Biogeochemical modelling of tropical marine ecosystems in the context of climate change

Submitted by
Chinenye Jane ANI

In September 2023

for the degree of Doctor of Philosophy in Oceanography within the College of Science and Engineering, James Cook University, Townsville, Queensland

Publications associated with this thesis

Ani, C.J., Baird, M., Robson, B. Modelling *Trichodesmium* photophysiology in the Great Barrier Reef using the eReefs model (*in prep*).

Ani, C.J., Baird, M., Robson, B. Modelling buoyancy-driven vertical movement of *Trichodesmium* application in the Great Barrier Reef (*under review Ecological Modelling*).

Ani, C.J., Baird, M.E. and Robson, B.J. Modelling *Trichodesmium* optics and buoyancy in the Great Barrier Reef using the eReefs models. In Vaze, J., Chilcott, C., Hutley, L. and Cuddy, S.M. (eds) MODSIM2023, 25th International Congress on Modelling and Simulation. Modelling and Simulation Society of Australia and New Zealand, July 2023, pp. 47. ISBN: 978-0-9872143-0-0. https://doi.org/10.36334/modsim.2023.ani317

Ani, C.J., Smithers, S.G., Lewis, S., Baird, M., Robson, B., 2023. eReefs modelling suggests *Trichodesmium* may be a major nitrogen source in the Great Barrier Reef. *Estuarine, Coastal and Shelf Science,* 108306.

Ani, C.J., Robson, B., 2021. Responses of marine ecosystems to climate change impacts and their treatment in biogeochemical ecosystem models. *Marine Pollution Bulletin* 166, 112223.

Ani, C.J., Robson, B., Lewis, S., Brodie, J., Smithers, S.G., 2019. Modelling the responses of marine ecosystems to climate change impacts. In MODSIM2019, 23rd International Congress on Modelling and Simulation. Modelling and Simulation Society of Australia and New Zealand, ISBN 978-0-9758400-8-5.

Conference presentations

Ani, C.J., Baird, M.E., Robson, B.J., 2023. "Modelling Trichodesmium optics and buoyancy in the Great Barrier Reef using the eReefs models" International Congress on Modelling and Simulation (MODSIM2023)

Ani, C.J., Smithers, S.G., Lewis, S., Robson, B, 2022. "Modelling *Trichodesmium* dynamics and its contribution to the Great Barrier Reef nitrogen budget" International Congress on Environmental Modelling and Software (iEMSs)

Ani, C.J., Smithers, S.G., Lewis, S., Robson, B, 2021. "Investigating the impacts of the temperature dependence of *Trichodesmium* on the timing and distribution of *Trichodesmium* blooms in the Great Barrier Reef" Advances in Marine Ecosystem Modelling Research (AMEMR) Virtual Conference

Ani, C.J., Robson, B., Lewis, S., Brodie, J., Smithers, S.G., 2019. "Modelling the responses of marine ecosystems to climate change impacts" International Congress on Modelling and Simulation (MODSIM2019)

Seminar presentations

Ani, C.J., Smithers, S.G., Lewis, S., Baird, M., Robson, B., 2022. "eReefs modelling suggests *Trichodesmium* may be a major nitrogen source in the Great Barrier Reef" AIMS@JCU Seminar Day

Acknowledgements

I acknowledge AIMS@JCU PhD Scholarship and Queensland Water Modelling Network Innovation Associates Program for funding this project.

I would like to thank my primary supervisor, Doctor Barbara Robson, for taking a chance on me and agreeing to have me as her PhD student. Barbara believed in my ability to successfully carry out this multidisciplinary research and guided me with patience through this study. She enriched my PhD experience by providing me with industry opportunities, which allowed me to apply the skills that I acquired during my PhD to solve real world problems. Special thanks to Doctor Stephen Lewis, my secondary supervisor, and Associate Professor Scott Smithers, my advisor mentor, for always encouraging me to think about the implications of my research work and for believing in my ability to successfully complete my PhD study. My supervisors are balanced, calm and kind, and I hope to emulate these throughout my life and career.

I thank my collaborator, Doctor Mark Baird, for helping me achieve my research goals. Without his contributions I would not have been able to improve the eReefs model. Thanks to him and the eReefs community in CSIRO, Hobart for their assistance in solving technical problems associated with my research and for making me enjoy my time in Hobart.

I would also like to thank my friends and the Nigerian Community in Townsville for making my PhD journey a memorable one. They helped me to find the right work-life balance.

Particular thanks to my mum and siblings for their support and prayers, and for always being my biggest cheer leaders although we are continents apart.

Finally, to my darling husband, Voluntia, thank you for your love and unwavering support, especially staying up late to listen to my research problems. I love you and I am thankful for having you in my life.

I could not have completed this adventure without your support.

Thank you, all.

Statement of contributions

Supervision

Dr Barbara Robson, Australian Institute of Marine Science
Dr Stephen Lewis, James Cook University
Associate Professor Scott Smithers, James Cook University

Funding

AIMS@JCU PhD Scholarship
Queensland Water Modelling Network (QWMN), a Programme of the Queensland Government Department of Environment and Science
2021 AIMS@JCU Science Communication Award

Contents

List of Figures

List of Tables

1. General introduction

The Great Barrier Reef (GBR) is a relevant case study to investigate nutrient cycling and climate change impacts on tropical marine ecosystems. The GBR is the world's largest coral reef system containing about 3000 individual reefs and stretching over 2,300 km along the north Queensland coast. An abundance of marine life is supported by the GBR. Despite being perhaps the most intensively managed coral reef system in the world, the GBR is exposed to threats from climate change and other human activities (Brodie et al., 2012; Hughes et al., 2017; Osborne et al., 2017; Great Barrier Reef Marine Park Authority, 2019; Emslie et al., 2020) and its condition is in decline.

Key drivers of this decline include reduced water quality from coastal catchments modified by agricultural activities that export three–four times higher riverine nutrients (nitrogen and phosphorus) and sediment loads than prior to European settlement (Brodie, 2013), tropical cyclones (Beeden et al., 2015), recurrent coral bleaching and ocean acidification (OA) associated with increased greenhouse gas emissions (Fabricius et al., 2011; Hughes et al., 2017). Increased nutrient loads reduce coral thermal tolerance, thereby increasing susceptibility to coral bleaching (Wooldridge, 2009). Increased riverine nutrient loads can enhance the growth of macroalgae (De'ath and Fabricius, 2010) and crown-of-thorns starfish (CoTS) larvae — the adults of which catastrophically reduce coral cover (Babcock et al., 2016). Storm events structurally damage coral cover (Beeden et al., 2015) and ocean acidification enhances decalcification thereby reducing the growth and survival of corals in the GBR (Albright et al., 2016). Given the sheer spatial size of the GBR, manual observations only capture an incomplete understanding of the complex hydrodynamic and biogeochemical processes that operate across various spatial and temporal scales and how these processes influence the health and productivity of the reef.

Biogeochemical models have been used to predict the impacts of terrestrial pollutants and climate change on the GBR to inform policy decisions (Mongin et al., 2016; Steven et al., 2019; Mongin et al., 2021; Baird et al., 2021). Biogeochemical models are process-based models that simulate nutrient cycling, optical conditions and the impacts of physical conditions on organism dynamics. Currently, the eReefs marine models are key tools used by the Australian and Queensland governments in managing and preserving the GBR. eReefs model applications include: assessment of catchment run-off impacts on the GBR health (Wolff et al., 2018; Margvelashvili et al., 2018; Baird et al., 2021), reporting the condition of the GBR, evaluating CoTS, fish and coral larvae dispersal (Hock et al., 2014, 2017, 2019; Gurdek-Bas et al., 2022), and investigating the vulnerability of the GBR to ocean acidification (Mongin et al., 2016, 2021) and coral bleaching (Baird et al., 2018).

The eReefs models are an implementation of the CSIRO Environmental Modelling Suite (EMS) (Baird et al., 2020) used to investigate the physical, biogeochemical and sediment processes in GBR marine ecosystems. EMS is a suite of hydrodynamic, biogeochemical and sediment models that simulates the physical conditions and water quality of the GBR. A regional hydrodynamic model is forced with river flow data, output from a global circulation model, the Ocean Modelling Analysis and Prediction System (OceanMAPS) and meteorological data from the Bureau of Meteorology's ACCESS models (Australian Community Climate and Earth-System Simulator). The hydrodynamic model (SHOC) simulates the physical conditions of the GBR (Herzfeld, 2006). Simulated physical conditions and transport are then used to drive a biogeochemical model, which simulates nitrogen, phosphorus, carbon and oxygen cycles, optical conditions, plankton, *Trichodesmium*, benthic organisms (i.e. coral, seagrass and macroalgae), detritus and sediment dynamics in the GBR. The EMS sediment transport model simulates the sinking, deposition and resuspension of suspended sediments and other particulate materials (Margvelashvili et al., 2008). Model parameterisation of the eReefs simulations of changes to biogeochemical processes

under climate change scenarios need to be evaluated to examine if the model performance may be further optimised.

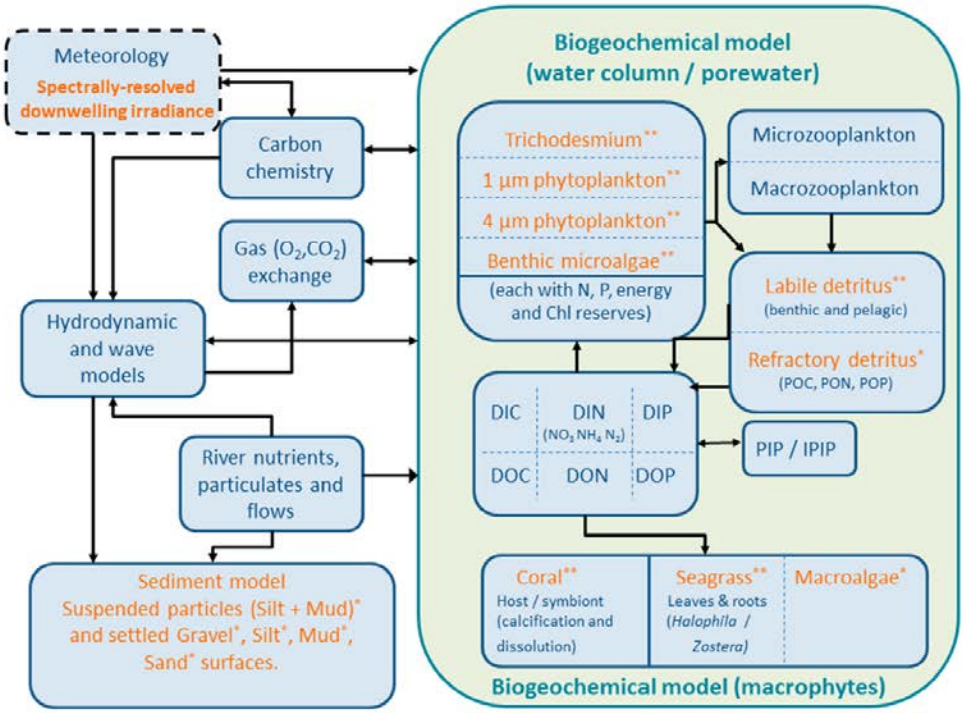

Figure 1.1: Schematic of the CSIRO Environmental Modelling Suite showing the connections between the hydrodynamic, biogeochemical, sediment, wave and optical models (Steven et al., 2019). The optically-active water components are represented by orange labels and asterisks, with the number of asterisks corresponding to the number of different optically-active elements with this component.

1.1 The representation of the responses of marine organisms to temperature increases and ocean acidification in coastal biogeochemical models

In this section, we will consider the representation of the responses of marine organisms (phytoplankton, zooplankton, corals and seagrasses) to temperature and ocean acidification in the EMS biogeochemical model (hereafter referred to as EMS-BGC). The parameterisation of relevant processes in EMS-BGC will be compared with three other leading coastal biogeochemical models, ERSEM (European Regional Seas Ecosystem Model), AED (Aquatic Ecodynamics) and GEM (Global Environmental Multiscale Model). This will set the context for the improvement of EMS-BGC and the application of the EMS to investigate nutrient cycling and climate change impacts on GBR ecosystems.

Full descriptions of these models can be found in (Baird et al., 2020; Butenschon et al., 2016; Hipsey et al., 2013; Blauw et al., 2009).

1.1.1 Water temperature

1.1.1.1 Phytoplankton physiological responses

EMS-BGC represents the temperature dependence of phytoplankton maximum growth rate as an exponential response function. Photosynthesis in EMS-BGC increases exponentially with increasing temperature, but also depends on light, cellular nutrient status and cell size. This approach has the advantage of simplicity and only requires a single parameter to describe the temperature response curve, but may not be appropriate in climate-change scenarios that may take conditions above the phytoplankton optimum temperature. An optimum temperature (T_{opt}) is the temperature at which an organism's physiological rate is maximal. Both ERSEM and AED use optimum response functions for the dependence of mass-specific gross primary production on temperature. With this function mass-specific gross primary production increases rapidly with increasing temperatures below T_{opt} and slowly declines when temperatures are above T_{opt}. GEM applies a simple linear response curve for the temperature dependence of maximum net growth rate of phytoplankton.

EMS-BGC, GEM and AED represent the temperature dependence of the phytoplankton mortality rate as exponential functions. This approach is ideal for high temperature conditions as laboratory observations have shown that phytoplankton mortality occur at very high temperatures (Boyd et al., 2013; Fu et al., 2014). In contrast to these, specific mortality due to lysis is temperature independent in ERSEM and is influenced by nutrient stress.

The temperature dependence of phytoplankton maintenance respiration in EMS-BGC, AED and GEM follow exponential response curves. In EMS-BGC, oxygen is also consumed when phytoplankton mortality releases carbon and is exponentially dependent on temperature. Respiration in ERSEM is split into maintenance and activity respirations. Maintenance respiration is not temperature-dependent in the model, while activity respiration is optimally dependent on temperature through the influence of temperature-dependent carbon assimilation and chlorophyll synthesis.

The maximum chlorophyll *a* synthesis rate in EMS-BGC is not temperature dependent, but the chlorophyll *a* synthesis rate has an exponential dependence on temperature since it is a function of temperature-dependent maximum growth rate and internal nutrient quota. However, the chlorophyll synthesis rate in ERSEM has an optimum temperature dependence and is also limited by internal nutrient quota.

Nutrient uptake in EMS-BGC is not temperature dependent, but is limited by diffusion, which is influenced by temperature. Nutrient uptake has an exponential temperature dependence in GEM and optimum temperature dependence in AED. Nutrient uptake in ERSEM is regulated by phytoplankton nutrient demand which has optimum temperature dependence except for silicate dynamics in diatoms.

It is important to note that the temperature dependence of the autotroph growth model in EMS-BGC is a combination of constant, exponential and polynomial functions. This is because its temperature dependence changes with respect to the physiological conditions of the autotroph.

1.1.1.2 Zooplankton responses

EMS-BGC represents zooplankton swimming velocities and maximum growth rates with an exponential temperature dependency. Zooplankton grazing rates in EMS-BGC are functions of the encounter rate of the predator and its prey, and are constant at saturated zooplankton growth. Since the encounter rate is a function of temperature-dependent swimming velocities, diffusive and shear velocities, zooplankton grazing rates have exponential temperature dependency. In ERSEM, zooplankton prey mass-specific uptake capacity has an optimum temperature dependence and its prey encounter rate is limited by a

predation efficiency constant. In addition, zoobenthos in ERSEM is also limited by oxygen and a growth limiting penalty function which accounts for overcrowding effects. AED calculates net zooplankton growth as a balance between food assimilation and losses from respiration, mortality, excretion and predation. Food assimilation is optimally dependent on temperature in AED. However, because primary consumers are not simulated as real state variables in GEM, the biomass of filter feeders are imposed as external forcings to allow their grazing effects to be simulated. Filter-feeders grazing activities, uptake, filtration and maximal growth rates are exponentially dependent on temperature.

Zooplankton respiration is implicitly modelled in EMS-BGC and has exponential dependency on temperature. It is simulated as oxygen consumption through carbon release from ingested phytoplankton biomass and detrital production resulting from zooplankton mortality and growth inefficiency. Zooplankton activity and maintenance respirations have an optimum temperature dependence in ERSEM. Zooplankton respiration in AED, and filter-feeder maintenance and growth respiration rates in GEM are exponentially dependent on temperature.

Zooplankton mortality rates are exponentially dependent on temperature in EMS-BGC and AED, as well as filter-feeders mortality rates in GEM. Further, zooplankton excretion fraction in loss rate and fecal pellet fraction in loss rate in AED have exponential temperature dependency, and mortality is also limited by salinity. In ERSEM, zooplankton mortality is independent of temperature but is limited by oxygen, and is a product of constant mortality rate and zooplankton biomass in hibernation.

1.1.1.3 Coral responses

Based on field observations, EMS-BGC specifies a temperature increase of 2°C above mean summer temperature as the critical thermal threshold beyond which bleaching occurs (Baird et al., 2018). The growth and mortality rates of coral polyps and symbionts have exponential temperature dependence. Coral symbiont maintenance respiration has exponential temperature dependency and its growth is enhanced by coral polyp remineralisation. Respiration is also simulated as oxygen consumption during coral symbiont expulsion, translocation of nutrients from symbiont to host, and coral polyp and symbiont mortalities. Coral larvae are not modelled in any of the four models and corals are not included in ERSEM, AED and GEM.

1.1.1.4 Seagrass responses

EMS-BGC represents the temperature dependence of maximum growth and mortality rates of seagrasses in the GBR as exponential functions, neglecting the potential for decline when temperatures exceed optimum values. As a result, the model will not simulate the dramatic decline of seagrasses that can occur during marine heat waves (Collier and Waycott, 2014; Arias-Ortiz et al., 2018), nor more subtle inhibition when the optimum temperature is exceeded to a smaller degree (Collier et al., 2017). Seagrasses are not represented in ERSEM, GEM and AED.

1.1.1.5 Microbial responses

EMS-BGC, AED and GEM specify nitrification and denitrificaton rates to have exponential temperature dependency. ERSEM represents the temperature dependence of nitrification and denitrification as optimum response functions. In addition, nitrification in ERSEM is also dependent on nitrogen, oxygen and pH states, but for benthic nitrification which is not dependent on pH state. Denitrification is also limited by available oxidised nitrogen in ERSEM. Remineralisation rates in EMS-BGC, GEM and AED have their temperature dependence represented by exponential response functions, whereas pelagic and

benthic remineralisation rates in ERSEM are not temperature independent as they are defined by constant mass-specific remineralisation rate. In ERSEM, mass-specific uptake of dissolved organic matter by heterotrophic bacteria has optimum temperature dependency and is limited by nutrients and oxygen, while mortality is a constant fraction of bacteria biomass and is regulated by oxygen. Heterotrophic bacteria maintenance and activity respirations have optimum temperature dependency.

A summary of temperature effects on marine organisms represented by EMS-BGC, ERSEM, AED and GEM is shown in Table 1.1.

1.1.2 Ocean acidification

1.1.2.1 Phytoplankton physiological responses

Overall, most coastal biogeochemical models, including EMS-BGC do not consider responses of phytoplankton physiological processes to pCO_2 increases. Most models have carbon uptake being growth rate and light dependent with no impact of carbon concentration (assumed to be unlimited). However, the impact of increased pCO_2 on phytoplankton is modelled as the enhancement of gross carbon uptake and activity respiration by a linearly pCO_2 dependent function in ERSEM.

1.1.2.2 Coral responses

The EMS-BGC represents the rate of coral calcification as a function of aragonite saturation in deep waters and fixed carbon of coral symbionts. Thus, decreased aragonite saturation due to pCO_2 increases will likely decrease coral calcification, but there is no dependency between coral calcification and coral growth. This is because coral growth is driven by light, nutrients and temperature, and calcification does not change coral biomass, rather it modifies alkalinity and dissolved inorganic carbon (DIC) concentration in the water. Although corals are not modelled in ERSEM, calcification rates are implicitly simulated from rain ratio — calcite production proxy — and are controlled by Michaelis-Menten terms for carbon, nutrients and temperature.

Overall, the effects of ocean acidification on the physiology of marine organisms are not often represented by coastal biogeochemical models.

1.1.3 Adaptation of marine organisms to changes in temperature and ocean acidification

The adaptation of marine organisms to rising temperatures and OA is not modelled by EMS-BGC, ERSEM, GEM and AED. Nevertheless, the phytoplankton module in GEM allows the simulation of the competition and adaptation of phytoplankton species to light or limiting nutrients. This involves the consideration of three phenotypes of each modelled phytoplankton group, with different phenotypes having distinct physiological parameters corresponding to changing environmental conditions.

Table 1.1: Summary of the representations of temperature dependence of marine organisms in EMS-BGC, ERSEM, GEM and AED. Primary consumers are modelled as filter-feeders in GEM and are categorised as zooplankton in this table. NA corresponds to not applicable.

Organism	Response function	EMS-BGC	ERSEM	GEM	AED	Advantage/Disadvantage
Phytoplankton	Optimum	NA	Mass-specific gross primary production Activity respiration Chl *a* synthesis rate Nutrient uptake	NA	Photosynthesis Nutrient uptake	Suitable for high temperature conditions
	Exponential	Photosynthesis Maximum growth rate Mortality rate Respiration Chl *a* synthesis rate	NA	Mortality rate Respiration rate Nutrient uptake	Mortality rate Respiration rate	Not suitable for high temperature conditions except for mortality and respiration rates
	Linear	NA	NA	Net growth rate	NA	Not suitable for high temperature conditions
Zooplankton	Optimum	NA	Prey mass-specific uptake capacity Maintenance and activity respirations	NA	Food assimilation	Suitable for high temperature conditions
	Exponential	Maximum growth rate Mortality rate Swimming velocity Grazing activity Respiration	NA	Maximal growth rate Grazing activity Maintenance and growth respiration rates Filtration rate Mortality rate	Respiration rate Mortality rate Excretion fraction of loss rate Fecal pellet fraction of loss rate	Not suitable for high temperature conditions except for mortality rate
Coral	Exponential	Maximum growth rate Mortality rate Respiration	NA	NA	NA	Not suitable for high temperature conditions except for mortality rate
Seagrass	Exponential	Maximum growth rate Mortality rate	NA	NA	NA	Not suitable for high temperature conditions except for mortality rate
Microbes	Optimum	NA	Mass-specific uptake of dissolved organic matter Maintenance and activity respirations Nitrification rate Denitrification rate	NA	NA	Suitable for high temperature conditions
	Exponential	Nitrification rate Denitrification rate Remineralisation rate	NA	Nitrification rate Denitrification rate Remineralisation rate	Nitrification rate Denitrification rate Remineralisation rate	Not suitable for high temperature conditions

1.2 How can the EMS biogeochemical model be modified?

The EMS-BGC does not consider the impacts of extreme events and the adaptation of marine organisms to climate change impacts. First, the use of exponential temperature response functions for all physiological rates of marine organisms modelled in EMS-BGC is not suitable for the reoccurring extreme temperature conditions in the GBR. Experimental studies have shown that higher temperatures inhibit physiological rates and can cause changes in community compositions of marine organisms (Boyd et al., 2013; Collier et al., 2017; Keys et al., 2018). Second, depending on location and species marine organisms have been shown to possess distinct thermal tolerance range and limits (Boyd et al., 2013; Collier et al., 2017). It is not a one-size-fits-all scenario. Thus, it is ideal to use their corresponding thermal tolerance and limits to parameterise the temperature dependence of their respective physiological rates. Third, it is imperative to incorporate the effects of ocean acidification on the physiology of marine organisms modelled in EMS-BGC as ocean acidification has been suggested to affect the physiology of some marine organisms (Smith et al., 2016; Keys et al., 2018; Alessi et al., 2019). Finally, the adaptation of marine organisms to changing environmental conditions need to be incorporated in EMS-BGC as these marine organisms have been reported to possess the potential to adapt to extreme environmental conditions (Schaum et al., 2017; Collier et al., 2018; Buerger et al., 2020).

Failure to adequately capture the effects of these extreme environmental conditions by EMS-BGC could result in uncertain predictions of marine ecosystem responses to increased temperature and ocean acidification in the GBR. With these additions, it is anticipated that the potential changes in benthic cover, plankton communities and calcifying organisms in response to temperature increases and ocean acidification in the GBR can be more reliably and accurately predicted. The review of the EMS-BGC identified that the knowledge of *Trichodesmium* abundance on the GBR, its contribution to nitrogen loads in the GBR and its parameterisation in the model is a major research gap and will be explored in this project.

1.3 Thesis aim and objectives

The aim of this project is to improve EMS-BGC by critically re-evaluating the assumptions underpinning the mathematical representation of biogeochemical processes in the existing model and use the EMS to investigate nutrient dynamics and climate change impacts on the GBR. To achieve this goal, we carried out key objectives which resulted in the following thesis chapters:

- Chapter 2 — a review of marine ecosystem parameters and processes that are expected to change as a result of climate change and ocean acidification, and a systematic review of published marine ecosystem climate change model applications. This chapter identifies important marine modelling practices that need to be implemented in future modelling studies for more reliable and accurate model predictions.

  Citation: Ani, C.J., Robson, B., 2021. Responses of marine ecosystems to climate change impacts and their treatment in biogeochemical ecosystem models. *Marine Pollution Bulletin* 166, 112223.

- Chapter 3 — quantification of the contribution of *Trichodesmium* to the total annual nitrogen budget of the GBR and the identification of potential drivers of *Trichodesmium* growth and nitrogen fixation. The knowledge gained in Chapter 2 was used to optimally parameterise the temperature dependence of *Trichodesmium* physiological processes in EMS-BGC model, thereby adequately representing the effects of rising temperature conditions in the GBR. The modified EMS-BGC model was used to simulate *Trichodesmium* dynamics in the GBR. This chapter provides a new line of evidence supporting the conjectured role of *Trichodesmium* as a major contributor

to the nitrogen budget of the GBR. Key research findings will help inform future water quality management strategies.

Citation: Ani, C.J., Smithers, S.G., Lewis, S., Baird, M., Robson, B., 2023. eReefs modelling suggests *Trichodesmium* may be a major nitrogen source in the Great Barrier Reef. *Estuarine, Coastal and Shelf Science,* 108306.

- Chapter 4 — modification of the parameterisation of *Trichodesmium* buoyancy regulation in the *Trichodesmium* growth submodel of the eReefs biogeochemical models. The modification involved the application of the form resistance factor to the sinking velocities of tuft-shaped *Trichodesmium* colonies. The model results compared well with observations from the Australian Institute of Marine Science Marine Monitoring Program sensor network sites and captured the emergent patterns of phytoplankton size spectrum observed in nature. The modified model formulations improve the physiological realism of the *Trichodesmium* growth submodel of the eReefs marine biogeochemical models, and can help to improve the understanding of *Trichodesmium* dynamics for effective GBR water quality management.

  Citation: Ani, C.J., Baird, M., Robson, B. Modelling buoyancy-driven vertical movement of *Trichodesmium* application in the Great Barrier Reef (*under review Ecological Modelling*).

- Chapter 5 — the parameterisation of the variation of *Trichodesmium* phycobilipigments under varying light conditions in the *Trichodesmium* growth submodel of the eReefs biogeochemical models. This involved the parameterisation of the interconversion between phycourobilin and phycoerythrobilin, and photosystem II reaction centre dynamics. The model results emphasise the need to validate *Trichodesmium* concentrations, phycourobilin or phycoerythrobilin concentrations, and/or nitrogen fixation rates against observations for increased confidence in the model's predictions.

All citations used in this thesis are included in a collective reference list at the end of the thesis, beginning on page 97.

2. Responses of marine ecosystems to climate change impacts and their treatment in biogeochemical ecosystem models

Summary

To predict the effects of climate change on marine ecosystems and the effectiveness of intervention and mitigation strategies, we need reliable marine ecosystem response models such as biogeochemical models that reproduce climate change effects. We reviewed marine ecosystem parameters and processes that are modified by climate change and examined their representations in biogeochemical ecosystem models. The interactions among important aspects of marine ecosystem modelling are not often considered due to complexity: these include the use of multiple IPCC scenarios, ensemble modelling approach, independent calibration datasets, the consideration of changes in cloud cover, ocean currents, wind speed, sea-level rise, storm frequency, storm intensity, and the incorporation of species adaptation to changing environmental conditions. Including our recommendations in future marine modelling studies could help improve the accuracy and reliability of model predictions of climate change impacts on marine ecosystems.

This chapter reproduces the following publication:

Ani, C.J., Robson, B., 2021. Responses of marine ecosystems to climate change impacts and their treatment in biogeochemical ecosystem models. *Marine Pollution Bulletin* 166, 112223.

Contribution of authors

Chinenye J. Ani: Methodology, Validation, Formal analysis, Investigation, Resources, Data curation, Writing – original draft.

Barbara Robson: Methodology, Validation, Formal analysis, Writing – review & editing, Supervision, Project administration, Conceptualisation, Funding acquisition.

2.1 Introduction

Marine ecosystems help to regulate the climate, protect coastal areas from storms (Shepard et al., 2011; Barbier, 2017), provide food for human communities, and support various livelihoods and recreational activities (Costanza et al., 2014; Barbier, 2017). Unfortunately, many marine ecosystems are in decline due to climate change or as a consequence of human activities. For example, Jones et al. (2018) estimate that 13.2% ($\approx$ 55 million km^2) of the world's oceans are marine wilderness and $<$ 100,000 km^2 wilderness remains in coastal ecosystems. From 1985 to 2012, coral cover on the Great Barrier Reef (GBR) declined from 28% to 13.8% (De'ath et al., 2012). Climate change impacts on marine ecosystems include global warming, ocean acidification, changes in ocean currents, sea-level rise and sea-ice retreat (Schweiger et al., 2008; IPCC, 2014; Hogg et al., 2015; Gattuso et al., 2015; Oliver et al., 2017). Human activities affect nearly all parts of the ocean. Eroded sediments, nutrients and chemicals from agricultural and urbanised catchments drain into coastal oceans, causing pollution (Brodie et al., 2011; Devlin et al., 2012). Discarded fishing nets and plastic waste entangle marine organisms as they swim (Wilcox et al., 2015) and some marine ecosystems such as mangrove forests have been cleared for development.

Oceans absorb more than 90% of heat generated from increased greenhouse gas (GHG) emissions from human activities such as the combustion of fossil fuels and land use (IPCC, 2014). The surface temperature of oceans is projected to increase by between 0.3°C to 1.7° C under Representative Pathway Concentration 2.6 (RCP2.6), 1.1° C to 2.6° C under RCP4.5, 1.4° C to 3.1° C under RCP6.0 and 2.6° C to 4.8° C under RCP8.5 IPCC scenarios by 2100 (IPCC, 2014). Ocean warming causes marine heat waves (Cavole et al., 2016; Oliver et al., 2017; Hughes et al., 2017), oxygen depletion (Vaquer-Sunyer and Duarte, 2011; Bruno et al., 2018) and coral bleaching (Hughes et al., 2017; Barkley et al., 2018), and may cause the loss of some marine habitats. An example is the potential loss of suitable spawning habitats for Atlantic cod (*Gadus morhua*) and Polar cod (*Boreogadus saida*) due to sea surface temperature increases (Dahlke et al., 2018).

More frequent extreme weather events associated with global warming (Mills et al., 2013; Pearce and Feng, 2013; Perry et al., 2014; Beeden et al., 2015; Hughes et al., 2017) and loss of coastal protection associated with increased storminess, sea-level rise and ecosystem changes such as reduced coral reef growth (Perry et al., 2014; Beeden et al., 2015; Cheal et al., 2017) may also negatively impact coastal communities.

Ocean warming intensifies oxygen depletion and can promote the growth of harmful algal blooms (Peperzak, 2003; Paul, 2008), leading to the death of marine organisms. Because warm water holds less dissolved oxygen than cooler water, hypoxia caused by severe oxygen depletion is projected to increase by 10% for each 1°C surface warming (Deutsch et al., 2011). Hypoxia can also occur due to increased oxygen demand as organics breakdown (Chen et al., 2007; Du et al., 2018; Rodríguez-Martínez et al., 2019).

Ocean CO_2 absorption increased from $1.0 \pm 0.5 \times 10^{12}$ kg Cyr^{-1} in 1960s to $2.4 \pm 0.5 \times 10^{12}$ kg Cyr^{-1} averaged over the period from 2008 to 2017 (Le Quéré et al., 2018). Although the absorption of CO_2 by oceans mitigates the atmospheric impacts of anthropogenic CO_2 emissions, it also causes ocean acidification (Wei et al., 2009). Ocean acidification is the reduction of ocean pH due to the dissolution of CO_2 in seawater. Global surface ocean pH naturally ranges between 8.0 and 8.5 (Bates et al., 2014), but has declined by 0.1 (Feely et al., 2004; Stocker et al., 2013; Gattuso et al., 2015) and is projected to decline by 0.3 to 0.4 by the end of 2100 under RCP8.5 (Mora et al., 2013; Gattuso et al., 2015). Ocean acidification reduces the growth, development, survival and abundance of marine calcifiers, and the abundance of their predators (Doney et al., 2009; Kroeker et al., 2013). Relative to current CO_2

conditions, marine calcifiers were shown to have a $11 - 19\%$ reduction in growth and development, a 27% decline in calcification and survival rate, and a 15% reduction in abundance under CO_2 conditions for the year 2100 (Kroeker et al., 2013).

Recently, several marine ecosystems around the world have experienced extreme marine heatwaves with catastrophic ecological outcomes (Filbee-Dexter et al., 2016; Hughes et al., 2017; Barkley et al., 2018; Brainard et al., 2018; Arias-Ortiz et al., 2018; Burt et al., 2019; Kendrick et al., 2019). The unprecedented coral bleaching events in the GBR in 2016 and 2017 (Hughes et al., 2017) are examples of such events. These unprecedented bleaching events reduced living hard coral cover by 51% over large areas of the GBR that experienced extreme temperatures (Stuart-Smith et al., 2018). The 2010/2011 marine heatwave damaged about 36% of seagrass meadows in Shark Bay, the largest and most diverse seagrass assemblages in the world (Arias-Ortiz et al., 2018). Ocean warming reduced mean kelp biomass by 85–99% over the past 40–60 years at Nova Scotia, Canada (Filbee-Dexter et al., 2016). However, global warming has enhanced the poleward expansion of mangrove forests into salt marshes in subtropical and temperate coastlines (Saintilan et al., 2014).

Modelling the effects of climate change on marine ecosystems can help with the predictions of climate change impacts and the effectiveness of intervention and mitigation strategies. Among the different modelling techniques, one has proven to be popular in its predictions (Fennel et al., 2019): the biogeochemical model.

Biogeochemical models – also known as ecosystem models or receiving water quality models – are process-based models that simulate optical conditions and the cycling of nutrients such as carbon (C), nitrogen (N) and phosphorous (P) throughout the ecosystem. They also simulate the effects of changes in the physical, chemical and biological environments on primary production (PP) and export of organic and inorganic matter. Biogeochemical models are different from end-to-end models as they do not simulate high trophic level (HTL) production, e.g., fishery production (Robson et al., 2017b). End-to-end models simulate the effects of the physical and hydrological environments on primary production and food-web interactions (Robson et al., 2017b). Biogeochemical models are ecological models but not all ecological models are biogeochemical models. Ecological models represent important processes and factors that influence ecological systems on different scales and hierarchical levels in a specific context (Jørgensen, 2008).

Among biogeochemical models, there are two main types of models: global and coastal. Global biogeochemical models simulate export of organic and inorganic matter, and water quality, but do not simulate benthic and sediment dynamics. Coastal biogeochemical models simulate water quality, organic matter, benthic and sediment dynamics. However, some coastal biogeochemical models ignore benthic and sediment dynamics and Soetaert et al. (2000) have shown that such models have poor predictions.

Research to predict climate change responses of marine ecosystems has led to the development of many biogeochemical models with varying process representations and complexities (Robson, 2014; Janssen et al., 2015). Despite these significant developments, there has until recently been little focus on the representation of climate change impacts on marine ecosystem response models. Understanding the effects of climate change on marine ecosystem processes in the laboratory and field is fundamentally important in predicting climate change impacts on marine ecosystems. Here, we review marine ecosystem parameters and processes that are expected to change as a result of climate change and ocean acidification and then present a systematic review of published marine ecosystem climate change model applications.

2.2 Methods

For the systematic review of marine ecosystem modelling of climate change scenarios, peer reviewed journal publications and proceeding papers were selected for inclusion based on their use of mechanistic models to project the effects of climate change on marine ecosystems. Mechanistic models represent processes through the application of known scientific laws describing the behaviour of components of the modelled system. The literature search was done on Web of Science on May 1, 2019 (Table 2.1). To obtain the most relevant studies, the search field "Topic" (which searches titles, abstract, author keywords and keywords plus) was selected. The search returned 353 papers published between 2005 and 2019. A subset of 131 papers was selected for inclusion based on relevance to modelling the responses of marine ecosystems to climate change impacts.

The selected 131 modelling studies used eighty-five different models, with others being different applications of the same model. References for all 131 modelling studies can be found on the Supporting Information document. The modelled systems include twenty-two coastal (including estuarine) ecosystems and 109 open ocean marine ecosystems. Further, seventy-two of these ecosystem models considered regional domains, while the remaining fifty-nine were global models.

Table 2.1: Literature search keywords.

Keyword type	**Search keywords**
Main keyword	Biogeochemical model OR ecosystem model OR water quality model
Context keyword	Climate change OR global warming OR ocean acidification
Scope keyword	Marine OR ocean OR sea OR bay OR coastal

To complement these results and expand the range of results returned, a second search was conducted using Google Scholar. Studies were selected for inclusion due to their use of field and laboratory experiments to assess the impacts of elevated temperature and pCO_2 on plankton, coral, seagrass, mangrove, kelp and microbes. These marine organisms are considered because they are important components of marine ecosystems around the world. Results from a range of latitudes and climates were included.

2.3 Marine ecosystem parameters modified by climate change

2.3.1 Meteorological conditions and sea level

Air temperatures, cloud cover, storm intensity and storm frequency have all changed and continue to change due to anthropogenically forced climate change associated with greenhouse gas emissions. Average global surface temperature increased by 0.37°C between 1925 and 1944 and by a further 0.32°C from 1978 to 1997 (Jones et al., 1999). Relative to 1850–1900, temperatures are projected to increase

throughout the 21st century with an increase of over 1.5°C by the end of the century (IPCC, 2014).

Warming-induced ocean thermal expansion, melting ice and changes in land water storage cause sea-level rise. Thermal expansion and melting ice have contributed about 75% of global sea-level rise since the early 1970s (IPCC, 2014). Sea-level rise exacerbates coastal flooding as it increases the vulnerability of coastal areas to floods in different parts of the world (French et al., 1995; Scott et al., 2012; Iwamura et al., 2013; Bhattachan et al., 2018; Knutson et al., 2020).

Despite several past disagreements on the reliability of model predictions of climate change impacts on tropical cyclones (Broccoli and Manabe, 1990; Evans and Allan, 1992; Bengtsson et al., 1996) recent studies agree on the use of high-resolution global models to predict climate change impacts on tropical cyclones (Knutson et al., 2010, 2020; Walsh et al., 2016). Relative to the end of the 20th century, a 2°C global temperature increase is projected to cause a 1 to 11% increase in the intensity of average global tropical cyclones and a 6 to 34% decrease in storm frequency by 2100 (Knutson et al., 2010, 2020). Overall, changes in storm intensity and frequency have been shown to greatly impact North and Central America, Australia, East and West Africa, Asia and South America (Ward et al., 2016). They have caused socio-economic damage and loss of human lives (Nordhaus, 2006), deteriorated the living conditions in some marine ecosystems and coastal communities (French et al., 1995).

2.3.2 River flows, sediment and nutrient loads

The impact of global warming on river flow regime is highly variable depending on the location. On a global scale, under SRES-A1B scenario Arnell and Gosling (2013) projected increases in mean annual runoff in Canada, high-latitude eastern Europe and Siberia by 2050 with respect to 1961–1990 averages. They also predicted declines in central Europe, around the Mediterranean, the Mashriq, central America and Brasil. Likewise, relative to 1950–1999 means, severe drought is predicted to be prevalent in North-central America from 2050 to 2099 under SRES-A1B scenario due to median declines in precipitation by 5 to 10% and runoff by 10 to 30% (Hidalgo et al., 2013). In South-western Australia, relative to averages from 1975 to 2007, a median decline by 25% in runoff resulting from a median decline by 8% in rainfall is predicted to occur by 2030 under future global temperature increases of 0.7°C, 1.0°C and 1.3°C (Silberstein et al., 2012).

Precipitation has been predicted to increase by 14 to 20% within 100km of tropical-cyclone activity (Knutson et al., 2010, 2020). Increased precipitation associated with tropical cyclones effectively generates runoff (Devlin et al., 2012; Darby et al., 2013) and contributes about 32% of the suspended sediment load draining into the Mekong Delta (Darby et al., 2016). During high flow events, large loads of nutrients and sediments from adjacent agricultural catchments drain into the GBR (Brodie et al., 2010, 2011; Devlin et al., 2012). Consequently, current mean annual suspended sediments increased 5.5 times, nitrogen increased 5.7 times and phosphorus increased 8.9 times since European settlement (Kroon et al., 2012). On the other hand, in Mekong Delta, 33.0 ± 7.1 megatonnes of an estimated 52.6 ± 10.2 megatonnes decline in suspended sediment load was caused by shift in tropical-cyclone activity (Darby et al., 2016).

These changes have the potential to alter marine biogeochemistry and consequently marine ecosystems, and can be manifested in eutrophication, hypoxia and sedimentation. Sediment loads from rivers influence the structure and maintenance of deltas, the turbidity and nutrient concentrations of coastal waters (Sklar and Browder, 1998). Increased sediment and nutrient loads from terrestrial runoff have been shown to impact coral health on the GBR and enhance the abundance of crown-of-thorns starfish (Wolanski and De'ath, 2005). In Bohai Sea, increased nutrient loads from rivers increased the frequency and area of red tide events, and the diversity of dominant phytoplankton species (Wang et al., 2019a).

On the other hand, in Chilika Lagoon, riverine nutrient loads and detritus have been shown to support fisheries (Bonthu et al., 2016).

2.3.3 Oceanic transport processes

Oceanic transport processes comprising ocean currents, stratification and upwelling are important factors influencing marine ecosystems as they transport plants, animals, heat and nutrients around the oceans. Changes in ocean currents in response to future climate change vary across locations. For instance, between the 1990s and 2060s, Sun et al. (2012) project declines in the transport of Leeuwin Current (15%) and Indonesian Throughflow (20%), and increases in East Australian Current core transport (12%) and extension (35%) under SRES-A1B. Further, Hogg et al. (2015) reported the intensification of Southern Ocean eddy field in recent decades, with largest trends observed in the Indian ($18.3 \pm 5.1 cm^2 s^{-2}$ decade^{-1}) and Pacific ($14.9 \pm 4.1 cm^2 s^{-2}$ decade^{-1}) regions of the Southern Ocean.

Ocean stratification is projected to largely increase by the end of the 21st century, relative to the end of the 20th century under SRES-A2 scenario (Capotondi et al., 2012; Hordoir and Meier, 2012). Temperature changes have been identified as the largest contributor to stratification increases on a global scale, with the largest effect in the tropics (Capotondi et al., 2012). However, salinity was reported to have the largest influence on stratification increases in the Arctic, North Atlantic and Northeast Pacific due to Arctic freshening and increased salinity in subtropical North Atlantic and in the Mediterranean Sea (Capotondi et al., 2012).

Increased greenhouse gas emissions have been suggested to increase coastal upwelling intensity (i.e. the eastern boundary upwelling systems (EBUS)) (Bakun, 1990; Snyder et al., 2003; Bakun et al., 2015; Wang et al., 2015). The EBUS – one of the most productive marine ecosystems in the world – are projected to expand poleward due to increased temperatures (Bakun et al., 2015). However, under global warming, open ocean upwelling is projected to weaken while coastal upwelling remains unchanged (Hsieh and Boer, 1992). This is due to the weakening of upwelling bands in equatorial and subpolar zones, and downwelling bands in subtropical zones.

These changes in oceanic transport processes will have implications on the dispersal of species larvae, distribution of nutrients and marine organisms, and nutrient cycling in marine ecosystems.

2.3.4 Water temperature

Global warming influences ocean temperature and will affect marine ecosystems. Temperature is arguably the most important physical variable that structures marine ecosystems. It influences the growth, composition and abundance of plankton communities, the abundance and distribution of fish, the growth and photosynthesis of seagrasses, mangroves, kelp and coral health. Extreme temperature increases caused by climate change alter marine ecosystems and the services they provide. A summary of temperature effects on marine ecosystems is shown in Figure 2.1. Temperature effects on plankton communities, corals, seagrasses, microbes, mangroves and kelp are detailed further below.

2.3.4.1 Phytoplankton physiological responses

Phytoplankton, the most important organism in marine food chains is sensitive to temperature increases. Some experiments have shown that growth rate, nitrogen fixation rate and photosynthetic rate increase with increasing temperature, peak at an optimum temperature T_{opt}, and decrease afterwards (Figure 2.2c) (Breitbarth et al., 2007; Boyd et al., 2013; Fu et al., 2014). Respiration of phytoplankton in temperate regions increased with increasing temperature (i.e. from 0 to 30°C), while gross photosynthesis

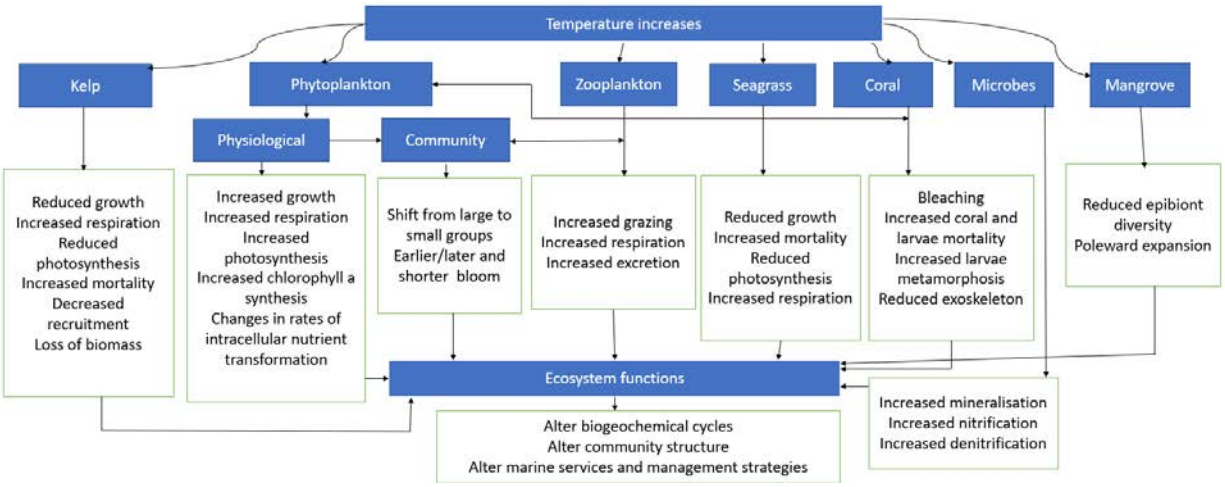

Figure 2.1: Summary of the responses of plankton, seagrasses, corals, microbes, mangroves and kelp to temperature increases.

increased below 10°C, peaked between 10°C and 15°C and decreased at higher temperatures (Andersson et al., 1994).

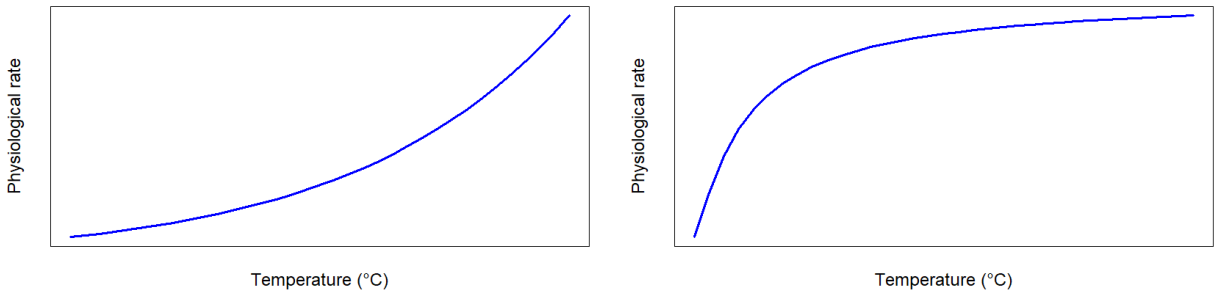

(a) Exponential response curve.

(b) Saturating response curve.

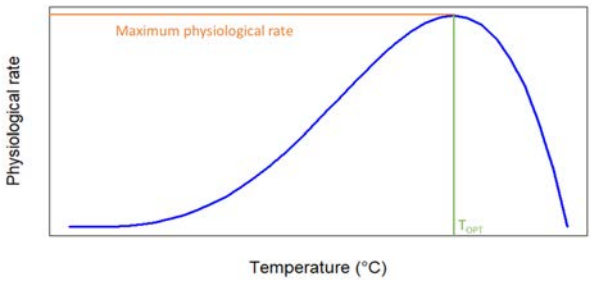

(c) Optimum response curve.

Figure 2.2: Temperature response curves.

Growth rate of polar diatoms increased by 25% with a temperature increase of 3°C and decreased rapidly with a further 1°C increase in temperature (Boyd et al., 2013). Temperate diatom species experience

a four-fold increase in growth rates with increasing temperature and no growth at temperatures above 20°C (Boyd et al., 2013). Maximum growth rates for polar and temperate phytoplankton species range between 0.3 d^{-1} and 1.4 d^{-1} (Boyd et al., 2013).

Tropical phytoplankton species have higher thermal tolerance than polar and temperate species as their thermal limits range between 18 and 34°C (Breitbarth et al., 2007; Boyd et al., 2013; Fu et al., 2014). *Trichodesmium* — a nitrogen fixing cyanobacterium — attained maximum growth of about 0.2 d^{-1} to 0.3 d^{-1} (Bell et al., 2005; Breitbarth et al., 2007; Boyd et al., 2013) at temperatures between 24 and 28°C (Bell et al., 2005; Breitbarth et al., 2007; Boyd et al., 2013; Fu et al., 2014) and gradually declined to zero at 35°C (Breitbarth et al., 2007; Boyd et al., 2013). Maximum nitrogen fixation by *Trichodesmium* (0.13 mmol N mol POC^{-1} h^{-1}) occurred at 27°C (Breitbarth et al., 2007), while maximum photosynthesis occurred at ≈ 26°C (Fu et al., 2014). *Crocosphaera*, another nitrogen fixer has been reported to have a higher thermal tolerance, with thermal limits ranging from 22°C to 34°C and optimum temperature at ≈ 28°C and 30°C (Boyd et al., 2013; Fu et al., 2014). Furthermore, the dinoflagellate *A. sanguinea* attained maximum growth at 25°C with an upper temperature limit between 30°C and 33°C, and a lower temperature limit between 10°C and 15°C (Boyd et al., 2013). A three-fold increase in dinoflagellate *P. donghaiense* growth rate was reported to occur between 15°C and 20°C, and ≈ 15% decrease at 30°C (Boyd et al., 2013). Although tropical phytoplankton have higher thermal limits than polar and temperate species, they are highly sensitive to increasing temperature changes since they live close to or at optimum temperatures.

Ocean warming alters the phenology of phytoplankton in different ways depending on local conditions. Warming-induced increased growth and photosynthetic rates caused an earlier peak of phytoplankton spring bloom by 1–1.4 $d°C^{-1}$ in the temperate-climate Kiel Fjord on the edge of the Baltic Sea (Sommer et al., 2007; Sommer and Lewandowska, 2011). However, in the northern Red Sea, a tropical marine ecosystem, phytoplankton blooms have recently started late (≈ 1–4 weeks), had a shorter duration (≈ 4 weeks) and finished earlier (≈ 4 weeks) (Gittings et al., 2018). This has been attributed to increased stratification and lower heat fluxes. The observed changes have implications on phytoplankton biomass.

The sensitivity of phytoplankton to pCO_2 is influenced by temperature. Elevated temperatures enhance growth and photosynthesis, and modulate the sensitivity of growth, photosynthesis and calcification of calcifying algae to pCO_2 increases (Sett et al., 2014). Likewise, the sensitivity of phytoplankton to temperature is influenced by other environmental factors, including light. Laboratory experiments for a mixed phytoplankton community conducted in conditions of light saturation and limitation, and weakly limiting nutrients have shown that maximum growth rate increases with temperature when light is saturated, while light limitation was found to reduce T_{opt} by ≈ 5°C (Edwards et al., 2016).

Temperature increases stimulate changes in intracellular nutrient transformation and can be represented as an optimum response function (Figure 2.2c) (Gao et al., 2000). Regardless of growth habitat, nitrate assimilation in multiple phytoplankton species cultured in nutrient-rich conditions and different light treatments exponentially increased at temperatures below 10°C, was optimised between T_{opt} of 10 and 20°C and decreased at temperatures above this range (Gao et al., 2000).

These observations suggest that many phytoplankton species have similar response curves to increasing temperature with distinct thermal tolerance and limits depending on location and species. Therefore, it is important to understand the ecological impact of these changes as they contribute to the oceans nitrogen and carbon inventories, bloom formation and to reef-building corals. These observed traits would be useful in modifying the parameterisation of biogeochemical models at the species level.

2.3.4.2 Phytoplankton community responses

The composition of phytoplankton communities changes as temperature varies. At higher temperatures, phytoplankton community composition shifts from large phytoplankton groups to small phytoplankton groups (Carpenter, 1973; Andersson et al., 1994; Hare et al., 2007; Keys et al., 2018), whereas large phytoplankton groups dominate when temperatures are low (Lassen et al., 2010).

At low temperatures, there is often reduced stratification and enhanced vertical mixing, hence elevated nutrient concentrations (Behrenfeld et al., 2006). At high temperatures, there is increased stratification and reduced vertical exchange, hence low nutrient concentrations (Schmittner, 2005; Behrenfeld et al., 2006). The dominance of small phytoplankton groups at higher temperatures (Falkowski and Oliver, 2007) might be attributed to their small cell size which results in higher surface area to volume ratio (Litchman et al., 2007). This attribute enables enhanced nutrient uptake by small phytoplankton under low nutrient concentrations.

2.3.4.3 Zooplankton responses

Zooplankton are fundamental in shaping phytoplankton structure through grazing and facilitate energy transfer from primary producers to upper trophic level consumers in the food chain (Truong et al., 2017). In addition, they supply organic matter through excretion and mortality which provides a food source for detrital feeders and is remineralised by bacteria to release dissolved nutrients that can be taken up by phytoplankton (Morais et al., 2017).

Increasing temperatures have been observed to increase respiration, excretion and zooplankton grazing rates (Ikeda et al., 2001; Ikeda, 2014; Alcaraz et al., 2014; George et al., 2015), although Alcaraz et al. (2014) reported declines above a threshold. Respiration and excretion rates of zooplankton from polar to tropical waters (-1.7°C to 30°C) have been shown to depend on body mass and temperature (Ikeda et al., 2001; Ikeda, 2014) as they increase with increasing temperatures (Ikeda, 2014). The rate at which meso- and macrozooplankton metabolic rates increase for a 10°C temperature rise (i.e. Q_{10}) ranges between 1.8 and 1.9 (Ikeda, 2014). Microzooplankton grazing rate increased from 0.15 ± 0.03 d^{-1} during the beginning of the spring bloom to 0.62 ± 0.11 d^{-1} during the peak and end of the bloom in the Long Island Sound (George et al., 2015).

Alcaraz et al. (2014) suggest that thermal thresholds and the balance between carbon loss and carbon gain are important in predicting warming impacts on zooplankton. They reported maximum grazing and respiration rates of Arctic *Calanus glacialis* at temperatures 2.5°C and 6°C, respectively, and that based on the balance between energetic gains and losses, the thermal threshold for *C. glacialis* survival is 6°C.

Although some experiments suggest increases in zooplankton physiological rates with increasing temperature (Ikeda et al., 2001; Ikeda, 2014; George et al., 2015), declines have been reported when temperature exceeds a thermal threshold in the Arctic (Alcaraz et al., 2014). Since tropical species live close to their thermal limits, extreme temperature increases could have similar implications for tropical zooplankton physiology. However, there is limited literature on warming effects on tropical zooplankton physiology. Thus, more work needs to be done to understand the physiological responses of tropical zooplankton to ocean warming for improved model parameterisations.

2.3.4.4 Coral responses

Corals provide habitats for many marine organisms through their reef-building ability. The symbiosis between reef-building corals and dinoflagellates is essential to coral calcification and coral reef growth.

However, warming has disrupted this symbiotic relationship and has led to more frequent and widespread mass coral bleaching events (Hughes et al., 2017).

Corals respond to temperature variations following an optimum response curve (Figure 2.2c) (Castillo and Helmuth, 2005; Rodolfo-Metalpa et al., 2014; Jurriaans and Hoogenboom, 2019) and their thermal responses vary among locations and between species (Warner et al., 1996; Jurriaans and Hoogenboom, 2019). For example, in the Gulf of Honduras, Southern Belize, *Orbicella annularis* (formerly *Montastrea annularis* and most abundant species in the Caribbean) photosynthetic and respiration rates are maximum at 33°C and decline to zero at 35°C (Castillo and Helmuth, 2005). Similarly, in the Mediterranean Sea, *O. annularis* photosynthesis and respiration are maximal at temperatures in the range $24 - 26$°C and $25 - 27$°C, respectively (Rodolfo-Metalpa et al., 2014).

Long-term exposure ($2 - 3$ days) of several coral species widespread and abundant in tropical western Atlantic Ocean and the Caribbean Sea, namely *O. annularis*, *Agaricia lamarcki*, *Agaricia agaricites* and *Siderastrea radians* from the Discovery Bay, Jamaica to elevated temperatures between 30°C and 36°C decreased their symbiont photosynthetic efficiency (Warner et al., 1996). Complete disruption of photosynthesis in highly sensitive *O. annularis* and *A. lamarcki* occurred at 32°C and 34°C, respectively, whereas the photosynthetic efficiencies of *A. agaricites* and *S. radians* declined less (Warner et al., 1996). Short-term exposure of *Acropora spp.* (*Acropora intermedia* and *Acropora valenciennesi*) and *Porites cylindrica* from three locations in the GBR, namely Orpheus Island, Lizard Island and Heron Island to temperature increase and decrease of 5°C above the mean summer temperature showed that coral thermal performance varies with species and with latitudes, and the variation in coral symbiont types could be responsible for the observed differences in coral thermal performance (Jurriaans and Hoogenboom, 2019). Coral symbionts were shown to acclimatise better than coral hosts as their thermal optimum is closer to environmental temperatures and are likely to support coral hosts during extreme temperature events (Jurriaans and Hoogenboom, 2019). *Acropora spp.* and *P. cylindrica* are abundant and widespread in the Indo-Pacific Ocean (Wallace and Rosen, 2006).

Coral thermal tolerance is influenced by the duration of thermal stress (Hughes et al., 2018) and other environmental factors such as light intensity (Jokiel and Coles, 1990; Brown, 1997; Anthony et al., 2007). Bleaching, which correlates with coral respiration, is exacerbated by high light intensity (Jokiel and Coles, 1990; Anthony et al., 2007) causing coral mortality (Anthony et al., 2007) and declines in hard coral cover (Guest et al., 2016; Hughes et al., 2018). Increased mortality of *A. intermedia* from the GBR was reported to occur by the second half of a six-week exposure to 31 ± 0.5°C temperature (Anthony et al., 2007). After the unprecedented 2016 and 2017 bleaching events on the GBR (Hughes et al., 2017, 2018), temperature-sensitive species of corals began to die immediately when exposed to temperatures above 3–4 degree-heating weeks in the GBR, and a further eight-month exposure to 6 degree-heating weeks shifted coral community assemblages (Hughes et al., 2018). As a consequence, coral calcification and production on Lizard Island in the GBR reduced by about 4–5% (McMahon et al., 2019). In general, short-term exposure (1–2 days) of corals to temperature increases of about 3–4°C above their thermal tolerance and long-term exposure ($>$ 1 week) to increases of about 1–2°C can induce bleaching (Jokiel and Coles, 1990).

Coral larvae *Porites astreoides* experienced increased metamorphosis (7%) and mortality (30%) rates, decreased photosynthetic rate ($\approx$ 50%) when exposed to high temperature 33°C (Edmunds et al., 2001). These observed changes are likely to reduce recruitment. Relative to ambient temperature (25°C), elevated temperature (29°C) reduced coral larvae *Pocillopora damicornis* respiration rates by 32%, rubisco protein expression 2.6 times and photochemical efficiency by $\approx$ 49% when compared to that of adult corals (Putnam et al., 2013). This suggests that coral larvae are more sensitive to temperature than adult corals and are physiologically more suited to changing temperatures.

In response to increasing temperatures *O. annularis* skeletal extension rate decreased, whereas skeletal density increased and for each 1°C increase calcification rate increased by $\approx 0.57 gcm^{-2}year^{-1}$ (Carricart-Ganivet, 2004). However, extreme temperature increases at 23.7°C in the Gulf of Mexico and 25.5°C in the Caribbean Sea cause zero calcification (Carricart-Ganivet, 2004).

These findings highlight the variability of coral thermal tolerance with respect to species, locations and duration of thermal stress. They assert that tropical and subtropical corals are highly susceptible to bleaching as they live close to their thermal limits during summer. Further, thermal stress reduces the autotrophic ability of coral larvae and symbionts, thereby deteriorating coral health and reducing coral recruitment.

2.3.4.5 Seagrass responses

Seagrasses are ecologically important as they are primary producers and provide habitats for many marine organisms. Growth rates of seagrasses are limited by light intensity and temperature. Temperature influences seagrass dynamics as their thermal adaptation and tolerance affect distribution, productivity and biomass dynamics. Short-term exposure of seagrasses to extreme temperatures has been shown to reduce growth rate and increase mortality (Collier and Waycott, 2014) and heat waves have been associated with massive loss of seagrass habitats in the tropics (Arias-Ortiz et al., 2018), and tropical temperate transition zones (Kendrick et al., 2019). At the critical temperature threshold of 40°C seagrass growth reduced and mortality followed 2 – 3 days after temperature increased to 43°C in the GBR (Collier and Waycott, 2014).

Within the limits of physiological tolerance photosynthetic rates of seagrasses increased with increasing temperature (Evans et al., 1986; Marsh Jr et al., 1986; Bulthuis, 1987; Masini et al., 1995; Collier and Waycott, 2014; Weisse et al., 2016; Collier et al., 2017). Temperature responses of seagrasses vary among species and across locations. In the GBR, the subtropical and temperate species *Zostera muelleri* photosynthesis has been found to reach a maximum at 31°C, whereas tropical species *Halodule uninervis* and *Cymodocea serrulata* attained maximum photosynthesis at 35°C which rapidly declined to zero between 44 and 45°C (Collier et al., 2017).

The maximum photosynthetic rates of *Zostera marina L.* and *Ruppia maritima L.* in the subtropical Chesapeake Bay, USA decreased at temperatures above 19°C and 23°C, respectively (Evans et al., 1986). In Great Harbour, Massachusetts, net photosynthesis of *Zostera marina L.* was optimised at temperature between 25 and 30°C (Marsh Jr et al., 1986). Masini et al. (1995) found the T_{opt} for net photosynthesis of *Posidonia sinuosa* in (Mediterranean climate) Princess Royal Harbour, Western Australia to range between 18 and 23°C. Dark respiration rates increased exponentially under temperatures between 5 and 30°C (Marsh Jr et al., 1986; Pérez and Romero, 1992). Further, low light intensity has been shown to limit the photosynthetic capacity of seagrasses under temperature increases (Bulthuis, 1987; Masini et al., 1995).

These results show that regardless of latitude and species, seagrasses follow an optimal temperature response curve. However, their thermal tolerances vary with latitude and among species as tropical seagrass species prefer higher temperatures than temperate and subtropical species. In general, short-term and long-term exposure of seagrasses to temperature increases above their thermal limits reduce their photosynthetic capacity and they are likely to suffer irreparable damage.

2.3.4.6 Microbial community responses

Marine microbes are fundamentally important in the health and productivity of marine ecosystems. They transform organic matter to nutrients through decomposition, transform nutrients into usable forms for marine plants and serve as a food source for some marine organisms. Marine microbes are also influenced by temperature. Marine microbial community responses to temperature increases could have positive or negative feedbacks to changing carbon and nitrogen cycles, and species that carry out important biogeochemical processes may be affected. Nitrogen mineralisation, nitrification and denitrification rates have been shown to follow an optimum response curve to temperature (Hansen et al., 1981; Thamdrup and Fleischer, 1998; Rysgaard et al., 2004). In one study of Arctic sediments, nitrogen mineralisation was found to be maximised at 20°C and decrease when temperatures are above 20°C (Thamdrup and Fleischer, 1998). In the same study, nitrification was found to increase with increasing temperatures below 8–16°C and rapidly decline for temperatures above this range (Thamdrup and Fleischer, 1998). Denitrification rates in Arctic sediments were found to be maximal at 24°C while anaerobic ammonia oxidation reached a maximum at 12°C (Rysgaard et al., 2004). We have not found studies reporting temperature response of microbial processes in tropical marine ecosystems.

2.3.4.7 Mangrove responses

Mangrove forests are found along the coast of tropical and subtropical oceans. Mangroves stabilise shorelines, protect coastal communities (Gedan et al., 2011) and sequester atmospheric carbon (Donato et al., 2011). They are one of the most productive ecosystems as they are sources of income, food and fuel for human communities and they provide nesting and nursery grounds for fish and invertebrates (Ewel et al., 1998; Aburto-Oropeza et al., 2008). Temperature greatly impacts mangroves as it limits the latitudinal distribution of mangroves. The minimum air temperature at which many mangroves are latitudinally limited is 16° C (Saenger, 2013) and leaf temperature between 22 and 30° C is optimal for CO_2 assimilation of tropical *Rhizophoraceae* species (Andrews et al., 1984). The 20°C winter isotherm of seawater coincides with the distributional limits of mangroves (Duke et al., 1998).

Short term exposure (2–24 hours) of *Avicennia germinans* (*Avicennia* is the most cold-tolerant genus) in three distinct life stages (dispersal, stranded, and seedling stages) to temperatures 5.7, 2.5 and -6.5° C reduced their survival, -6.5°C at 24 hours exposure had the greatest reducing effect on survival and dispersal had the greatest survival (Pickens and Hester, 2011). This shows that mangrove seedlings do not thrive in very low temperature conditions. *A. germinans* seedling photosynthetic rate was shown to be optimal (i.e., between 7.5 and 9.4 μmol cm$^{-1}s^{-1}$) at the range 24–25° C and zero between 39 and 42° C under low and high nutrient conditions (Reef et al., 2016). *A. germinans* is widespread in coastal wetlands in the Caribbean and Gulf of Mexico.

Field studies indicate the expansion of mangroves into salt marshes on subtropical and temperate shorelines including, North America (Comeaux et al., 2012; Osland et al., 2013), Australia (Rogers et al., 2005; Straw and Saintilan, 2006), New Zealand (Morrisey et al., 2010; Stokes et al., 2010), China (Durango-Cordero et al., 2013) and Mozambique (De Boer, 2002). The expansion of mangroves into salt marshes corresponds to the expansion of temperature thresholds to the North and South Poles and sea-level rise (Saintilan et al., 2014). A moderate increase of ocean temperature by 1.2° C increased the overall cover of algal epibionts of mangrove roots by 24% but reduced epibiont diversity by 33% due to the occurrence of warming-induced shorter, weedy algal turfs (Walden et al., 2019).

These findings suggest that although continued temperature increases will enhance the poleward extension of mangrove forests it will modify the quality of mangrove habitats.

2.3.4.8 Kelp responses

Kelp species mostly occur along the coastlines of the world's temperate regions. They form structurally complex beds or forests which are one of the most diverse and productive ecosystems in the world (Steneck et al., 2002; Graham et al., 2016; Smale, 2020). Ocean temperature primarily determines the distribution of kelp. Elevated temperatures have been shown to reduce the growth of kelp due to direct effects of temperature on photosynthesis (Davison, 1991; Andersen et al., 2013). The maximum photosynthetic rate, photosynthetic efficiency and respiration of Norwegian *Saccharina latissima* were constant at 10 and 15° C, but at 20° C, maximum photosynthetic rate and photosynthetic efficiency reduced whereas respiration greatly increased (Andersen et al., 2013). Simonson et al. (2015b) exposed three dominant species in Nova Scotia (*Agarum clathratum* and *S. latissima* and *Laminaria digitata*) to four temperature treatments (11, 14, 18 and 21° C) for three weeks. They reported mortality in all species at 18 and 21° C, with mortality and tissue loss occurring at 21° C within two weeks exposure. *A. clathratum* growth rates reduced at 18° C after three weeks exposure. After one week exposure to 21° C, the strength and extensibility of *S. latissima* and *L. digitata* reduced by 40–70% although all species experienced reduced strength at 18° C after three weeks exposure. Simonson et al. (2015b) identified *A. clathratum* as the least vulnerable to warming-induced tissue weakening and loss. However, elevated temperature had no effect on kelp quality as food source for the gastropod mesograzer *Lacuna vincta* and the invasive bryozoan *Membranipora membranacea*, thereby exacerbating the direct temperature effects on kelp causing increased kelp biomass loss (Simonson et al., 2015a).

The interactive effects of temperature, nutrients, pCO_2 and competitive species have been reported to alter kelp ecosystem (Connell and Russell, 2010; Moy and Christie, 2012). A fourteen-week experimental study involving the removal of turfs from a phase-shifted system indicated the inhibition of kelp recruitment by algal turfs (Connell and Russell, 2010). Relative to ambient temperature (17° C), elevated temperature (20° C) and pCO_2 enrichment increased the abundance of algal turfs, thereby reducing kelp abundance (Connell and Russell, 2010). All juveniles of the perennial kelp *Ecklonia cava* (dominant from central to southern Japan) exposed to nutrient-enriched seawater at temperatures 20, 26, 28 and 30° C survived, whereas mortality occurred in nutrient-deplete conditions at all temperatures (Gao et al., 2016). *E. cava* photosynthetic rate peaked at 28° C and decreased greatly at 30° C under nutrient-replete conditions, but was constant at 20 to 28° C in non-enriched conditions (Gao et al., 2016). Further, increasing temperatures from 20 to 30° C decreased growth rate under nutrient enrichment, while growth rate remained constant at 20 and 26° and decreased at 28° C under non-enriched conditions (Gao et al., 2016). Overall, photosynthetic and growth rates were greater in nutrient-enriched seawater than in nutrient-deplete conditions at temperatures between 20 and 28° C (Gao et al., 2016). However, Muth et al. (2019) showed that regardless of nutrient levels, increasing temperatures from 12 to 18° C reduced kelp recruitment in the eastern Pacific.

Over the past 40–60 years in Nova Scotia, ocean warming reduced mean kelp biomass by 85–99% and caused a shift from kelp beds to rocky reefs dominated by invasive algal turfs (Filbee-Dexter et al., 2016). Between 2004 and 2009 in the Skagerrak region along the coast of southern Norway, large-scale loss of *S. latissima* occurred leading to filamentous, ephemeral macroalgae dominance (Moy and Christie, 2012). This large-scale community shift is mainly attributed to rising temperature and eutrophication.

These findings suggest that rising temperature is a major contributor to the decline of kelp ecosystems. Continued loss of kelp forests will have implications for coastal marine production and management.

2.3.5 Ocean acidification

Ocean acidification caused by increased pCO_2 inhibits the ability of marine calcifiers to form shells and skeletons (Orr et al., 2005; Hoegh-Guldberg et al., 2007; Fabry et al., 2008; Chan and Connolly, 2013), affects their growth, reproduction and survival rates (Kroeker et al., 2013), and may enhance the dissolution of existing shells and skeleton material (Feely et al., 2004; Orr et al., 2005; Andersson et al., 2009; Kroeker et al., 2013).

2.3.5.1 Phytoplankton responses

Phytoplankton are carbon fixers, thus they influence the carbon pump of oceans. Increased seawater CO_2 concentrations has been shown to increase photosynthesis, increase primary production of calcifying phytoplankton and likely alter phytoplankton community composition (Tortell et al., 2008; Yang and Gao, 2012; Grear et al., 2017). Coccolithophore species *Emiliania huxleyi* – the most cosmopolitan species – and *Gephyrocapsa oceanica* – the most abundant species in tropical and subtropical oceans (Bendif et al., 2015) – have been shown to have pCO_2-dependent optimum-curve responses for growth, photosynthesis and calcification rates (Sett et al., 2014). Temperature modulates the optimum response of these processes. Optimum [pCO_2] of *E. huxleyi* and *G. oceanica* for growth, photosynthesis and calcification increased to $\approx$ 600 and 1300 ppm pCO_2, $\approx$ 835 and 1535 ppm pCO_2, and $\approx$ 550 and 875 ppm pCO_2 when temperature increased to 20 and 25°C, respectively.

In various contexts, elevated pCO_2 concentrations (800 and 1000 ppm) increased carbon fixation by 25%, dark respiration by 35% (Yang and Gao, 2012), phytoplankton biomass by 6.5-fold (Keys et al., 2018) and growth rate by $\approx$ 10–20% (Tortell et al., 2008). Elevated pCO_2 (1000 ppm) increased the Southern Ocean bloom-forming *Chaetoceros debilis* growth rate by 63%, but had no effect on other bloom-forming species such as *Phaeocystis antarctica*, *Pseudo-nitzschia subcurvata* and *Fragilariopsis kerguelensis* (Trimborn et al., 2013). Cellular particulate inorganic and organic carbon (PIC and POC) concentrations increased by 80% and 90% at 600 ppmV pCO_2, and a further 150 ppmV pCO_2 increase caused 48% and 45% increase in PIC and POC concentrations (Iglesias-Rodriguez et al., 2008). Likewise, *Trichodesmium* nitrogen fixation increased by 60% when pCO_2 increased from 180 to 1400 ppmV and intracellular nutrient concentrations (i.e. POC and PON) increased by 33% when pCO_2 increased from 380 to 1400 ppmV (Eichner et al., 2014). In contrast, Böttjer et al. (2014) found no significant effect on nitrogen fixation by short-term (1–3 days) exposure of natural occurring nitrogen fixers in North Pacific subtropical gyre to elevated pCO_2 ($\approx$ 1000 ppm).

There is mixed evidence on elevated pCO_2 effects on phytoplankton community composition. Bermúdez et al. (2016); Keys et al. (2018) found that temperate phytoplankton community composition shifted towards smallest size fractions due to pCO_2 increases while Tortell et al. (2002) found the opposite in phytoplankton assemblages in the Southern Ocean. The dominance of small-sized phytoplankton can be attributed to increased growth rate of small-sized phytoplankton caused by elevated pCO_2 (Grear et al., 2017). Rising pCO_2 from ambient to 1981 ppm reduced essential polyunsaturated fatty acids (PUFA) in North Sea phytoplankton and the observed nanophytoplankton PUFA reduction caused $\approx$ 10% reduction of dominant copepod *Calanus finmarchicus* PUFA (Bermúdez et al., 2016).

The findings described above suggest that phytoplankton is most likely to benefit from ocean acidification, although a reduction in phytoplankton fatty acids will reduce the nutritional quality of phytoplankton available for zooplankton and other grazers.

2.3.5.2 Zooplankton responses

Ocean acidification has been found in some studies to have little or no direct effect on zooplankton (McConville et al., 2013; Hildebrandt et al., 2014). Short-term exposure (4 days) of copepod species *Centropages typicus* and *Temora longicornis* to elevated pCO_2 (750 ppm) had no effect on egg production and hatching success (McConville et al., 2013). Similarly, elevated pCO_2 3000 ppm had no effect on Arctic copepods *C. glacialis* and *C. hyperboreus* (Hildebrandt et al., 2014). However, exposing pelagic copepods to about 98,000 ppm for a day increased copepod mortality in subarctic to subtropical waters (Watanabe et al., 2006). Copepods living in deep waters were shown to be more sensitive than shallow-living copepods, and deep-living copepods in subarctic and transitional waters were shown to have higher pCO_2 tolerance than subtropical copepods (Watanabe et al., 2006).

In tropical coral reefs located in Papau New Guinea, rising pCO_2 leading to average pH reduction from 8 to $\approx$ 7.8 pH reduced demersal zooplankton biomass (by a factor of three), while zooplankton community composition and fatty acid composition remained unchanged (Smith et al., 2016). Demersal zooplankton biomass reduction could be attributed to the shift from branching corals to massive bouldering corals due to progressing ocean acidification. This observation highlights the importance of in situ experiments in understanding ocean acidification effects on zooplankton as they are likely to produce results different to results obtained from laboratory experiments.

We found little information on tropical zooplankton responses to ocean acidification. More experiments are needed to understand the short- and long-term effects of ocean acidification on tropical zooplankton species.

2.3.5.3 Coral responses

Corals are likely to experience direct effects of increased pCO_2 as they build their skeletons from calcium carbonate. Elevated pCO_2 (635 ppm) enlarged the body size of *P. damicornis* larvae by $\approx 10\%$ (Putnam et al., 2013). *P. damicornis* larvae was shown to favour skeletal growth at the expense of asexual budding when exposed to 896 and 1681 ppm pCO_2 (Jiang et al., 2015). Combined effects of elevated pCO_2 ($\approx$ 1100 ppm) and temperature (2°C above ambient) decreased respiration by $\approx$ 30% and recruitment of *Dendropoma cristatum* larvae by $\approx$ 60% (Alessi et al., 2019). Coral *Stylophora pistillata* calcification decreased by 50% when exposed to increased pCO_2 (734 and 798 ppm) and temperature at 28°C, but remained constant at 25°C (Reynaud et al., 2003). Increased pCO_2 (750 ppm) increased coral *Acropora pulchra* biomass by 31% and 38% at 29.8°C and 27.2°C under light saturation (Comeau et al., 2014). This supports the influence of irradiance on the responses of reef-building corals to elevated pCO_2. *P. damicornis* and *S. pistillata* are common in the Indo-Pacific Ocean.

Across the globe, there is concern that the interacting effects of ocean acidification and rising temperatures will cause a decline in calcification of coral species. For example, across the GBR, a 11.4% decline in calcification of massive *Posites* from 1990 to 2005 has been confirmed (De'ath et al., 2009, 2013). Between 390 and 750 ppm pCO_2 coral diversity, recruitment and abundance of structural corals declined, but coral cover remained unchanged due to the dominance of *Posites* over structural corals despite its low calcification (Fabricius et al., 2011). Further, in the eastern tropical Pacific *P. damicornis* extension declined by approximately 33% from 1974 to 2006 (Manzello, 2010).

These findings suggest that although the effects of pCO_2 increases on corals at their early life stages vary, they could have major consequences on their ecological functions and coupled with thermal stress pCO_2 effects on corals are exacerbated.

2.3.5.4 Seagrass responses

Ocean acidification has been shown to have positive effects on seagrass (Palacios and Zimmerman, 2007; Fabricius et al., 2011; Ow et al., 2015; Takahashi et al., 2016) due to the potential ability of seagrass to increase its productivity with ocean acidification (Burnell et al., 2014; Borum et al., 2016). Long-term (one year) exposure of *Z. marina* to 16–1123 μM pCO_2 under light-limited and saturating light conditions did not change shoot production and leaf photosynthesis (Palacios and Zimmerman, 2007). However, under saturating light conditions, rising pCO_2 enhanced seagrass productivity as below-ground biomass, vegetative proliferation and reproduction increased (Palacios and Zimmerman, 2007). Short-term (45 days) exposure of *Z. marina* to 3673 μM pCO_2 caused a reduction in light requirements for survival and growth, and a three-fold increase in leaf photosynthesis and shoot production (Zimmerman et al., 1997). Similarly, a two-week exposure of warm water species *Cymodocea serrulata*, *Halodule uninervis* and *Thalassia hemprichii* to rising pCO_2 (442–1204 ppm) increased net production and gross photosynthesis to respiration ratio in all species, and reduced light requirements for growth and survival in *C. serrulata* and *H. uninervis* (Ow et al., 2015).

In the GBR, Fabricius et al. (2011) showed that long-term enrichment of pCO_2 from 390 to 750 ppm caused an eight-fold increase in seagrass cover. Likewise, at three shallow volcanic CO_2 vents in Papua New Guinea, pCO_2 enrichment resulting to decreased average pH from 7.9 to 7.5 increased seagrass cover three times and seagrass biomass 5 times, with varying seagrass community composition (Takahashi et al., 2016).

These results suggest that continued ocean acidification could enhance the survival and growth of seagrass in coastal waters by reducing light requirements and enhancing productivity, but due to the varying seagrass community composition it could alter seagrass community structures.

2.3.5.5 Microbial responses

For heterotrophic bacteria, pCO_2 increases had direct positive effects such as increased growth, photosynthesis and reduced respiration. These changes could affect their ecological functions in marine ecosystems. A five-day exposure of two bacterial isolates, *Rhodobacteraceae* and *Flavobacteriaceae*, from the Mediterranean Sea to 1000 ppmV pCO_2 had positive effects on their metabolic rates (Teira et al., 2012). *Rhodobacteraceae* photosynthetic rate increased, and *Flavobacteriaceae* growth efficiency and photosynthetic rate increased, while respiration rate reduced (Teira et al., 2012). *Rhodobacteraceae* contribute about 20% of coastal bacterioplankton community (Buchan et al., 2005), while *Flavobacteriaceae* is abundant in eutrophic waters (Alderkamp et al., 2006).

Relative to pH 8, nitrification rates reduced by 50% at pH 7, reduced by $\geq$ 90% at pH 6.5 and was inhibited at pH 6 in deep sea waters (Huesemann et al., 2002). This shows that pCO_2 increases could cause an accumulation of ammonia in bottom waters and when transported into the euphotic zone could alter phytoplankton abundance and community composition structure.

2.3.5.6 Mangrove responses

Elevated atmospheric CO_2 effects on mangroves are influenced by other environmental factors such as salinity, nutrient availability and water use (Lovelock et al., 2016). A fourteen-week exposure of two Australian mangroves *Rhizophora apiculata* and *R. stylosa* to a two-fold increase in ambient atmospheric CO_2 (340 μl L^{-1}) increased growth under low saline conditions but had no effect on growth under high saline conditions (Ball et al., 1997). The observed growth increase is caused by enhanced photosynthetic water use efficiency, increased net assimilation rate and increased leaf area ratio (Ball

et al., 1997). Relative to 400 ppm pCO_2, elevated pCO_2 (800 ppm) increased *A. germinans* seedling maximum photosynthetic rate, T_{opt} for photosynthetic rate and the temperature at which the photosynthetic rate is zero (Reef et al., 2016). Thereby causing increased growth in above-ground biomass and root volume under high and low nutrient conditions, respectively (Reef et al., 2016). Similarly, an eighteen-month exposure of *A. germinans* to 365 and 720 μl L^{-1} CO_2 concentrations increased its growth and biomass under high nitrogen concentrations, but when grown with cordgrass *Spartina alterniflora*, the seedling growth reduces (McKee, 2006). This indicates that competition from other species limits seedling growth under elevated CO_2 conditions. Mangrove seedlings of *R. mangle* exposed to ambient (350 μl L^{-1}) and double-ambient CO_2 conditions for a year experienced increased growth and biomass and increased branching activity due to CO_2 enrichment (Farnsworth et al., 1996). In general, CO_2 enrichment increased mangrove seedling growth by 12–47% (Lovelock et al., 2016). On the other hand, elevated CO_2 was shown to have no effect on *R. mangle*, *A. germinans* and *Conocarpus erectus* net productivity but reduced the productivity of *Laguncularia racemosa* (Snedaker and Araújo, 1998). Increased CO_2 increased the transpiration efficiency, reduced the stomatal conductance and transpiration of all four species (Snedaker and Araújo, 1998).

Relative to ambient pCO_2 (350 ppm), elevated pCO_2 (500 ppm) had no effect on the total cover of algal epibiont on mangrove roots but its interacting effect with a 1.2° C temperature increase reduced epibiont diversity and increased the total algal epibiont cover (Walden et al., 2019).

These findings suggest that CO_2 enrichment will enhance mangrove production, but the composition and structural complexity of mangrove communities will most likely be altered due to the species-specific responses to the interacting effects of CO_2 enrichment and other biotic and abiotic factors.

2.3.5.7 Kelp responses

Kelp canopy effectively removes inorganic carbon from water column during photosynthesis and accumulates fixed carbon in its biomass. Seasonal carbon storage and increased photosynthetic material are provided by dense kelp canopy for more carbon uptake. Ocean acidification has been shown to have little or no effect on kelp (Fernández et al., 2015; Leal et al., 2017; Mora-Soto et al., 2020; Fernández et al., 2021). Reducing the pH from 8 to 7.59 had no effect on the photosynthesis and growth of giant *Macrocystis pyrifera*, but the combined effects of pCO_2, nutrient availability and temperature could change *M. pyrifera* physiological responses to pCO2 enrichment (Fernández et al., 2015). *M. pyrifera* is the most widely distributed kelp species in the world's temperate shorelines (Mora-Soto et al., 2020). Relative to pH 8.01 and 8.4, low pH 7.2 and 7.65 did not affect the development of *M. pyrifera* and *Undaria pinnatifida* in south-eastern New Zealand (Leal et al., 2017). pCO_2 enrichment of juvenile *M. pyrifera* had no effect on their photosynthesis and growth but it increased the gene expression of nitrate reductase (Fernández et al., 2021). However, increased mortality and germination rates of *M. pyrifera* spores occurred due to the interacting effects of temperatures (13 and 18° C) and pCO_2 (400 ppm and 1800 ppm) (Gaitán-Espitia et al., 2014).

These findings indicate that ocean acidification is not a major threat to kelp health but the interacting effects of ocean acidification and other environmental factors could have adverse effects on kelp ecosystems.

2.3.6 Adaptation of marine organisms to changes in temperature and ocean acidification

The potential ability of marine organisms to adapt and acclimate to environmental stressors may reduce the severity of detrimental effects of a changing environment. Long-term acclimation (e.g. 1–2 weeks

or a decade) of phytoplankton to high temperatures has been shown to improve their thermal tolerance. These improvements include reduced respiration rates, increased optimum temperatures for growth and photosynthesis (Staehr and Birkeland, 2006; Padfield et al., 2016; Schaum et al., 2017), increased growth rate and cellular pigment content, decreased cell size and Chl a-specific light absorption (Staehr and Birkeland, 2006). Accordingly, when compared to phytoplankton in ambient conditions, warm-adapted phytoplankton competes better in warm conditions and loses its competitive fitness in ambient conditions (Schaum et al., 2017).

Z. muelleri has been identified as the most thermal tolerant seagrass species after a seven-week exposure of different tropical species, namely *Cymodocea serrulata* and *Halodule uninervis* to increasing temperatures and pCO_2 under saturating light conditions (Collier et al., 2018). *Z. muelleri* maximum net production was positive at 15°C to 35°C, while rapid declines in growth, production and shoot density exacerbated by high pCO_2 at 35°C were reported in other species.

Enhanced thermal tolerance of heat-evolved strains of coral microalgal endosymbiont at 31°C increased the bleaching tolerance of coral host larvae when symbiosis is established (Buerger et al., 2020).

Epigenetic effects have the ability to buffer the impacts of changing environmental conditions by generating phenotypic plasticity. Increased DNA methylation likely reduced ocean acidification effects on coral, *S. pistillata* by contributing to its phenotypic acclimation (Liew et al., 2018). Offsprings of individuals grown in warm temperatures have been shown to grow better in warm temperatures. Warmer egg production temperature of *Acartia* copepod induced positive maternal effects which increased the egg hatching rate in warmer temperatures (Vehmaa et al., 2012).

At the ecosystem level, the low connectivity of coral reefs in Nikko Bay due to the long residence time of the bay water enables local adaptation of these coral reefs to ocean acidification (Golbuu et al., 2016).

2.4 How well are climate change impacts represented by marine ecosystem response models?

2.4.1 Model performance assessment

Model performance indicates how well model results agree with observational datasets. Model evaluation provides modellers the needed confidence in model performance. To this end, 107 out of the 131 studies reviewed reported metrics comparing predicted and measured results. Seventy-six studies had parameter values fine-tuned to better match observations (i.e. calibration), but only nine studies were validated using independent datasets. This is consistent with the findings of previous reviews of biogeochemical model assessment (Arhonditsis and Brett, 2004; Robson, 2014). Although these models have varying complexity, evaluation was mostly done by comparing model results of physical, chemical and biological variables against historical observational data.

The physical variables most commonly assessed were salinity (twelve studies), water temperature (fourteen studies) and water level (sea surface elevation) (five studies), while the most common biogeochemical variables analysed included concentrations of chlorophyll a (Chl a) (twenty-three studies), dissolved oxygen (DO) (twelve studies), dissolved inorganic carbon (DIC) (seven studies), nitrate and phosphate (NO_3 and PO_4) (fifteen studies), total alkalnity (TA) (seven studies), net primary production (NPP) (eight studies), export fluxes (three studies) and pH (four studies). The biomass of lower and higher trophic level species, and the annual catch of fisheries were also assessed for model performance in fourteen studies.

Multiple metrics were used to assess model performance in twenty studies. These metrics include the standard deviation (SD), the root mean square error (RMSE), average absolute error (AAE), average error (AE), the modelling efficiency (MEF), the robustness index, percent model agreement, Spearman and Kendall tau-b correlation coefficients (Holzwarth and Wirtz, 2018; Lachkar et al., 2018; Irby et al., 2018; Pilcher et al., 2018; Fulton et al., 2018; Bauer et al., 2018; Bryndum-Buchholz et al., 2019). However, Suprenand and Ainsworth (2017) calibrated model parameters with trophic vulnerabilities due to insufficient observational data, although they are less suited for time series fitting when observations are available. Travers-Trolet et al. (2014) calibrated their model with an automatic method involving evolutionary algorithms based on the selection of the best set of model parameters that simulate model results (biomasses) that are closest to observed biomasses. Automatic calibration is more thorough and less labour-intensive than manual calibration, but is more likely to obtain unrealistic parameter sets unless parameter ranges and parameter priors are specified carefully (e.g., (Robson et al., 2018)), and requires greater computational resources.

Multiple metrics are used for thorough model performance assessment because they capture different aspects of model performance (Stow et al., 2009). For example, AAE, AE and RMSE measure accuracy, i.e. they measure the difference between model results and observations, while MEF evaluates both accuracy and precision, but is less sensitive to lack of correlation and should be used with a correlation metric. Olsen et al. (2016) recommend the use of at least four metrics, namely MEF, RMSE, AAE, and Spearman rank correlation for effective model performance assessment.

2.4.2 Time period of simulations

The long-term aspects of global climate change prompted sixty-one studies to continuously run their models from the past to the future with dates ranging between 1850 - 2100 (Meier et al., 2017; Lefort et al., 2015; Patara et al., 2013; Vancoppenolle et al., 2013; Lehodey et al., 2010) and 1950 - 2100 (Richon et al., 2019; Carozza et al., 2019; Dutkiewicz et al., 2013). However, sixteen models considered twenty-year or ten-year runs of present and future climate conditions to save computational cost (Hodgson et al., 2018). Nine studies ran their models for at most two years under future conditions. In particular, Guyondet et al. (2015) and (Irby et al., 2018) considered a model run in isolation for a year (2050) of projected future conditions, while Herrmann et al. (2013) considered 7 one-year simulations under future conditions. Thirty-eight studies performed hindcast runs (Pilcher et al., 2018) and six studies ran future simulations for over a thousand years (Yamamoto et al., 2018). Marshall et al. (2017) ran simulations for 100 years, but looped a single year ROMS oceanography 100 times. This was done to reduce the computational cost, control inter-annual variability of oceanic conditions and isolate the impacts of distinct drivers of change.

Depending on model formulation, long and continuous runs could allow the simulation of cumulative climate impacts and assessment of intermediate climate change conditions. However, short runs comparing current with future conditions have lower computational costs, therefore they are suitable for high resolution modelling and multiple scenarios examination.

2.4.3 IPCC Scenarios

IPCC scenarios describe future dynamics of GHG emissions, air pollutant emissions and land use, and are used to assess how causes of future emissions influence future emission outcomes and examine the associated uncertainties. Descriptions of IPCC scenarios can be found in (Nakicenovic et al., 2000; Watson et al., 2001; Pachauri and Reisinger, 2008; IPCC, 2014). Only sixty-two of the 131 selected studies used IPCC scenarios. Among these sixty-two studies, forty-three used a single scenario and

nineteen used multiple IPCC scenarios. Twenty-seven studies dynamically downscaled IPCC climate change predictions with regional ocean models such as the Regional Ocean Modelling System (ROMS) to get daily local predictions (Carozza et al., 2019; Laurent et al., 2018) and one study considered statistical downscaling (Brown et al., 2016). Seven studies forced experiments with prescribed atmospheric CO_2, increased by 1% per year to double or quadruple its initial concentration and constant afterwards (Park et al., 2015; Yamamoto et al., 2018) for future predictions. Eleven studies used prescribed atmospheric CO_2 from observational data (Wallhead et al., 2017; Van Oostende et al., 2018) to force experiments for hindcast runs.

The use of only one IPCC scenario provides limited information regarding uncertainties, but has a lower computational cost than using multiple scenarios. Downscaled climate predictions are suitable for policy decisions as they offer better temporal and spatial resolutions. Downscaling involves the use of information from broad-scale ($\approx$ 200km grids) General Circulation Models (GCMs) to predict climate change impacts on regional scales ($\approx$ 10–50km) (Queensland Water Modelling Network). Dynamical downscaling is the use of high-resolution regional models to simulate broad-scale climate change processes on regional or local scales. Dynamical downscaling allows explicit representation of physical principles that influence climate conditions, has high computational cost and is sensitive to large-scale biases (Queensland Water Modelling Network). On the other hand, statistical downscaling uses statistical techniques to relate local climate observations to GCM outputs and produce new environmental conditions. Statistical downscaling is cost-effective, but is more likely to produce incorrect results than dynamical downscaling due to the ability of climate change to alter the statistical relationships, or large-scale climate features used as predictors are not well captured by GCMs or have strong biases (Queensland Water Modelling Network).

2.4.4 Scenario Analysis

Most studies compared scenarios of baseline reference of natural and current conditions against a group of scenarios representing perturbed conditions. This comparison isolates the impacts of the perturbations.

2.4.5 Meteorological conditions

2.4.5.1 Air temperature

Twelve studies represented changes in meteorological conditions as projections of climate models under high air temperatures. Parameters used in two of these studies showed direct increases in air temperature (Guyondet et al., 2015; Laurent et al., 2018). Laurent et al. (2018) represented changes in meteorological conditions as projections of a climate model forced with 3°C warmer air temperature and 10% river discharge increase. The 3°C increase in air temperature was projected by the same model used for the future run under the same IPCC scenario. Likewise, a 4°C increase in air temperature and a 10% increase in river discharge were used to force the 2050 scenario run in (Guyondet et al., 2015). This approach is simple but has the potential to overestimate or underestimate climate change impacts.

2.4.5.2 Wind speed

Changes in wind speed/stress were considered in only five studies. Jiang and Xia (2018) interpolated wind data from the National Center for Environmental Prediction/North America Regional Reanalysis (NCEP/NARR) and directly increased/decreased the magnitude of Southerly winds on the shelf for wind scenarios. In two studies, monthly and daily wind stress climatology were obtained from satellite data. In particular, Lachkar et al. (2018) forced their model with satellite data under nine wind stress

scenarios by directly increasing and decreasing wind stress seasonally and annually, while Mogollón and R. Calil (2018) ran future model runs under increased winds scenario by directly increasing the zonal and meridional wind stress components. These studies found that changes in wind speed impact marine ecosystems. Increased wind speed reduced the residence time in coastal regions, increased phytoplankton production and nutrient export, and expanded offshore plumes (Mogollón and R. Calil, 2018; Jiang and Xia, 2018). Lachkar et al. (2018) identified the summer monsoon wind as the major driver of change in the size and intensity of the Arabian Sea oxygen minimum zone (OMZ). Strong monsoon winds expand the OMZ due to increased oxygen consumption resulting from increased productivity. Further, changing Indian monsoon influences the biological pump and the nitrogen cycle on a longer timescale, as intensified winds increased N_2O production, thereby exacerbating climate change.

Changes in cloud cover, storm intensity and storm frequency were not considered as forcings for the biogeochemical models in any of the studies reviewed. This means that the current state of the art in biogeochemical modelling of climate change impacts considers neither the effects of changes in incident light on photosynthesis, nor the effects of storms on vertical mixing, sediment resuspension nor shear stress, which can directly damage benthic habitats.

2.4.6 River flows, sediment and nutrient loads

Of the 131 studies reviewed, forty-nine studies considered the effects of modified river discharge as boundary conditions and forty examined changes in nutrient loads. Changes in river discharge were modelled using four main approaches, and changes in nutrient loads using five main methods (Table 2.2). Providing more and better observations of river discharge/nutrient loads will improve the accuracy of hindcast model predictions and model assessments. Although the use of fixed percent increase or decrease in river discharge/nutrient loads data based on climate predictions eliminates complexities and is cost-effective, it can produce unreliable results. Likewise, using statistical models to determine input river discharge/nutrient loads is cost-effective and can produce unreliable results as the effects of underlying physical processes are not taken into account. However, the application of a hydrological model under climate change scenarios to produce input river discharge/nutrient load time series produces more reliable projections but requires high computational cost.

2.4.7 Ocean transport processes

None of the modelling studies included in the literature reviewed explicitly considered changes in ocean stratification, upwelling or ocean currents as forcing factors. However, thirteen studies used global or downscaled Earth System Model outputs to force biogeochemical models (Vancoppenolle et al., 2013; Hodgson et al., 2018; Park et al., 2015; Kwiatkowski et al., 2019) and may have implicitly taken the effects of these ocean transport processes into account.

2.4.8 Water temperature

Fifty-five studies simulated changes in water temperature in response to changes in meteorological conditions represented as IPCC climate change projections from global climate models. Five studies directly increased water temperature based on future climate predictions. Fulton et al. (2018) applied 0.2°C, 0.5°C, 1.0°C and 2.0°C water temperature increases simulated under RCP scenarios at the end of 2050 and Irby et al. (2018) directly applied a 1.75°C increase in water temperature by mid-century. Three studies directly applied the time series of monthly water temperature from observational data (Lachkar et al., 2018; Holzwarth and Wirtz, 2018; Shen et al., 2019). Direct increase of water temperature by Irby et al. (2018) is consistent with temperature predictions from downscaled global

Table 2.2: Summary of the approaches used to model the impacts of changes in river discharge and nutrient loads on marine ecosystems.

Consideration	Approach	Advantages/Disadvantages	Number of studies using this approach	Citations
Changes in river discharge	Application of past river discharge datasets.	Computationally cost-efficient. Suitable for hindcast runs and model validation. Limited observational datasets.	23	(Ruiz et al., 2013), (Guyennon et al., 2015), (Laurent et al., 2017), (Strååt et al., 2018), (Holzwarth and Wirtz, 2018).
	Fixed percent increase or decrease in river discharge data based on climate predictions.	Computationally cost-efficient. Eliminates complexity and uncertainties associated with climate model runs such as model and forcing incompatibilities. May overestimate/underestimate the impacts of changes in river discharge.	11	(Tanaka et al., 2013), (Guyondet et al., 2015), (Wakelin et al., 2015), (Etemad-Shahidi et al., 2015), (Brown et al., 2016).
	Use of a statistical model to determine input river discharge.	Based on the relationship between observations of inputs and outputs of the modelled system. Does not require detailed information on physical processes. Computationally cost-efficient. Can omit important factors influencing river discharge changes.	5	(Allin et al., 2017), (Bauer et al., 2018).
	Application of a hydrological model under climate change scenarios to obtain input river discharge.	Requires detailed information on physical processes, thus provides an understanding of hydrological processes affecting river discharge behaviour. Captures the impacts of climate variability. Most accurate in simulating river discharge changes. Large computational cost. Existence of complexity and uncertainties associated with climate model runs.	10	(Lazzari et al., 2014), (Glibert et al., 2014), (Fernandes et al., 2015), (Feng et al., 2015), (Ryabchenko et al., 2016).
Changes in nutrient loads	Application of past river nutrient loads datasets.	Suitable for hindcast runs and model validation. Limited observational datasets.	17	(Herrmann et al., 2013), (Bianucci et al., 2015) (Meier et al., 2017), (Laurent et al., 2017) (Van Oostende et al., 2018).
	Fixed nutrient loads or fixed nutrient concentrations.	Allows the manifestation of climate change impacts. May overestimate or underestimate the impacts of climate change on riverine nutrient loads.	2	(Glibert et al., 2014), (Jiang and Xia, 2018).
	Fixed percent increase or decrease of nutrient loads.	Computationally cost-efficient. Can overestimate/underestimate the impacts of changes in nutrient loads.	8	(Hardman-Mountford et al., 2013), (Guyondet et al., 2015) (Wakelin et al., 2015), (Ryabchenko et al., 2016).
	Synthesis of input nutrient loads using a statistical model	Captures statistical features of nutrient load variability. Computationally cost-efficient. Can omit important factors affecting changes in nutrient loads.	3	(Allin et al., 2017), (Bauer et al., 2018).
	Application of a hydrological model under climate change scenarios to produce input nutrient load time series.	Captures the impacts of climate variability. Most accurate in simulating nutrient load changes. Large computational cost. Existence of complexity and uncertainties associated with climate model runs.	10	(Lessin et al., 2014), (Meire et al., 2013), (Lazzari et al., 2014), (Fernandes et al., 2015), (Irby et al., 2018).

climate models (Muhling et al., 2018), but it is greater than observed temperature and slightly lower than the temperature predictions from a high resolution climate model (Saba et al., 2016). This approach reduces the complexity and computational cost of creating downscaled climate predictions but has the potential to produce misleading results by overestimating or underestimating the impacts of warming. Therefore, for better accuracy, changes in water temperature should ideally be dynamically simulated when developing scenarios for biogeochemical modelling.

2.4.9 Ocean acidification

As mentioned in Section 2.3.5, increased CO_2 ocean uptake alters carbonate chemistry which directly affects marine calcifiers and indirectly affects their predators. Six studies considered effects of changes in pCO_2 as ocean acidification effects on marine biota. They predict declines in primary production (Yool et al., 2013), fish and invertebrates growth (Cornwall and Eddy, 2015), the biomass of low pH sensitive benthic biota and the abundance of demersal fish, sharks and epibenthic invertebrates that feed on these benthic biota (Marshall et al., 2017; Fay et al., 2017). Van Oostende et al. (2018) project a shift to a pelagic-oriented marine ecosystem.

2.4.10 Adaptations of biota and ecosystems to climate change

The adaptation of ecosystems to climate change was modelled in three studies as phytoplankton adaptation to varying stoichiometry (Glibert et al., 2014; Kwiatkowski et al., 2019) and as the alignment of whale distribution to changing prey (krill) distributions (Tulloch et al., 2019).

Twelve studies modified their model algorithms to simulate changes in responses in changed-climate conditions. Tulloch et al. (2018, 2019) introduced a climate-growth parameter and a predator-prey interaction term to explore krill response to food availability and physical changes, and the effects of prey availability on the survival of baleen whales, respectively. Kwiatkowski et al. (2019) considered varying stoichiometry of phytoplankton and the habitat capacity model was incorporated into Ecospace to describe the response of functional groups to changing environmental drivers (Bauer et al., 2018). Irby et al. (2018) introduced temperature dependence to rates for phytoplankton/zooplankton growth, nitrification, detrital solubilisation and remineralisation, while optimum, minimum and maximum temperatures of species were converted to species temperature response functions (Serpetti et al., 2017). These functions were centred on the optimum temperature and thermal tolerance of species. Finally, pteropods were considered as individual functional groups to allow the investigation of pteropods as indicators of trophic shifts under climate change (Suprenand and Ainsworth, 2017).

2.4.11 Sea-level rise

Five studies considered sea-level rise (Etemad-Shahidi et al., 2015; Brown et al., 2016; Wang et al., 2017; Meier et al., 2017; Irby et al., 2018). In these studies, sea level was directly increased in scenario runs based on projected sea-level rises. Direct increase of sea level instead of the use of runs with continuous sea-level rise enables the study of equilibrium conditions without overlying long-term trends.

Depending on location, sea-level rise was found to increase salinity, residence time, sea water intrusion, the salinity intrusion depth, stratification and phosphate concentration. Increased residence time and sea water intrusion increased Chl a concentration and decreased total suspended solids (TSS), respectively, thereby enhancing phytoplankton growth (Wang et al., 2017; Meier et al., 2017). Further, increased stratification amplified hypoxia in bottom waters (Meier et al., 2017; Irby et al., 2018). On the other hand, Etemad-Shahidi et al. (2015) suggest that sea-level rise is likely to reduce warming in the lower part of the estuary because of enhanced inflow of cold bottom ocean waters.

2.4.12 Human activities

The impacts of climate change on marine ecosystems can be amplified by human activities and it is sometimes difficult to disentangle the impacts of multiple drivers of change. A combination of well-managed marine protected areas where human activities are controlled (Rilov et al., 2020) and statistical modelling (Castro-Sanguino et al., 2021) can be used to separate the impacts of climate change and anthropogenic stressors. Currently, oceans have active fishing vessels and exploited species are over-fished, thereby reducing fish stock (Pauly and Zeller, 2016). Untreated sewage discharge and industrial waste from highly populated, industrialised cities, and nutrients from agricultural land use increase riverine nutrient loads and chemicals. River flow capture, use and diversion for water management in highly urbanised areas have greatly modified river discharge, riverine sediment and nutrient loads causing coastal ecosystem alterations (Cloern et al., 2016; Elliott et al., 2019), which are enhanced by climate change-related impacts (Elliott et al., 2019).

Therefore, to effectively model the responses of marine ecosystems to impacts of climate change it is important to consider the direct and indirect effects of population growth, resource demands and use over model projection time frames. To this end, twenty-nine studies considered the impacts of changes in fishing efforts, nutrient loads, land-based and marine-based management practices, and fishing vessel activities alongside climate change impacts (Tian et al., 2015; Bauer et al., 2018; Holzwarth and Wirtz, 2018; Carozza et al., 2019). They found that intense fishing reduced the abundance of high trophic species and increased the abundance of low trophic species. They suggest that sustainable land use and effective management policies could help improve marine ecosystem functions under future climate change. Finally, increased nutrient loads enhanced hypoxia in bottom waters, while reduced nutrient loads expanded fishing habitats (Bauer et al., 2018).

2.4.12.1 Other forcing factors

Thirty nine studies obtained atmospheric forcing from observational data (Lachkar et al., 2018; Mogollón and R. Calil, 2018; Laurent et al., 2018) and existing reanalysis datasets, while other studies obtained atmospheric forcing data from climate model outputs (Barange et al., 2017; Nakamura et al., 2018). Klein et al. (2018) forced their model with climatological Chl a data from SeaWiFs within the model domain. Four studies obtained tidal forcing from a tidal model (Wakelin et al., 2015; Brown et al., 2016; Shen et al., 2019) and observed changes in greenhouse gases and aerosol concentrations were used to force the climate model in (Richon et al., 2019). Tanaka et al. (2013) scaled surface radiation by 10% and assumed a 10% decrease in water mixing for future climate predictions. Seven studies forced ecosystem models with simulated primary production (Suprenand and Ainsworth, 2017; Piroddi et al., 2017; Stäbler et al., 2019). Ortega-Cisneros et al. (2018) forced the Atlantis model with fish mortality rates to easily construct multiple scenarios and compare results with the Ecopath with Ecosim and Ecospace (EwE) model. The integration of simulated primary production eliminates IPCC scenario complexities associated with data accessibility and model output reliability.

2.5 What has been neglected? Where to from here?

It is important to note that the limits of the distribution and productivity of phytoplankton (the most important marine organism in the food chain) and other marine organisms depend on their physiological tolerance to extreme temperatures and elevated pCO_2. More experiments need to be carried out by observational scientists to provide information needed for model parameterisation on the physiological responses of marine organisms to climate change impacts, particularly in tropical waters. Marine mod-

ellers need to interact more with observational scientists to ensure that models adequately represent available understanding of marine ecosystems.

At present, the representation of climate change impacts on marine response models is missing some key factors. Future models need to include important marine ecosystem parameters that are modified by climate change. For instance, changes in cloud cover, storm intensity and frequency, ocean stratification, upwelling and ocean currents were not considered as forcings in the reviewed literature. Few studies considered sea-level rise and changes in wind speed. It has been shown that reduced sea ice cover resulting from reduced cloud cover could increase SST (Liu et al., 2009). Also, warming and sea-level rise have been shown to affect storm intensity and frequency, and exacerbate coastal flooding (Iwamura et al., 2013; Bhattachan et al., 2018). Therefore, some important aspects of climate change could be omitted by excluding these changing environmental factors since they have been shown to affect marine ecosystems.

Better observational datasets are needed for accurate predictions of marine ecosystem responses to climate change impacts and for model assessment. Limited observational datasets hinder the effective assessment of models since for better model evaluation and uncertainty analysis calibration datasets need to be independent of validation datasets (Flynn and McGillicuddy, 2018). Improved collection of detailed and long-term observational datasets would help improve the assessment, accuracy and reliability of marine ecosystem response model predictions.

A good number of studies considered IPCC scenarios, but few studies considered the impacts of climate change under multiple IPCC scenarios. Future studies should where possible include multiple IPCC scenarios and utilise ensemble modelling approaches to capture essential effects of climate change in marine ecosystems and for better uncertainty analysis.

Some studies coupled ecosystem/biogeochemical models with physical-ocean-atmosphere models with reasonable computational efficiency (Richon et al., 2019; Hodgson et al., 2018; Mogollón and R. Calil, 2018). Regional climate models were coupled with hydrological models to represent changes in river discharge and nutrient loads as boundary conditions (Fernandes et al., 2015; Feng et al., 2015; Ryabchenko et al., 2016). Coupling regional models with hydrological models at catchment scales captures climate variability and provides information on underlying hydrological processes. Future modelling studies should continue to follow this modelling practice for improved accuracy of model predictions.

Finally, the adaptation of marine organisms to changing environmental conditions has so far been considered by very few modelling studies and should be a priority for future model development.

3. eReefs modelling suggests *Trichodesmium* may be a major nitrogen source in the Great Barrier Reef

Summary

Trichodesmium can fix nitrogen that is later released into the water column. This process may be a major source of 'new' nitrogen in the Great Barrier Reef (GBR), but to date this contribution is poorly resolved. We have estimated the seasonal, spatial and annual contributions of *Trichodesmium* to the annual nitrogen budget of the GBR using the eReefs marine models. Models were run for the interval December 2010 to November 2012. During this period La Niña conditions produced record rainfalls and widespread flooding of GBR catchments. Model outputs suggest nitrogen fixation by *Trichodesmium* in the GBR (which covers about 348,000 km^2) contributes approximately 0.5 MT/yr, exceeding the total average annual riverine nitrogen loads (0.05–0.08 MT/yr). Nitrogen fixation loads are exceeded by riverine loads only if the comparison is restricted to inshore waters and during the wet season. The river pollution is likely to have impacts in freshwater wetlands, mangroves, seagrasses and in-shore coral reefs; while *Trichodesmium* blooms are likely to be less intense but more widespread and affect offshore coral reefs and other oceanic ecosystems. Phosphorus and iron are suggested to be potential drivers of *Trichodesmium* growth and nitrogen fixation. This result is provisional but reinforces the need for more detailed assessment and reliable quantification of the annual nitrogen contribution from nitrogen fixation in the GBR and other coastal waters. Such advances will improve understandings of the role of terrestrial nitrogen loads in the GBR and of terrestrial phosphorus and iron loads which can modulate *Trichodesmium* abundance. These findings will help to broaden the focus of water quality management programs and support management to improve GBR water quality.

This chapter reproduces the following publication:

Ani, C.J., Smithers, S.G., Lewis, S., Baird, M., Robson, B., 2023. eReefs modelling suggests *Trichodesmium* may be a major nitrogen source in the Great Barrier Reef. *Estuarine, Coastal and Shelf Science,* 108306.

Contribution of authors

Chinenye J. Ani: Writing – original draft, Visualisation, Validation, Software, Resources, Methodology, Conceptualisation, Investigation, Formal analysis, Data curation.

Scott G. Smithers: Writing – review & editing, Supervision.

Stephen Lewis: Writing – review & editing, Supervision.

Mark Baird: Writing – review & editing, Methodology.

Barbara Robson: Writing – review & editing, Validation, Supervision, Resources, Project administration, Methodology, Funding acquisition, Conceptualisation.

3.1 Introduction

3.1.1 *Trichodesmium* and surface blooms

Trichodesmium is a non-heterocystous, nitrogen-fixing (i.e., diazotrophic) cyanobacterium that is common in the surface waters of tropical and subtropical oligotrophic oceans (Capone et al., 1997; Westberry and Siegel, 2006). *Trichodesmium* can form extensive blooms, especially when skies and seas are clear and calm (Capone et al., 1997). Surface blooms range in colour from yellow to red and have been observed in the eastern tropical Atlantic Ocean (Ramos et al., 2005), south-western Pacific Ocean (Dupouy et al., 2011; McKinna et al., 2011), eastern Pacific Ocean, Arabian Sea and southern Indian Ocean (Westberry and Siegel, 2006). Nitrogen fixed from atmospheric dinitrogen (N_2) by *Trichodesmium* may later be released into the water column by remineralisation (Mulholland et al., 2006) and may enhance the growth of other phytoplankton species (Wang et al., 2019b; Zehr and Capone, 2020) and cause eutrophication of oligotrophic waters (Higgins et al., 2018).

Trichodesmium cells aggregate and form single trichomes (colonies) or larger colonies (tufts or puffs) in the water column (Capone et al., 1997). *Trichodesmium* possess very strong intracellular gas vesicles that allow them to occur at up to 200 m depth but also enable buoyancy that can lead to surface blooms in calm conditions (Heimann and Cirés, 2015). *Trichodesmium* buoyancy allows the shading of other non-buoyant phytoplankton species in the water column thereby interrupting light influx (Huisman et al., 2018). Additionally, *Trichodesmium* gas vesicles provide a high backscatter cross-section (Borstad et al., 1992). *Trichodesmium* possess unique phycobilipigments, phycourobilin (PUB) and phycoerythrobilin (PEB). PUB has an absorption peak at 495 nm and PEB has absorption peaks at 545 and 565 nm (Subramaniam et al., 1999). These distinctive bio-optical features allow surface blooms of *Trichodesmium* to be readily detected and differentiated from unicellular cyanobacteria by satellites (Subramaniam et al., 1999).

Surface blooms form when *Trichodesmium* grows rapidly in surface waters due to elevated concentrations of certain nutrients (especially phosphorus and iron (Rodier and Le Borgne, 2008, 2010; Rahav and Bar-Zeev, 2017)) and when sea surface temperatures are between 24 °C and 28 °C (Paerl, 1996; Rodier and Le Borgne, 2008, 2010). Environmental conditions that favour accumulation at the surface also promote bloom development (Paerl, 1996; Rodier and Le Borgne, 2008, 2010). For example, low wind speed ($<$ 4 m s^{-1}) limits vertical mixing and enhances the surface accumulation of *Trichodesmium* colonies. However, blooms have also reportedly formed during higher wind conditions (up to 7.3 m s^{-1}), when temperature is $>$ 26 °C (Rodier and Le Borgne, 2008). Low light ($<$ 10 μmol quanta m^{-2} s^{-1}) (Bell and Fu, 2005; Breitbarth et al., 2008) and salinity conditions ($<$ 22 PSU) (Fu and Bell, 2003) constrain growth and thus may limit bloom development. High temperatures ($>$ 28 °C) also reduce *Trichodesmium* growth and nitrogen fixation (Boyd et al., 2013; Hutchins et al., 2019; Ani and Robson, 2021). During bloom events, reddish-pink discolourations due to the leaching of PEB have been observed as an early indicator of bloom decay (Padmakumar et al., 2010).

The unique bio-optical properties of *Trichodesmium* enable the detection and mapping of surface blooms on marine environments using ocean-colour satellites (Westberry and Siegel, 2006; McKinna, 2015; Rousset et al., 2018; Blondeau-Patissier et al., 2018; Bell, 2021). The capability of satellites to detect dispersed single trichomes at greater depths below the water surface is limited, and thus estimates of *Trichodesmium* abundance and associated fixed-nitrogen loads calculated from satellite observations typically only capture surface bloom events (often associated with *Trichodesmium* senescence rather than peak growth (Bell et al., 2005; Jyothibabu et al., 2017)).

3.1.2 The need for quantifying the nitrogen contributed by *Trichodesmium* to marine ecosystems

The contribution of *Trichodesmium* to marine nitrogen budgets must be considered to understand the potential impacts of blooms on water quality. However, such estimates are difficult to calculate and are often variable. For example, an early attempt demonstrated that approximately half of the "new" nitrogen (i.e., nitrogen that is not generated from remineralised organic matter) in the subtropical North Pacific Ocean was produced by *Trichodesmium* (Karl et al., 1997). In the same year, Capone et al. (1997) reported that *Trichodesmium* added around 80 MT N annually to the world's tropical oceans (which cover about 1.5×10^8 km^2) during non-bloom conditions. A decade later, Westberry and Siegel (2006) used satellite ocean-colour data to map *Trichodesmium* occurrence and estimate the nitrogen it contributes to the world's oceans. Using this approach, they calculated that $\sim$ 42 MT N yr^{-1} were added during bloom conditions and $\sim$ 20 MT N yr^{-1} during non-bloom conditions. More recently, Wang et al. (2019b) used an inverse biogeochemical and a prognostic ocean model to calculate a global nitrogen fixation rate of 163 MT N yr^{-1}, these vastly different loads demonstrate the uncertainty associated with these estimates. We also note that *Trichodesmium* influence on coastal waters nitrogen budgets has received little attention. As eutrophication driven by nitrogen (and other nutrients) is a major management challenge in many coastal settings (Bell et al., 2014; Damar et al., 2019; Barcellos et al., 2019; Bonsdorff, 2021), quantifying the nitrogen contributed by *Trichodesmium* is a fundamental knowledge gap.

3.1.3 Great Barrier Reef and water quality management

One high value marine ecosystem under pressure from increased nutrient loads is the Great Barrier Reef (GBR) of north-eastern Australia (Brodie et al., 2011, 2012). The GBR is the world's largest coral reef system containing about 3,700 individual reefs and stretching over 2,300 km along the north Queensland coast. The GBR is approximately 330 km across at its widest point and extends over an area of 348,000 km^2. Enshrined as a World Heritage Area (United Nations Educational, Scientific and Cultural Organisation), the GBR supports an abundance of marine life, provides economic, social and recreational services, and is worth about $56 billion (in uncorrected 2013 Australian dollars) to the Australian economy (Deloitte). However, landuse changes since European settlement in coastal catchments draining into the GBR have increased riverine nutrient and sediment loads three–fourfold, reducing GBR water quality (McCloskey et al., 2021b,a). Increased nutrient loads have been linked to increased phytoplankton growth (Bell et al., 2014) and macroalgal growth (Chen et al., 2019), changes in the coral community composition (Thompson et al., 2014), increased coral disease (Willis et al., 2004) and the enhanced growth of crown-of-thorns starfish (COTS) larvae whose adults prey on corals (Fabricius et al., 2010; Babcock et al., 2016).

Addressing the negative impacts of eutrophication is a priority for the management agency responsible for the GBR (GBRMPA, 2021). However, monitoring and management programmes implemented over many years to improve GBR water quality caused by increased riverine nutrient loads have had limited success (Kroon et al., 2016; Dale et al., 2018). The Reef Water Quality Protection Plan (RWQPP, 2013) focuses on improving water quality by reducing the inflow of sediments and dissolved inorganic nitrogen to the GBR via the adoption of improved land management practices. The management focus on riverine nutrient loads exported to the GBR is appropriate, but the dynamics of these loads and possible interactions with nutrient sources originating within the GBR may have been overlooked. The possibility that *Trichodesmium* is a significant source of nitrogen in the GBR and may, in some years and areas, be more significant than terrestrial sources has long been suggested (Bell et al., 1999; Furnas et al., 2011; Messer et al., 2017; Erler et al., 2020; Bell, 2021). These studies used various methods to

estimate nitrogen fixation. Bell et al. (1999) measured concentrations of *Trichodesmium* and nitrogen fixation rates from available observations of *Trichodesmium* whereas Furnas et al. (2011) used weakly-constrained values for *Trichodesmium* nitrogen fixation rates and abundance to derive their estimate. Bell (2021) used satellite ocean-colour data to determine his estimate. None of these studies provide a detailed understanding of the drivers of *Trichodesmium* growth and nitrogen fixation, nor of its spatial and temporal occurrence in the GBR.

To date *in situ* measurements of nitrogen fixation in the GBR are limited because measurement of nitrogen fixation has not been done in the region. However, the measurement of nitrogen fixation has been reported to be challenging and expensive (Mohr et al., 2010; Großkopf et al., 2012; Luo et al., 2012; Zehr and Capone, 2020). Accurate measurement and reporting of *Trichodesmium* concentrations are also challenging. The ability of *Trichodesmium* to form surface aggregations during bloom events will make it difficult to meaningfully and consistently quantify its abundance. For example, water quality sampling in the GBR follows standard oceanic sampling techniques and hence typically takes samples 0.5 m below the sea surface (and approximately 1 m off the seafloor). This routine monitoring approach is likely to miss surface aggregations of *Trichodesmium*. Another reason for limited field observations is the uneven distribution of buoyant surface aggregations of *Trichodesmium* due to the influence of wind stress (Capone et al., 1997). The vertical movement of *Trichodesmium* due to buoyancy changes add further complexities to the effective monitoring and measurement of *Trichodesmium* quantities in the water column. This is because the occurrence of a surface bloom does not indicate *Trichodesmium* are abundant at depth and the lack of a surface bloom does not confirm low *Trichodesmium* concentrations below the surface. Finally, even when population counts are available, it is unclear how they relate to the cellular abundance as *Trichodesmium* colonies range from individual trichomes to larger “puffs" and “tufts" (Heimann and Cirés, 2015). Clearly, the effective management of water quality on the GBR must also understand the drivers of *Trichodesmium* growth and nitrogen fixation, and correctly measure nitrogen fixation.

3.1.4 The contribution of *Trichodesmium* to the Great Barrier Reef nitrogen budget

Trichodesmium surface blooms have been detected and mapped on the GBR using ocean-colour satellites (Rousset et al., 2018; Blondeau-Patissier et al., 2018; Bell, 2021). As indicated above, these estimates generally omit *Trichodesmium* growing outside of bloom events, *Trichodesmium* located below the surface, and *Trichodesmium* located in cloud-covered areas. The accuracy of satellite-derived estimates of *Trichodesmium* fixed-nitrogen loads in the GBR may be substantially limited by these omissions (Bell, 2021).

Another approach to estimate the contribution of nitrogen fixation to GBR waters is to use a 3D coupled hydrodynamic-biogeochemical-sediment model that simulates nitrogen fixation as a function of environmental conditions and numerical representations of the key physical and biological processes involved. We adopted this approach and applied the eReefs marine modelling suite (Steven et al., 2019) to estimate the contribution of nitrogen fixation by *Trichodesmium* to the total annual nitrogen budget of the GBR. One key advantage of this approach over ocean-colour estimates is that the models allow a 3D calculation of *Trichodesmium* dynamics, which is important as *Trichodesmium* is often distributed vertically through the water column and not only as surface blooms detected by satellites (Rousset et al., 2018; Bell, 2021). Furthermore, the models can be used to dynamically calculate changing nitrogen fixation rates in response to the availability of dissolved inorganic nitrogen in the water, intracellular nitrogen, phosphorus and carbon stores, and light and temperature conditions. The capacity for such nuanced analysis is an important advance over coarse estimations. For example, *Trichodesmium* does not always fix nitrogen due to the energetic cost of nitrogen fixation relative to taking up available ammonium

and nitrate (Oliver et al., 2012) and appropriate adjustments can be made with this modelling approach.

Here we use the eReefs marine models to provide more detail of spatial and temporal occurrences of *Trichodesmium* in the GBR, and of the contribution of *Trichodesmium* to the total GBR nitrogen budget. The eReefs models using the CSIRO-EMS (CSIRO Environmental Modelling Suite) suite of models (here-after, "EMS") were developed for prediction of ecosystem dynamics in the GBR at broad spatial (4 km and 1 km nominal grid resolutions) and temporal scales. EMS is a coupled 3D hydrodynamic, biogeochemical and sediment modelling system that simulates the physical state and water quality of the GBR (Steven et al., 2019). The eReefs EMS simulations have been used to study riverine nutrients exported from coastal catchments (Wolff et al., 2018; Baird et al., 2021), ocean acidification impacts on the GBR (Mongin et al., 2016, 2021), coral bleaching (Baird et al., 2018) and the redistribution of sediment loads delivered from terrestrial catchments (Margvelashvili et al., 2018). We use EMS simulations to quantify the annual nitrogen load produced by *Trichodesmium* in the GBR for under the conditions experienced in our model years. Although very few *in situ* measurements of nitrogen fixation in the GBR exist, our results support earlier claims (Bell et al., 1999; Furnas et al., 2011; Messer et al., 2017; Bell, 2021) that in many years *Trichodesmium* may contribute more to the annual nitrogen budget of the GBR than riverine runoff.

3.2 Methods

3.2.1 Model

The EMS code is available from https://github.com/csiro-coasts/EMS/ and the algorithms and scientific basis of its biogeochemical model are fully described by Baird et al. (2020). Details of its application to the GBR are well described in many references (Herzfeld, 2006; Margvelashvili et al., 2018; Baird et al., 2018, 2021; Mongin et al., 2016, 2021). A detailed skill assessment and model evaluation for the biogeochemical model are given by Skerratt et al. (2019) and Robson et al. (2020). The hydrodynamic model (SHOC — Sparse Hydrodynamic Ocean Code (Herzfeld, 2006)) uses a curvilinear orthogonal grid in the horizontal and fixed 'z' coordinates in the vertical. SHOC simulates the physical conditions of the GBR. The biogeochemical model simulates nutrient cycles, optical conditions, plankton (two size-based phytoplankton groups plus, *Trichodesmium* and two size-based zooplankton groups), benthic organisms (coral metabolism and symbionts, three seagrass groups, microalgae and macroalgae), detritus and sediment dynamics in the GBR. The sediment transport model simulates sinking, deposition and resuspension of suspended sediments and other particulate materials, and the vertical movements of *Trichodesmium* due to buoyancy changes.

In the version of EMS described by Baird et al. (2020), the temperature dependence of *Trichodesmium* physiological processes is assumed to increase exponentially with increasing temperature. However, the exponential parameterisation in the EMS is no longer suitable for the ongoing temperature increases in the GBR because high temperatures ($>$ 28 °C) reduce *Trichodesmium* growth and nitrogen fixation (Boyd et al., 2013; Ani and Robson, 2021). To accurately capture the effects of extreme temperatures occurring in the GBR, the temperature dependence of *Trichodesmium* physiological processes is optimally parameterised using the function developed by Norberg (2004):

$$\mu^{max}_{Tricho} = \Big(1 - \Big(\frac{T - T_{opt}}{0.5w}\Big)^2\Big) 0.059 e^{0.0633T}. \tag{3.2.1}$$

μ^{max}_{Tricho} is a fraction reduction from the maximum physiological rate at temperature T, T_{opt} is the optimum temperature at which μ^{max}_{Tricho} is maximal (μ^{max}_{Tricho} decreases when T $> T_{opt}$) and w is the

width of the thermal niche of *Trichodesmium*. The values of w and T_{opt} used in the model are 18 °C and 26 °C, respectively.

From (Baird et al., 2020), *Trichodesmium* growth rate is defined in the EMS as

$$\frac{\partial Tricho}{\partial t} = \mu_{Tricho}^{max} P^* N^* C^*. \tag{3.2.2}$$

See Tables 3.1 and 3.2 for variable and parameter descriptions. Nitrogen fixation by *Trichodesmium* occurs when dissolved inorganic nitrogen (DIN) is less than a critical threshold DIN_{crit}. In the EMS, it is assumed that DIN = NO_3 + NH_4. As a result, nitrogen fixation rate (N_{fix}) per cell is defined as:

$$N_{fix} = max\Big(4\pi r D_{NO_3} DIN_{crit} C^* P^* (1 - N^*) - 4\pi r D_{NO_3} [NO_3 + NH_4](1 - N^*), 0\Big). \tag{3.2.3}$$

The energetic cost of nitrogen fixation is given as a fixed proportion of fixed carbon ($f_{N_{fix}}$) equivalent to a reduction in quantum efficiency, and as a proportion, $f_{nitrogenase}$, of fixed nitrogen:

$$\frac{\partial C_R}{\partial t} = -(1 - f_{N_{fix}})(1 - f_{nitrogenase}) k_I. \tag{3.2.4}$$

The buoyancy adjustment of *Trichodesmium* in the water column is represented as the density difference between the cell (ρ_c) and the water (ρ_w). By Stoke's law approximation,

$$\frac{\partial Tricho}{\partial t} = -\frac{2 g r_{col}^2 (\rho_c - \rho_w)}{9\mu} \frac{\partial Tricho}{\partial z}, \tag{3.2.5}$$

where

$$\rho_c = \rho_{min} + C^* (\rho_{max} - \rho_{min}), \tag{3.2.6}$$

z is the distance in the vertical and μ is the dynamic viscosity of water. Detailed descriptions of the EMS *Trichodesmium* growth model are available in Robson et al. (2013) and Baird et al. (2020).

Table 3.1: State and derived variables for the *Trichodesmium* growth model.

Variable	**Symbol**	**Units**
Structural *Trichodesmium* biomass	$Tricho$	mg N m^{-3}
Nitrogen reserves	N_R	mg N $cell^{-1}$
Carbon reserves	C_R	mg C $cell^{-1}$
Phosphorus reserves	P_R	mg P $cell^{-1}$
Maximum nitrogen reserves	N_R^{max}	mg N $cell^{-1}$
Maximum carbon reserves	C_R^{max}	mg C $cell^{-1}$
Maximum phosphorus reserves	P_R^{max}	mg P $cell^{-1}$
Normalised nitrogen reserves	$N^* = N_R/N_R^{max}$	–
Normalised carbon reserves	$C^* = C_R/C_R^{max}$	–
Normalised phosphorus reserves	$P^* = P_R/P_R^{max}$	–
Molecular diffusivity of NO_3	D_{NO_3}	m^2 s^{-1}
Photon absorption rate	k_I	mol photon $cell^{-1}$ s^{-1}

Table 3.2: Constants and parameters for the *Trichodesmium* growth model.

Variable	Symbol	Units	Reference
Acceleration due to gravity	g	9.81 m s^{-2}	–
Trichodesmium cell radius	r	5 μm	(Robson et al., 2013)
Trichodesmium colony radius	r_{col}	5 μm	(Robson et al., 2013)
Minimum cell density	ρ_{min}	900 kg m^{-3}	Calculated from observed sinking rates in (Villareal and Carpenter, 2003)
Maximum cell density	ρ_{max}	1050 kg m^{-3}	Calculated from observed sinking rates in (Villareal and Carpenter, 2003)
Critical threshold for N fixation	DIN_{crit}	10 mg N m^{-3}	(Robson et al., 2013)
Fraction of energy used for nitrogenase	$f_{nitrogenase}$	0.07	(Robson et al., 2013)
Fraction of energy used for N fixation	$f_{N_{fix}}$	0.33	(Robson et al., 2013)

3.2.2 Model forcing

The regional hydrodynamic model was forced with outputs from a global circulation model, the 10 km Ocean Modelling Analysis and Prediction System (OceanMAPS — https://researchdata.edu.au/oceanmaps-analysis/1440629), meteorological data obtained from the 12 km Australian Community Climate and Earth-System Simulator (ACCESS-R — http://www.bom.gov.au/nwp/doc/access/NWPData.shtml) and observations of 22 river flows. Simulated physical conditions used to drive the biogeochemical model included: a) wave data (wave amplitude, direction and period from the Bureau of Meteorology (BoM) regional wave model AUSWAVE-R (which is a 0.1° regional configuration of WAVEWATCH III)); and b) P2R GBR Dynamic SedNet with 2019 catchment conditions of nutrient and sediment loads (McCloskey et al., 2017, 2021b,a).

The EMS hydrodynamic model configured at 4 km resolutions (GBR4 grid) with the modified temperature response function described above was used in this study. The GBR4 grid extends from 7.518° S to 28.679° S (Figure 3.1) and has 600 × 180 grid cells in the horizontal, with 47 vertical layers. The 4km resolution EMS has been thoroughly validated for the GBR region by Skerratt et al. (2019) and Robson et al. (2020), but the *Trichodesmium* growth model has not been evaluated against field observations due to a scarcity of relevant observational data. The model was run for two years from December 1, 2010 to November 30, 2012 because during this period, La Niña conditions were established and peaked between late 2010 and early 2011. Northern and eastern Australia, including the GBR catchments experienced severe storms and record high rainfall causing widespread flooding. As a result, most rivers discharging into the GBR lagoon experienced large flood flows, particularly in the southern half of the GBR causing increased riverine nutrient and sediment loads. The storms damaged 15% of the total coral reef area within the GBR, with approximately 4% experiencing structural damage (Beeden et al., 2015). Likewise, about 16% of mangroves in Hinchinbrook Island experienced severe windthrow (Asbridge et al., 2018) and seagrass habitats declined (Mckenzie and Unsworth, 2011; McKenna et al., 2015).

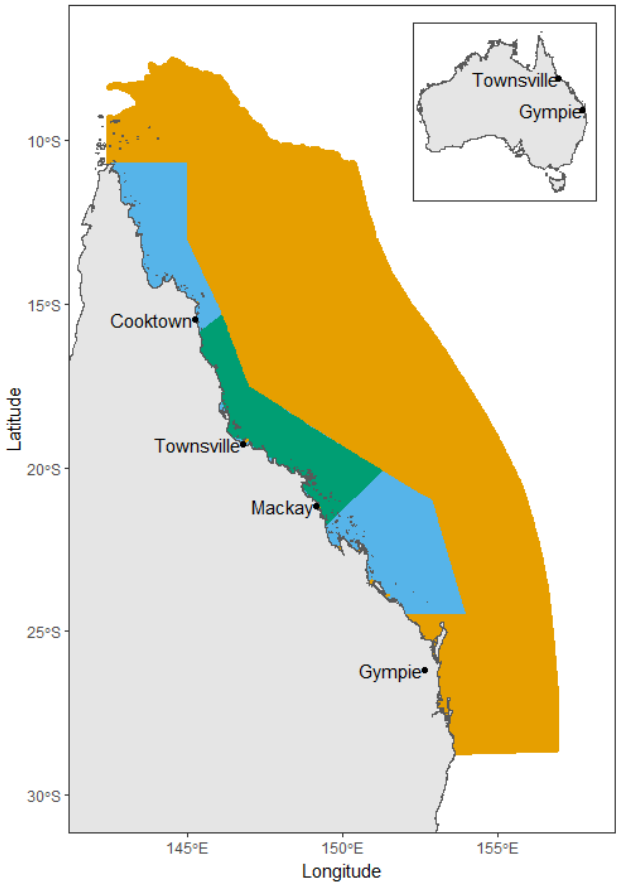

Figure 3.1: Map showing the GBR4 domain (orange), the Great Barrier Reef Marine Park (GBRMP) Boundary (soft blue and green) and Central GBR (green).

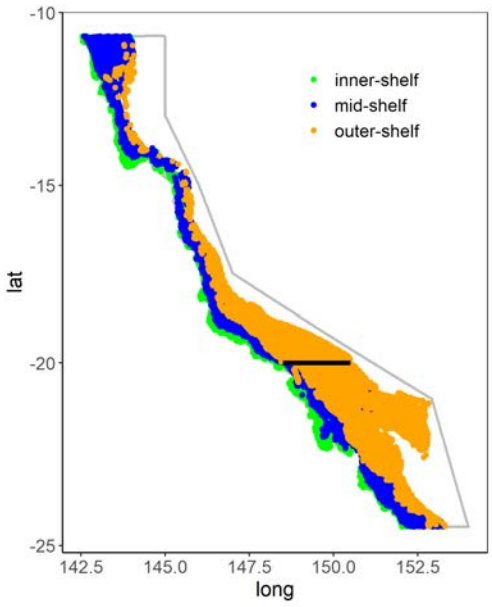

Figure 3.2: Map showing the cross-shelf waterbodies in the Great Barrier Reef Marine Park (GBRMP) boundary (grey). Inner-shelf is 0–20 m deep, mid-shelf is 20–40 m deep and outer-shelf is 40–80 m deep (Belperio, 1983). The black line represents a transect on the cross-shelf waters that starts from the geolocation (20°S,148.5°E) and ends at (20°S,150.5°E).

3.2.3 Quantification of nitrogen load from nitrogen fixation

R software version 4.0.5 (R Core Team, 2021) was used for simulated data extraction, analysis and visualisation. The depth-integrated cumulative moving mean of the *Trichodesmium* nitrogen fixation rate ($Nfix_{rate}$ — mg N m^{-3} s^{-1}) of *Trichodesmium* was extracted from simulated data using the eReefs R package (Robson, 2018). The fixed-nitrogen load was calculated for the area of the Great Barrier Reef Marine Park (GBRMP) rather than the whole 4km EMS domain (Figure 3.1). Modelled nitrogen fixation was calculated daily and integrated over the 3D volume of the GBRMP, obtained from https://www.gbrmpa.gov.au/about-us/resources-and-publications/spatial-data-information-services.

To estimate the total annual fixed-nitrogen loads in the GBR cross-shelf waterbodies, $Nfix_{rate}$ was extracted from simulated data using the three cross-shelf waterbodies defined by Belperio (1983). The waterbodies distinguished by Belperio (1983) include: the inner-shelf between 0–20 m deep dominated by terrigenous sedimentation; mid-shelf between 20–40 m deep characterised by palimpsest sedimentary zone; and the outer-shelf between 40–80 m deep where reefal sediments dominate. Figure 3.2 shows the cross-shelf waterbodies in the GBR based on our extracted simulated datasets. As the size of cross-shelf waterbodies varies significantly (inner-shelf $\sim$ 25,390 km^2; mid-shelf $\sim$ 64,180 km^2; outer-shelf $\sim$ 92,360 km^2) the total annual fixed-nitrogen load is estimated in both kg m^{-2} and tonnes.

3.2.4 Statistical models

Generalised additive models (GAMs) were used to relate simulated *Trichodesmium* concentrations and nitrogen fixation rates to environmental factors. While EMS provides a complex mechanistic model to predict *Trichodesmium*, statistical analysis of the results can provide a simpler predictive model and shed light on environmental drivers of *Trichodesmium* growth. GAMs were used to identify the emergent properties/patterns of simulated results.

Emergent properties are relationships or patterns observed in nature that occur as ecosystem functions and are key indicators to assess that models correctly capture important biogeochemical processes. To create simulated datasets of *Trichodesmium* concentrations and nitrogen fixation rates that are used for GAM analyses, 15,000 depth-integrated data points were randomly selected from GBRMP grid coordinates. The GAMs implemented in R (R Core Team, 2021) using the splines package are defined as:

$$\begin{aligned} lm(\text{Trichodesmium N} \sim\ & ns(\text{DIN}, df = 5) + ns(\text{SST}, df = 5) + ns(\text{day}, df = 3) \\ & + ns(\text{salinity}, df = 4) + ns(\text{depth}, df = 4) \\ & + ns(\text{DIP}, df = 4) + ns(\text{PAR}, df = 5)) \end{aligned} \tag{3.2.7}$$

and

$$\begin{aligned} lm(\text{N-fixation rate} \sim\ & ns(\text{DIN}, df = 2) + ns(\text{SST}, df = 5) + ns(\text{day}, df = 1) \\ & + ns(\text{salinity}, df = 4) + ns(\text{DIP}, df = 5) + \\ & + ns(\text{PAR}, df = 5)), \end{aligned} \tag{3.2.8}$$

where df values represent the degrees of freedom of variables that are statistically significant (p-value ≤ 0.05) and best fit the data. Depth variable was not included in (3.2.8) because it was non-significant. *Trichodesmium* N is the structural *Trichodesmium* nitrogen indicating *Trichodesmium* abundance (biomass), day is day of the year (1 to 365) and SST is simulated sea surface temperature. DIN is the simulated concentration of dissolved inorganic nitrogen, DIP is the simulated concentration of dissolved inorganic phosphorus, depth is depth of the seafloor at the corresponding latitude/longitude geolocation and PAR is simulated photosynthetic active radiation at midday.

3.3 Results

3.3.1 Estimated total annual fixed nitrogen for the Great Barrier Reef and for cross-shelf waters

The annual load of nitrogen fixed by *Trichodesmium* in the GBRMP estimated using the eReefs marine models is approximately 0.5 MT/yr; $\sim$ 0.2 MT/yr is estimated for the Central GBR region alone (Figure 3.3). The highest nitrogen load was fixed during spring (126 KT) and the lowest during summer (118 KT), however seasonal variations were small. In all seasons less nitrogen was fixed in the inner-shelf waters of the GBR and the highest nitrogen loads were fixed on the outer-shelf (Table 3.3). The total annual nitrogen load fixed in the inner-shelf is 5.6 $\times$ 10^{-4} kg m^{-2} or 14 KT, mid-shelf is 1.3 $\times$ 10^{-3} kg m^{-2} or 83 KT, and outer-shelf is 1.9 $\times$ 10^{-3} kg m^{-2} or 171 KT. Together these sum to 268 KT or approximately 0.3 MT/yr, noting that this yield is produced in shelf waters shallower than 80 m and thus does not include the entire GBRMP (see Figure 3.2), which when included gives the total fixed nitrogen of 0.5 MT/yr. The total annual nitrogen produced per unit area in the GBR is 1.4 $\times$ 10^{-3} Kg N m^{-2} yr^{-1}.

3.3.2 Seasonality of nitrogen fixation and environmental drivers

During summer and spring *Trichodesmium* is abundant ($>$ 0.8 mg N m^{-3}) in coastal (inner-shelf) areas especially in the Central and Southern GBR (Figures 3.4 and 3.5). Fixed-nitrogen loads are also highest in the inner-shelf during summer and spring (Table 3.3). Mean SSTs range from 28 °C to 31 °C in

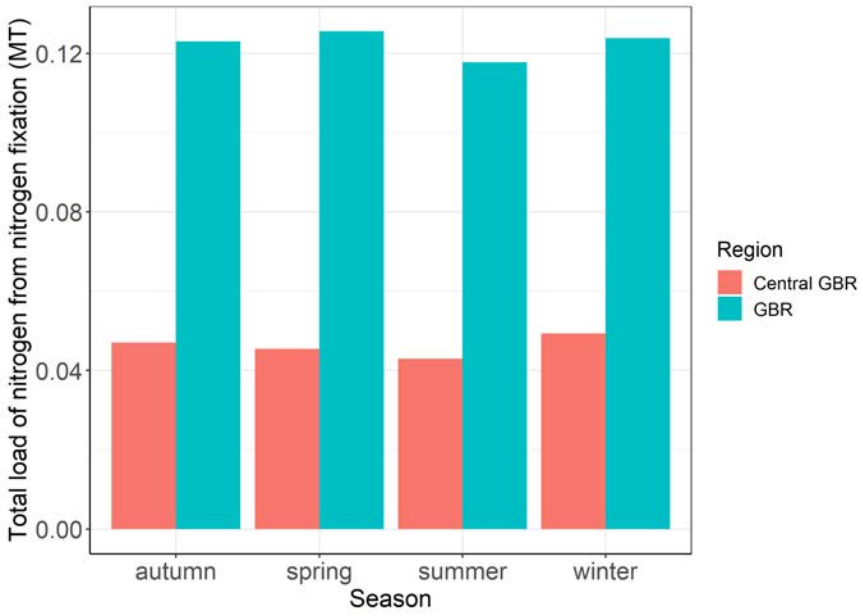

Figure 3.3: EMS estimates of seasonal contribution of *Trichodesmium* nitrogen fixation to the nitrogen budget of the Great Barrier Reef and Central Great Barrier Reef from December 1, 2010 to November 30, 2011. Seasons are defined as summer (from December 2 to March 1), autumn (from March 2 to June 1), winter (from June 2 to September 1) and spring (from September 2 to December 1).

Table 3.3: EMS estimates of the seasonal differences in annual total (tonnes (T)) and per unit surface area (kg m^{-2}) *Trichodesmium* nitrogen fixation contributions to the nitrogen budget within inner-, mid- and outer-shelf waters of the Great Barrier Reef from December 1, 2010 to November 30, 2011. The total N load (T) values consider area and depth (volume) differences between the different water bodies. Inner-shelf is 0–20 m deep, mid-shelf is 20–40 m deep and outer-shelf is 40–80 m deep. Seasons are defined as summer (from December 2 to March 1), autumn (from March 2 to June 1), winter (from June 2 to September 1) and spring (from September 2 to December 1).

Waterbody	**Season**	**Total N yield (KT)**	**N production per unit area (kg m^{-2})**
Inner-shelf	Summer	3.7	1.5×10^{-4}
	Autumn	3.3	1.3×10^{-4}
	Winter	3.1	1.2×10^{-4}
	Spring	4.0	1.6×10^{-4}
Mid-shelf	Summer	21.0	3.3×10^{-4}
	Autumn	21.1	3.3×10^{-4}
	Winter	19.1	3.0×10^{-4}
	Spring	22.2	3.5×10^{-4}
Outer-shelf	Summer	36.3	3.9×10^{-4}
	Autumn	45.5	4.9×10^{-4}
	Winter	44.4	4.8×10^{-4}
	Spring	45.2	4.9×10^{-4}

summer (Figure 3.4) and between 24 °C and 28 °C in spring (Figure 3.5) in the regions where modelling indicates abundant *Trichodesmium*.

Simulated DIP is $\leq$ 25 mg P m^{-3} (0.807 mol L $^{-1}$) in regions of high *Trichodesmium* concentrations ($>$ 0.8 mg N m^{-3}) during summer in the GBR (Figure 3.4). In contrast, during spring, simulated concentrations of DIP in most parts of the northern inner-shelf areas are $\leq$ 4 mg P m^{-3} (0.129 mol L $^{-1}$) (Figure 3.5).

Trichodesmium concentrations decreased with depth across the cross-shelf waterbodies (Figure 3.6). This is supported by the emergent patterns of the simulated data in Figure 3.7 as *Trichodesmium* concentrations (biomass) decreased with depth (i.e., 0–200 m deep). Figure 3.7 also shows that DIP predicts *Trichodesmium* concentrations in the GBR and that *Trichodesmium* concentrations slightly peak at 26 °C and increased in 34 ppt sea water salinity. The emergent relationships in Figure 3.8 show that *Trichodesmium* nitrogen fixation rate increased with DIP, PAR, in 32 ppt seawater salinity and at temperatures between 20 and 30 °C whereas elevated DIN concentrations inhibit nitrogen fixation rates (Figure 3.8).

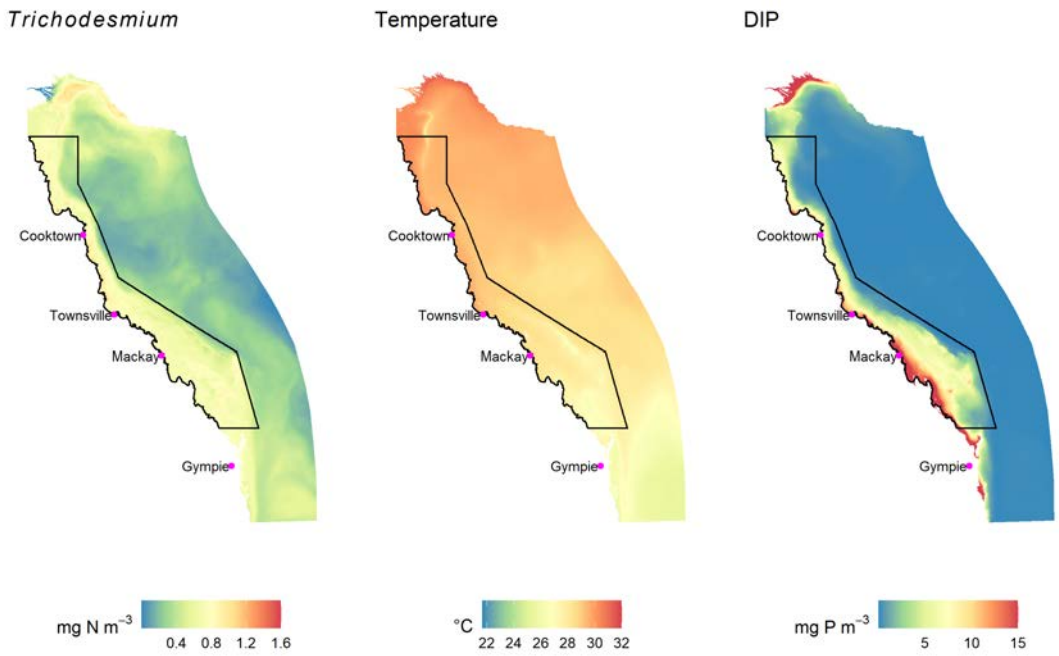

Figure 3.4: Spatially-resolved simulated mean *Trichodesmium* concentrations, sea surface temperature and Dissolved Inorganic Phosphorus (DIP) during summer (from 2 December 2010 to 1 March 2011) in the Great Barrier Reef.

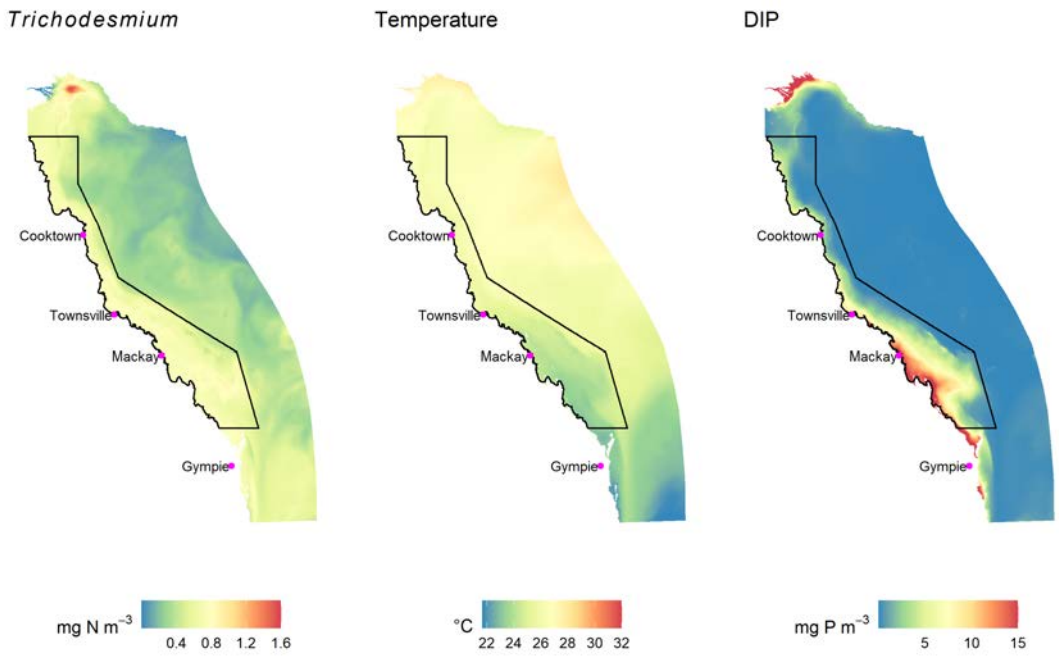

Figure 3.5: Spatially-resolved simulated mean *Trichodesmium* concentrations, sea surface temperature and Dissolved Inorganic Phosphorus (DIP) during spring (from 2 September 2011 to 1 December 2011) in the Great Barrier Reef.

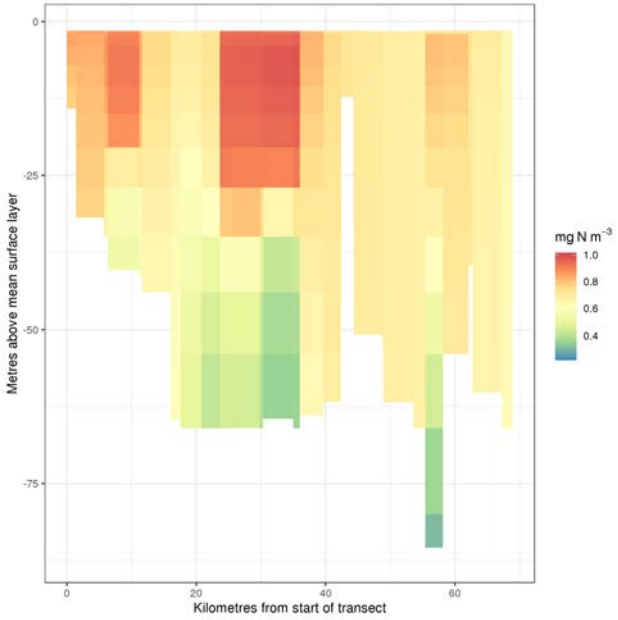

Figure 3.6: The vertical distribution of simulated *Trichodesmium* concentrations observed along a transect on the cross-shelf waters of the Great Barrier Reef (see Figure 3.2) on 10-08-2011. The transect starts from the geolocation (20°S,148.5°E) and ends at (20°S,150.5°E).

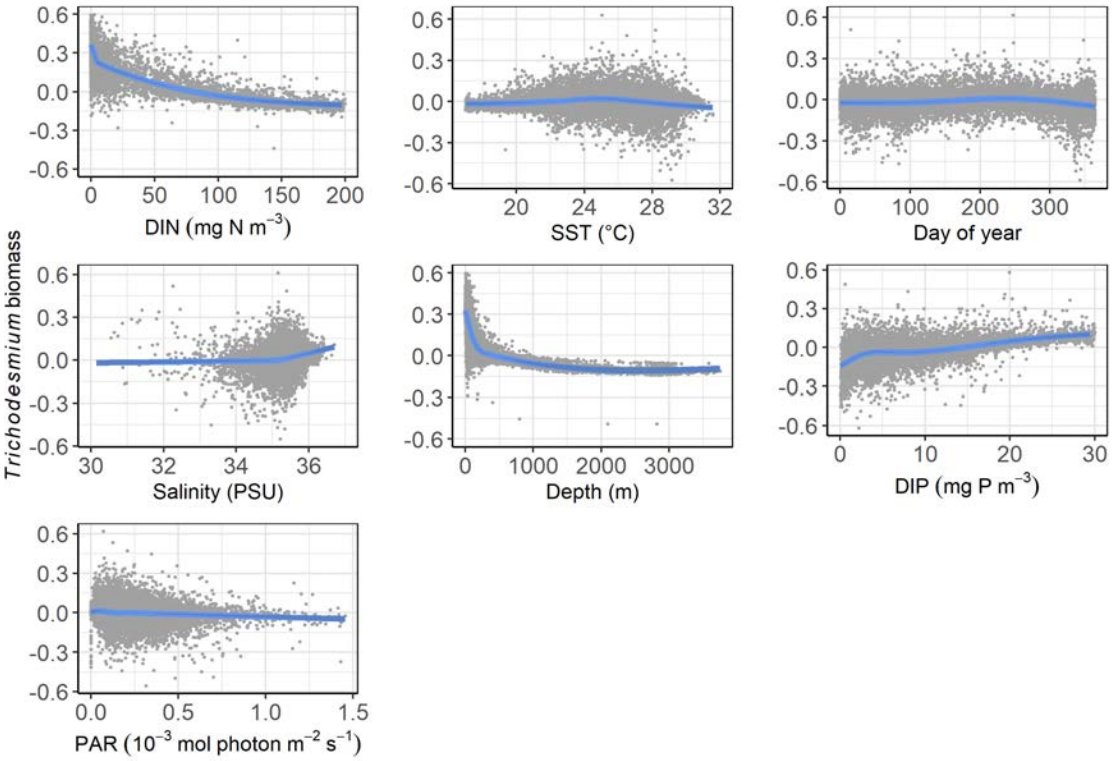

Figure 3.7: Additive effects plots from the generalised additive model (GAM) of simulated depth-integrated environmental variables relative to simulated *Trichodesmium* biomass (concentrations — mg N m^{-3}) (Adjusted $R^2 = 0.94$). DIN is dissolved inorganic nitrogen, DIP is dissolved inorganic phosphorus, PAR is photosynthetic active irradiance, SST is sea surface temperature, depth is depth of the bathymetry at the corresponding geolocation and R^2 is coefficient of determination. To avoid fitting to outliers the x-axis of DIP and DIN were limited to a maximum of 30 mg P m^{-3} and 200 mg N m^{-3}, which correspond to about 95% of the simulated data.

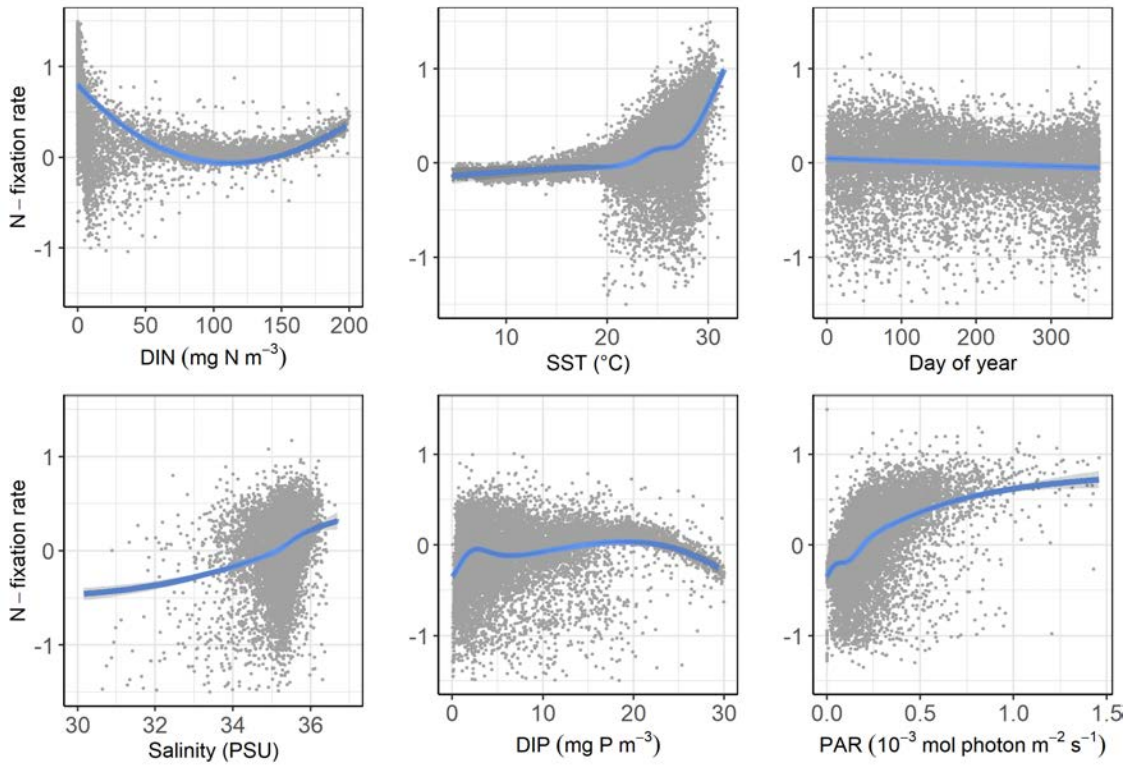

Figure 3.8: Additive effects plots from the generalised additive model (GAM) of simulated depth-integrated environmental variables relative to simulated *Trichodesmium* nitrogen fixation rate (10^{-6} mg N m^{-3} s^{-1}) (Adjusted $R^2 = 0.8$). DIN is dissolved inorganic nitrogen, DIP is dissolved inorganic phosphorus, PAR is photosynthetic active irradiance, SST is sea surface temperature and R^2 is coefficient of determination. To avoid fitting to outliers the x-axis of DIP and DIN were limited to a maximum of 30 mg P m^{-3} and 200 mg N m^{-3}, which correspond to about 95% of the simulated data.

3.4 Discussion

3.4.1 Comparison of the contribution of *Trichodesmium* and river-derived nutrients to the annual nitrogen budget of the Great Barrier Reef

The annual nitrogen load produced by *Trichodesmium* nitrogen fixation within the GBRMP calculated using our method was $\sim$ 0.5 MT, with a smaller load of $\sim$ 0.3 MT estimated for the restricted area included in the cross-shelf waterbodies which do not include the outer shelf waters exceeding 80 m depth. Importantly, both estimates are markedly larger than the 2010-2011 annual total nitrogen load of $\sim$ 0.1 MT exported to the GBR from its catchments (Turner et al., 2013). Similarly, the annual nitrogen load contributed to the GBR by nitrogen fixation of 0.5 MT is well above published estimates of mean-annual riverine nitrogen load to the GBR of 0.08 MT estimated by Kroon et al. (2012) and 0.05 MT modelled by McCloskey et al. (2017, 2021b,a). Kroon et al.'s (2012) estimate is at the higher end compared to McCloskey et al.'s (2017; 2021b; 2021a) because the particulate nitrogen loads they used relied on an earlier and less accurate soil database. Although our model-derived fixed nitrogen loads for the entire GBR significantly exceed earlier estimates of mean-annual riverine loads of nitrogen, the fixed load added by *Trichodesmium* in inner-shelf areas ($\sim$ 14 KT) is less than the catchment-derived nitrogen load. It is, nonetheless, "new" nitrogen which to date has not been reliably quantified, and in dry years with limited runoff may comprise the major nitrogen source.

Our eReefs model-derived annual estimate of 200 KT/yr of *Trichodesmium* fixed nitrogen within the Central GBR also markedly exceeds the 14 KT estimated by Bell (2021) using ocean-colour satellite estimates of surface *Trichodesmium* distribution. Bell (2021) assumed a concentration of 20 mg m^{-3} over a 1 m surface mixed layer where surface blooms were observed, and that most nitrogen contained within *Trichodesmium* is derived from nitrogen fixation. Although Bell's (2021) estimate is comparable to earlier average fixed-nitrogen load estimates (Bell et al. (1999) $\sim$ 3.3 KT/yr; Erler et al. (2020) $\sim$ 6.7 KT/yr), he acknowledged his approach did not include variations in *Trichodesmium* concentrations with depth which would significantly influence load outputs. The eReefs model simulations applied here capture vertical distributions of *Trichodesmium* in GBR waters (Figure 3.6). This important difference accounts for the much higher nitrogen yields calculated in this study compared to those derived from surface observations only.

3.4.2 Comparison of EMS simulations and satellite-derived and field observations of *Trichodesmium* bloom dynamics in the Great Barrier Reef

Our EMS simulated results are consistent with satellite and field observations of *Trichodesmium* bloom dynamics in the GBR. Satellite observations from Blondeau-Patissier et al. (2018) showed increases in bloom sizes from the northern to southern GBR and specifically more frequent surface blooms of *Trichodesmium* during July–August in the northern GBR and during November–December in the southern GBR. They also showed that the largest and most frequent surface blooms occurred in the southern GBR at temperatures > 24 °C and suggested that the increased bloom frequency observed in 2009–2011 could be attributed to the strong La Niña phases in 2010–2011 when temperatures were relatively high. Although Blondeau-Patissier et al. (2018) reported a clear seasonal pattern in *Trichodesmium* surface blooms in the GBR, our model suggests little seasonal variability. This may be because *Trichodesmium* are less concentrated at the surface and more evenly distributed with depth outside these months, or it may indicate an important missing environmental driver of bloom variability in the model. Our results agree with the latitudinal patterns reported by Blondeau-Patissier et al. (2018), which showed an increase in bloom sizes from the northern to southern GBR and the occurrence of the largest blooms at temperatures > 24 °C. Davies et al. (2020) showed that the two tropical Integrated Marine Observing

System (IMOS) National Reference Stations (NRS), Yongala and North Stradbroke Island, experienced higher *Trichodesmium* abundance relative to NRS in Australian coastal locations outside the GBR. High *Trichodesmium* abundance was observed at Yongala during September–November and March–May, and lowest abundance during June–July. A decadal decline in *Trichodesmium* abundance was observed at North Stradbroke Island. Although Davies et al. (2020) showed decreased *Trichodesmium* abundance from the northern to southern GBR, they showed maximum *Trichodesmium* abundance at temperatures > 24 °C.

3.4.3 Environmental factors that influence *Trichodesmium* abundance and nitrogen fixation in the Great Barrier Reef

Our results suggest seasonal, spatial and emergent patterns of *Trichodesmium* abundance and nitrogen fixation in the GBR. The emergent relationships suggested by the GAM analyses indicate that the observed spatial and temporal patterns of *Trichodesmium* abundance and nitrogen fixation reflect a range of environmental factors. Simulated *Trichodesmium* concentrations and distribution are greatest during spring when mean temperatures range from 24 °C to 28 °C and the emergent patterns show peak *Trichodesmium* concentrations at 26 °C and increased nitrogen fixation at temperatures between 20 °C and 30 °C. Field observations in the GBR by Davies et al. (2020) note abundant *Trichodesmium* at temperatures between 24 °C and 26 °C and Blondeau-Patissier et al. (2018) established that larger *Trichodesmium* blooms were more probable as sea temperatures warm. *Trichodesmium* abundance may be increasing globally with climate change. Global warming has been projected to increase ocean stratification and reduce the mixed layer depth (Capotondi et al., 2012). These factors have been associated with surface blooms of *Trichodesmium* and may increase the frequency of future blooms (Bergman et al., 2013). Increased temperatures (up to a threshold) will likely result in more frequent surface blooms and increased fixed-nitrogen loads in the GBR. This will have implications for nutrient cycling and other ecosystem processes such as phytoplankton growth.

In the GBR *Trichodesmium* grows best when DIP concentrations are between 0.08 and 0.12 μmol L^{-1} (Furnas, 1997) and fixes nitrogen at increased rates in conditions of elevated DIP concentrations (Erler et al., 2020). Our simulations indicate that the spatial distribution and timing of *Trichodesmium* abundance coincide with the seasons and regions (i.e., inner-shelf) of higher DIP concentrations (mostly > 0.12 μmol L^{-1}) (Figures 3.4 and 3.5). This is supported by the emergent patterns in Figures 3.7 and 3.8 that indicate DIP is a predictor of *Trichodesmium* concentrations and nitrogen fixation. Summer has the second highest contribution of fixed nitrogen on the inner-shelf regions (Table 3.3). This trend is likely driven by the higher DIP loads supplied from rivers during the summer wet season months which may reduce the inhibiting effect of high temperatures on *Trichodesmium* growth and nitrogen fixation (Mulholland and Bernhardt, 2005). Elevated DIP concentrations during summer in our models are likely due to increased and widespread river flows associated with Tropical Cyclone Tasha (December–January 2010/2011), Tropical Cyclone Anthony (January 2011) and severe Tropical Cyclone Yasi (February 2011) in northern Queensland. Frequent *Trichodesmium* blooms in the GBR have been attributed to the interacting effects of optimal temperature range and DIP availability (Davies et al., 2020). Therefore, the abundance of *Trichodesmium* in conditions of high temperatures and DIP concentrations suggest that temperature or the availability of DIP alone does not control *Trichodesmium* blooms. There are complex interactions, and more favourable conditions in one environmental variable may offset less optimal conditions in others so that predicting *Trichodesmium* bloom occurrence using single factors can be problematic.

Dust storms and atmospheric input of nutrients via rainfall also deliver nutrients to the world's oceans (Herut and Krom, 1996). In particular, aeolian additions of iron and phosphorus are known to influ-

ence *Trichodesmium* growth and distribution. For example, high iron concentrations in the North Atlantic Ocean and Arabian Sea have been linked to *Trichodesmium* abundance (Sohm et al., 2011) and phytoplankton community composition has been shown to shift from small to large phytoplankton groups (e.g., *Trichodesmium* and diatoms) following episodes of dust influx (Shaw et al., 2008). In waters with low nitrogen concentrations but rich in iron and phosphorus *Trichodesmium* have a competitive advantage over other phytoplankton (Huisman et al., 2018). The dynamics of iron and phosphorus in the GBR are thus likely to influence *Trichodesmium* and associated fixed nitrogen loads. However, at present they remain poorly known and cannot yet be included in our model or estimates of nitrogen fixation.

Our results suggest that the highest fixed-nitrogen loads on the GBR occur in spring, when usually winds are relatively light and seawater salinities are normal. High loads of fixed nitrogen in the mid- and outer-shelf during spring (Table 3.3) suggest shelf-edge upwelling as a possible source of the phosphorus and iron needed for *Trichodesmium* nitrogen fixation. Upwelling is known to occur on the shelf adjacent to the Central GBR (Berkelmans et al., 2010) and may contribute to the high fixed nitrogen loads indicated for this region by our modelling. The emergent patterns show that in the model normal seawater salinity favours *Trichodesmium* growth and nitrogen fixation. Our results also indicate that the lowest nitrogen load from *Trichodesmium* occurs during the summer (wet season) months (Figure 3.3). It is possible that the stronger winds ($>$ 6 m s^{-1}) and low light and salinity conditions ($<<$ 33 PSU due to flood events) that often accompany wet season storms contribute to this outcome; Blondeau-Patissier et al. (2018) noted such conditions are suboptimal for *Trichodesmium* bloom formation.

3.4.4 Comparison of the spatial and temporal variation of river-derived and *Trichodesmium*-derived nitrogen in the Great Barrier Reef

We note that while our estimate of the annual nitrogen contributed by *Trichodesmium* to the GBR is around fivefold greater than that delivered by rivers from the adjacent catchments, there are spatial and temporal (and possibly bioavailability) differences that warrant further appreciation. Firstly, much of the terrestrial nitrogen load is generally delivered to the GBR over a short period (typically weeks) over the summer wet season (December to April) (Brodie et al., 2011). Hence the $\sim$ 100 KT of nitrogen contributed by terrestrial inputs in the 2010-2011 year (Turner et al., 2013) is comparable to the nitrogen contribution of 120 KT from *Trichodesmium* during the summer months. Secondly, the riverine flood plumes, which disperse the terrestrial nitrogen loads, cover a much smaller spatial area of the GBR. Because of these localised areas (particularly the nearshore areas) the inner-shelf (Table 3.3) may be exposed to more terrestrially derived nitrogen than *Trichodesmium* during the summer months ($\sim$ 3.7 KT), although the annual loads are comparable. Thirdly, the period of assimilation of nitrogen in the GBR from the terrestrial and *Trichodesmium* sources may be different, although *Trichodesmium* is very bioavailable. For example, the DIN component of terrestrial runoff is immediately bioavailable and triggers widespread algal growth (Brodie et al., 2011) that can be observed as green colouring in satellite images of flood plumes (Devlin and Schaffelke, 2009; Brodie et al., 2010). These features only persist while the plumes remain intact, but our modelling indicates nitrogen from *Trichodesmium* clearly dominates the nitrogen loadings from external sources over the remaining seasons and is an essential component of nitrogen cycling in the GBR.

The much higher river-derived nitrogen concentrations in nearshore areas of the GBR will have more direct impacts on nearshore reefs. Since the vast majority of fixed nitrogen occurs in the mid- and outer-shelf waters, the potential increase in *Trichodesmium*-derived nitrogen loads due to increased bloom frequency could be important for the long-term health of offshore reefs in the GBR. However, high DIN concentrations have been reported to enhance coral heterotrophy and reduce bleaching (Ezzat

et al., 2019). About 80–90% of nitrogen fixed by *Trichodesmium* is released as DIN in seawater during the exponential growth and surface accumulation phases (Mulholland and Bernhardt, 2005). The concentration of DIN may not always be high within and around areas where surface blooms occur if the released DIN is rapidly taken up by other nearby phytoplankton. During and after surface bloom demise, *Trichodesmium* mortality produces large dissolved or particulate organic matter that is most likely buried in sediments (Furnas et al., 2011) or remineralised by bacteria (Furnas et al., 2005; Lønborg et al., 2018) both with potential oxygen-demand implications. Furthermore, nutrients stored in sediments may be released and transported to the water column to again promote *Trichodesmium* bloom formation and the growth of other phytoplankton species (Garzon-Garcia et al., 2021). Thus, the river pollution is likely to have impacts in freshwater wetlands, mangroves, seagrasses and in-shore coral reefs; while *Trichodesmium* blooms are likely to be less intense but more widespread and affect offshore coral reefs and other oceanic ecosystems.

3.4.5 Limitations of the EMS *Trichodesmium* growth model

The EMS allows the calculation of the vertical distribution of *Trichodesmium* dynamics and the rate of change of nitrogen fixation in response to changing environmental conditions. These are key advantages over satellite image informed estimates of *Trichodesmium* contributions to the annual nitrogen budget of the GBR. However, there are several areas where the model could be improved, most particularly by including physiological features not yet considered by the EMS *Trichodesmium* growth model. The physiological features include but are not limited to:

- Salinity effects on *Trichodesmium* growth, nitrogen fixation and pigmentation (Fu and Bell, 2003).
- Variations of phycobilipigments and their influence on light absorption and photoprotection (Subramaniam et al., 1999).
- Iron as a limiting nutrient for growth and nitrogen fixation (Sohm et al., 2011).
- Wind effects on the occurrence of surface aggregates of *Trichodesmium* (Capone et al., 1997).
- CO_2 effects on *Trichodesmium* nitrogen and carbon fixations (Hutchins et al., 2007).

We acknowledge that the EMS *Trichodesmium* growth model has not been evaluated against field observations in the GBR because very few *in situ* observations of *Trichodesmium* concentrations or nitrogen fixation rates are available. Despite these limitations, EMS simulated results are in accord with satellite-derived and field observations of *Trichodesmium* bloom dynamics in the GBR as indicated in Section 3.4.2. Our total-annual-production-per-unit-area estimate of 1.4 $\times$ 10^{-3} Kg N m^{-2} yr^{-1} is also comparable to global fixed nitrogen estimates. These global estimates include Capone et al.'s (1997) estimate of 0.53 $\times$ 10^{-3} Kg N m^{-2} yr^{-1} in the world's tropical oceans and Wang et al.'s (2019b) 0.61 $\times$ 10^{-3} Kg N m^{-2} yr^{-1} and 0.45 $\times$ 10^{-3} Kg N m^{-2} yr^{-1} estimates in the Pacific Ocean and global oceans, respectively. Thus although validation of the model must be a priority, we are nonetheless confident that the outputs discussed here are reasonable.

3.5 Conclusions and implications for GBR management

This study provides a new line of evidence supporting the conjectured role of *Trichodesmium* as a major contributor to the nitrogen budget of the GBR. We quantified the annual nitrogen budget from *Trichodesmium* nitrogen fixation using the 3D EMS and showed that the total annual fixed-nitrogen load is much greater than the riverine nitrogen input. It is not yet possible to validate the *Trichodesmium*

model and resulting nitrogen budget with currently available data, but our results highlight the need for further monitoring and measurement of *Trichodesmium* and nitrogen fixation in the GBR. We also identified key environmental factors that predict *Trichodesmium* growth and nitrogen fixation in the GBR (e.g., phosphorus). Our model results, which support estimates based on satellite observations suggest iron and phosphorus in catchment runoff may be more important drivers of nitrogen fixation in the GBR than previously understood. Validation of these results will enable managers to better target activities to reduce the influence of these nutrients and excess nitrogen loads.

Understanding the drivers of *Trichodesmium* growth and nitrogen fixation is essential for GBR water quality management. The modelling approach used in this study provides a valuable perspective on spatial and temporal variability critical for targeted monitoring and management —– from assessing exposure and risks to developing adaptive management approaches. Targeted monitoring will help provide field observations for the evaluation of the accuracy of EMS and satellite-derived estimates of fixed nitrogen, measurements of iron riverine loads and will help commence iron studies in the GBR. Adaptive management plans and catchment regulations may need to change by incorporating the management of terrestrial phosphorus and iron loads if our findings of phosphorus and iron as important drivers of *Trichodesmium* growth and nitrogen fixation prove to be correct.

These recommendations will help inform management to better detect, monitor, and manage the occurrence and impacts of *Trichodesmium* blooms in the GBR. Our findings will enable a more holistic understanding of nitrogen budgets and cycling in the GBR and recognise the importance of *Trichodesmium* growth and nitrogen fixation as well as other nutrient sources such as dust storms and upwelling. Our findings will help broaden the focus of water quality management programmes in providing more information on improving GBR water quality. We recommend that future modelling studies on the contribution of nitrogen fixation by *Trichodesmium* should focus on understanding the spatial and inter-annual variability of *Trichodesmium* nitrogen and other nutrient sources, their impacts across the GBR and the drivers of *Trichodesmium* growth and nitrogen fixation.

4. Modelling buoyancy-driven vertical movement of *Trichodesmium* application in the Great Barrier Reef

Summary

Trichodesmium cells aggregate and form single trichomes or larger colonies and possess strong intracellular gas vesicles that generate strong positive buoyancy and facilitate the vertical migration of colonies. *Trichodesmium* is proposed to be an important source of nitrogen in the Great Barrier Reef (GBR) with implications for nutrient cycling and eutrophication. To understand the dynamics of *Trichodesmium* in the GBR ecosystem, reliable model predictions of *Trichodesmium* growth, nitrogen fixation and distribution are required. The sinking rates of *Trichodesmium* colonies have been reported to be dependent on the shape and size of colonies, and the orientation of colonies in seawater. Therefore, to better simulate the vertical movement of *Trichodesmium* in the GBR, and subsequent biogeochemical dynamics, the *Trichodesmium* processes in the eReefs biogeochemical model was modified by applying the form resistance factor to the sinking velocities of tuft-shaped *Trichodesmium* colonies. Our model results compare well with observations from the Australian Institute of Marine Science Marine Monitoring Program sensor network sites and capture the emergent patterns of phytoplankton size spectrum observed in nature. The modified model formulations improve the physiological realism of the *Trichodesmium* growth submodel of the eReefs marine biogeochemical models, and can help to improve the understanding of *Trichodesmium* dynamics for effective GBR water quality management.

This chapter is under review for journal publication:

Ani, C.J., Baird, M., Robson, B. Modelling buoyancy-driven vertical movement of *Trichodesmium* application in the Great Barrier Reef. *Ecological Modelling*.

Contribution of authors

Chinenye J. Ani: Writing – original draft, Visualisation, Validation, Software, Resources, Methodology, Conceptualisation, Investigation, Formal analysis, Data curation.

Mark Baird: Methodology, Writing – review & editing.

Barbara Robson: Writing – review & editing, Validation, Supervision, Resources, Project administration, Methodology, Funding acquisition, Conceptualisation.

4.1 Introduction

Trichodesmium is a unique diazotrophic marine cyanobacterium that is widely spread in tropical and subtropical oceans. *Trichodesmium* cells aggregate and form single trichomes or larger colonies and form extensive surface blooms when conditions are favourable (Capone et al., 1997). *Trichodesmium* colony morphology include puff colony, tuft colony, raft colony and bowtie colony (Janson et al., 1995; Hynes et al., 2012). One important and unique characteristic of *Trichodesmium* is its ability to regulate the vertical movement of its colonies in the water column. This process, also known as buoyancy, is facilitated by the strong gas vesicles possessed by *Trichodesmium* (Walsby, 1978; Heimann and Cirés, 2015). These gas vesicles allow *Trichodesmium* to survive in poor nutrient conditions.

In the euphotic zone, *Trichodesmium* fixes and stores carbon and nitrogen (Romans et al., 1994; Held et al., 2022), sinks with this carbon ballast into deep waters where phosphorus can be assimilated (Villareal and Carpenter, 2003; Hewson et al., 2009). *Trichodesmium* gas vesicles are adapted to withstand high pressure experienced in deep waters so that turgor pressure collapse of gas vesicles does not occur (Walsby, 1978). In deep waters, the carbon ballast is metabolised and since gas vesicles are not collapsed, lighter *Trichodesmium* colonies are able to regain buoyancy and float back to surface waters. This enables them to spend more time in the euphotic zone while optimising its access to light and nutrients and may outcompete other phytoplankton species for light and nutrients needed for growth (Huisman et al., 2018). Thus, *Trichodesmium* buoyancy allows *Trichodesmium* to occur in conditions of varying irradiance and nutrient availability common in tropical and subtropical oceans.

The sinking rates of *Trichodesmium* colonies depend on the shape and size of colonies (Walsby, 1992). Reynolds and Walsby (1975) suggest that larger colonies may sink to greater depth than small colonies due to high sinking velocities. However, Kromkamp and Walsby (1992) reported that larger colonies did not migrate to greater depth: rather they sank faster and the number of colonies that migrated vertically increased. *Trichodesmium* buoyancy varies as a function of the varying balance between gas vesicles and carbohydrate ballast due to changing light conditions, nutrients and other environmental conditions (Kromkamp and Walsby, 1992; Oliver, 1994) or by consuming carbohydrate ballast through the supply of energy to nitrogenase for nitrogen fixation (Held et al., 2022). *Trichodesmium* colonies become more buoyant in low light conditions (because they consume intracellular carbon stores to fuel respiration) and gradually lose their buoyancy in high light conditions (because photosynthesis increases carbon stores) (Walsby, 1969).

Surface *Trichodesmium* bloom is formed as a result of the occurrence of buoyancy in very calm conditions (Capone et al., 1997). At the surface *Trichodesmium* photosynthesise and shade out other phytoplankton species, and experience increased mortality due to UV exposure and spread of viral phages through the population. Thus, the persistence of *Trichodesmium* in surface waters demonstrates that *Trichodesmium* is not able to perfectly regulate buoyancy. *Trichodesmium* buoyancy variations can impact marine ecosystems as they can facilitate optimal utilisation of light while preventing cell damage due to high irradiance (Subramaniam et al., 1999; Ueno et al., 2016). Buoyancy variations also influence *Trichodesmium* dispersal and distribution in sea waters (Capone et al., 1997; Heimann and Cirés, 2015).

Trichodesmium is proposed to be an important source of nitrogen in the Great Barrier Reef (GBR) — the world's largest coral reef system — with implications for nutrient cycling and eutrophication (Bell, 2021; Ani et al., 2023). Effective GBR water quality management requires an understanding of the contribution of *Trichodesmium* to the total annual nitrogen budget of the GBR. Satellite ocean-colour data (Bell, 2021) and the eReefs models (coupled hydrodynamic-biogeochemical model (Baird et al., 2020)) (Ani et al., 2023), have been used to estimate the annual contribution of *Trichodesmium* fixed nitrogen to the nitrogen budget of the GBR. Both approaches suggested that the nitrogen fixed by *Trichodesmium* was

greater than riverine nitrogen loads exported to the GBR. Therefore, an understanding of *Trichodesmium* buoyancy regulation is important to improve the understanding of *Trichodesmium* dynamics in GBR ecosystems.

In this study, the influence of *Trichodesmium* colony shape and orientation in seawater on *Trichodesmium* buoyancy was parameterised in the *Trichodesmium* growth submodel of the eReefs biogeochemical models by applying the form resistance factor to the sinking velocities of tuft-shaped *Trichodesmium* colonies found in the GBR (Bell et al., 2005). This would help to provide reliable model simulations of *Trichodesmium* growth, nitrogen fixation and distribution, which are important for improved understanding of *Trichodesmium* dynamics in GBR ecosystems.

4.2 Methods

4.2.1 *Trichodesmium* buoyancy

The sinking velocity of particles is influenced by cell size, shape and density. For a spherical particle, Stoke's law is applied to the sinking velocity, which is given as

$$\mu = \frac{2gr^2(\rho_c - \rho_w)}{9\eta}, \tag{4.2.1}$$

where r is the cell radius, g is gravity, ρ_w is the water density, ρ_c is the cell density and η is the coefficient of the dynamic viscosity of the water. The version of the *Trichodesmium* growth model described by Robson et al. (2013); Baird et al. (2020) assumes a spherical *Trichodesmium* colony with radius $r = 5$ μm and used (4.2.1) to represent *Trichodesmium* sinking velocity. However, *Trichodesmium erythraeum* colonies in the GBR have been reported to be tuft shaped (Bell et al., 2005).

McNown and Malaika (1950) applied the form resistance factor Φ to the sinking velocity of non-spherical cells. The sinking velocity of non-spherical cells with volume V is defined as

$$\mu = \frac{2gr_e^2(\rho_c - \rho_w)}{9\eta\Phi}, \tag{4.2.2}$$

where r_e is the effective radius given by

$$r_e = \left(\frac{3V}{4\pi}\right)^{\frac{1}{3}}. \tag{4.2.3}$$

The form resistance factor is the factor by which the sinking velocity of a non-spherical particle differs from that of a sphere of equal volume and density. A spherical cell has $\Phi = 1$. At low Reynolds number, symmetrically weighted non-spherical objects remain in their original orientation when sinking and the settling velocity of a cylindrical object is similar to that of an ellipsoid of the same axial ratio, density and volume (McNown and Malaika, 1950).

Here, we represent *Trichodesmium* tufts as ellipsoids. Although in reality, tufts do not have the smooth surface of an ellipsoid, given the small size of the tufts and laminar fluid dynamics involved, this surface roughness will not significantly affect form resistance.

Following (Walsby and Holland, 2006), the form resistance coefficient of an ellipsoid with semi-axes a, b and c is given as

$$\Phi = \frac{16}{3D(\Psi + \Omega)}, \tag{4.2.4}$$

where Ψ is a shape factor independent of orientation, Ω is an orientation-dependent shape factor relative to the direction of movement, and $D = 2(abc)^{\frac{1}{3}}$ is the nominal diameter. The filaments of a cylindrical cell of width w and length l have volume

$$V = \pi\Big(\frac{w}{2}\Big)^2 l \tag{4.2.5}$$

and from (4.2.3), the effective radius

$$r_e = \Big(\frac{3}{16}w^2 l\Big)^{\frac{1}{3}}. \tag{4.2.6}$$

For a vertically oriented cell (Figure 4.1),

$$a > b = c, a = \frac{l}{2}, b = \frac{w}{2}, \Psi = \Psi_{vert}, \Omega = \Omega_{vert}.$$

A horizontally oriented cell (Figure 4.1) has

$$a = c < b, b = \frac{l}{2}, a = \frac{w}{2}, \Psi = \Psi_{hor}, \Omega = \Omega_{hor}.$$

See (Walsby and Holland, 2006) for detailed derivations of Ψ_{vert}, Ψ_{hor}, Ω_{vert} and Ω_{hor}. The form resistance coefficient and effective radius of a tuft-shaped *Trichodesmium erythraeum* colony with length 1000–2000 μm and width (diameter) 50–150 μm (Post et al., 2002) are calculated using (4.2.4) where

$$\Psi = \frac{\Psi_{vert} + \Psi_{hor}}{2} \tag{4.2.7}$$

and

$$\Omega = \frac{\Omega_{vert} + \Omega_{hor}}{2}. \tag{4.2.8}$$

Using (4.2.2) the buoyancy regulation of *Trichodesmium* in the water column is represented by the model as

$$\frac{\partial Tricho}{\partial t} = -\frac{2gr_e^2(\rho_c - \rho_w)}{9\eta\Phi}\frac{\partial Tricho}{\partial z}, \tag{4.2.9}$$

where

$$\rho_c = \rho_{min} + R_C^*(\rho_{max} - \rho_{min}), \tag{4.2.10}$$

z is the distance in the vertical. The parameters ρ_{min} and ρ_{max} constrain the calculation of *Trichodesmium* colony density and R_C^* represents carbon reserves. These modified formulations increase the sinking rate of a *Trichodesmium* colony in the model and are in the range -0.8 to 0.8 mm s^{-1} reported by Walsby (1978). Figure 4.2 shows the relationship between the sinking velocity, the effective radius and the form resistance factor of a tuft-shaped *Trichodesmium* colony in the model. Detailed descriptions of the EMS *Trichodesmium* growth model are available in (Robson et al., 2013) and (Baird et al., 2020).

4.2.2 Model forcing

The eReefs hydrodynamic model was forced with outputs from the 10 km Ocean Modelling Analysis and Prediction System (OceanMAPS – https://researchdata.edu.au/oceanmaps-analysis/1440629), the 12 km Australian Community Climate and Earth-System Simulator (ACCESS-R – http://www.bom.gov.au/nwp/doc/access/NWPData.shtml) and river flow data from 22 rivers. The biogeochemical model was forced with simulated hydrodynamic model outputs, wave data from the Bureau of Meteorology (BoM)

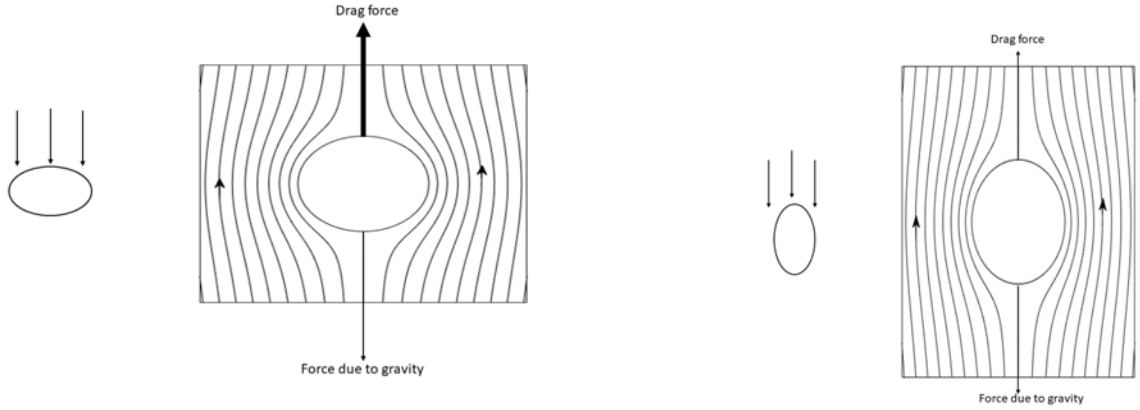

Figure 4.1: Theoretical streamlines for flow around a sinking ellipsoid. The insets at the left show the perspective of the flow. Horizontally oriented sinking ellipsoid (left) and a vertically oriented sinking ellipsoid (right).

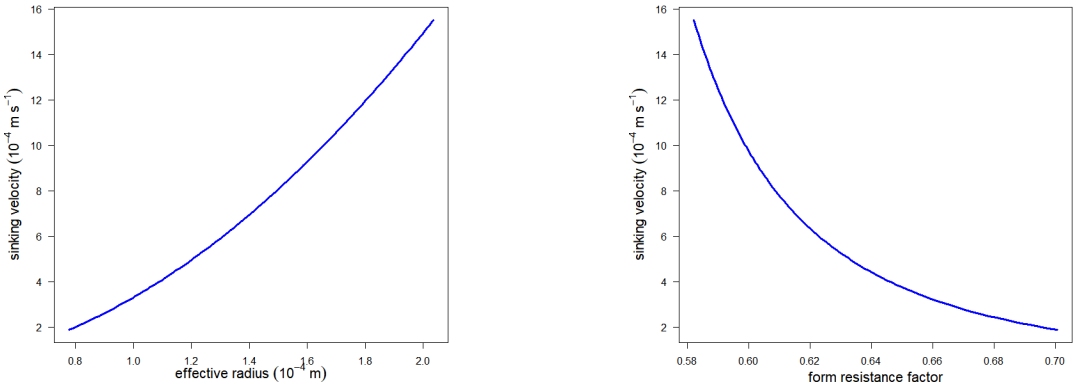

Figure 4.2: Relationships between the sinking velocity and the effective radius (left), the sinking velocity and the form resistance factor (right) of a tuft-shaped *Trichodesmium* colony of length 1000–2000 μm and width (diameter) 50–150 μm (Post et al., 2002).

Table 4.1: Constants and parameters for the *Trichodesmium* growth model.

Variable	Symbol	Units	Reference
Constants			
Acceleration due to gravity	g	9.81 m s^{-2}	–
Dynamic viscosity of water at 20 °C	μ	0.001 Pa.s	–
Parameters			
Trichodesmium cell radius	r	$5\ \mu m$	(Robson et al., 2013)
Trichodesmium colony effective radius	r_e	$140\ \mu m$	–
Trichodesmium form resistance factor	Φ	0.61	–
Minimum cell density	ρ_{min}	1010 kg m^{-3}	Calculated from observed maximum rising rates in (Walsby, 1978)
Maximum cell density	ρ_{max}	1030 kg m^{-3}	Calculated from observed maximum sinking rates in (Walsby, 1978)

regional wave model AUSWAVE-R and P2R GBR Dynamic SedNet with 2019 catchment conditions of nutrient and sediment loads (McCloskey et al., 2017, 2021b,a). The eReefs hydrodynamic model (version 2.0) configured at 4 km resolutions (GBR4 grid) with the modified sinking velocity and the *Trichodesmium* growth model in (Ani et al., 2023) was run from December 1, 2010 to November 30, 2012. The modified model is denoted as GBR4-BGC-cyl.

4.2.3 Model evaluation

Fourteen observation sites from the Australian Institute of Marine Science (AIMS) Marine Monitoring Program (MMP) sensor network sites (Australian Institute of Marine Science , AIMS) (Figure 4.2) sampled tri-annually and time series of simulated model outputs from version 3.2 of the biogeochemical model of the eReefs model described in (Baird et al., 2020) (hereafter referred to as GBR4-BGC-sph) were used to evaluate the modified model. Observations obtained from the fourteen monitoring sites were available throughout the period of model simulation (See (Skerratt et al., 2019) for more information on AIMS MMP sites).

The variables considered for validation include Chl-*a* extractions, dissolved inorganic phosphorus (DIP), ammonium (NH_4) and nitrate + nitrite [NO_x]. The skill metrics used to validate the modified model include, bias, Willmott score, root mean square error (RMS) and mean absolute error (MAE). Bias examines the model's over- or under-prediction of observations. The Willmott score varies between 0 and 1 and is a ratio of the mean square error and the mean absolute deviation about the observed mean (Willmott et al., 1985). A Willmott score of 1 indicates a perfect match and 0 indicates no match. For this study, following Skerratt et al. (2019); Robson et al. (2020), a Willmott score of 0.6 against simulated water quality variables was used as a benchmark for excellent model fit. RMS measures model accuracy, i.e., the difference between model predictions and observations. An RMS of 0 indicates perfect fit.

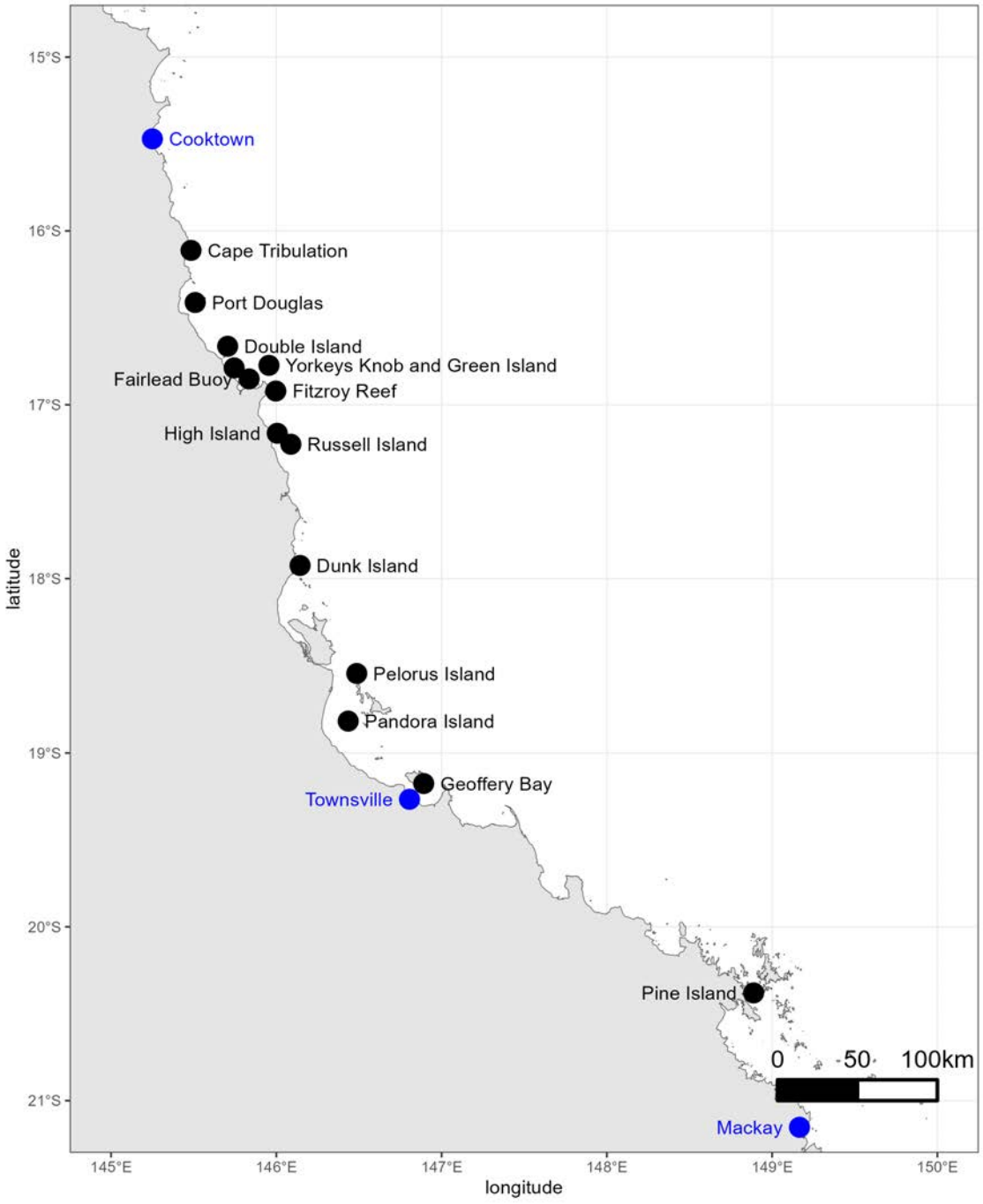

Figure 4.3: Sample sites: the Australian Institute of Marine Science (AIMS) Marine Monitoring Program (MMP) sensor locations (black symbol) and towns (blue symbol).

The emergent properties of phytoplankton community structure were assessed using 15,000 randomly sampled simulated surface data points from December 2010 to November 2012. The variation of the percentage of chlorophyll *a* contained in large phytoplankton (including *Trichodesmium*) and small phytoplankton as a function of chlorophyll were examined. These relationships were compared with observed relationships reported by Brewin et al. (2010); Hirata et al. (2011) from analyses on a global marine phytoplankton database. Additionally, the relationship between simulated zooplankton biomass and chlorophyll *a* were compared with that of GBR4-BGC-sph using 15,000 randomly sampled surface data points.

4.3 Results

4.3.1 Skill assessment

Simulated GBR4-BGC-sph Chl-*a* extractions and observations of Chl-*a* extractions had an average Willmott index of 0.47 and mean bias of 0.12 mg Chl-*a* m^{-3} (Figure 4.4). Chl-*a* extractions from samples at MMP sites and simulated Chl-*a* extractions from GBR4-BGC-cyl had a lower average Willmott index (0.43) and higher bias of 0.18 mg Chl-*a* m^{-3} when compared to the GBR4-BGC-sph Chl-*a* extractions at the same sites. Both models overestimate Chl-*a* extractions at all sites except at Yorkey's knob, Dunk Island Pandora Island which are in waters very close to the mainland and are surrounded by shallow and muddy seabed.

Figure 4.5 shows that the comparison of simulated GBR4-BGC-sph NH_4 and NH_4 observations had an average bias of -0.36 mg N m^{-3} and Willmott index of 0.39. Simulated NH_4 from the modified model had a lower average Willmott index (0.37) and mean bias -0.36 mg N m^{-3}. Both GBR4-BGC-sph and GBR4-BGC-cyl underestimate NH_4 at all the sites expect at Fitzroy Reef and Pelorus Island.

Simulated NO_3 from GBR4-BGC-sph and GBR4-BGC-cyl were compared with tri-annually sampled NO_3 and had an average Willmott index of 0.25 and -0.07 mg N m^{-3} bias (Figure 4.6). On the other hand, simulated NO_3 from GBR4-BGC-cyl model had a mean Willmott index (0.25) and lower mean bias (-0.19 mg N m^{-3}). NO_3 was underestimated by both models at 65% of the MMP sites.

The comparison of simulated GBR4-BGC-sph DIP and DIP observations from the MMP sites had an average Willmott index of 0.29 and bias 1.16 mg P m^{-3} (Figure 4.7). Simulated DIP from the modified GBR4-BGC-cyl had a higher mean Willmott index (0.30) and a higher bias (1.31 mg P m^{-3}). DIP concentrations were overestimated by both models.

Overall, simulated Chl-*a* extractions, NH_4, NO_3 and DIP concentrations during 2011/2012 wet season (from December to February) were higher when compared with the 2010/2011 wet season (Figure 4.8). This is likely due to La Niña conditions peaked between late 2010 and early 2011 and caused record high rainfall in north and eastern Australia.

4.3.2 Emergent relationships and *Trichodesmium* dynamics

Emergent relationships are system-level patterns observed in nature that occur as ecosystem functions and are used as indicators to assess that models accurately capture important biogeochemical processes especially when there are limited observations for model assessment (Robson et al., 2017a; Hipsey et al., 2020; Robson et al., 2020). Emergent relationship between the percentage of small vs large phytoplankton and chlorophyll *a* in global ocean data sets (Brewin et al., 2010; Hirata et al., 2011) was used by Robson et al. (2017a, 2020) to provide an additional layer for the assessment of the eReefs marine models.

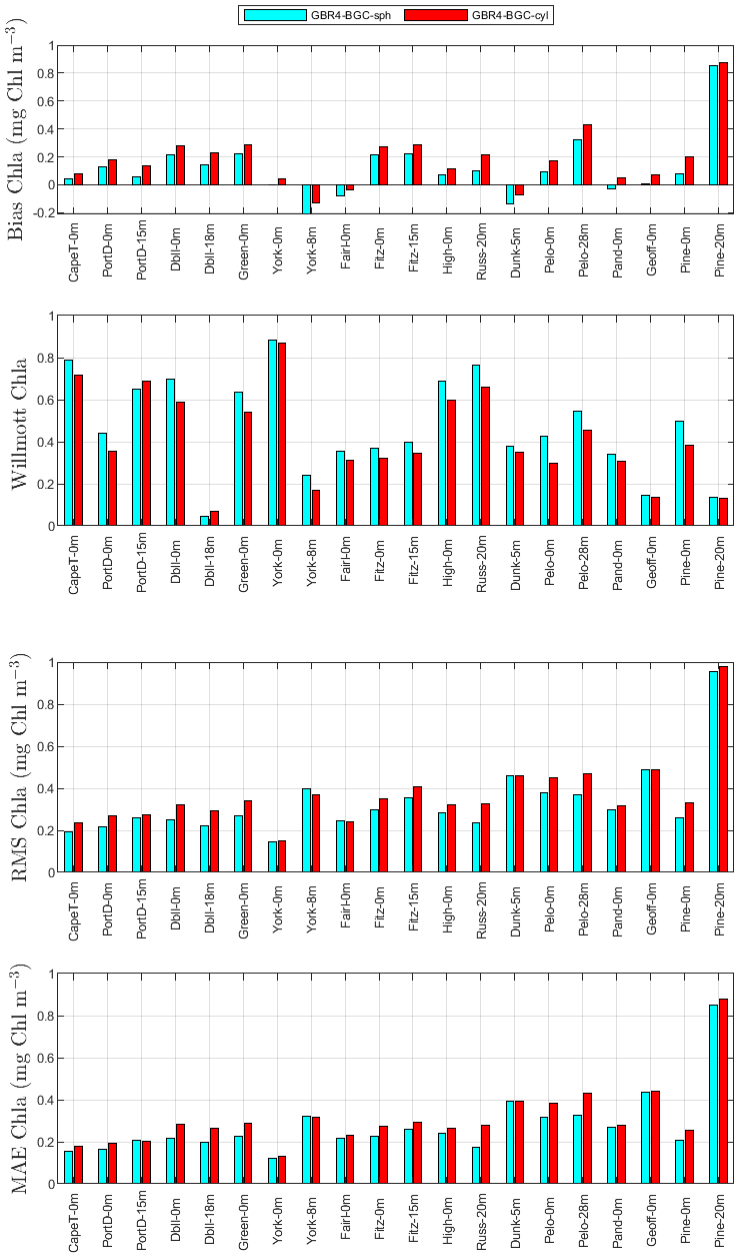

Figure 4.4: From top to bottom: bias, Willmott score, root mean square error and mean absolute error for simulated cholorophyll *a* (Chl-*a*) versus monthly observations of surface Chl-*a* pigment concentrations from December 2010 to November 2012 (Moran et al., 2022). Sites are arranged from North to South and locations are shown in Figure 4.3. Water quality sampling was done at more than one depth at some sites. The x-axis labels represent the short form of the station name followed by the depth in metres below the surface. Index of short names to full station names: CapeT = "Cape Tribulation"; PortD = "Port Douglas"; Dbll = "Double Island"; Green = "Green Island"; York = "Yorkeys Knob"; Fairl = "Fairlead Buoy"; Fitz = "Fitzroy Reef"; High = "High Island"; Russ = "Russell Island"; Dunk = "Dunk Island"; Pelo = "Pelorus Island"; Pand = "Pandora Island"; Geoff = "Geoffery Bay"; Pine = "Pine Island". "GBR4-BGC-sph" corresponds to the version of the model described in (Baird et al., 2020) whereas "GBR4-BGC-cyl" is the modified model.

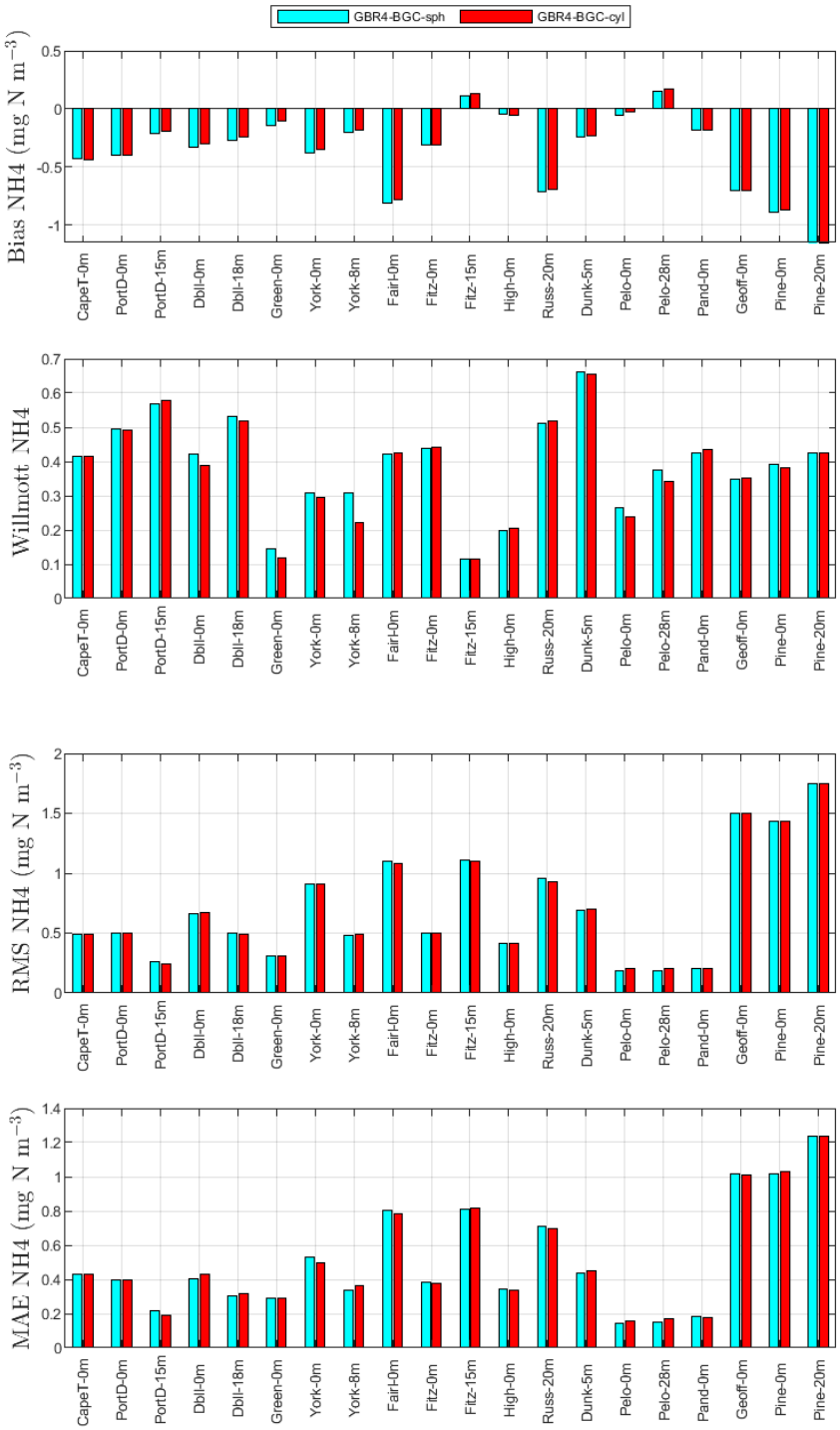

Figure 4.5: From top to bottom: bias, Willmott score, root mean square error and mean absolute error for simulated ammonium versus monthly observations from December 2010 to November 2012. Sites are arranged from North to South and locations are shown in Figure 4.3. “GBR4-BGC-sph" corresponds to the version of the model described in (Baird et al., 2020) and “GBR4-BGC-cyl" is the modified model. See Figure 4.4 for more information on sites.

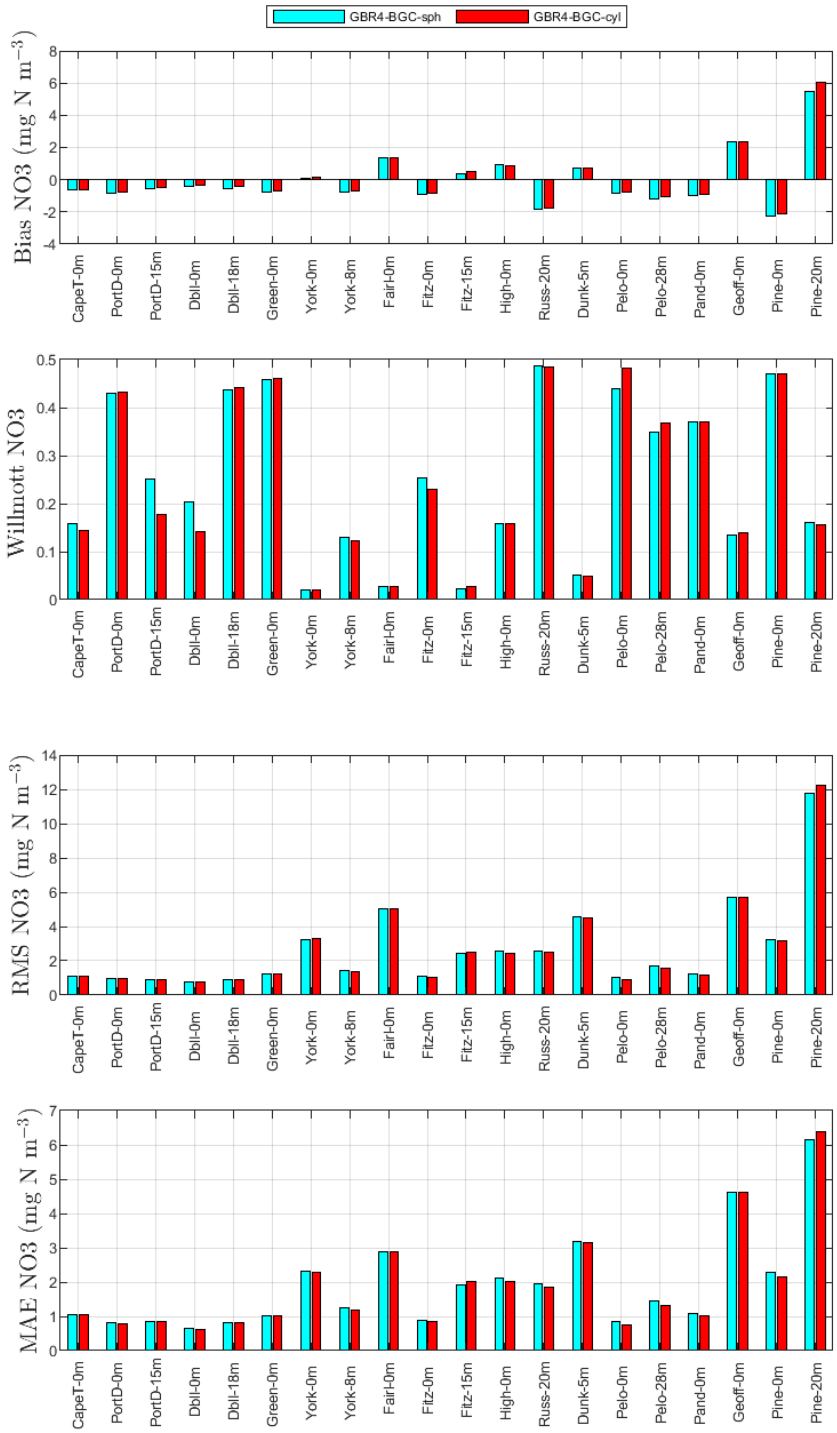

Figure 4.6: From top to bottom: bias, Willmott score, root mean square error and mean absolute error for simulated nitrate versus monthly observations from December 2010 to November 2012. Sites are arranged from North to South and locations are shown in Figure 4.3. "GBR4-BGC-sph" corresponds to the version of the model described in (Baird et al., 2020) and "GBR4-BGC-cyl" is the modified model. See Figure 4.4 for more information on sites. See Figure 4.4 for more information on sites.

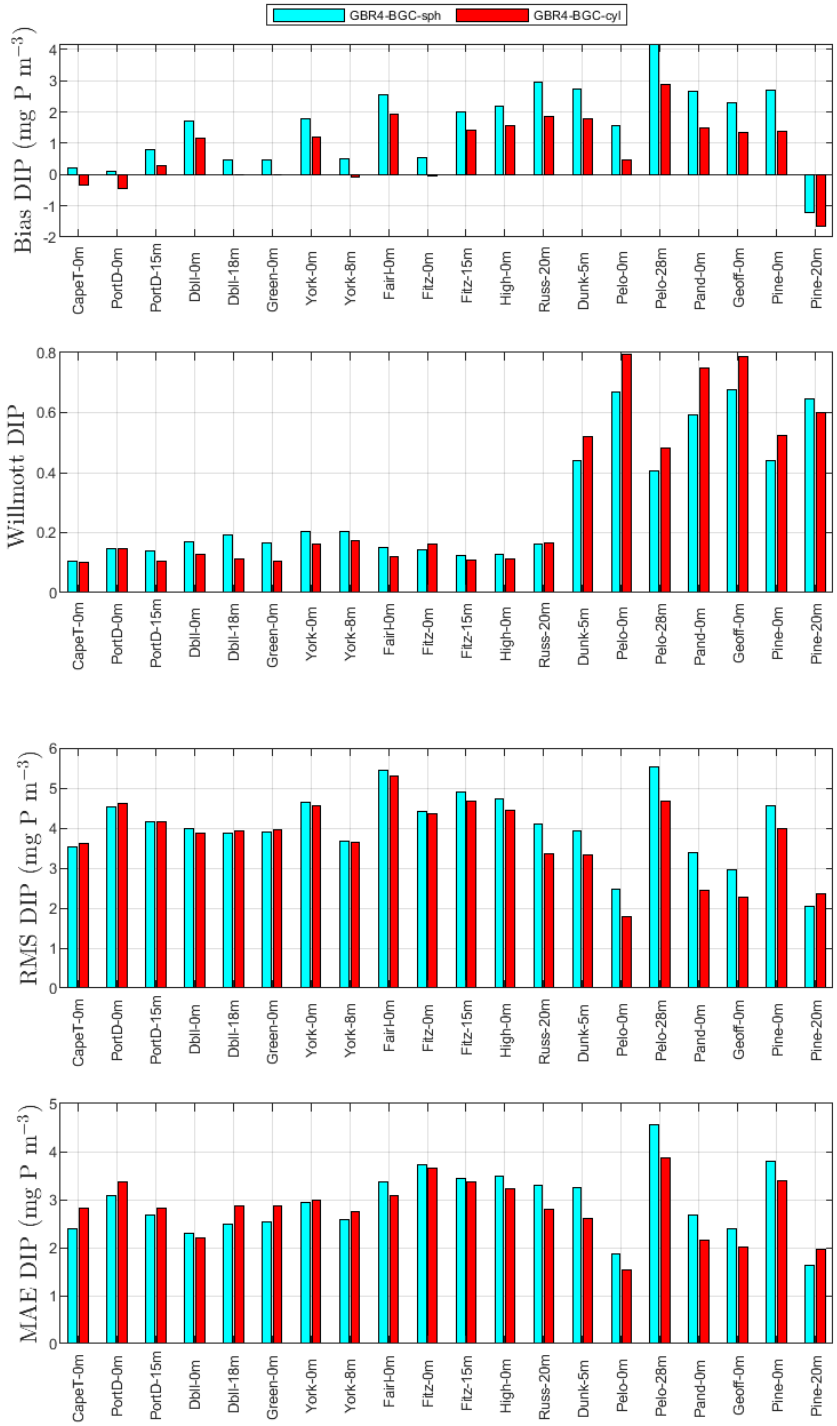

Figure 4.7: From top to bottom: bias, Willmott score, root mean square error and mean absolute error for simulated dissolved inorganic phosphorus (DIP) versus monthly observations from December 2010 to November 2012. Sites are arranged from North to South and locations are shown in Figure 4.3. “GBR4-BGC" corresponds to the version of the model described in (Baird et al., 2020) and “modified GBR4-BGC" is the modified model. See Figure 4.4 for more information on sites.

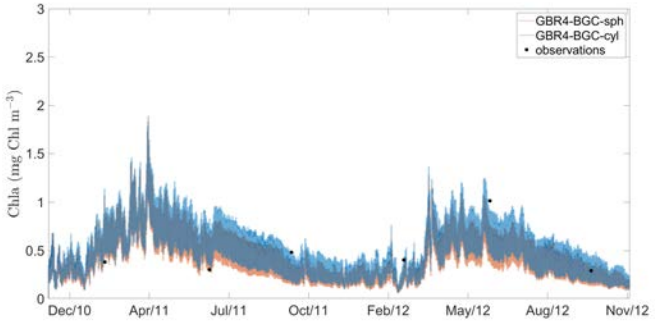

(a) Total chlorophyll a concentrations.

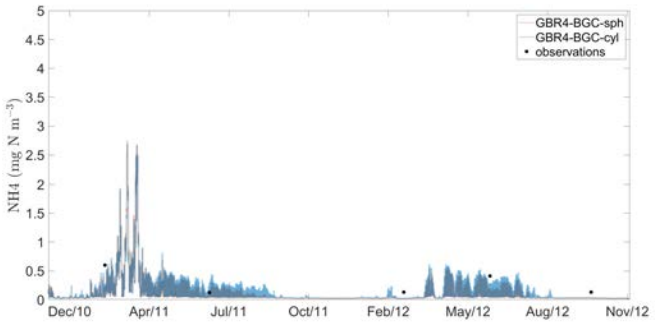

(b) NH_4 concentrations.

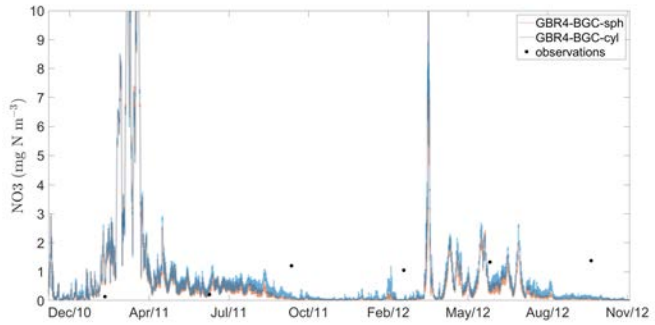

(c) NO_3 concentrations.

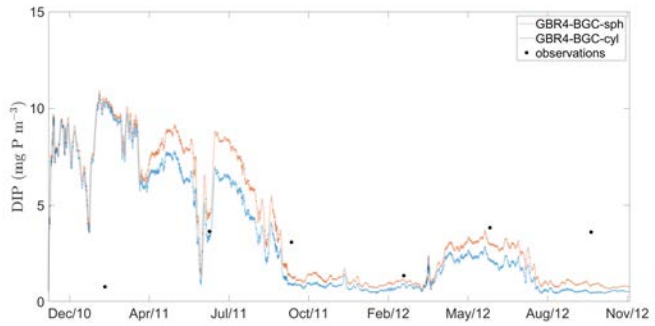

(d) DIP concentrations.

Figure 4.8: Comparison of the time series of simulated and observed chlorophyll *a* extractions, NH_4, NO_3 and DIP at 15 m Port Douglas. GBR4-BGC (orange), modified GBR4-BGC (blue) and observations (black).

Figure 4.9 shows the relationship between small and large phytoplankton and total chlorophyll from GBR4-BGC-sph, GBR4-BGC-cyl and observations. GBR4-BGC-cyl better captures the emergent patterns observed in nature. This increases our confidence that the model is correctly simulating the processes that underlie competition and co-existence of phytoplankton of different size classes. Figure 4.10 shows that both models are similar with respect to their ability to reproduce the expected emergent relationship between zooplankton concentrations and chlorophyll *a* concentrations.

The difference between mean surface *Trichodesmium* concentrations from GBR4-BGC-cyl and GBR4-BGC-sph during summer is shown in Figure 4.11. GBR4-BGC-cyl *Trichodesium* concentrations are slightly higher than that of GBR4-BGC-sph in southern GBR cross-shelf waters, lower in central and northern cross-shelf waters and northern GBR domain, and are similar to GBR4-BGC-sph *Trichodesium* concentrations in other parts of the GBR domain.

The modified model simulates the vertical distribution of *Trichodesmium*. Intracellular *Trichodesmium* total nitrogen are highest at the surface (Figure 4.12a) but intracellular *Trichodesmium* chlorophyll *a* concentrations are higher at intermediate depths (Figure 4.12b). Intracellular *Trichodesmium* carbon reserves and nitrogen fixation rates are lowest in deep and dark conditions (Figures 4.12c and 4.12d).

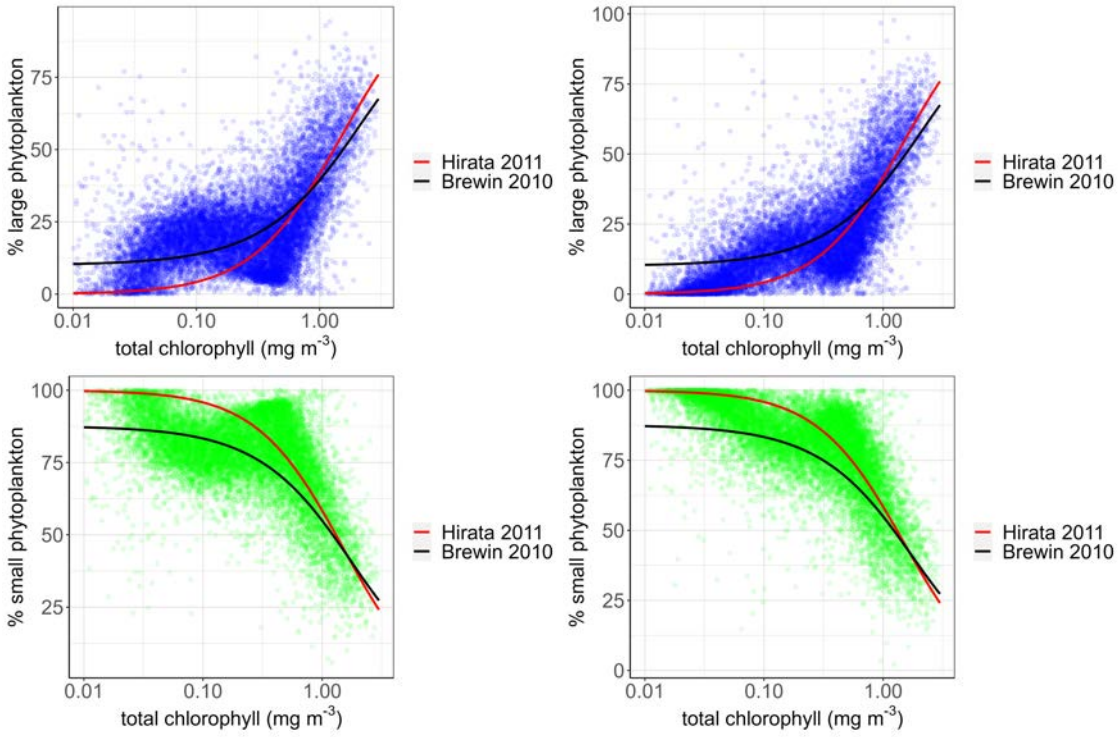

(a) GBR4-BGC-sph. (b) GBR4-BGC-cyl.

Figure 4.9: Relationship between the percentage of randomly sampled simulated surface large phytoplankton and chlorophyll *a* concentrations (top), simulated surface small phytoplankton and chlorophyll *a* concentrations (bottom). Dots represent randomly sampled simulated data points and lines show fits to observations from a global marine database taken from Brewin et al. (2010); Hirata et al. (2011). Large phytoplankton comprises microphytoplankton and *Trichodesium* and small phytoplankton consists of nano- and pico-phytoplankton.

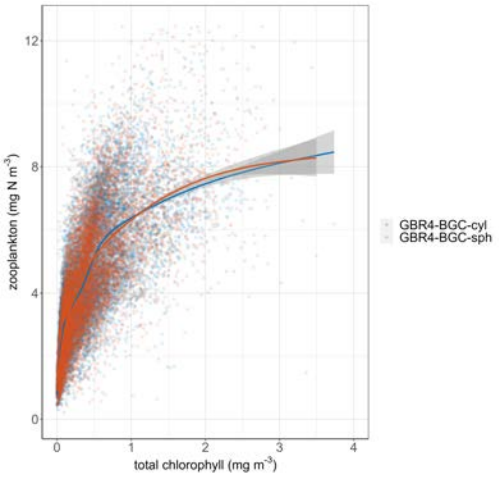

Figure 4.10: Relationship between 15,000 randomly sampled simulated surface zooplankton and chlorophyll *a* concentrations. The smoothing functions applied to the data are represented by lines and grey-shaded confidence intervals.

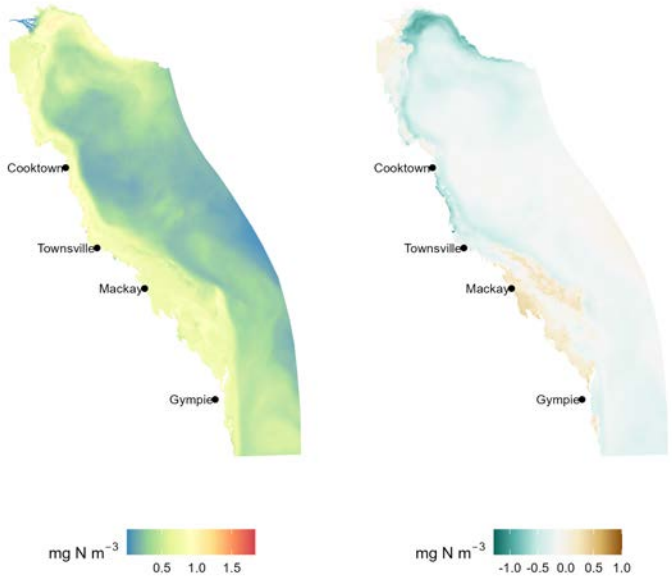

Figure 4.11: Spatially-resolved GBR4-BGC-sph mean surface *Trichodesmium* concentrations (left), and the difference between GBR4-BGC-cyl and GBR4-BGC-sph mean surface *Trichodesmium* concentrations (right) during summer (from 2 December 2010 to 1 March 2011) in the Great Barrier Reef.

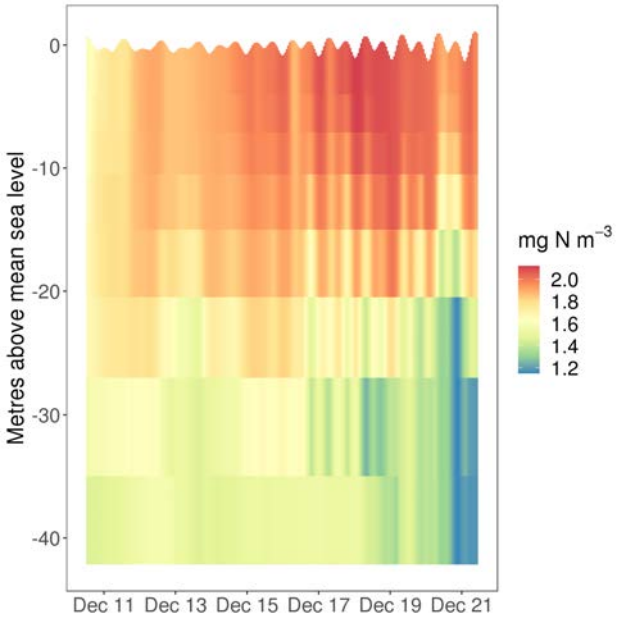

(a) *Trichodesmium* total nitrogen.

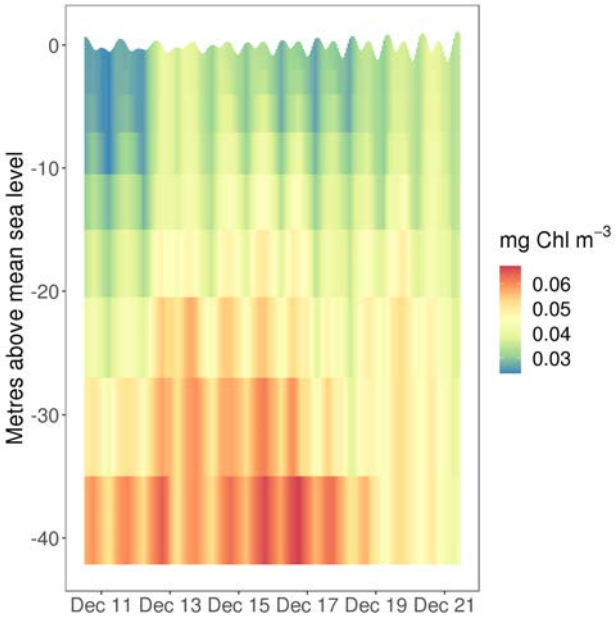

(b) *Trichodesmium* chlorophyll *a* concentrations.

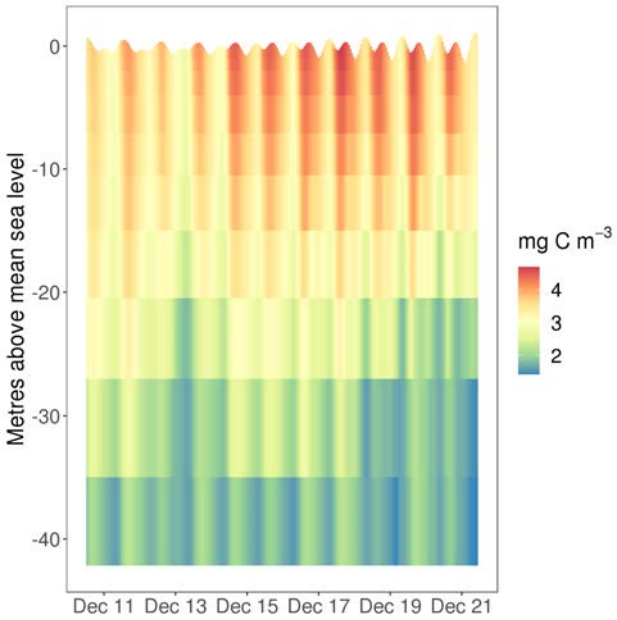

(c) *Trichodesmium* carbon reserves.

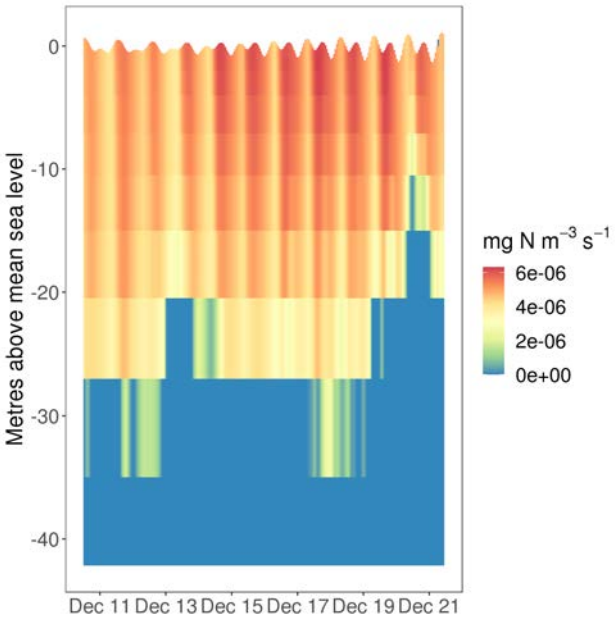

(d) *Trichodesmium* nitrogen fixation rate.

Figure 4.12: Depth profile over time of simulated intracellular *Trichodesmium* nitrogen store (combination of nitrogen and nitrogen reserves), intracellular chlorophyll *a* concentrations, intracellular carbon reserves, and *Trichodesmium* nitrogen fixation rate at the geolocation (17.75°S, 146.6° E) from midday 10/12/2010 to midday 22/12/2010.

4.4 Discussion

The vertical distribution of *Trichodesmium* dynamics is influenced by buoyancy regulation. The interactions between buoyancy regulation and changing environmental conditions such as light, temperature and nutrient availability can alter the occurrence of *Trichodesmium* and other marine organisms. Benavides et al. (2022) suggest that increased sinking of *Trichodesmium* colonies can increase the growth of other phytoplankton species due to increased influx of light and nutrient availability for other phytoplankton growth. Buoyancy regulation allows *Trichodesmium* colonies to overcome the inhibiting effect of low phosphorus concentration on growth in oligotrophic waters by migrating to deeper waters to assimilate both inorganic and organic phosphorus (Beversdorf et al., 2010; White et al., 2010). Thus, the reduced DIP concentrations from the modified GBR4-BGC at 15 m below the sea surface shown in Figure 4.8d could be due to increased phosphorus uptake by fast-sinking *Trichodesmium* colonies.

Trichodesmium colonies mostly photosynthesise and fix nitrogen at the surface under high irradiance. Decreased mean surface GBR4-BGC-cyl *Trichodesmium* concentrations during summer (wet season) shown in most parts of the GBR cross-shelf waters and northern GBR domain (Figure 4.11) is likely due to increased number of sinking *Trichodesmium* colonies, which sink faster to deep waters where reduced carbon and nitrogen fixation occur (Benavides et al., 2022; Ani et al., 2023). This agrees with Kromkamp and Walsby's (1992) report that large *Trichodesmium* colonies sink faster and the number of colonies that migrate vertically increased. However, increased mean surface GBR4-BGC-cyl *Trichodesmium* concentrations shown in southern cross-shelf waters could be as a result of increased number of trapped colonies due to the inadequacy of *Trichodesmium* to perfectly regulate buoyancy and the effects of high DIP concentrations from river discharge on *Trichodesmium* growth.

The decrease in simulated *Trichodesmium* total nitrogen with depth (Figure 4.12a) is likely influenced by the inhibiting effects of low irradiance on *Trichodesmium* growth. However, *Trichodesmium* chlorophyll *a* concentrations are higher at intermediate depths (Figure 4.12b) because the model's production of chlorophyll is stimulated in low light conditions when sufficient intracellular carbon, nitrogen and phosphorus are available. The model results suggest that the dynamics of *Trichodesmium* nitrogen and chlorophyll stores may be quite different and cannot be assumed to covary.

Trichodesmium colonies in deep waters will continue to fix nitrogen, but at a reduced rate because nitrogen fixation is inhibited by high DIN concentrations (Benavides et al., 2022; Ani et al., 2023). This is supported by the reduced *Trichodesmium* nitrogen fixation rate in deep waters shown in Figure 4.12d. Below the euphotic zone, *Trichodesmium* uses carbon stores acquired before sinking to fix nitrogen and can also obtain carbon from dissolved organic matter. This can reduce *Trichodesmium* growth in deep waters and is evident in Figure 4.12a as the structural *Trichodesmium* nitrogen indicating *Trichodesmium* abundance decreased with depth. Our model results show the reduction of intracellular carbon reserves in deep and dark conditions (Figure 4.12c). Also, Figures 4.12c and 4.12d show that nitrogen fixation rate is highest when intracellular carbon reserves are high. This is because of the energetic cost of nitrogen fixation as *Trichodesmium* utilizes fixed carbon to fix nitrogen from atmospheric dinitrogen (Oliver et al., 2012). The decrease in temperature in deep waters (which reduces *Trichodesmium* metabolism (Boyd et al., 2013; Ani and Robson, 2021)), increased oxygen saturation at depth and reduced nitrogen fixation reduce the consumption of fixed carbon, thus allowing *Trichodesmium* to survive below the euphotic zone before recovering buoyancy. Moreover, the ability of *Trichodesmium* to occur in lower temperature conditions (White et al., 2006) can allow them survive in deep and dark conditions.

It is important to note that the model developed here does not consider all phenomena relevant to *Trichodesmium* buoyancy regulation. For example, the model formulations used in this study do not include effects of obliquely oriented colonies on *Trichodesmium* sinking rates or variations in tuft size

and shape. Obliquely oriented non-spherical colonies or cells have been shown to drift sideways while sinking thereby enhancing their lateral dispersion (Holland, 2010). In addition, *Trichodesmium* colonies were assumed to be symmetrically weighted. However, all asymmetrically weighted colonies have been reported to sink in one orientation (McNown and Malaika, 1950) and can alter their sinking rates.

4.5 Conclusions

The model formulations developed in this study improve the physiological realism of the *Trichodesmium* growth submodel of the eReefs marine biogeochemical models, and should therefore improve the accuracy of the model outputs. However, the skill assessment results show that the modified model's skill is similar to that of the version of the model in (Baird et al., 2020) and where it is different it is slightly worse, although the modified model better captures the emergent patterns of phytoplankon size spectrum observed in nature, thus increasing our confidence in the model's predictions. Therefore, there is need to validate *Trichodesmium* concentrations or nitrogen fixation rates against observations but at present, very limited observational data are available.

Finally, our model results suggest that observations of the presence or absence of *Trichodesmium* surface blooms are not sufficient to characterise the role of this cyanobacterium in the GBR.

5. Modelling *Trichodesmium* photophysiology in the Great Barrier Reef using the eReefs models

Summary

The nitrogen-fixing cyanobacterium, *Trichodesmium*, is proposed to be a major source of nitrogen in the Great Barrier Reef (GBR). Effective GBR water quality management requires an understanding of the contribution of *Trichodesmium* to the total annual nitrogen budget of the GBR. Reliable model simulations of *Trichodesmium* growth, nitrogen fixation and distribution are required to understand the dynamics of *Trichodesmium* in the GBR ecosystem. The variation of the major light-harvesting *Trichodesmium* phycobilipigments (phycourobilin (PUB) and phycoerythrobilin (PEB)) under varying light conditions was represented in the *Trichodesmium* growth submodel of the eReefs biogeochemical model. This involved parameterising the interconversion between PUB and PEB, and the photosystem II reaction centre dynamics. Our model formulations provide improved representations of *Trichodesmium* photophysiology and can help to improve the understanding of *Trichodesmium* dynamics for effective GBR water quality management.

This chapter is under preparation for journal publication:

Ani, C.J., Baird, M., Robson, B.. Modelling *Trichodesmium* photophysiology in the Great Barrier Reef using the eReefs models.

Contribution of authors

Chinenye J. Ani: Writing – original draft, Visualisation, Validation, Software, Resources, Methodology, Conceptualisation, Investigation, Formal analysis, Data curation.

Mark Baird: Methodology, Writing – review & editing.

Barbara Robson: Writing – review & editing, Validation, Supervision, Resources, Project administration, Methodology, Funding acquisition.

5.1 Introduction

5.1.1 *Trichodesmium* phycobilipigments

Trichodesmium is a diazotrophic cyanobacterium that occurs in fields of dynamic light conditions and has developed intracellular mechanisms for optimal light harvesting and utilisation. *Trichodesmium* possess light-harvesting phycobilisomes made up of phycobilipigments, which are the main contributors to light absorption and photosynthesis (Subramaniam et al., 1999; Hynes et al., 2012). The phycobilipigment phycoerythrin (PE) dominates *Trichodesmium* phycobilisomes. PE comprises phycourobilin (PUB) and phycoerythrobilin (PEB). PUB has absorption peaks at 490–500 nm and PEB has absorption peaks at 545–565 nm (Hynes et al., 2012) (Figure 5.1). The phycobilisomes also consist of phycocyanin (PC) with absorption peak at $\sim$ 620 nm and allophycocyanin (APC), which has an absorption peak at 650 nm (Hynes et al., 2012). The ratio of PE to chlorophyll *a* (Chl-*a*) in *Trichodesmium* has been reported to be between 2.8 and 4 and is influenced by light intensity and other environmental factors (Hogetsu and Watanabe, 1975; Bell and Fu, 2005).

Light-harvesting phycobilisomes absorb light over a wide range of wavelengths and transfer the absorbed energy to photosynthetic reaction centres, photosystems I and II (PSI and PSII), thereby increasing the absorption cross-section of *Trichodesmium*. A large fraction of absorbed energy is transferred from PSII to PSI and utilised for nitrogen fixation resulting in reduced oxygen evolution and growth (Subramaniam et al., 1999).

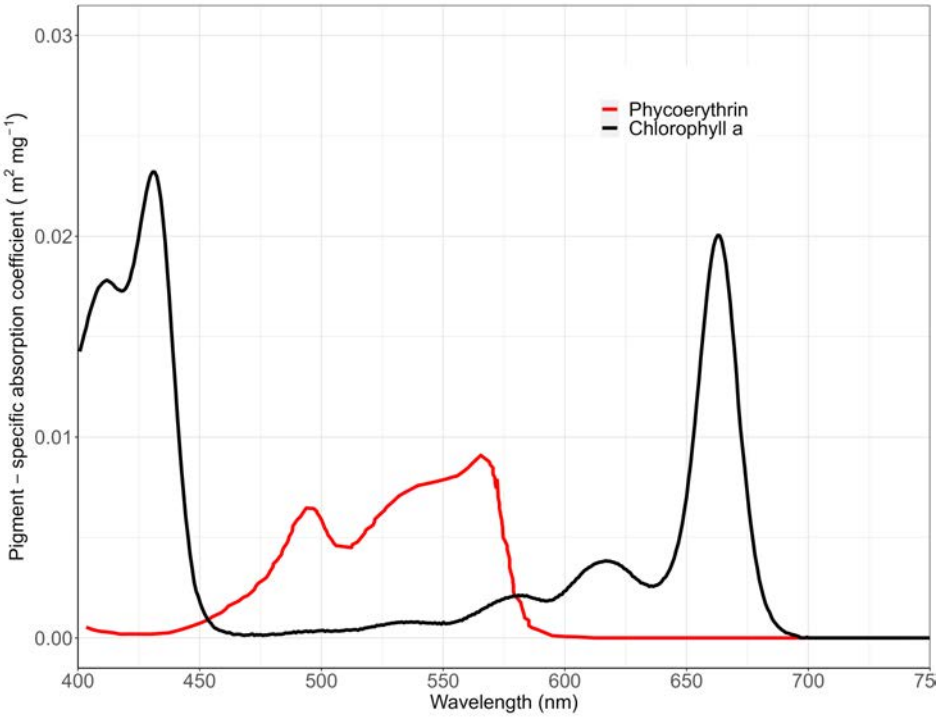

Figure 5.1: Pigment-specific absorption coefficients for *Trichodesmium* phycoerythrin (phycourobilin + phycoerythrobilin) and chlorophyll *a* pigments. The absorption peaks of phycourobilin and phycoerythrobilin are at 495 nm and 565 nm, respectively. See (Baird et al., 2020) for details on the laboratory standards used to determine the absorption coefficients.

Subramaniam et al. (1999) suggested that changes in *Trichodesmium* PE concentrations occur via the rapid interconversion between PUB and PEB under varying light conditions, which corresponds to the

transfer of absorbed energy between PSII and PSI in *Trichodesmium* (Andresen et al., 2010). In high light conditions, PSII is greatly reduced causing a reduction in PEB concentrations and an increase in PUB concentrations. Light absorbed by PUB is emitted at 565 nm, whereas energy absorbed by PEB is efficiently transferred to PSII through PC and APC. Contrarily, at low irradiance, PEB concentrations increase and are greater than PUB concentrations, which are greatly reduced. Light absorbed by both PUB and PEB is efficiently transferred to PSII for photosynthesis. The absorbed energy transfer pathway, phycobilisomes→PSII→PSI (also called "spillover"), suggested by Subramaniam et al. (1999) (Figure 5.2) is supported by other research studies (Vernotte et al., 1990; Olive et al., 1997; Ueno et al., 2016). The increase in PUB concentrations and the emission of absorbed light at high irradiance have been likened to the photoprotective xanthophyll cycle in phytoplankton and higher plants (Rodriguez, 1998; Cai et al., 2015).

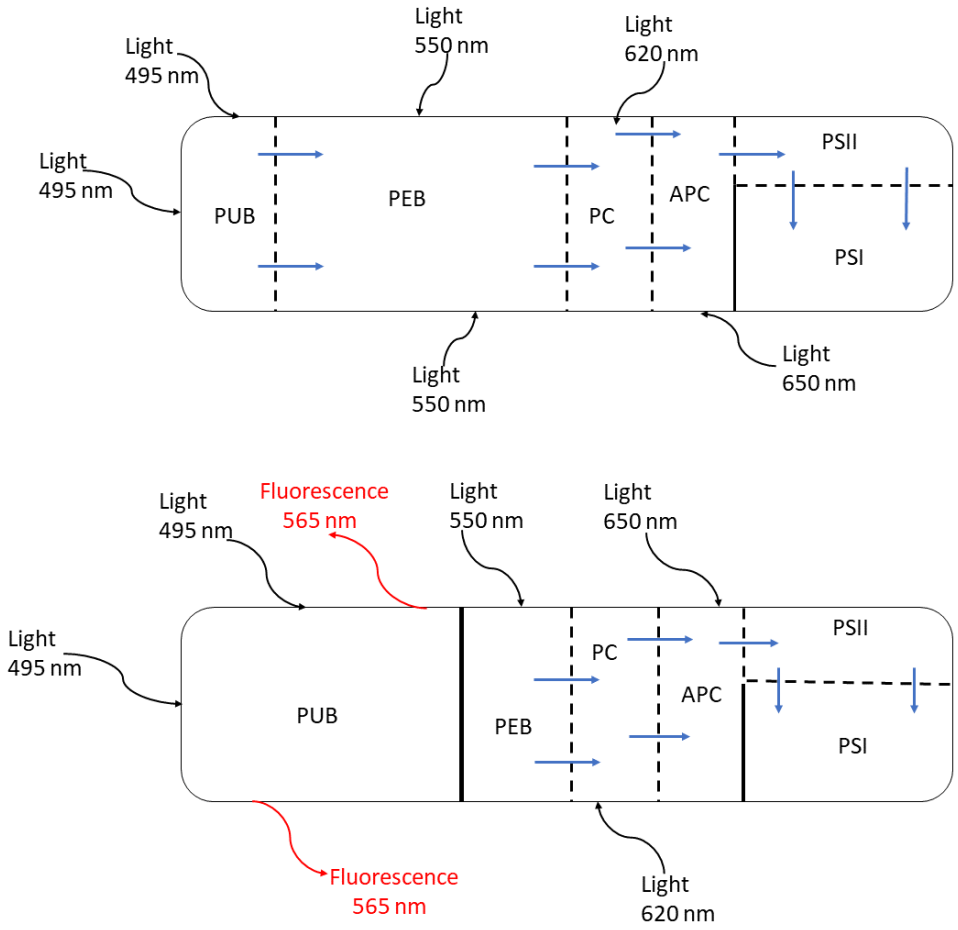

Figure 5.2: Schematic showing the photosynthetic energy transfer from phycobilisomes to the photosynthetic reaction centres in *Trichodesmium*. Blue arrows depict fluxes of absorbed energy. Low light conditions (top) and high light conditions (bottom). Adapted from (Subramaniam et al., 1999).

5.1.2 *Trichodesmium* dynamics in the Great Barrier Reef

Trichodesmium is proposed to be a major source of nitrogen in the Great Barrier Reef (GBR) with implications for nutrient cycling and eutrophication (Messer et al., 2017; Bell, 2021; Ani et al., 2023).

To effectively manage GBR water quality it is essential to understand the contribution of *Trichodesmium* to the total annual nitrogen budget of the GBR. Previous work by Bell (2021); Ani et al. (2023) used satellite ocean-colour data and the eReefs models to quantify the annual contribution of *Trichodesmium* fixed nitrogen to the nitrogen budget of the GBR. In both studies, *Trichodesmium* nitrogen estimates over the GBR and Central GBR were reported to be greater than riverine nitrogen loads exported to the GBR.

The *Trichodesmium* growth model (Robson et al., 2013) incorporated into the eReefs biogeochemical model (https://research.csiro.au/ereefs/), an application of the CSIRO Environmental Modelling Suite (CSIRO EMS) (Baird et al., 2020), simulates *Trichodesmium* dynamics in the GBR. The eReefs marine model is a coupled hydrodynamic, biogeochemical and sediment model that simulates the environmental conditions of the GBR at multiple temporal and spatial scales.

To understand the dynamics of *Trichodesmium* in the GBR ecosystem, reliable model simulations of *Trichodesmium* growth, nitrogen fixation and distribution are required. Although the eReefs models have been used to provide detailed spatial and temporal occurrences of *Trichodesmium* in the GBR and quantify its contribution to the total annual nitrogen budget of the GBR (Ani et al., 2023), not all important *Trichodesmium* physiological processes were represented by the *Trichodesmium* growth submodel. A key process that was not considered is the variation of *Trichodesmium* phycobilipigments under varying light conditions. This study modifies the CSIRO EMS model of *Trichodesmium* photophysiology by parameterising the interconversion between PUB and PEB under varying light conditions, and photosystem II reaction centre dynamics.

5.2 Methods

To incorporate the variation of *Trichodesmium* phycobilipigments under varying light conditions in the eReefs *Trichodesmium* growth submodel, we adopt the mechanistic approach for zooxanthellae xanthophyll cycle in (Baird et al., 2018). *Trichodesmium* light absorption is modelled by considering concentrations of Chl-*a*, PUB ($Tricho_{PUB}$) and PEB ($Tricho_{PEB}$) as time-varying state variables. For simplicity, a constant PE (PUB+PEB) to Chl-*a* ratio, Θ_{PE2Chl}, is assumed by the model and PE synthesis is a product of Θ_{PE2Chl} and synthesised Chl-*a*.

5.2.1 Light absorption by *Trichodesmium* and carbon fixation

To simulate light absorption by *Trichodesmium*, a spectrally-resolved optical model that resolves the total rate of light absorption due to photosynthetic pigments across all wavelengths, λ, is used (see (Baird et al., 2013, 2020) for more details). The model assumes that the ratio of Chl-*a* and other photosynthetic pigments is constant and uses it with *Trichodesmium* Chl-*a* concentrations and the number of *Trichodesmium* cells in the population to calculate the Chl-*a* specific absorption coefficient due to all light harvesting pigments. The Chl-*a* specific absorption coefficient due to all light harvesting pigments for *Trichodesmium*, $\gamma_{Tricho,\lambda}$, in the model is given as

$$\gamma_{Tricho,\lambda} = 2.5\gamma_{PE,\lambda} + 0.02\gamma_{Myxo,\lambda} + 0.09\gamma_{\beta-car,\lambda} + 0.1\gamma_{Zea,\lambda} + \gamma_{Chl-a,\lambda}, \tag{5.2.1}$$

where Myxo is myxoxanthophyll, β-car is β carotene and Zea is zeaxanthin.

The absorption cross-section of *Trichodesmium* (α_{Tricho}) defined as

$$\alpha_{Tricho} = \pi r^2 \Big[1 - \frac{2(1-(1+2\gamma_{Tricho,\lambda}c_i r)e^{-2\gamma_{Tricho,\lambda}c_i r})}{(2\gamma_{Tricho,\lambda}c_i r)^2}\Big] \tag{5.2.2}$$

is a function of cell radius (r) and wavelength-dependent absorption coefficient of *Trichodesmium*, $\gamma_{Tricho,\lambda}$, with c_i representing intracellular Chl-*a* concentrations and πr^2 corresponding to the projected area of a spherical cell. When there is no light absorption the expression in square brackets is 0 because $\gamma_{Tricho,\lambda} c_i r = 0$ and tends to 1 as the cell becomes fully opaque (i.e., $\gamma_{Tricho,\lambda} c_i r \to \infty$).

The rate of photons absorbed, k_I, is given by

$$k_I = \frac{(10^9 hc)^{-1}}{A_V} \int \alpha_{Tricho} E_{d,\lambda} \lambda d\lambda, \tag{5.2.3}$$

where h is Planck constant, c is the speed of light, A_V is Avagrado constant and E_d is downwelling irradiance.

The energy transferred to oxidised reaction centres ($\frac{Q_{ox}}{Q_T}$) that is used for photosynthesis is

$$k_{I_{fix}} = k_I \Big(\frac{Q_{ox}}{Q_T}\Big)(1 - R_C^*), \tag{5.2.4}$$

where R_C^* is intracellular carbon reserves. Oxygen release,

$$\frac{138}{1060} 32 \; k_I \Big(\frac{Q_{ox}}{Q_T}\Big)(1 - R_C^*), \tag{5.2.5}$$

and dissolved inorganic carbon uptake,

$$\frac{106}{1060} 12 \; k_I \Big(\frac{Q_{ox}}{Q_T}\Big)(1 - R_C^*), \tag{5.2.6}$$

are associated with the absorption of photons.

5.2.2 *Trichodesmium* pigments synthesis

The rate of Chl-*a* synthesis is based on the incremental benefit of adding pigment to the photosynthetic rate, the reduced benefits of surplus carbon reserves ($1 - R_C^*$), self-shading χ and the fraction of inhibited reaction centres ($\frac{Q_{in}}{Q_T}$). Self-shading, χ, is the derivative of α_{Tricho} per unit projected area ($\frac{\alpha_{Tricho}}{PA}$) with respect to ρ, where $\rho = \gamma_{Tricho,\lambda} c_i r$. Therefore,

$$\chi = \frac{1}{PA} \frac{\partial \alpha_{Tricho}}{\partial \rho} = \frac{1 - e^{-2\rho}(2\rho^2 + 2\rho + 1)}{\rho^3}. \tag{5.2.7}$$

The rate of Chl-*a* synthesis is given as

$$\frac{\partial c_i}{\partial t} = Chl_{max}(1 - R_C^*)\Big(1 - \frac{Q_{in}}{Q_T}\Big)\bar{\chi} \qquad \text{if C:Chl} > \theta_{min}, \tag{5.2.8}$$

where $\bar{\chi}$ is the quantum-weighted mean of χ, Chl_{max} is the maximum rate of Chl-*a* synthesis and θ_{min} is the minimum C:Chl ratio below which Chl-*a* synthesis is zero. Since Θ_{PE2Chl} is 2.5 from (5.2.1) and PUB:PEB ratio has been reported to be approximately 0.81 (Hynes et al., 2012), the rates of PEB and PUB syntheses are defined as

$$\frac{\partial Tricho_{PEB}}{\partial t} = 1.38 \frac{\partial c_i}{\partial t} \tag{5.2.9}$$

and

$$\frac{\partial Tricho_{PUB}}{\partial t} = 1.12 \frac{\partial c_i}{\partial t}, \tag{5.2.10}$$

respectively.

5.2.3 The variation of *Trichodesmium* phycoerythrin under varying light conditions

To simulate the variation of *Trichodesmium* phycoerythin under varying light conditions, the interconversion between PUB and PEB, and PSII reaction centre dynamics are parameterised by including time-varying concentrations of oxidised (Q_{ox}), reduced (Q_{red}) and inhibited (Q_{in}) reaction centres as state variables. The rate at which the interconversion between PUB and PEB occurs is assumed to be relatively fast when compared to the rate of pigments syntheses. This process is reversible and is given by

$$\frac{\partial Tricho_{PEB}}{\partial t} = -8\Big(\frac{Q_{in}}{Q_T} - 0.5\Big)^3 \tau_{PE}\ \Phi(Tricho_{PEB} + Tricho_{PUB}) = -\frac{\partial Tricho_{PUB}}{\partial t}, \quad (5.2.11)$$

where τ_{PE} is the switching time-scale and Φ is a parabolic term (see (Baird et al., 2018) for detailed description) that slows down the conversion rate when one pigment pool has near-zero concentration.

Photons are absorbed by phycobiligments in the ratio of their concentrations and transferred to PSII. Since energy absorbed by PUB at low irradiance have a low quantum yield (Subramaniam et al., 1999), for model simplicity, we assume that photons absorbed by PUB are emitted whereas photons absorbed by PEB cause a change in the state of PSII or in R_C^*. If a photon interacts with Q_{ox} and R_C^* is depleted, carbon fixation occurs and R_C^* is increased. If a photon interacts with Q_{ox} and carbon fixation is inhibited, Q_{ox} is reduced to Q_{red}. Finally, if a photon interacts with Q_{in}, the reaction centre remains inhibited. The following equations represent the rates of change of the reaction centres:

$$\frac{\partial Q_{ox}}{\partial t} = -k_I\ n\ m_{RCII}\ \frac{Q_{ox}}{Q_T}(1 - R_C^*), \quad (5.2.12)$$

$$\frac{\partial Q_{red}}{\partial t} = k_I\ n\ m_{RCII}\ \frac{Q_{ox}}{Q_T}(1 - R_C^*) - k_I\ n\ m_{RCII}\ \frac{Q_{red}}{Q_T}, \quad (5.2.13)$$

$$\frac{\partial Q_{in}}{\partial t} = k_I\ n\ m_{RCII}\ \frac{Q_{red}}{Q_T}. \quad (5.2.14)$$

n is the number of *Trichodesmium* cells and m_{RCII} is a stoichiometric coefficient. The amount of absorbed photon that is not used by Q_{ox} for carbon fixation is given by

$$k_{I_{unfix}} = k_I\Big(\frac{Q_{in}}{Q_T}\Big) - k_{I_{fix}}, \quad (5.2.15)$$

and is used to change an oxidised reaction centre to a reduced reaction centre.

Table 5.1: Model state variables for the *Trichodesmium* growth model.

Variable	**Symbol**	**Units**
Structural *Trichodesmium* biomass	$Tricho$	mg N m^{-3}
Trichodesmium phycourobilin concentration	$Tricho_{PUB}$	mg PUB m^{-3}
Trichodesmium phycoerythrobilin concentration	$Tricho_{PEB}$	mg PEB m^{-3}
Carbon reserves	R_C^*	mg C m^{-3}
Oxidised reaction centre concentration	Q_{ox}	mg m^{-3}
Reduced reaction centre concentration	Q_{red}	mg m^{-3}
Inhibited reaction centre concentration	Q_{in}	mg m^{-3}

Table 5.2: Derived variables for the *Trichodesmium* growth model.

Variable	**Symbol**	**Units**
Downwelling irradiance	E_d	W m^{-2}
Wavelength	λ	m
Intracellular chlorophyll *a* concentration	c_i	mg m^{-3}
Total reaction centre concentration	Q_T	mg m^{-3}
Concentration of *Trichodesmium* cells	n	cell m^{-3}
Absorption cross-section	α_{Tricho}	m^2 $cell^{-1}$
Photon absorption rate	k_I	mol photon $cell^{-1}$ s^{-1}
Maximum chlorophyll *a* synthesis rate	Chl_{max}	mg Chl m^{-3} d^{-1}

Table 5.3: Constants and parameters for the *Trichodesmium* growth model.

Variable	**Symbol**	**Units**	**Reference**
Constants			
Avagadro constant	A_V	6.02 $\times$ 10^{24} mol^{-1}	–
Planck constant	h	6.626 $\times$ 10^{-34} J s^{-1}	–
Speed of light	c	2.998 $\times$ 10^8 m s–1	–
Parameters			
Minimum C:Chl ratio	θ_{min}	50 g g^{-1}	(Breitbarth et al., 2008)
Trichodesmium cell radius	r	5 μm	(Robson et al., 2013)
Rate coefficient of phycobilipigment switching	τ_{PE}	1/600 s^{-1}	(Baird et al., 2018)
Stoichiometric ratio of RCII units to photons	m_{RCII}	0.1 mol RCII mol $photon^{-1}$	(Baird et al., 2018)

5.2.4 Model forcing

Outputs from the 12 km Australian Community Climate and Earth-System Simulator (ACCESS-R – http://www.bom.gov.au/nwp/doc/access/NWPData.shtml), the 10 km Ocean Modelling Analysis and Prediction System (OceanMAPS – https://researchdata.edu.au/oceanmaps-analysis/1440629) and river flow data from 22 rivers were used to force the eReefs hydrodynamic model. The biogeochemical model forcing include the hydrodynamic model (SHOC) outputs, wave data from the Bureau of Meteorology (BoM) regional wave model AUSWAVE-R and P2R GBR Dynamic SedNet with 2019 catchment conditions of sediment and nutrient loads (McCloskey et al., 2017, 2021b,a). The eReefs hydrodynamic model configured at 4 km resolutions (GBR4 grid) with the model formulations developed here, the temperature dependence in (Ani et al., 2023) and the buoyancy regulation formulations described in Chapter 4 was run from December 1, 2010 to November 30, 2012.

5.2.5 Model Validation

To evaluate the model, fourteen observation sites from the Australian Institute of Marine Science (AIMS) Marine Monitoring Program (MMP) sensor network sites (Australian Institute of Marine Science , AIMS) (Figure 5.3) sampled thrice yearly and time series of simulated model outputs from the version of the eReefs model described by Baird et al. (2020) (i.e., version 3.2 of the biogeochemical model run with version 2.0 of the hydrodynamic model, hereafter referred to as GBR4-BGC) were used to assess the model. Observational datasets from the AIMS MMP sites used for model assessment were available throughout the period the model was simulated (For more information on AIMS MMP sites see Skerratt et al. (2019); Moran et al. (2022)).

The variables considered for model assessment include Chl-*a* concentrations from pigment extractions, nitrate + nitrite [NO_x], ammonium (NH_4) and dissolved inorganic phosphorus (DIP). The skill metrics bias, Willmott score, root mean square error (RMS) and mean absolute error (MAE) were used to evaluate the modified model. Bias assesses the model's capability to under- or over-predict observations. The Willmott score is a ratio of the mean square error and the mean absolute deviation about the observed mean, and varies between 0 and 1 (Willmott et al., 1985). A Willmott score of 0 indicates no match and 1 indicates a perfect match. For this study, a Willmott score of 0.6 against simulated water quality variables was used as a benchmark for excellent model fit (Skerratt et al., 2019; Robson et al., 2020). RMS measures the accuracy of the model by calculating the difference between model predictions and observations. An RMS of 0 indicates perfect fit.

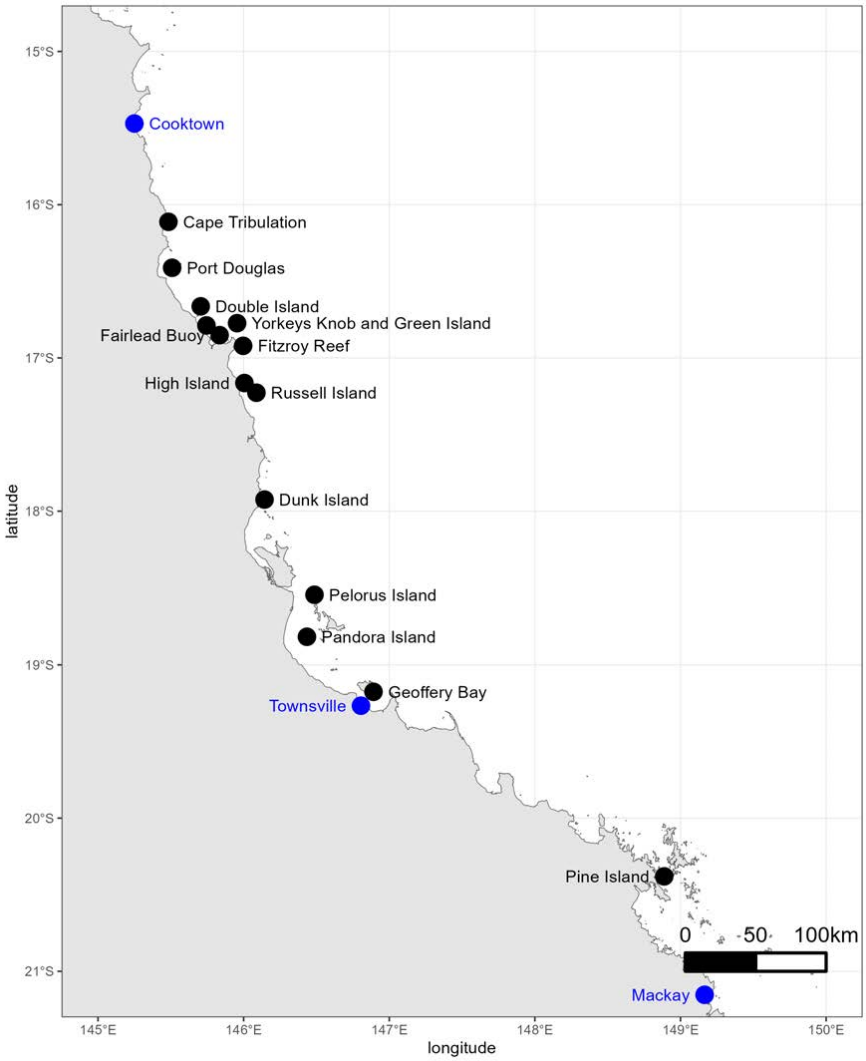

Figure 5.3: Sample sites: the Australian Institute of Marine Science (AIMS) Marine Monitoring Program (MMP) sensor locations (black symbol) and towns (blue symbol).

5.3 Results

5.3.1 Skill assessment

The comparison of observations of Chl-*a* extractions and simulated GBR4-BGC Chl-*a* extractions had a mean Willmott index of 0.47 and mean bias of 0.12 mg Chl-*a* m^{-3} (Figure 5.4). Simulated modified GBR4-BGC Chl-*a* extractions and observations of Chl-*a* extractions had a lower average Willmott index of 0.43 and higher mean bias of 0.18 mg Chl-*a* m^{-3} (Figure 5.4). Chl-*a* extractions were overestimated in both model simulations and at all sites except at sites located in waters very close to the mainland and are surrounded by shallow and muddy seabed, namely Yorkey's knob, Dunk Island and Pandora Island.

Simulated GBR4-BGC NH_4 and NH_4 observations had an average Willmott index of 0.39 and bias of -0.36 mg N m^{-3}. (Figure 5.5). Simulated NH_4 from the modified model had a lower average Willmott

index (0.38) and mean bias -0.36 mg N m^{-3}. NH_4 concentrations were underestimated by both models at all the sites expect at Fitzroy Reef and Pelorus Island.

Figure 5.6 shows that simulated GBR4-BGC NO_3 had an average Willmott index of 0.25 and -0.07 mg N m^{-3} mean bias. Simulated NO_3 from the modified GBR4-BGC model had a lower average bias of -0.19 mg N m^{-3} and a 0.25 mean Willmott index. Both models underestimated NO_3 concentrations at 65% of the MMP sites.

In Figure 5.7, simulated GBR4-BGC DIP concentrations had a mean Willmott index of 0.29 and 1.16 mg P m^{-3} bias. Simulated DIP from the modified GBR4-BGC had a higher mean Willmott index (0.30) and a higher bias (1.31 mg P m^{-3}). Both models overestimated DIP concentrations.

In general, skill metrics for the modified model were similar to those for the original model.

During 2011/2012 wet season (from December to February), simulated Chl-*a* extractions, NH_4, NO_3 and DIP concentrations were higher when compared with the 2010/2011 wet season (Figure 5.8). This is most likely due to record high rainfall in north and eastern Australia caused by peak La Niña conditions between late 2010 and early 2011. Figure 5.9 shows the difference between the modified GBR4-BGC and GBR4-BGC simulations, thus highlighting the divergence of the models.

5.3.2 Emergent relationships and *Trichodesmium* dynamics

Emergent relationships are system-level patterns that arise from underlying processes, often in a way that is not immediately obvious by inspecting the equations representing those processes. Examining emergent relationships can be used to provide an enhanced level of model assessment, especially when observational data are limited (Robson et al., 2017a; Hipsey et al., 2020; Robson et al., 2020). Previous work by Robson et al. (2017a, 2020) have used the emergent relationship between the proportion of small vs large phytoplankton and Chl-*a* in global ocean data sets (Brewin et al., 2010; Hirata et al., 2011) to provide an additional layer of model evaluation for the eReefs marine models. The relationship between small and large phytoplankton and total chlorophyll from GBR4-BGC, modified GBR4-BGC and observations is shown in Figure 5.10. Relative to the modified GBR4-BGC, the GBR4-BGC better captures the emergent patterns observed in nature. Both models have similar emergent relationships between zooplankton and chlorophyll as simulated surface zooplankton concentrations increased with chlorophyll (Figure 5.11).

Figure 5.12a show increased *Trichodesmium* PUB concentrations under high irradiance (day) and decreased PUB concentrations in dark conditions (night). Conversely, simulated *Trichodesmium* PEB concentrations increased in deep and dark conditions, and decreased in surface waters (high irradiance) (Figure 5.12b). Our model results also show the vertical distribution of *Trichodesmium*. In Figure 5.12c, at intermediate depths intracellular *Trichodesmium* chlorophyll a concentrations are higher (Figure 5.12d) whereas *Trichodesmium* total nitrogen stores are highest at the surface. In the model, chlorophyll is synthesised in low light and high nutrient conditions.

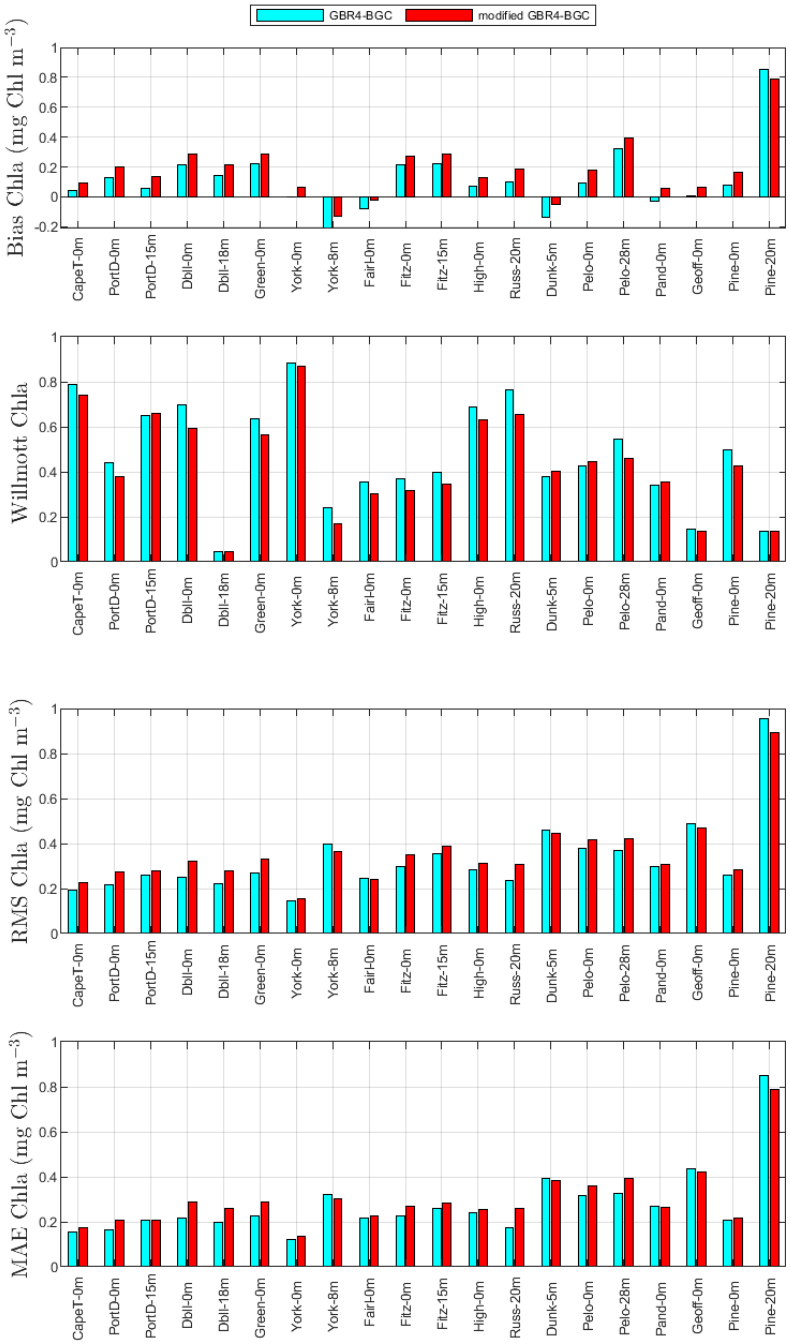

Figure 5.4: From top to bottom: bias, Willmott score, root mean square error and mean absolute error for simulated cholorophyll *a* (Chl-*a*) versus monthly observations of Chl-*a* extractions from December 2010 to November 2012. Sites are arranged from North to South and locations are shown in Figure 5.3. Water quality sampling was done at more than one depth at some sites. The x-axis labels represent the short form of the station name followed by the depth in metres below the surface. Index of short names to full station names: CapeT = "Cape Tribulation"; PortD = "Port Douglas"; Dbll = "Double Island"; Green = "Green Island"; York = "Yorkeys Knob"; Fairl = "Fairlead Buoy"; Fitz = "Fitzroy Reef"; High = "High Island"; Russ = "Russell Island"; Dunk = "Dunk Island"; Pelo = "Pelorus Island"; Pand = "Pandora Island"; Geoff = "Geoffery Bay"; Pine = "Pine Island".

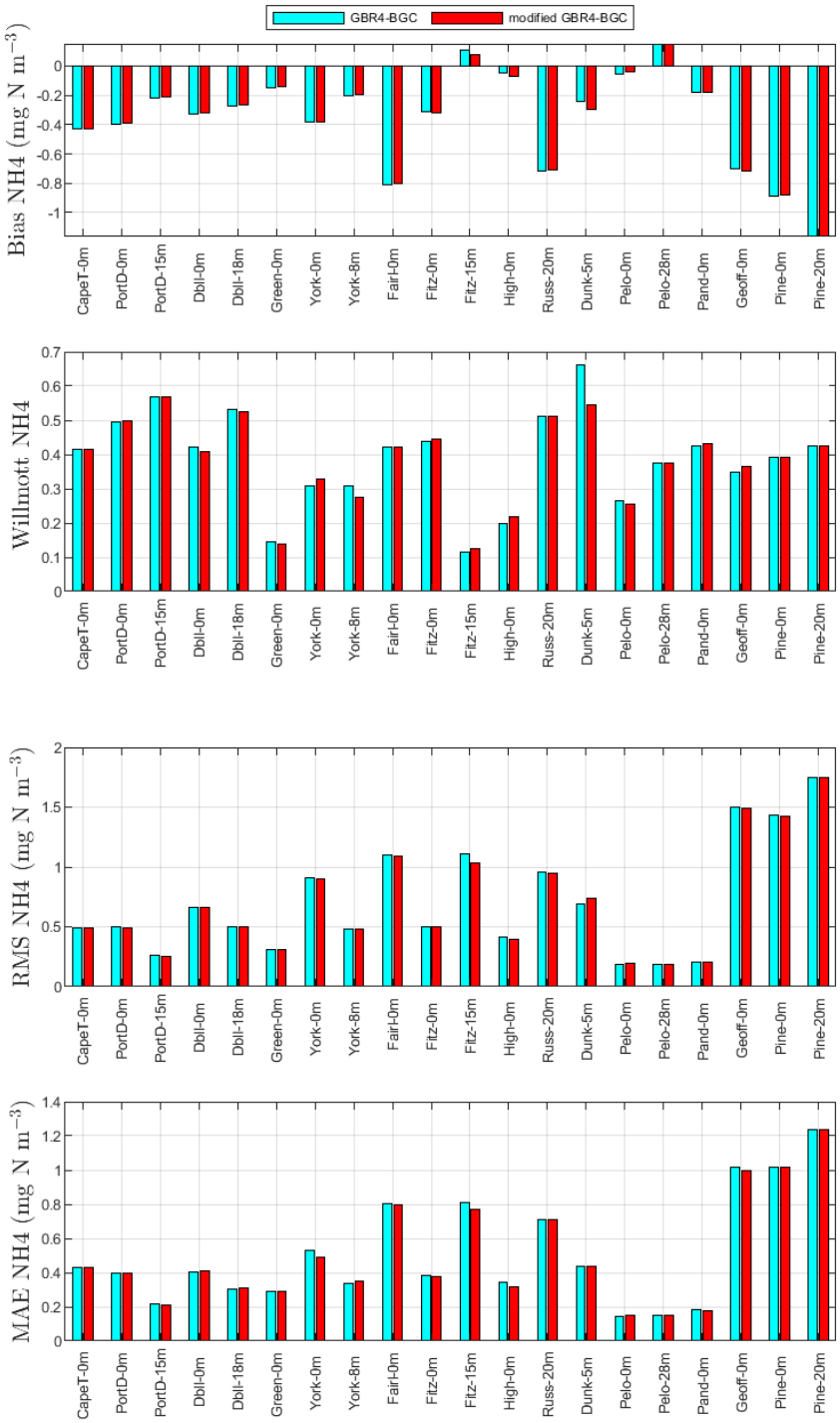

Figure 5.5: From top to bottom: bias, Willmott score, root mean square error and mean absolute error for simulated ammonium versus monthly observations from December 2010 to November 2012. Sites are arranged from North to South and locations are shown in Figure 5.3. See Figure 5.4 for more information on sites.

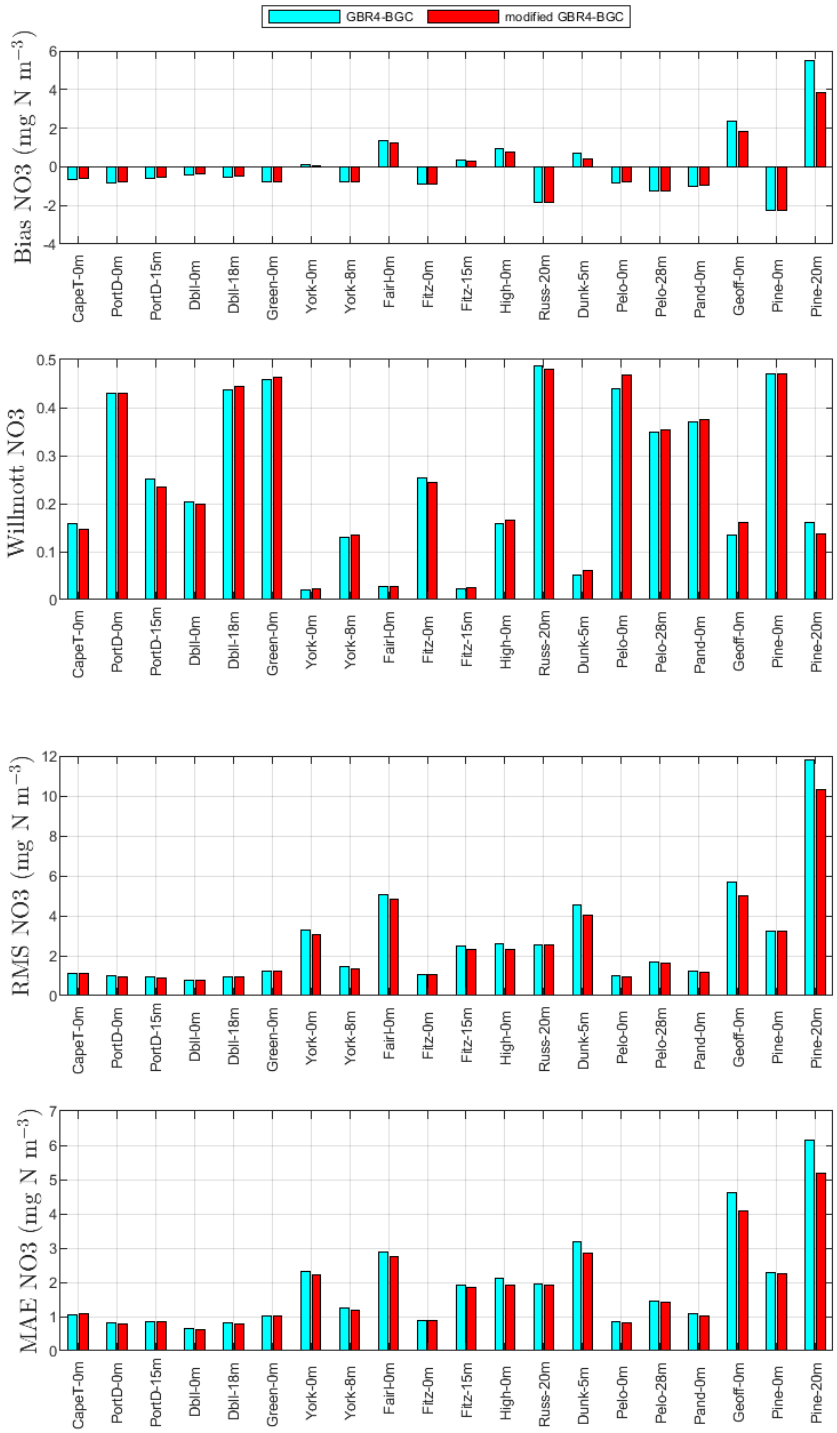

Figure 5.6: From top to bottom: bias, Willmott score, root mean square error and mean absolute error for simulated nitrate versus monthly observations from December 2010 to November 2012. Sites are arranged from North to South and locations are shown in Figure 5.3. See Figure 5.4 for more information on sites.

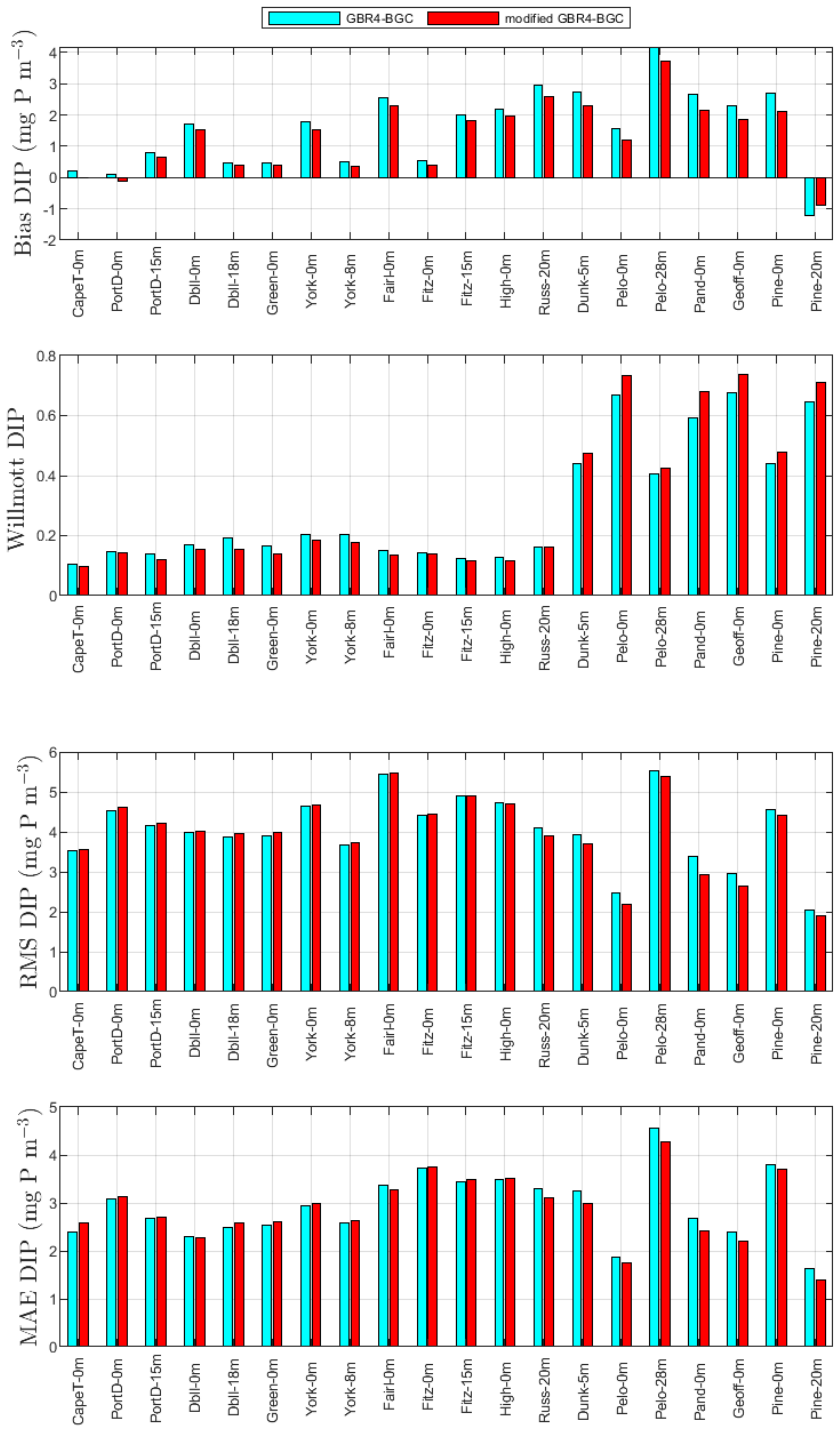

Figure 5.7: From top to bottom: bias, Willmott score, root mean square error and mean absolute error for simulated dissolved inorganic phosphorus (DIP) versus monthly observations from December 2010 to November 2012. Sites are arranged from North to South and locations are shown in Figure 5.3. See Figure 5.4 for more information on sites.

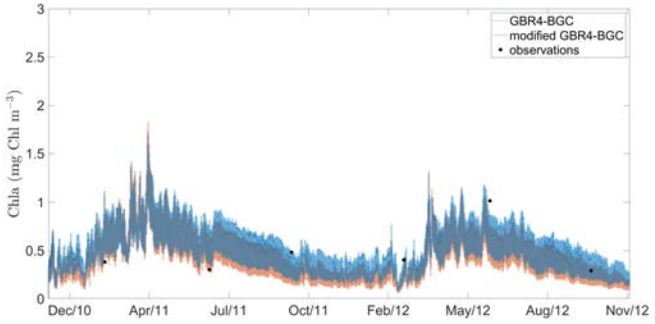

(a) Total chlorophyll a concentrations.

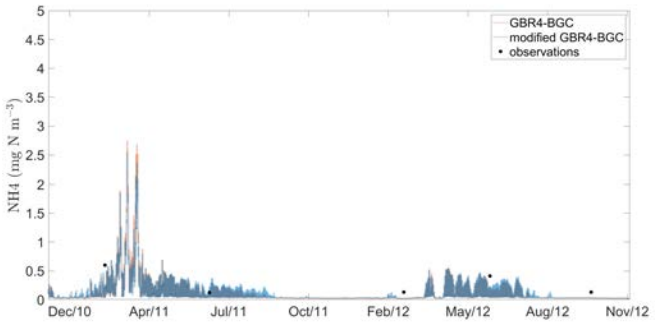

(b) NH_4 concentrations.

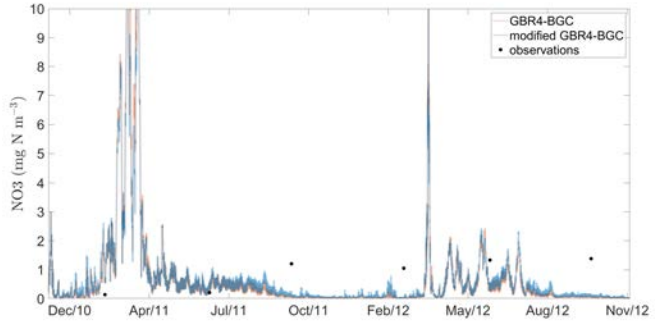

(c) NO_3 concentrations.

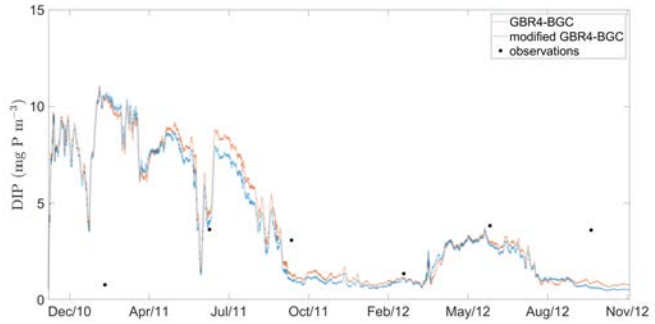

(d) DIP concentrations.

Figure 5.8: Comparison of the time series of simulated and observed chlorophyll a extractions, NH_4, NO_3 and DIP at 15 m Port Douglas. GBR4-BGC (orange), modified GBR4-BGC (blue) and observations (black).

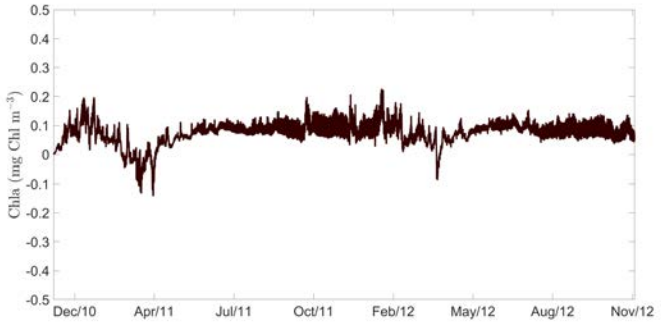

(a) Total chlorophyll a concentrations.

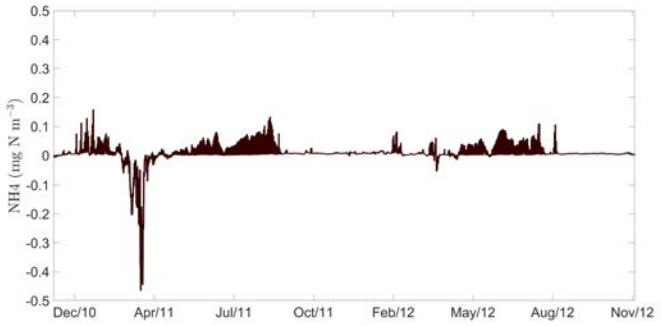

(b) NH_4 concentrations.

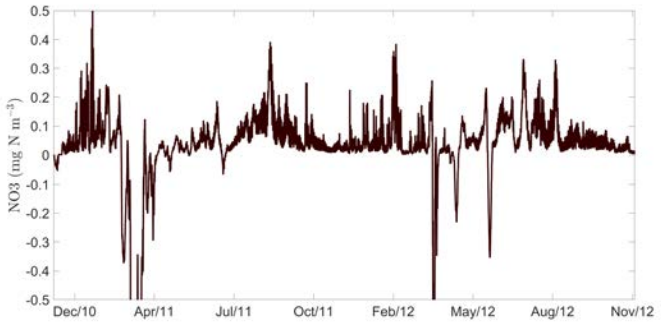

(c) NO_3 concentrations.

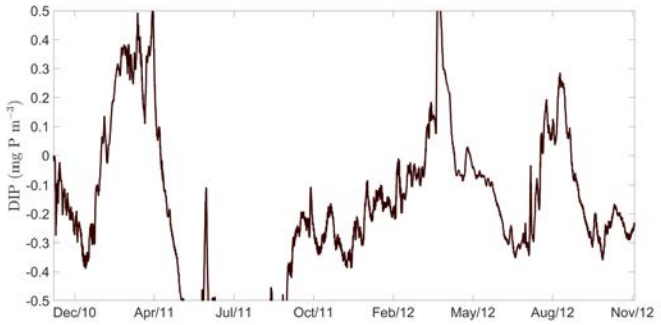

(d) DIP concentrations.

Figure 5.9: Difference between the time series of simulated chlorophyll a extractions, NH_4, NO_3 and DIP from modified GBR4-BGC and GBR4-BGC at 15 m Port Douglas.

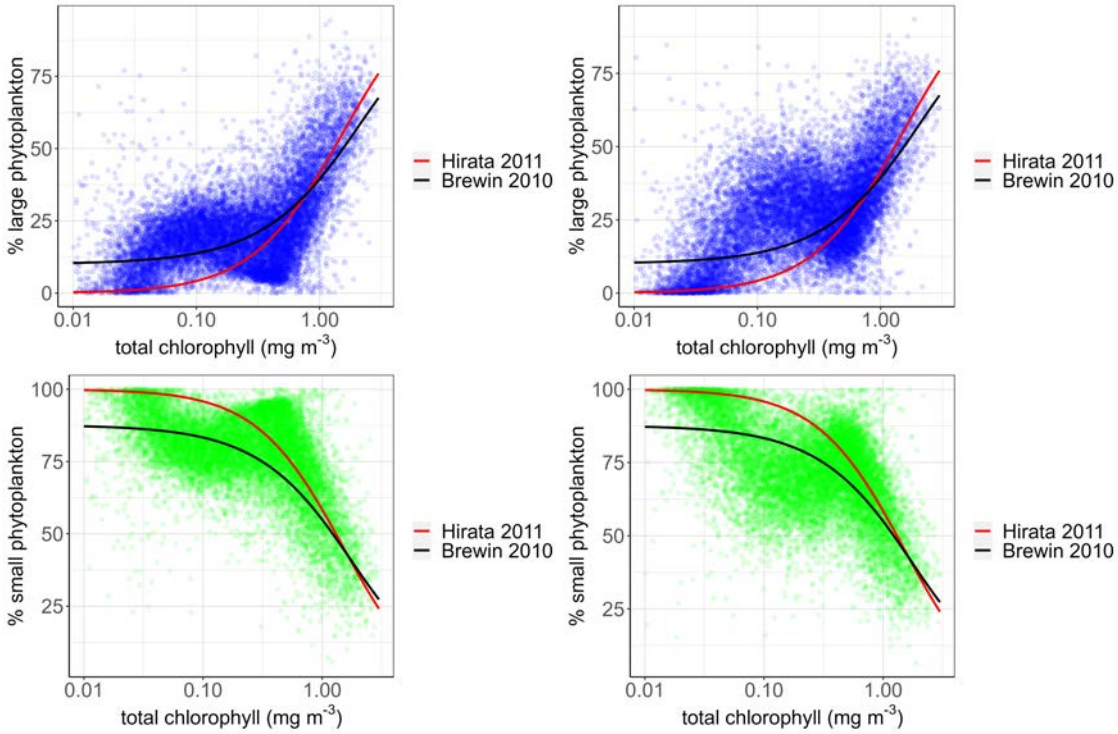

(a) GBR4-BGC.

(b) Modified GBR4-BGC.

Figure 5.10: Relationship between the percentage of randomly sampled simulated surface large phytoplankton and chlorophyll a concentrations (top), simulated surface small phytoplankton and chlorophyll a concentrations (bottom). Dots represent randomly sampled simulated data points and lines show fits to observations from a global marine database taken from Brewin et al. (2010); Hirata et al. (2011). Large phytoplankton comprises microphytoplankton and *Trichodesium* and small phytoplankton consists of nano- and pico-phytoplankton.

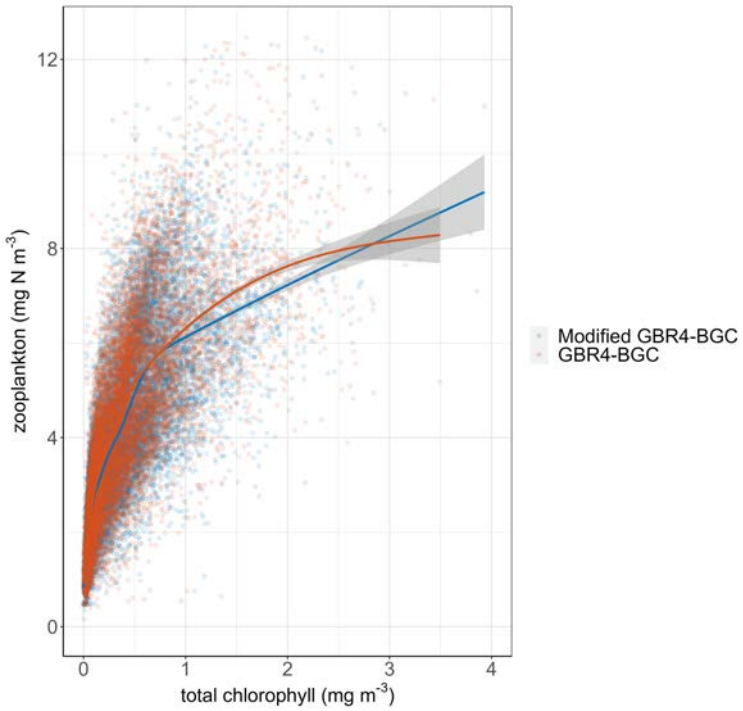

Figure 5.11: Relationship between 15,000 randomly sampled simulated surface zooplankton and chlorophyll a concentrations. The smoothing functions applied to the data are represented by lines and grey-shaded confidence intervals.

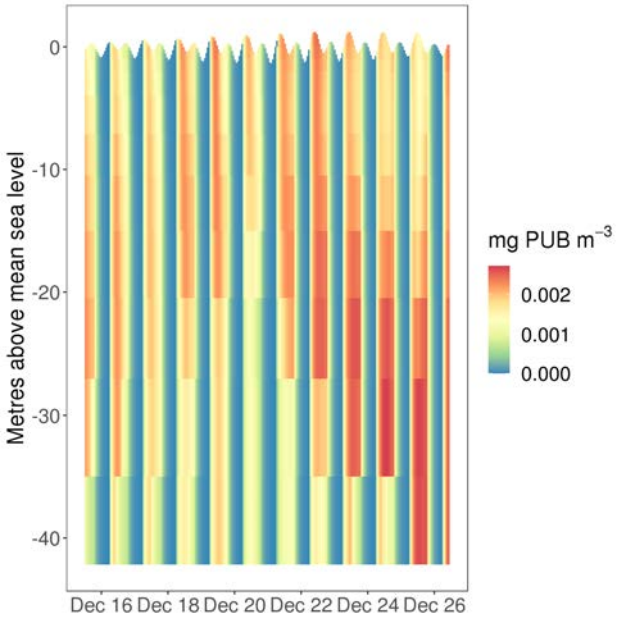

(a) *Trichodesmium* phycourobilin.

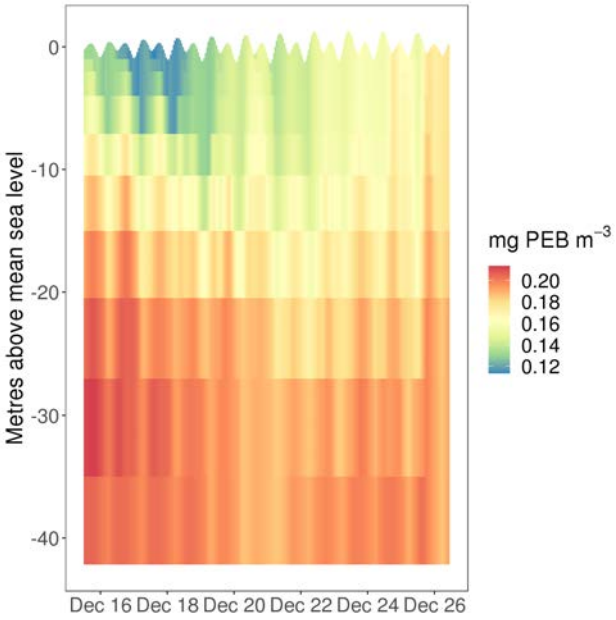

(b) *Trichodesmium* phycoerythrobilin.

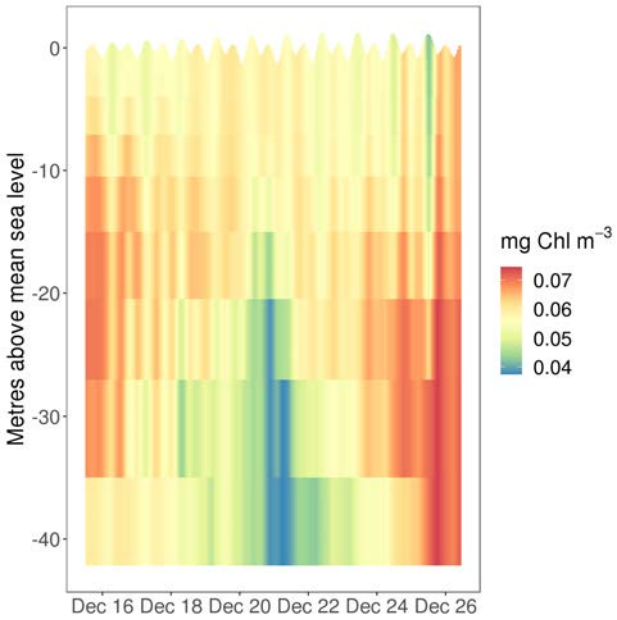

(c) *Trichodesmium* chlorophyll *a*.

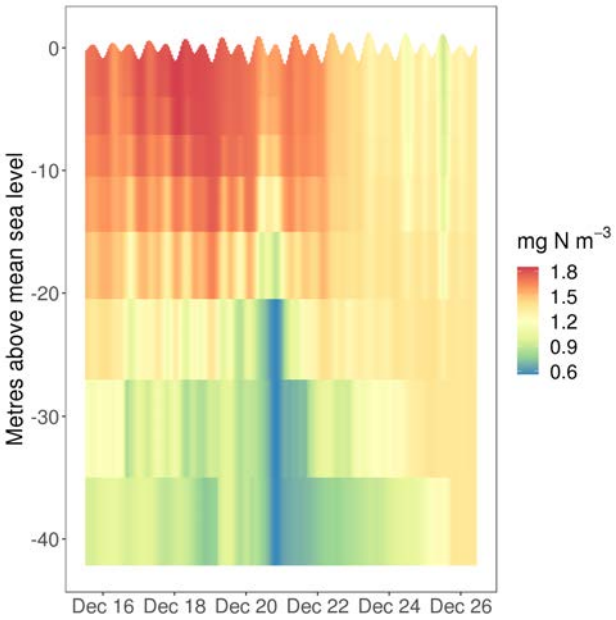

(d) *Trichodesmium* total nitrogen store.

Figure 5.12: Depth profile over time of simulated concentrations of intracellular *Trichodesmium* phycourobilin (PUB), phycoerythrobilin (PEB), chlorophyll *a* and total nitrogen store (combination of intracellular structural nitrogen and intracellular nitrogen reserves) at the geolocation (17.75°S, 146.6° E) from midday 15/12/2010 to midday 27/12/2010.

5.4 Discussion

Trichodesmium phycobilipigments enable the maximisation of photosynthetic efficiency, which is important for growth and surface bloom formation. Our model results show that *Trichodesmium* acclimates to high light conditions obtainable during the day and in surface waters by increasing the concentration of PUB and decreasing PEB concentrations (Figures 5.12a and 5.12b). Contrarily, in deep waters or dark conditions, *Trichodesmium* PUB concentrations decreased and PEB concentrations increased. These results agree with the suggestions of Subramaniam et al. (1999), which include an increase in PUB concentrations and decrease in PEB concentrations when irradiance is high. Additionally, they suggested that the increase in PUB concentrations when light conditions are high may serve as photoprotection since the photons absorbed by PUB are emitted.

Simulated *Trichodesmium* total nitrogen stores are shown to be maximal at the surface and decreased with depth (Figure 5.12d). This is likely due to the acclimation of *Trichodesmium* to high irradiance. *Trichodesmium* acclimation to high light has been associated with increased growth due to reduced cell size, reduction of light-harvesting pigments and increased synthesis of light-protective pigments (Andresen et al., 2010). Furthermore, the interacting effects of other environmental variables in the GBR such as dissolved inorganic nitrogen (DIN) and temperature on *Trichodesmium* growth might have contributed to decreased *Trichodesmium* biomass in deep waters. This is because increased DIN concentrations and reduced temperatures have been suggested to inhibit *Trichodesmium* growth in GBR deep waters (Ani et al., 2023).

PEB is a major light-harvesting pigment and is essential for photosynthesis. A decrease in PEB concentrations in surface waters should lead to reduced light absorption and consequently a decrease in growth. However, our results show that *Trichodesmium* nitrogen stores — consist of structural material used for growth — are highest at the surface. Likewise, increased PEB concentrations in deep and dark conditions should enhance *Trichodesmium* growth but simulated *Trichodesmium* nitrogen stores are shown to reduce with depth. These could be due to the influence of a combination of various environmental factors such as temperature, nutrient availability and light on *Trichodesmium* growth. Therefore, while changes in PEB concentrations will impact growth, this impact can be offset by the interacting effects of other important environmental factors.

The model formulations developed in this study more accurately presents what is known about *Trichodesmium* photophysiology and have been shown to alter simulated *Trichodesmium* dynamics. However, some important processes that drive *Trichodesmium* dynamics have not been implemented in our model. For example, the limitation of *Trichodesmium* growth by iron (Sohm et al., 2011), effects of salinity on *Trichodesmium* growth, nitrogen fixation and pigmentation (Fu and Bell, 2003), and wind effects on *Trichodesmium* vertical movement (Capone et al., 1997) are not represented in the model.

5.5 Conclusions

In this study, new formulations for *Trichodesmium* optics were developed for improved parameterisation of the *Trichodesmium* growth submodel of the eReefs marine biogeochemical models. Although these new formulations should improve model predictions and have been shown to modify the dynamics of simulated *Trichodesmium* populations, we do not have sufficient *Trichodesmium* observational data to assess whether this has made the model more accurate. The skill of the modified model when compared against available monitoring data (surface chlorophyll *a* and nutrient concentrations) is similar to that of the version in (Baird et al., 2020) and is slightly worse where it is different.

To increase our confidence in the modified model's predictions, it is critical to validate *Trichodesmium* concentrations, PEB or PUB concentrations, and/or nitrogen fixation rates against observations. Additional improvements to the model could include representing the role of iron in nitrogen fixation or simulating the dynamics of *Trichodesmium* colony formation and growth, however both of these would require additional observational and experimental data.

6. Summary and Conclusions

The previous chapters of this thesis presented an effort to modify EMS-BGC and apply the EMS for efficient spatial management by investigating *Trichodesmium* dynamics in the GBR.

In the first chapter, the parameterisation of important biogeochemical processes in EMS-BGC was compared with three other leading coastal biogeochemical models, namely ERSEM, AED and GEM. The study reported that EMS-BGC does not consider the impacts of extreme events and the adaptation of marine organisms to climate change impacts and presented important biogeochemical processes that need to be improved. The use of exponential temperature response functions for all physiological rates of marine organisms modelled in EMS-BGC is not suitable for the reoccurring extreme temperature conditions in the GBR and the use of optimum response functions was recommended. The study highlighted the importance of incorporating the effects of ocean acidification on the physiology of marine organisms modelled in EMS-BGC as ocean acidification has been suggested to affect the physiology of some marine organisms. A further recommendation includes the incorporation of the adaptation of marine organisms to changing environmental conditions in EMS-BGC as these marine organisms have been reported to possess the potential to adapt to extreme environmental conditions. These findings helped set the context for the improvement of EMS-BGC and the application of EMS to the investigation of nutrient cycling and climate change impacts on the GBR ecosystem.

Chapter 2 presented a review on marine ecosystem parameters and processes that are modified by climate change and their representations in biogeochemical ecosystem models. The study found that the limits of the distribution and productivity of phytoplankton and other marine organisms depend on their physiological tolerance to extreme temperatures and elevated pCO_2. The study results indicated the need for more experimental studies and observational datasets, and synergy between experimental (observational) scientists and marine modellers for adequate model parameterisation. This is because improved collection of detailed and long-term observational datasets would help improve the assessment, accuracy and reliability of marine ecosystem response model predictions. The review study recommended the inclusion of important marine ecosystem parameters that are modified by climate change in marine response models and the use of ensemble modelling approaches for better uncertainty analysis. Future modelling studies were recommended to continue coupling regional models with hydrological models at catchment scales to capture climate variability and provide information on underlying hydrological processes. These recommendations would help improve the assessment, accuracy and reliability of marine ecosystem response model predictions of climate change impacts.

The *Trichodesmium* growth model of EMS-BGC was modified by optimally parameterising the temperature dependence of *Trichodesmium* physiological processes in Chapter 3, with knowledge gained from Chapter 2 since *Trichodesmium* dynamics is likely to change due to climate change impacts. This captured the ongoing temperature increases occurring in the GBR. The contribution of *Trichodesmium* to the total annual nitrogen budget of the GBR was estimated for the areas of GBRMP and GBR cross-shelf waters. The model results suggested that nitrogen fixation by *Trichodesmium* in the GBR contributed approximately 0.5 MT/yr, exceeding the total average annual riverine nitrogen loads (0.05–0.08 MT/yr). Nitrogen fixation loads are exceeded by riverine loads only if the comparison is restricted to inshore waters and during the wet season. The river pollution was suggested to likely impact freshwater wetlands, mangroves, seagrasses and in-shore coral reefs; while *Trichodesmium* blooms are likely to be less intense but more widespread and affect offshore coral reefs and other oceanic ecosystems. Phosphorus and iron were identified as potential drivers of *Trichodesmium* growth and nitrogen fixation. Although the model result is provisional due to limited observations for model assessment, the model outputs reinforced the

need for more detailed assessment and reliable quantification of the annual nitrogen contribution from nitrogen fixation in the GBR and other coastal waters. Such advances will improve understandings of the role of terrestrial nitrogen loads in the GBR and of terrestrial phosphorus and iron loads which can modulate *Trichodesmium* abundance. The model findings will help to broaden the focus of water quality management programs and support management to improve GBR water quality.

In Chapter 4, the *Trichodesmium* growth submodel of the eReefs biogeochemical models was modified by applying the form resistance factor to the sinking velocities of tuft-shaped *Trichodesmium* colonies in the GBR. The improved model results compared well with observations from the Australian Institute of Marine Science Marine Monitoring Program sensor network sites and captured the emergent patterns of phytoplankton size spectrum observed in nature. The modified model formulations improved the physiological realism of the *Trichodesmium* growth submodel of the eReefs marine biogeochemical models, and can help to improve the understanding of *Trichodesmium* dynamics for effective GBR water quality management. The model results suggested that observations of the presence or absence of *Trichodesmium* surface blooms are not sufficient to characterise the role of this cyanobacterium in the GBR and highlighted the need for enhanced *Trichodesmium* monitoring for better model evaluation.

The variation of the major light-harvesting *Trichodesmium* phycobilipigments (phycourobilin (PUB) and phycoerythrobilin (PEB)) under varying light conditions was represented in the *Trichodesmium* growth submodel of the eReefs biogeochemical model in Chapter 5. This involved parameterising the interconversion between PUB and PEB, and the photosystem II reaction centre dynamics. The new formulations should improve model predictions and have been shown to modify the dynamics of simulated *Trichodesmium* populations. However, due to limited availability of *Trichodesmium* observational data the accuracy of the improved model was not assessed. The skill of the modified model when compared against available monitoring data (surface chlorophyll *a* and nutrient concentrations) was similar to that of the original eReefs model. Also, the model results support previous findings on the need for sufficient *Trichodesmium* observations for model validation.

In conclusion, the modelling approach used in this study provides a valuable perspective on spatial and temporal variability of *Trichodesmium*, which is critical for targeted monitoring and management —- from assessing exposure and risks to developing adaptive management approaches. Targeted monitoring will help provide field observations for the evaluation of the accuracy of EMS and satellite-derived estimates of fixed nitrogen, measurements of iron riverine loads and will help commence iron studies in the GBR, whereas targeted management will help increase the impacts of spatially limited GBR water quality management plans. Finally, this research work recognises that the EMS is not a perfect model and recommends continuous model improvement and validation for reliable and accurate predictions of climate change impacts on the GBR.

References

O. Aburto-Oropeza, E. Ezcurra, G. Danemann, V. Valdez, J. Murray, and E. Sala. Mangroves in the Gulf of California increase fishery yields. *Proceedings of the National Academy of Sciences*, 105(30): 10456–10459, 2008.

R. Albright, K. R. Anthony, M. Baird, R. Beeden, M. Byrne, C. Collier, S. Dove, K. Fabricius, O. Hoegh-Guldberg, R. P. Kelly, et al. Ocean acidification: Linking science to management solutions using the Great Barrier Reef as a case study. *Journal of Environmental Management*, 182:641–650, 2016.

M. Alcaraz, J. Felipe, U. Grote, E. Arashkevich, and A. Nikishina. Life in a warming ocean: thermal thresholds and metabolic balance of Arctic zooplankton. *Journal of Plankton Research*, 36(1):3–10, 2014.

A.-C. Alderkamp, E. Sintes, and G. J. Herndl. Abundance and activity of major groups of prokaryotic plankton in the coastal North Sea during spring and summer. *Aquatic microbial ecology*, 45(3): 237–246, 2006.

C. Alessi, F. Giomi, F. Furnari, G. Sarà, R. Chemello, and M. Milazzo. Ocean acidification and elevated temperature negatively affect recruitment, oxygen consumption and calcification of the reef-building *Dendropoma cristatum* early life stages: Evidence from a manipulative field study. *Science of The Total Environment*, 693:133476, 2019.

A. Allin, G. Schernewski, R. Friedland, T. Neumann, and H. Radtke. Climate change effects on denitrification and associated avoidance costs in three Baltic river basin-coastal sea systems. *Journal of Coastal Conservation*, 21(4):561–569, 2017.

G. S. Andersen, M. F. Pedersen, and S. L. Nielsen. Temperature acclimation and heat tolerance of photosynthesis in Norwegian *Saccharina latissima* (*Laminariales, Phaeophyceae*). *Journal of phycology*, 49(4):689–700, 2013.

A. Andersson, P. Haecky, and Å. Hagström. Effect of temperature and light on the growth of micro-nano-and pico-plankton: impact on algal succession. *Marine Biology*, 120(4):511–520, 1994.

A. Andersson, I. Kuffner, F. Mackenzie, P. Jokiel, K. Rodgers, and A. Tan. Net Loss of $CaCO_3$ from a subtropical calcifying community due to seawater acidification: mesocosm-scale experimental evidence. *Biogeosciences*, 6(8):1811–1823, 2009.

E. Andresen, J. Lohscheider, E. Šetlikova, I. Adamska, M. Šimek, and H. Küpper. Acclimation of *Trichodesmium erythraeum ISM101* to high and low irradiance analysed on the physiological, biophysical and biochemical level. *New Phytologist*, 185(1):173–188, 2010.

T. Andrews, B. Clough, and G. Muller. Photosynthetic gas exchange properties and carbon isotope ratios of some mangroves in North Queensland. In *Physiology and management of mangroves*, pages 15–23. Springer, 1984.

C. J. Ani and B. Robson. Responses of marine ecosystems to climate change impacts and their treatment in biogeochemical ecosystem models. *Marine Pollution Bulletin*, 166:112223, 2021.

C. J. Ani, S. G. Smithers, S. Lewis, M. Baird, and B. Robson. eReefs modelling suggests *Trichodesmium* may be a major nitrogen source in the Great Barrier Reef. *Estuarine, Coastal and Shelf Science*, page 108306, 2023.

K. R. Anthony, S. R. Connolly, and O. Hoegh-Guldberg. Bleaching, energetics, and coral mortality risk: Effects of temperature, light, and sediment regime. *Limnology and oceanography*, 52(2):716–726, 2007.

G. B. Arhonditsis and M. T. Brett. Evaluation of the current state of mechanistic aquatic biogeochemical modeling. *Marine Ecology Progress Series*, 271:13–26, 2004.

A. Arias-Ortiz, O. Serrano, P. Masqué, P. S. Lavery, U. Mueller, G. A. Kendrick, M. Rozaimi, A. Esteban, J. W. Fourqurean, N. Marbà, et al. A marine heatwave drives massive losses from the world's largest seagrass carbon stocks. *Nature Climate Change*, 8(4):338, 2018.

N. W. Arnell and S. N. Gosling. The impacts of climate change on river flow regimes at the global scale. *Journal of Hydrology*, 486:351–364, 2013.

E. Asbridge, R. Lucas, K. Rogers, and A. Accad. The extent of mangrove change and potential for recovery following severe Tropical Cyclone Yasi, Hinchinbrook Island, Queensland, Australia, 2018.

Australian Community Climate and Earth-System Simulator. ACCESS NWP Data Information. http://www.bom.gov.au/nwp/doc/access/NWPData.shtml, Accessed September 2019.

Australian Institute of Marine Science (AIMS), 2023. Great Barrier Reef Marine Monitoring Program for Inshore Water Quality (MMP WQ). https://apps.aims.gov.au/metadata/view/2b2aa4e4-1368-49e0-8b25-1559ee297854, Accessed 10 December 2020.

R. C. Babcock, J. M. Dambacher, E. B. Morello, É. E. Plagányi, K. R. Hayes, H. P. Sweatman, and M. S. Pratchett. Assessing different causes of crown-of-thorns starfish outbreaks and appropriate responses for management on the Great Barrier Reef. *PLoS One*, 11(12):e0169048, 2016.

M. Baird, K. Wild-Allen, J. Parslow, M. Mongin, B. Robson, J. Skerratt, F. Rizwi, M. Soja-Wozniak, E. Jones, M. Herzfeld, et al. CSIRO Environmental Modelling Suite (EMS): scientific description of the optical and biogeochemical models (vB3p0). *Geoscientific Model Development*, 13:4503–4553, 2020.

M. E. Baird, P. J. Ralph, F. Rizwi, K. Wild-Allen, and A. D. Steven. A dynamic model of the cellular carbon to chlorophyll ratio applied to a batch culture and a continental shelf ecosystem. *Limnology and oceanography*, 58(4):1215–1226, 2013.

M. E. Baird, M. Mongin, F. Rizwi, L. K. Bay, N. E. Cantin, M. Soja-Woźniak, and J. Skerratt. A mechanistic model of coral bleaching due to temperature-mediated light-driven reactive oxygen build-up in zooxanthellae. *Ecological Modelling*, 386:20–37, 2018.

M. E. Baird, M. Mongin, J. Skerratt, N. Margvelashvili, S. Tickell, A. D. Steven, C. Robillot, R. Ellis, D. Waters, P. Kaniewska, et al. Impact of catchment-derived nutrients and sediments on marine water quality on the Great Barrier Reef: An application of the eReefs marine modelling system. *Marine Pollution Bulletin*, 167:112297, 2021.

A. Bakun. Global climate change and intensification of coastal ocean upwelling. *Science*, 247(4939): 198–201, 1990.

A. Bakun, B. A. Black, S. J. Bograd, M. Garcia-Reyes, A. J. Miller, R. R. Rykaczewski, and W. J. Sydeman. Anticipated effects of climate change on coastal upwelling ecosystems. *Current Climate Change Reports*, 1(2):85–93, 2015.

M. Ball, M. Cochrane, and H. Rawson. Growth and water use of the mangroves *Rhizophora apiculata* and *R. stylosa* in response to salinity and humidity under ambient and elevated concentrations of atmospheric CO_2. *Plant, Cell & Environment*, 20(9):1158–1166, 1997.

M. Barange, M. Butenschön, A. Yool, N. Beaumont, J. A. Fernandes, A. P. Martin, and J. Allen. The cost of reducing the North Atlantic Ocean biological carbon pump. *Frontiers in Marine Science*, 3: 290, 2017.

E. B. Barbier. Marine ecosystem services. *Current Biology*, 27(11):R507–R510, 2017.

D. Barcellos, H. M. Queiroz, G. N. Nóbrega, R. L. de Oliveira Filho, S. T. Santaella, X. L. Otero, and T. O. Ferreira. Phosphorus enriched effluents increase eutrophication risks for mangrove systems in northeastern Brazil. *Marine pollution bulletin*, 142:58–63, 2019.

H. C. Barkley, A. L. Cohen, N. R. Mollica, R. E. Brainard, H. E. Rivera, T. M. DeCarlo, G. P. Lohmann, E. J. Drenkard, A. E. Alpert, C. W. Young, et al. Repeat bleaching of a central Pacific coral reef over the past six decades (1960–2016). *Communications biology*, 1(1):1–10, 2018.

N. R. Bates, Y. M. Astor, M. J. Church, K. Currie, J. E. Dore, M. González-Dávila, L. Lorenzoni, F. Muller-Karger, J. Olafsson, and J. M. Santana-Casiano. A Time-Series View of Changing Surface Ocean Chemistry Due to Ocean Uptake of Anthropogenic CO_2 and Ocean Acidification. *Oceanography*, 27(1):126–141, 2014.

B. Bauer, H. M. Meier, M. Casini, A. Hoff, P. Margoński, A. Orio, S. Saraiva, J. Steenbeek, M. T. Tomczak, and H. editor: Marta Coll. Reducing eutrophication increases spatial extent of communities supporting commercial fisheries: a model case study. *ICES Journal of Marine Science*, 75(4):1306–1317, 2018.

R. Beeden, J. Maynard, M. Puotinen, P. Marshall, J. Dryden, J. Goldberg, and G. Williams. Impacts and recovery from severe tropical Cyclone Yasi on the Great Barrier Reef. *PloS one*, 10(4):e0121272, 2015.

M. J. Behrenfeld, R. T. O'Malley, D. A. Siegel, C. R. McClain, J. L. Sarmiento, G. C. Feldman, A. J. Milligan, P. G. Falkowski, R. M. Letelier, and E. S. Boss. Climate-driven trends in contemporary ocean productivity. *Nature*, 444(7120):752–755, 2006.

P. Bell, I. Elmetri, and P. Uwins. Nitrogen fixation by *Trichodesmium spp.* in the Central and Northern Great Barrier Reef Lagoon: relative importance of the fixed-nitrogen load. *Marine Ecology Progress Series*, 186:119–126, 1999.

P. R. Bell. Analysis of satellite imagery using a simple algorithm supports evidence that *Trichodesmium* supplies a significant new nitrogen load to the GBR lagoon. *Ambio*, 50(6):1200–1210, 2021.

P. R. Bell and F.-X. Fu. Effect of light on growth, pigmentation and N_2 fixation of cultured *Trichodesmium* sp. from the Great Barrier Reef lagoon. *Hydrobiologia*, 543(1):25–35, 2005.

P. R. Bell, P. J. Uwins, I. Elmetri, J. A. Phillips, F.-X. Fu, and A. J. Yago. Laboratory culture studies of *Trichodesmium* isolated from the Great Barrier Reef Lagoon, Australia. *Hydrobiologia*, 532(1-3): 9–21, 2005.

P. R. Bell, I. Elmetri, and B. E. Lapointe. Evidence of large-scale chronic eutrophication in the Great Barrier Reef: quantification of chlorophyll a thresholds for sustaining coral reef communities. *Ambio*, 43(3):361–376, 2014.

A. Belperio. Terrigenous sedimentation in the central Great Barrier Reef lagoon: a model from the Burdekin region. *BMR Journal of Australian Geology and Geophysics*, 8(3):179–190, 1983.

M. Benavides, S. Bonnet, F. A. Le Moigne, G. Armin, K. Inomura, S. Hallstrøm, L. Riemann, I. Berman-Frank, E. Poletti, M. Garel, et al. Sinking *Trichodesmium* fixes nitrogen in the dark ocean. *The ISME Journal*, pages 1–8, 2022.

E. M. Bendif, I. Probert, J. R. Young, and P. von Dassow. Morphological and phylogenetic characterization of new *Gephyrocapsa* isolates suggests introgressive hybridization in the *Emiliania/Gephyrocapsa* complex (haptophyta). *Protist*, 166(3):323–336, 2015.

L. Bengtsson, M. Botzet, and M. Esch. Will greenhouse gas-induced warming over the next 50 years lead to higher frequency and greater intensity of hurricanes? *Tellus A*, 48(1):57–73, 1996.

B. Bergman, G. Sandh, S. Lin, J. Larsson, and E. J. Carpenter. *Trichodesmium*–a widespread marine cyanobacterium with unusual nitrogen fixation properties. *FEMS microbiology reviews*, 37(3):286–302, 2013.

R. Berkelmans, S. J. Weeks, and C. R. Steinberga. Upwelling linked to warm summers and bleaching on the Great Barrier Reef. *Limnology and Oceanography*, 55(6):2634–2644, 2010.

J. R. Bermúdez, U. Riebesell, A. Larsen, and M. Winder. Ocean acidification reduces transfer of essential biomolecules in a natural plankton community. *Scientific reports*, 6:27749, 2016.

L. Beversdorf, A. White, K. Björkman, R. Letelier, and D. Karl. Phosphonate metabolism by *Trichodesmium* IMS101 and the production of greenhouse gases. *Limnology and oceanography*, 55(4): 1768–1778, 2010.

A. Bhattachan, M. Jurjonas, A. Moody, P. Morris, G. Sanchez, L. Smart, P. Taillie, R. Emanuel, and E. Seekamp. Sea level rise impacts on rural coastal social-ecological systems and the implications for decision making. *Environmental Science & Policy*, 90:122–134, 2018.

L. Bianucci, K. Fennel, D. Chabot, N. Shackell, and D. Lavoie. Ocean biogeochemical models as management tools: a case study for Atlantic wolffish and declining oxygen. *ICES Journal of Marine Science*, 73(2):263–274, 2015.

A. N. Blauw, H. F. Los, M. Bokhorst, and P. L. Erftemeijer. GEM: a generic ecological model for estuaries and coastal waters. *Hydrobiologia*, 618(1):175, 2009.

D. Blondeau-Patissier, V. E. Brando, C. Lønborg, S. M. Leahy, and A. G. Dekker. Phenology of *Trichodesmium* spp. blooms in the Great Barrier Reef lagoon, Australia, from the ESA-MERIS 10-year mission. *PloS one*, 13(12):e0208010, 2018.

E. Bonsdorff. Eutrophication: Early warning signals, ecosystem-level and societal responses, and ways forward. *Ambio*, 50(4):753–758, 2021.

S. Bonthu, D. Ganguly, P. Ramachandran, R. Ramachandran, A. K. Pattnaik, and E. Wolanski. Both riverine detritus and dissolved nutrients drive lagoon fisheries. *Estuarine, Coastal and Shelf Science*, 183:360–369, 2016.

G. A. Borstad, E. J. Carpenter, and J. F. Gower. Development of algorithms for remote sensing of *Trichodesmium* blooms. In *Marine pelagic cyanobacteria: Trichodesmium and other diazotrophs*, pages 193–210. Springer, 1992.

J. Borum, O. Pedersen, L. Kotula, M. W. Fraser, J. Statton, T. D. Colmer, and G. A. Kendrick. Photosynthetic response to globally increasing CO_2 of co-occurring temperate seagrass species. *Plant, Cell & Environment*, 39(6):1240–1250, 2016.

D. Böttjer, D. M. Karl, R. M. Letelier, D. A. Viviani, and M. J. Church. Experimental assessment of diazotroph responses to elevated seawater pCO_2 in the North Pacific Subtropical Gyre. *Global biogeochemical cycles*, 28(6):601–616, 2014.

P. W. Boyd, T. A. Rynearson, E. A. Armstrong, F. Fu, K. Hayashi, Z. Hu, D. A. Hutchins, R. M. Kudela, E. Litchman, M. R. Mulholland, et al. Marine phytoplankton temperature versus growth responses from polar to tropical waters–outcome of a scientific community-wide study. *PloS one*, 8(5):e63091, 2013.

R. E. Brainard, T. Oliver, M. J. McPhaden, A. Cohen, R. Venegas, A. Heenan, B. Vargas-Ángel, R. Rotjan, S. Mangubhai, E. Flint, et al. Ecological impacts of the 2015/16 El Niño in the central equatorial Pacific. *Bulletin of the American Meteorological Society*, 99(1):S21–S26, 2018.

E. Breitbarth, A. Oschlies, and J. LaRoche. Physiological constraints on the global distribution of *Trichodesmium*? effect of temperature on diazotrophy. *Biogeosciences*, 4(1):53–61, 2007.

E. Breitbarth, J. Wohlers, J. Kläs, J. LaRoche, and I. Peeken. Nitrogen fixation and growth rates of *Trichodesmium* IMS-101 as a function of light intensity. *Marine Ecology Progress Series*, 359:25–36, 2008.

R. J. Brewin, S. Sathyendranath, T. Hirata, S. J. Lavender, R. M. Barciela, and N. J. Hardman-Mountford. A three-component model of phytoplankton size class for the Atlantic Ocean. *Ecological Modelling*, 221(11):1472–1483, 2010.

A. J. Broccoli and S. Manabe. Can existing climate models be used to study anthropogenic changes in tropical cyclone climate? *Geophysical Research Letters*, 17(11):1917–1920, 1990.

J. Brodie, T. Schroeder, K. Rohde, J. Faithful, B. Masters, A. Dekker, V. Brando, and M. Maughan. Dispersal of suspended sediments and nutrients in the Great Barrier Reef lagoon during river-discharge events: conclusions from satellite remote sensing and concurrent flood-plume sampling. *Marine and Freshwater Research*, 61(6):651–664, 2010.

J. Brodie, M. Devlin, D. Haynes, and J. Waterhouse. Assessment of the eutrophication status of the Great Barrier Reef lagoon (Australia). *Biogeochemistry*, 106(2):281–302, 2011.

J. E. Brodie. *2013 Scientific Consensus Statement: Land Use Impacts on the Great Barrier Reef Water Quality and Ecosystem Condition*. Reef Water Quality Protection Plan Secretariat, 2013.

J. E. Brodie, F. Kroon, B. Schaffelke, E. Wolanski, S. Lewis, M. Devlin, I. Bohnet, Z. Bainbridge, J. Waterhouse, and A. Davis. Terrestrial pollutant runoff to the Great Barrier Reef: an update of issues, priorities and management responses. *Marine pollution bulletin*, 65(4-9):81–100, 2012.

B. Brown. Coral bleaching: causes and consequences. *Coral reefs*, 16(1):S129–S138, 1997.

C. A. Brown, D. Sharp, and T. C. M. Collura. Effect of climate change on water temperature and attainment of water temperature criteria in the Yaquina Estuary, Oregon (USA). *Estuarine, Coastal and Shelf Science*, 169:136–146, 2016.

J. F. Bruno, A. E. Bates, C. Cacciapaglia, E. P. Pike, S. C. Amstrup, R. van Hooidonk, S. A. Henson, and R. B. Aronson. Climate change threatens the world's marine protected areas. *Nature Climate Change*, 8(6):499–503, 2018.

A. Bryndum-Buchholz, D. P. Tittensor, J. L. Blanchard, W. W. Cheung, M. Coll, E. D. Galbraith, S. Jennings, O. Maury, and H. K. Lotze. Twenty-first-century climate change impacts on marine animal biomass and ecosystem structure across ocean basins. *Global change biology*, 25(2):459–472, 2019.

A. Buchan, J. M. González, and M. A. Moran. Overview of the marine Roseobacter lineage. *Applied and environmental microbiology*, 71(10):5665–5677, 2005.

P. Buerger, C. Alvarez-Roa, C. Coppin, S. Pearce, L. Chakravarti, J. Oakeshott, O. Edwards, and M. van Oppen. Heat-evolved microalgal symbionts increase coral bleaching tolerance. *Science Advances*, 6 (20):eaba2498, 2020.

D. A. Bulthuis. Effects of temperature on photosynthesis and growth of seagrasses. *Aquatic Botany*, 27(1):27–40, 1987.

O. W. Burnell, S. D. Connell, A. D. Irving, J. R. Watling, and B. D. Russell. Contemporary reliance on bicarbonate acquisition predicts increased growth of seagrass *Amphibolis antarctica* in a high-CO_2 world. *Conservation physiology*, 2(1), 2014.

J. A. Burt, F. Paparella, N. Al-Mansoori, A. Al-Mansoori, and H. Al-Jailani. Causes and consequences of the 2017 coral bleaching event in the southern Persian/Arabian Gulf. *Coral Reefs*, 38(4):567–589, 2019.

M. Butenschon, J. Clark, J. N. Aldridge, J. I. Allen, Y. Artioli, J. Blackford, J. Bruggeman, P. Cazenave, S. Ciavatta, S. Kay, et al. ERSEM 15.06: a generic model for marine biogeochemistry and the ecosystem dynamics of the lower trophic levels. *Geoscientific Model Development*, 9(4):1293–1339, 2016.

X. Cai, K. Gao, F. Fu, D. A. Campbell, J. Beardall, and D. A. Hutchins. Electron transport kinetics in the diazotrophic cyanobacterium *Trichodesmium* spp. grown across a range of light levels. *Photosynthesis research*, 124(1):45–56, 2015.

D. G. Capone, J. P. Zehr, H. W. Paerl, B. Bergman, and E. J. Carpenter. *Trichodesmium*, a globally significant marine cyanobacterium. *Science*, 276(5316):1221–1229, 1997.

A. Capotondi, M. A. Alexander, N. A. Bond, E. N. Curchitser, and J. D. Scott. Enhanced upper ocean stratification with climate change in the CMIP3 models. *Journal of Geophysical Research: Oceans*, 117(C04031), 2012.

D. A. Carozza, D. Bianchi, and E. D. Galbraith. Metabolic impacts of climate change on marine ecosystems: Implications for fish communities and fisheries. *Global Ecology and Biogeography*, 28 (2):158–169, 2019.

E. J. Carpenter. Brackish-water phytoplankton response to temperature elevation. *Estuarine and Coastal Marine Science*, 1(1):37–44, 1973.

J. P. Carricart-Ganivet. Sea surface temperature and the growth of the West Atlantic reef-building coral *Montastraea annularis*. *Journal of Experimental Marine Biology and Ecology*, 302(2):249–260, 2004.

K. Castillo and B. Helmuth. Influence of thermal history on the response of *Montastraea annularis* to short-term temperature exposure. *Marine Biology*, 148(2):261–270, 2005.

C. Castro-Sanguino, J. C. Ortiz, A. Thompson, N. H. Wolff, R. Ferrari, B. Robson, M. M. Magno-Canto, M. Puotinen, K. E. Fabricius, and S. Uthicke. Reef state and performance as indicators of cumulative impacts on coral reefs. *Ecological Indicators*, 123:107335, 2021.

L. M. Cavole, A. M. Demko, R. E. Diner, A. Giddings, I. Koester, C. M. Pagniello, M.-L. Paulsen, A. Ramirez-Valdez, S. M. Schwenck, N. K. Yen, et al. Biological impacts of the 2013–2015 warm-water anomaly in the Northeast Pacific: winners, losers, and the future. *Oceanography*, 29(2): 273–285, 2016.

N. C. Chan and S. R. Connolly. Sensitivity of coral calcification to ocean acidification: a meta-analysis. *Global change biology*, 19(1):282–290, 2013.

A. J. Cheal, M. A. MacNeil, M. J. Emslie, and H. Sweatman. The threat to coral reefs from more intense cyclones under climate change. *Global change biology*, 23(4):1511–1524, 2017.

C.-C. Chen, G.-C. Gong, and F.-K. Shiah. Hypoxia in the East China Sea: one of the largest coastal low-oxygen areas in the world. *Marine Environmental Research*, 64(4):399–408, 2007.

X. Chen, K. Yu, X. Huang, Y. Wang, Z. Liao, R. Zhang, Q. Yao, J. Wang, W. Wang, S. Tao, et al. Atmospheric nitrogen deposition increases the possibility of macroalgal dominance on remote coral reefs. *Journal of Geophysical Research: Biogeosciences*, 124(5):1355–1369, 2019.

J. E. Cloern, P. C. Abreu, J. Carstensen, L. Chauvaud, R. Elmgren, J. Grall, H. Greening, J. O. R. Johansson, M. Kahru, E. T. Sherwood, et al. Human activities and climate variability drive fast-paced change across the world's estuarine–coastal ecosystems. *Global change biology*, 22(2):513–529, 2016.

C. Collier and M. Waycott. Temperature extremes reduce seagrass growth and induce mortality. *Marine pollution bulletin*, 83(2):483–490, 2014.

C. J. Collier, Y. X. Ow, L. Langlois, S. Uthicke, C. L. Johansson, K. R. O'Brien, V. Hrebien, and M. P. Adams. Optimum temperatures for net primary productivity of three tropical seagrass species. *Frontiers in Plant Science*, 8:1446, 2017.

C. J. Collier, L. Langlois, Y. Ow, C. Johansson, M. Giammusso, M. P. Adams, K. R. O'Brien, and S. Uthicke. Losing a winner: thermal stress and local pressures outweigh the positive effects of ocean acidification for tropical seagrasses. *New Phytologist*, 219(3):1005–1017, 2018.

S. Comeau, R. C. Carpenter, and P. J. Edmunds. Effects of irradiance on the response of the coral *Acropora pulchra* and the calcifying alga *Hydrolithon reinboldii* to temperature elevation and ocean acidification. *Journal of experimental marine biology and ecology*, 453:28–35, 2014.

R. S. Comeaux, M. A. Allison, and T. S. Bianchi. Mangrove expansion in the Gulf of Mexico with climate change: Implications for wetland health and resistance to rising sea levels. *Estuarine, Coastal and Shelf Science*, 96:81–95, 2012.

S. D. Connell and B. D. Russell. The direct effects of increasing CO_2 and temperature on non-calcifying organisms: increasing the potential for phase shifts in kelp forests. *Proceedings of the Royal Society B: Biological Sciences*, 277(1686):1409–1415, 2010.

C. E. Cornwall and T. D. Eddy. Effects of near-future ocean acidification, fishing, and marine protection on a temperate coastal ecosystem. *Conservation Biology*, 29(1):207–215, 2015.

R. Costanza, R. De Groot, P. Sutton, S. Van der Ploeg, S. J. Anderson, I. Kubiszewski, S. Farber, and R. K. Turner. Changes in the global value of ecosystem services. *Global environmental change*, 26: 152–158, 2014.

F. T. Dahlke, M. Butzin, J. Nahrgang, V. Puvanendran, A. Mortensen, H.-O. Pörtner, and D. Storch. Northern cod species face spawning habitat losses if global warming exceeds 1.5°C. *Science advances*, 4(11):eaas8821, 2018.

A. P. Dale, K. Vella, M. Gooch, R. Potts, R. L. Pressey, J. Brodie, and R. Eberhard. Avoiding implementation failure in catchment landscapes: a case study in governance of the Great Barrier Reef. *Environmental management*, 62(1):70–81, 2018.

A. Damar, K.-J. Hesse, F. Colijn, and Y. Vitner. The eutrophication states of the Indonesian sea large marine ecosystem: Jakarta Bay, 2001–2013. *Deep Sea Research Part II: Topical Studies in Oceanography*, 163:72–86, 2019.

S. E. Darby, J. Leyland, M. Kummu, T. A. Räsänen, and H. Lauri. Decoding the drivers of bank erosion on the Mekong river: The roles of the Asian monsoon, tropical storms, and snowmelt. *Water Resources Research*, 49(4):2146–2163, 2013.

S. E. Darby, C. R. Hackney, J. Leyland, M. Kummu, H. Lauri, D. R. Parsons, J. L. Best, A. P. Nicholas, and R. Aalto. Fluvial sediment supply to a mega-delta reduced by shifting tropical-cyclone activity. *Nature*, 539(7628):276–279, 2016.

C. Davies, R. Eriksen, and A. J. Richardson. Spatial and seasonal trends in *Trichodesmium*. 2020.

I. R. Davison. Environmental effects on algal photosynthesis: temperature. *Journal of phycology*, 27 (1):2–8, 1991.

W. De Boer. The rise and fall of the mangrove forests in Maputo Bay, Mozambique. *Wetlands Ecology and Management*, 10(4):313–322, 2002.

G. De'ath and K. Fabricius. Water quality as a regional driver of coral biodiversity and macroalgae on the Great Barrier Reef. *Ecological Applications*, 20(3):840–850, 2010.

G. De'ath, J. M. Lough, and K. E. Fabricius. Declining coral calcification on the Great Barrier Reef. *Science*, 323(5910):116–119, 2009.

G. De'ath, K. E. Fabricius, H. Sweatman, and M. Puotinen. The 27–year decline of coral cover on the Great Barrier Reef and its causes. *Proceedings of the National Academy of Sciences*, 109(44): 17995–17999, 2012.

G. De'ath, K. Fabricius, and J. Lough. Yes-Coral calcification rates have decreased in the last twenty-five years! *Marine Geology*, 346:400–402, 2013.

Deloitte. http://www2.deloitte.com/au/en/pages/economics/articles/great-barrier-reef.html, Accessed 1 September 2020.

C. Deutsch, H. Brix, T. Ito, H. Frenzel, and L. Thompson. Climate-forced variability of ocean hypoxia. *science*, 333(6040):336–339, 2011.

M. Devlin and B. Schaffelke. Spatial extent of riverine flood plumes and exposure of marine ecosystems in the Tully coastal region, Great Barrier Reef. *Marine and Freshwater Research*, 60(11):1109–1122, 2009.

M. Devlin, L. McKinna, J. Alvarez-Romero, C. Petus, B. Abott, P. Harkness, and J. Brodie. Mapping the pollutants in surface riverine flood plume waters in the Great Barrier Reef, Australia. *Marine pollution bulletin*, 65(4-9):224–235, 2012.

D. C. Donato, J. B. Kauffman, D. Murdiyarso, S. Kurnianto, M. Stidham, and M. Kanninen. Mangroves among the most carbon-rich forests in the tropics. *Nature geoscience*, 4(5):293–297, 2011.

S. C. Doney, V. J. Fabry, R. A. Feely, and J. A. Kleypas. Ocean acidification: the other CO_2 problem. *Annual Review of Marine Science*, 1:169–192, 2009.

J. Du, J. Shen, K. Park, Y. P. Wang, and X. Yu. Worsened physical condition due to climate change contributes to the increasing hypoxia in Chesapeake Bay. *Science of the Total Environment*, 630: 707–717, 2018.

N. Duke, M. Ball, and J. Ellison. Factors influencing biodiversity and distributional gradients in mangroves. *Global Ecology & Biogeography Letters*, 7(1):27–47, 1998.

C. Dupouy, D. Benielli-Gary, J. Neveux, Y. Dandonneau, and T. Westberry. An algorithm for detecting *Trichodesmium* surface blooms in the South Western Tropical Pacific. *Biogeosciences*, 8(12):3631–3647, 2011.

J. S. Durango-Cordero, B. Satyanarayana, J. Zhang, J. Wang, M. Chen, X. Fanghong, J. C. Chan, L. Kangying, J. Bogaert, N. Koedam, et al. Vegetation structure at Zhangiang Mangrove National Nature Reserve (ZMMNR), PR China: a comparison between original and non-original trees using ground-truthing, remote sensing and GIS techniques, 2013.

S. Dutkiewicz, J. R. Scott, and M. Follows. Winners and losers: Ecological and biogeochemical changes in a warming ocean. *Global Biogeochemical Cycles*, 27(2):463–477, 2013.

P. Edmunds, R. Gates, and D. Gleason. The biology of larvae from the reef coral *Porites astreoides*, and their response to temperature disturbances. *Marine Biology*, 139(5):981–989, 2001.

K. F. Edwards, M. K. Thomas, C. A. Klausmeier, and E. Litchman. Phytoplankton growth and the interaction of light and temperature: A synthesis at the species and community level. *Limnology and Oceanography*, 61(4):1232–1244, 2016.

M. Eichner, S. A. Kranz, and B. Rost. Combined effects of different CO_2 levels and N sources on the diazotrophic cyanobacterium *Trichodesmium*. *Physiologia Plantarum*, 152(2):316–330, 2014.

M. Elliott, J. W. Day, R. Ramachandran, and E. Wolanski. A synthesis: what is the future for coasts, estuaries, deltas and other transitional habitats in 2050 and beyond? In *Coasts and Estuaries*, pages 1–28. Elsevier, 2019.

M. J. Emslie, P. Bray, A. J. Cheal, K. A. Johns, K. Osborne, T. Sinclair-Taylor, and C. A. Thompson. Decades of monitoring have informed the stewardship and ecological understanding of Australia's Great Barrier Reef. *Biological Conservation*, 252:108854, 2020.

D. V. Erler, H. T. Farid, T. D. Glaze, N. L. Carlson-Perret, and J. M. Lough. Coral skeletons reveal the history of nitrogen cycling in the coastal Great Barrier Reef. *Nature communications*, 11(1):1–8, 2020.

A. Etemad-Shahidi, M. Rohani, J. Parsa, and C. Lemckert. Effects of sea level rise on the salinity of Bahmanshir estuary. *International journal of environmental science and technology*, 12(10):3329–3340, 2015.

A. S. Evans, K. L. Webb, and P. A. Penhale. Photosynthetic temperature acclimation in two coexisting seagrasses, *Zostera marina L.* and *Ruppia maritima L. Aquatic Botany*, 24(2):185–197, 1986.

J. L. Evans and R. J. Allan. El Niño/Southern Oscillation modification to the structure of the monsoon and tropical cyclone activity in the Australasian region. *International Journal of Climatology*, 12(6): 611–623, 1992.

K. Ewel, R. TWILLEY, and J. Ong. Different kinds of mangrove forests provide different goods and services. *Global Ecology & Biogeography Letters*, 7(1):83–94, 1998.

L. Ezzat, J.-F. Maguer, R. Grover, C. Rottier, P. Tremblay, and C. Ferrier-Pagès. Nutrient starvation impairs the trophic plasticity of reef-building corals under ocean warming. *Functional Ecology*, 33(4): 643–653, 2019.

K. Fabricius, K. Okaji, and G. De'Ath. Three lines of evidence to link outbreaks of the crown-of-thorns seastar *Acanthaster planci* to the release of larval food limitation. *Coral Reefs*, 29(3):593–605, 2010.

K. E. Fabricius, C. Langdon, S. Uthicke, C. Humphrey, S. Noonan, G. De'ath, R. Okazaki, N. Muehllehner, M. S. Glas, and J. M. Lough. Losers and winners in coral reefs acclimatized to elevated carbon dioxide concentrations. *Nature Climate Change*, 1(3):165–169, 2011.

V. J. Fabry, B. A. Seibel, R. A. Feely, and J. C. Orr. Impacts of ocean acidification on marine fauna and ecosystem processes. *ICES Journal of Marine Science*, 65(3):414–432, 2008.

P. G. Falkowski and M. J. Oliver. Mix and match: how climate selects phytoplankton. *Nature reviews microbiology*, 5(10):813–819, 2007.

E. Farnsworth, A. Ellison, and W. Gong. Elevated CO_2 alters anatomy, physiology, growth, and reproduction of red mangrove (*Rhizophora mangle L.*). *Oecologia*, 108(4):599–609, 1996.

G. Fay, J. S. Link, and J. A. Hare. Assessing the effects of ocean acidification in the Northeast US using an end-to-end marine ecosystem model. *Ecological Modelling*, 347:1–10, 2017.

R. A. Feely, C. L. Sabine, K. Lee, W. Berelson, J. Kleypas, V. J. Fabry, and F. J. Millero. Impact of anthropogenic CO_2 on the $CaCO_3$ system in the oceans. *Science*, 305(5682):362–366, 2004.

Y. Feng, M. A. Friedrichs, J. Wilkin, H. Tian, Q. Yang, E. E. Hofmann, J. D. Wiggert, and R. R. Hood. Chesapeake Bay nitrogen fluxes derived from a land-estuarine ocean biogeochemical modeling system: Model description, evaluation, and nitrogen budgets. *Journal of Geophysical Research: Biogeosciences*, 120(8):1666–1695, 2015.

K. Fennel, M. Gehlen, P. Brasseur, C. W. Brown, S. Ciavatta, G. Cossarini, A. Crise, C. A. Edwards, D. Ford, M. A. Friedrichs, et al. Advancing marine biogeochemical and ecosystem reanalyses and forecasts as tools for monitoring and managing ecosystem health. *Frontiers in Marine Science*, 6:89, 2019.

J. A. Fernandes, S. Kay, M. A. Hossain, M. Ahmed, W. W. Cheung, A. N. Lazar, and M. Barange. Projecting marine fish production and catch potential in Bangladesh in the 21st century under long-term environmental change and management scenarios. *ICES Journal of Marine Science*, 73(5): 1357–1369, 2015.

P. A. Fernández, M. Y. Roleda, and C. L. Hurd. Effects of ocean acidification on the photosynthetic performance, carbonic anhydrase activity and growth of the giant kelp *Macrocystis pyrifera*. *Photosynthesis Research*, 124(3):293–304, 2015.

P. A. Fernández, J. M. Navarro, C. Camus, R. Torres, and A. H. Buschmann. Effect of environmental history on the habitat-forming kelp *Macrocystis pyrifera* responses to ocean acidification and warming: a physiological and molecular approach. *Scientific reports*, 11(1):1–15, 2021.

K. Filbee-Dexter, C. J. Feehan, and R. E. Scheibling. Large-scale degradation of a kelp ecosystem in an ocean warming hotspot. *Marine Ecology Progress Series*, 543:141–152, 2016.

K. J. Flynn and D. J. McGillicuddy. Modeling marine harmful algal blooms: Current status and future prospects. *Harmful Algal Blooms: A Compendium Desk Reference*, pages 115–134, 2018.

G. T. French, L. F. Awosika, and C. Ibe. Sea-level rise and Nigeria: Potential impacts and consequences. *Journal of Coastal Research*, pages 224–242, 1995.

F.-X. Fu and P. Bell. Effect of salinity on growth, pigmentation, N_2 fixation and alkaline phosphatase activity of cultured *Trichodesmium* sp. *Marine Ecology Progress Series*, 257:69–76, 2003.

F.-X. Fu, E. Yu, N. S. Garcia, J. Gale, Y. Luo, E. A. Webb, and D. A. Hutchins. Differing responses of marine N_2 fixers to warming and consequences for future diazotroph community structure. *Aquatic Microbial Ecology*, 72(1):33–46, 2014.

E. Fulton, C. Bulman, H. Pethybridge, and S. Goldsworthy. Modelling the Great Australian Bight Ecosystem. *Deep Sea Research Part II: Topical Studies in Oceanography*, 157:211–235, 2018.

M. Furnas. Shelf-scale nitrogen and phosphorus budgets for the central Great Barrier Reef. In *Proc. 8th Int. Coral Reef Symp., 1997*, volume 1, pages 809–814, 1997.

M. Furnas, A. Mitchell, M. Skuza, and J. Brodie. In the other 90%: phytoplankton responses to enhanced nutrient availability in the Great Barrier Reef Lagoon. *Marine pollution bulletin*, 51(1-4): 253–265, 2005.

M. Furnas, D. Alongi, D. McKinnon, L. Trott, and M. Skuza. Regional-scale nitrogen and phosphorus budgets for the northern (14° S) and central (17° S) Great Barrier Reef shelf ecosystem. *Continental Shelf Research*, 31(19-20):1967–1990, 2011.

J. D. Gaitán-Espitia, J. R. Hancock, J. L. Padilla-Gamiño, E. B. Rivest, C. A. Blanchette, D. C. Reed, and G. E. Hofmann. Interactive effects of elevated temperature and pCO_2 on early-life-history stages of the giant kelp *Macrocystis pyrifera*. *Journal of Experimental Marine Biology and Ecology*, 457: 51–58, 2014.

X. Gao, H. Endo, M. Nagaki, and Y. Agatsuma. Growth and survival of juvenile sporophytes of the kelp *Ecklonia cava* in response to different nitrogen and temperature regimes. *Fisheries science*, 82 (4):623–629, 2016.

Y. Gao, G. J. Smith, and R. S. Alberte. Temperature dependence of nitrate reductase activity in marine phytoplankton: biochemical analysis and ecological implications. *Journal of phycology*, 36(2): 304–313, 2000.

A. Garzon-Garcia, J. M. Burton, S. Lewis, Z. Bainbridge, R. De Hayr, P. Moody, and J. Brodie. The bioavailability of nitrogen associated with sediment in riverine plumes of the Great Barrier Reef. *Marine Pollution Bulletin*, 173:112910, 2021.

J.-P. Gattuso, A. Magnan, R. Billé, W. W. Cheung, E. L. Howes, F. Joos, D. Allemand, L. Bopp, S. R. Cooley, C. M. Eakin, et al. Contrasting futures for ocean and society from different anthropogenic CO_2 emissions scenarios. *Science*, 349(6243), 2015.

GBRMPA. Great Barrier Reef Marine Park Authority 2021, Annual Report 2020–21, GBRMPA, Townsville. 2021.

K. B. Gedan, M. L. Kirwan, E. Wolanski, E. B. Barbier, and B. R. Silliman. The present and future role of coastal wetland vegetation in protecting shorelines: answering recent challenges to the paradigm. *Climatic change*, 106(1):7–29, 2011.

J. A. George, D. J. Lonsdale, L. R. Merlo, and C. J. Gobler. The interactive roles of temperature, nutrients, and zooplankton grazing in controlling the winter–spring phytoplankton bloom in a temperate, coastal ecosystem, Long Island Sound. *Limnology and Oceanography*, 60(1):110–126, 2015.

J. A. Gittings, D. E. Raitsos, G. Krokos, and I. Hoteit. Impacts of warming on phytoplankton abundance and phenology in a typical tropical marine ecosystem. *Scientific reports*, 8(1):1–12, 2018.

P. M. Glibert, J. Icarus Allen, Y. Artioli, A. Beusen, L. Bouwman, J. Harle, R. Holmes, and J. Holt. Vulnerability of coastal ecosystems to changes in harmful algal bloom distribution in response to climate change: projections based on model analysis. *Global change biology*, 20(12):3845–3858, 2014.

Y. Golbuu, M. Gouezo, H. Kurihara, L. Rehm, and E. Wolanski. Long-term isolation and local adaptation in Palau's Nikko Bay help corals thrive in acidic waters. *Coral Reefs*, 35(3):909–918, 2016.

M. H. Graham, M. D. Fox, and S. L. Hamilton. Macrophyte productivity and the provisioning of energy and habitat to nearshore systems. *Marine macrophytes as foundation species*, 2016.

J. S. Grear, T. A. Rynearson, A. L. Montalbano, B. Govenar, and S. Menden-Deuer. pCO_2 effects on species composition and growth of an estuarine phytoplankton community. *Estuarine, coastal and shelf science*, 190:40–49, 2017.

Great Barrier Reef Marine Park Authority. *Great Barrier Reef Outlook Report 2019*. Great Barrier Reef Marine Park Authority, 2019.

T. Großkopf, W. Mohr, T. Baustian, H. Schunck, D. Gill, M. M. Kuypers, G. Lavik, R. A. Schmitz, D. W. Wallace, and J. LaRoche. Doubling of marine dinitrogen-fixation rates based on direct measurements. *Nature*, 488(7411):361–364, 2012.

J. Guest, J. Low, K. Tun, B. Wilson, C. Ng, D. Raingeard, K. Ulstrup, J. T. I. Tanzil, P. Todd, T. Toh, et al. Coral community response to bleaching on a highly disturbed reef. *Scientific Reports*, 6(1): 1–10, 2016.

R. Gurdek-Bas, J. A. Benthuysen, H. B. Harrison, K. R. Zenger, and L. van Herwerden. The El Niño Southern Oscillation drives multidirectional inter-reef larval connectivity in the Great Barrier Reef. *Scientific Reports*, 12(1):21290, 2022.

A. Guyennon, M. Baklouti, F. Diaz, J. Palmieri, J. Beuvier, C. Lebeaupin-Brossier, T. Arsouze, K. Béranger, J.-C. Dutay, and T. Moutin. New insights into the organic carbon export in the Mediterranean Sea from 3-D modeling. *Biogeosciences*, 12(23):7025–7046, 2015.

T. Guyondet, L. Comeau, C. Bacher, J. Grant, R. Rosland, R. Sonier, and R. Filgueira. Climate change influences carrying capacity in a coastal embayment dedicated to shellfish aquaculture. *Estuaries and coasts*, 38(5):1593–1618, 2015.

J. I. Hansen, K. Henriksen, and T. H. Blackburn. Seasonal distribution of nitrifying bacteria and rates of nitrification in coastal marine sediments. *Microbial Ecology*, 7(4):297–304, 1981.

N. J. Hardman-Mountford, L. Polimene, T. Hirata, R. J. Brewin, and J. Aiken. Impacts of light shading and nutrient enrichment geo-engineering approaches on the productivity of a stratified, oligotrophic ocean ecosystem. *Journal of The Royal Society Interface*, 10(89):20130701, 2013.

C. E. Hare, K. Leblanc, G. R. DiTullio, R. M. Kudela, Y. Zhang, P. A. Lee, S. Riseman, and D. A. Hutchins. Consequences of increased temperature and CO_2 for phytoplankton community structure in the Bering Sea. *Marine Ecology Progress Series*, 352:9–16, 2007.

K. Heimann and S. Cirés. N_2-fixing cyanobacteria: ecology and biotechnological applications. In *Handbook of Marine Microalgae*, pages 501–515. Elsevier, 2015.

N. A. Held, J. B. Waterbury, E. A. Webb, R. M. Kellogg, M. R. McIlvin, M. Jakuba, F. W. Valois, D. M. Moran, K. M. Sutherland, and M. A. Saito. Dynamic diel proteome and daytime nitrogenase activity supports buoyancy in the cyanobacterium *Trichodesmium*. *Nature Microbiology*, 7(2):300–311, 2022.

M. Herrmann, F. Diaz, C. Estournel, P. Marsaleix, and C. Ulses. Impact of atmospheric and oceanic interannual variability on the Northwestern Mediterranean Sea pelagic planktonic ecosystem and associated carbon cycle. *Journal of Geophysical Research: Oceans*, 118(10):5792–5813, 2013.

B. Herut and M. Krom. Atmospheric input of nutrients and dust to the SE Mediterranean. In *The impact of desert dust across the Mediterranean*, pages 349–358. Springer, 1996.

M. Herzfeld. An alternative coordinate system for solving finite difference ocean models. *Ocean Modelling*, 14(3-4):174–196, 2006.

I. Hewson, R. S. Poretsky, S. T. Dyhrman, B. Zielinski, A. E. White, H. J. Tripp, J. P. Montoya, and J. P. Zehr. Microbial community gene expression within colonies of the diazotroph, *Trichodesmium*, from the Southwest Pacific Ocean. *The ISME journal*, 3(11):1286–1300, 2009.

H. G. Hidalgo, J. A. Amador, E. J. Alfaro, and B. Quesada. Hydrological climate change projections for Central America. *Journal of Hydrology*, 495:94–112, 2013.

S. N. Higgins, M. J. Paterson, R. E. Hecky, D. W. Schindler, J. J. Venkiteswaran, and D. L. Findlay. Biological nitrogen fixation prevents the response of a eutrophic lake to reduced loading of nitrogen: evidence from a 46-year whole-lake experiment. *Ecosystems*, 21(6):1088–1100, 2018.

N. Hildebrandt, B. Niehoff, and F. J. Sartoris. Long-term effects of elevated CO_2 and temperature on the Arctic calanoid copepods *Calanus glacialis* and *C. hyperboreus*. *Marine pollution bulletin*, 80 (1-2):59–70, 2014.

M. Hipsey, L. Bruce, and D. Hamilton. Aquatic Ecodynamics (AED) Model Library Science Manual. *The University of Western Australia Technical Manual, Perth, Australia*, 34, 2013.

M. R. Hipsey, G. Gal, G. B. Arhonditsis, C. C. Carey, J. A. Elliott, M. A. Frassl, J. H. Janse, L. de Mora, and B. J. Robson. A system of metrics for the assessment and improvement of aquatic ecosystem models. *Environmental Modelling & Software*, 128:104697, 2020.

T. Hirata, N. Hardman-Mountford, R. Brewin, J. Aiken, R. Barlow, K. Suzuki, T. Isada, E. Howell, T. Hashioka, M. Noguchi-Aita, et al. Synoptic relationships between surface Chlorophyll-a and diagnostic pigments specific to phytoplankton functional types. *Biogeosciences*, 8(2):311–327, 2011.

K. Hock, N. H. Wolff, S. A. Condie, K. R. Anthony, and P. J. Mumby. Connectivity networks reveal the risks of crown-of-thorns starfish outbreaks on the Great Barrier Reef. *Journal of applied ecology*, 51 (5):1188–1196, 2014.

K. Hock, N. H. Wolff, J. C. Ortiz, S. A. Condie, K. R. Anthony, P. G. Blackwell, and P. J. Mumby. Connectivity and systemic resilience of the Great Barrier Reef. *PLoS biology*, 15(11):e2003355, 2017.

K. Hock, C. Doropoulos, R. Gorton, S. A. Condie, and P. J. Mumby. Split spawning increases robustness of coral larval supply and inter-reef connectivity. *Nature communications*, 10(1):3463, 2019.

E. E. Hodgson, I. C. Kaplan, K. N. Marshall, J. Leonard, T. E. Essington, D. S. Busch, E. A. Fulton, C. J. Harvey, A. Hermann, and P. McElhany. Consequences of spatially variable ocean acidification in the California Current: Lower pH drives strongest declines in benthic species in southern regions while greatest economic impacts occur in northern regions. *Ecological modelling*, 383:106–117, 2018.

O. Hoegh-Guldberg, P. J. Mumby, A. J. Hooten, R. S. Steneck, P. Greenfield, E. Gomez, C. D. Harvell, P. F. Sale, A. J. Edwards, K. Caldeira, et al. Coral reefs under rapid climate change and ocean acidification. *science*, 318(5857):1737–1742, 2007.

K. Hogetsu and M. Watanabe. Photosynthetic pigments in *Trichodesmium*–identification and determination of carotenoids. *Studies on the community of marine pelagic blue-green algae. Univ. of Tokyo*, pages 36–40, 1975.

A. M. Hogg, M. P. Meredith, D. P. Chambers, E. P. Abrahamsen, C. W. Hughes, and A. K. Morrison. Recent trends in the southern ocean eddy field. *Journal of Geophysical Research: Oceans*, 120(1): 257–267, 2015.

D. P. Holland. Sinking rates of phytoplankton filaments orientated at different angles: theory and physical model. *Journal of plankton research*, 32(9):1327–1336, 2010.

I. Holzwarth and K. Wirtz. Anthropogenic impacts on estuarine oxygen dynamics: A model based evaluation. *Estuarine, Coastal and Shelf Science*, 211:45–61, 2018.

R. Hordoir and H. Meier. Effect of climate change on the thermal stratification of the Baltic Sea: a sensitivity experiment. *Climate Dynamics*, 38(9-10):1703–1713, 2012.

W. W. Hsieh and G. J. Boer. Global climate change and ocean upwelling. *Fisheries Oceanography*, 1 (4):333–338, 1992.

M. H. Huesemann, A. D. Skillman, and E. A. Crecelius. The inhibition of marine nitrification by ocean disposal of carbon dioxide. *Marine Pollution Bulletin*, 44(2):142–148, 2002.

T. P. Hughes, J. T. Kerry, M. Álvarez-Noriega, J. G. Álvarez-Romero, K. D. Anderson, A. H. Baird, R. C. Babcock, M. Beger, D. R. Bellwood, R. Berkelmans, et al. Global warming and recurrent mass bleaching of corals. *Nature*, 543(7645):373, 2017.

T. P. Hughes, J. T. Kerry, A. H. Baird, S. R. Connolly, A. Dietzel, C. M. Eakin, S. F. Heron, A. S. Hoey, M. O. Hoogenboom, G. Liu, et al. Global warming transforms coral reef assemblages. *Nature*, 556(7702):492–496, 2018.

J. Huisman, G. A. Codd, H. W. Paerl, B. W. Ibelings, J. M. Verspagen, and P. M. Visser. Cyanobacterial blooms. *Nature Reviews Microbiology*, 16(8):471–483, 2018.

D. Hutchins, F.-X. Fu, Y. Zhang, M. Warner, Y. Feng, K. Portune, P. Bernhardt, and M. Mulholland. CO_2 control of *Trichodesmium* N_2 fixation, photosynthesis, growth rates, and elemental ratios: Implications for past, present, and future ocean biogeochemistry. *Limnology and oceanography*, 52(4): 1293–1304, 2007.

D. A. Hutchins, P. Qu, F.-x. Fu, J. Kling, M. Huh, and X. Wang. Distinct responses of the nitrogen-fixing marine cyanobacterium *Trichodesmium* to a thermally-variable environment as a function of phosphorus availability. *Frontiers in microbiology*, 10:1282, 2019.

A. M. Hynes, E. A. Webb, S. C. Doney, and J. B. Waterbury. Comparison of cultured *Trichodesmium* (Cyanophyceae) with species characterized from the field 1. *Journal of phycology*, 48(1):196–210, 2012.

M. D. Iglesias-Rodriguez, P. R. Halloran, R. E. Rickaby, I. R. Hall, E. Colmenero-Hidalgo, J. R. Gittins, D. R. Green, T. Tyrrell, S. J. Gibbs, P. von Dassow, et al. Phytoplankton calcification in a high-CO_2 world. *science*, 320(5874):336–340, 2008.

T. Ikeda. Respiration and ammonia excretion by marine metazooplankton taxa: synthesis toward a global-bathymetric model. *Marine biology*, 161(12):2753–2766, 2014.

T. Ikeda, Y. Kanno, K. Ozaki, and A. Shinada. Metabolic rates of epipelagic marine copepods as a function of body mass and temperature. *Marine Biology*, 139(3):587–596, 2001.

IPCC. Climate change 2014: Synthesis Report. Contribution of Working Groups I, II and III to the fifth assessment report of the Intergovernmental Panel on Climate Change. page 151, 2014.

I. D. Irby, M. A. Friedrichs, F. Da, and K. E. Hinson. The competing impacts of climate change and nutrient reductions on dissolved oxygen in Chesapeake Bay. *Biogeosciences*, 15(9):2649–2668, 2018.

T. Iwamura, H. P. Possingham, I. Chadès, C. Minton, N. J. Murray, D. I. Rogers, E. A. Treml, and R. A. Fuller. Migratory connectivity magnifies the consequences of habitat loss from sea-level rise for shorebird populations. *Proceedings of the Royal Society B: Biological Sciences*, 280(1761):20130325, 2013.

S. Janson, P. J. Siddiqui, A. E. Walsby, K. M. Romans, E. J. Carpenter, and B. Bergman. CYTOMORPHOLOGICAL CHARACTERIZATION OF THE PLANKTONIC DIAZOTROPHIC CYANOBACTERIA *TRICHODESMIUM SPP.* FROM THE INDIAN OCEAN AND CARIBBEAN AND SARGASSO SEAS 1. *Journal of Phycology*, 31(3):463–477, 1995.

A. B. Janssen, G. B. Arhonditsis, A. Beusen, K. Bolding, L. Bruce, J. Bruggeman, R.-M. Couture, A. S. Downing, J. A. Elliott, M. A. Frassl, et al. Exploring, exploiting and evolving diversity of aquatic ecosystem models: a community perspective. *Aquatic ecology*, 49(4):513–548, 2015.

L. Jiang and M. Xia. Modeling investigation of the nutrient and phytoplankton variability in the Chesapeake Bay outflow plume. *Progress in oceanography*, 162:290–302, 2018.

L. Jiang, H. Huang, X.-C. Yuan, T. Yuan, Y.-Y. Zhang, C. K.-C. Wen, X.-B. Li, and G.-W. Zhou. Effects of elevated pCO_2 on the post-settlement development of *Pocillopora damicornis*. *Journal of Experimental Marine Biology and Ecology*, 473:169–175, 2015.

P. Jokiel and S. Coles. Response of Hawaiian and other Indo-Pacific reef corals to elevated temperature. *Coral reefs*, 8(4):155–162, 1990.

K. R. Jones, C. J. Klein, B. S. Halpern, O. Venter, H. Grantham, C. D. Kuempel, N. Shumway, A. M. Friedlander, H. P. Possingham, and J. E. Watson. The location and protection status of Earth's diminishing marine wilderness. *Current Biology*, 28(15):2506–2512, 2018.

P. D. Jones, M. New, D. E. Parker, S. Martin, and I. G. Rigor. Surface air temperature and its changes over the past 150 years. *Reviews of Geophysics*, 37(2):173–199, 1999.

S. E. Jørgensen. Overview of the model types available for development of ecological models. *Ecological Modelling*, 215(1-3):3–9, 2008.

S. Jurriaans and M. Hoogenboom. Thermal performance of scleractinian corals along a latitudinal gradient on the Great Barrier Reef. *Philosophical Transactions of the Royal Society B*, 374(1778): 20180546, 2019.

R. Jyothibabu, C. Karnan, L. Jagadeesan, N. Arunpandi, R. Pandiarajan, K. Muraleedharan, and K. Balachandran. *Trichodesmium* blooms and warm-core ocean surface features in the Arabian Sea and the Bay of Bengal. *Marine Pollution Bulletin*, 121(1-2):201–215, 2017.

D. Karl, R. Letelier, L. Tupas, J. Dore, J. Christian, and D. Hebel. The role of nitrogen fixation in biogeochemical cycling in the subtropical North Pacific Ocean. *Nature*, 388(6642):533–538, 1997.

G. A. Kendrick, R. Nowicki, Y. S. Olsen, S. Strydom, M. W. Fraser, E. A. Sinclair, J. Statton, R. K. Hovey, J. A. Thomson, D. Burkholder, et al. A systematic review of how multiple stressors from an extreme event drove ecosystem-wide loss of resilience in an iconic seagrass community. *Frontiers in Marine Science*, 6:455, 2019.

M. Keys, G. Tilstone, H. S. Findlay, C. E. Widdicombe, and T. Lawson. Effects of elevated CO_2 and temperature on phytoplankton community biomass, species composition and photosynthesis during an experimentally induced autumn bloom in the western English Channel. *Biogeosciences*, 15(10): 3203–3222, 2018.

E. S. Klein, S. L. Hill, J. T. Hinke, T. Phillips, and G. M. Watters. Impacts of rising sea temperature on krill increase risks for predators in the Scotia Sea. *PloS one*, 13(1):e0191011, 2018.

T. Knutson, S. J. Camargo, J. C. Chan, K. Emanuel, C.-H. Ho, J. Kossin, M. Mohapatra, M. Satoh, M. Sugi, K. Walsh, et al. Tropical cyclones and climate change assessment: Part II: Projected response to anthropogenic warming. *Bulletin of the American Meteorological Society*, 101(3):E303–E322, 2020.

T. R. Knutson, J. L. McBride, J. Chan, K. Emanuel, G. Holland, C. Landsea, I. Held, J. P. Kossin, A. Srivastava, and M. Sugi. Tropical cyclones and climate change. *Nature geoscience*, 3(3):157–163, 2010.

K. J. Kroeker, R. L. Kordas, R. Crim, I. E. Hendriks, L. Ramajo, G. S. Singh, C. M. Duarte, and J.-P. Gattuso. Impacts of ocean acidification on marine organisms: quantifying sensitivities and interaction with warming. *Global change biology*, 19(6):1884–1896, 2013.

J. Kromkamp and A. E. Walsby. Buoyancy regulation and vertical migration of *Trichodesmium*: a computer-model prediction. In *Marine pelagic Cyanobacteria: Trichodesmium and Other Diazotrophs*, pages 239–248. Springer, 1992.

F. J. Kroon, P. M. Kuhnert, B. L. Henderson, S. N. Wilkinson, A. Kinsey-Henderson, B. Abbott, J. E. Brodie, and R. D. Turner. River loads of suspended solids, nitrogen, phosphorus and herbicides delivered to the Great Barrier Reef lagoon. *Marine pollution bulletin*, 65(4-9):167–181, 2012.

F. J. Kroon, P. Thorburn, B. Schaffelke, and S. Whitten. Towards protecting the Great Barrier Reef from land-based pollution. *Global change biology*, 22(6):1985–2002, 2016.

L. Kwiatkowski, O. Aumont, and L. Bopp. Consistent trophic amplification of marine biomass declines under climate change. *Global change biology*, 25(1):218–229, 2019.

Z. Lachkar, M. Lévy, and S. Smith. Intensification and deepening of the Arabian Sea oxygen minimum zone in response to increase in Indian monsoon wind intensity. *Biogeosciences*, 15(1):159–186, 2018.

M. K. Lassen, K. D. Nielsen, K. Richardson, K. Garde, and L. Schlüter. The effects of temperature increases on a temperate phytoplankton community–a mesocosm climate change scenario. *Journal of Experimental Marine Biology and Ecology*, 383(1):79–88, 2010.

A. Laurent, K. Fennel, W.-J. Cai, W.-J. Huang, L. Barbero, and R. Wanninkhof. Eutrophication-induced acidification of coastal waters in the northern Gulf of Mexico: Insights into origin and processes from a coupled physical-biogeochemical model. *Geophysical Research Letters*, 44(2):946–956, 2017.

A. Laurent, K. Fennel, D. S. Ko, and J. Lehrter. Climate change projected to exacerbate impacts of coastal eutrophication in the northern Gulf of Mexico. *Journal of Geophysical Research: Oceans*, 123 (5):3408–3426, 2018.

P. Lazzari, G. Mattia, C. Solidoro, S. Salon, A. Crise, M. Zavatarelli, P. Oddo, and M. Vichi. The impacts of climate change and environmental management policies on the trophic regimes in the Mediterranean Sea: Scenario analyses. *Journal of Marine Systems*, 135:137–149, 2014.

C. Le Quéré, R. M. Andrew, P. Friedlingstein, S. Sitch, J. Hauck, J. Pongratz, P. A. Pickers, J. I. Korsbakken, G. P. Peters, J. G. Canadell, et al. Global carbon budget 2018. *Earth System Science Data*, 10(4):2141–2194, 2018.

P. P. Leal, C. L. Hurd, P. A. Fernández, and M. Y. Roleda. Ocean acidification and kelp development: reduced pH has no negative effects on meiospore germination and gametophyte development of *Macrocystis pyrifera* and *Undaria pinnatifida*. *Journal of phycology*, 53(3):557–566, 2017.

S. Lefort, O. Aumont, L. Bopp, T. Arsouze, M. Gehlen, and O. Maury. Spatial and body-size dependent response of marine pelagic communities to projected global climate change. *Global change biology*, 21(1):154–164, 2015.

P. Lehodey, I. Senina, J. Sibert, L. Bopp, B. Calmettes, J. Hampton, and R. Murtugudde. Preliminary forecasts of Pacific bigeye tuna population trends under the A2 IPCC scenario. *Progress in Oceanography*, 86(1-2):302–315, 2010.

G. Lessin, U. Raudsepp, I. Maljutenko, J. Laanemets, J. Passenko, and A. Jaanus. Model study on present and future eutrophication and nitrogen fixation in the Gulf of Finland, Baltic Sea. *Journal of Marine Systems*, 129:76–85, 2014.

Y. J. Liew, D. Zoccola, Y. Li, E. Tambutté, A. A. Venn, C. T. Michell, G. Cui, E. S. Deutekom, J. A. Kaandorp, C. R. Voolstra, et al. Epigenome-associated phenotypic acclimatization to ocean acidification in a reef-building coral. *Science advances*, 4(6):eaar8028, 2018.

E. Litchman, C. A. Klausmeier, O. M. Schofield, and P. G. Falkowski. The role of functional traits and trade-offs in structuring phytoplankton communities: scaling from cellular to ecosystem level. *Ecology letters*, 10(12):1170–1181, 2007.

Y. Liu, J. R. Key, and X. Wang. Influence of changes in sea ice concentration and cloud cover on recent Arctic surface temperature trends. *Geophysical Research Letters*, 36(20), 2009.

C. Lønborg, X. A. Álvarez-Salgado, S. Duggan, and C. Carreira. Organic matter bioavailability in tropical coastal waters: The Great Barrier Reef. *Limnology and Oceanography*, 63(2):1015–1035, 2018.

C. E. Lovelock, K. W. Krauss, M. J. Osland, R. Reef, and M. C. Ball. The physiology of mangrove trees with changing climate. In *Tropical tree physiology*, pages 149–179. Springer, 2016.

Y.-W. Luo, S. Doney, L. Anderson, M. Benavides, I. Berman-Frank, A. Bode, S. Bonnet, K. H. Boström, D. Böttjer, D. Capone, et al. Database of diazotrophs in global ocean: abundance, biomass and nitrogen fixation rates. *Earth System Science Data*, 4(1):47–73, 2012.

D. Manzello. Coral growth with thermal stress and ocean acidification: lessons from the eastern tropical Pacific. *Coral reefs*, 29(3):749–758, 2010.

N. Margvelashvili, F. Saint-Cast, and S. Condie. Numerical modelling of the suspended sediment transport in Torres Strait. *Continental Shelf Research*, 28(16):2241–2256, 2008.

N. Margvelashvili, J. Andrewartha, M. Baird, M. Herzfeld, E. Jones, M. Mongin, F. Rizwi, B. Robson, J. Skerratt, K. Wild-Allen, et al. Simulated fate of catchment-derived sediment on the Great Barrier Reef shelf. *Marine pollution bulletin*, 135:954–962, 2018.

J. A. Marsh Jr, W. C. Dennison, and R. S. Alberte. Effects of temperature on photosynthesis and respiration in eelgrass (*Zostera marina L.*). *Journal of Experimental Marine Biology and Ecology*, 101 (3):257–267, 1986.

K. N. Marshall, I. C. Kaplan, E. E. Hodgson, A. Hermann, D. S. Busch, P. McElhany, T. E. Essington, C. J. Harvey, and E. A. Fulton. Risks of ocean acidification in the California Current food web and fisheries: ecosystem model projections. *Global change biology*, 23(4):1525–1539, 2017.

R. Masini, J. Cary, C. Simpson, and A. McComb. Effects of light and temperature on the photosynthesis of temperate meadow-forming seagrasses in Western Australia. *Aquatic Botany*, 49(4):239–254, 1995.

G. McCloskey, D. Waters, R. Baheerathan, S. Darr, C. Dougall, R. Ellis, B. Fentie, and L. Hateley. Modelling pollutant load changes due to improved management practices in the Great Barrier Reef catchments: updated methodology and results – Technical Report for Reef Report Card 2014. *Queensland Department of Natural Resources and Mines, Brisbane, Queensland*, 2017.

G. McCloskey, R. Baheerathan, C. Dougall, R. Ellis, F. Bennett, D. Waters, S. Darr, B. Fentie, L. Hateley, and M. Askildsen. Modelled estimates of fine sediment and particulate nutrients delivered from the Great Barrier Reef catchments. *Marine pollution bulletin*, 165:112163, 2021a.

G. McCloskey, R. Baheerathan, C. Dougall, R. Ellis, F. Bennett, D. Waters, S. Darr, B. Fentie, L. Hateley, and M. Askildsen. Modelled estimates of dissolved inorganic nitrogen exported to the Great Barrier Reef lagoon. *Marine Pollution Bulletin*, 171:112655, 2021b.

K. McConville, C. Halsband, E. S. Fileman, P. J. Somerfield, H. S. Findlay, and J. I. Spicer. Effects of elevated CO_2 on the reproduction of two calanoid copepods. *Marine pollution bulletin*, 73(2): 428–434, 2013.

K. McKee. Where temperate meets tropical: relative responses of salt marsh and mangrove species to nitrogen and CO_2 enrichment. In *Society of Wetland Scientists 27th International Conference, Cairns, Australia*, pages 83–84, 2006.

S. McKenna, J. Jarvis, T. Sankey, C. Reason, R. Coles, and M. Rasheed. Declines of seagrasses in a tropical harbour, North Queensland, Australia, are not the result of a single event. *Journal of biosciences*, 40(2):389–398, 2015.

L. Mckenzie and R. Unsworth. Surviving the flood: How long can seagrass 'hold its breath'? *Seagrass-Watch Magazine*, 43:2–4, 2011.

L. I. McKinna. Three decades of ocean-color remote-sensing Trichodesmium spp. in the World's oceans: A review. *Progress in Oceanography*, 131:177–199, 2015.

L. I. McKinna, M. J. Furnas, and P. V. Ridd. A simple, binary classification algorithm for the detection of *Trichodesmium* spp. within the Great Barrier Reef using MODIS imagery. *Limnology and Oceanography: Methods*, 9(2):50–66, 2011.

A. McMahon, I. R. Santos, K. G. Schulz, A. Scott, J. Silverman, K. L. Davis, and D. T. Maher. Coral reef calcification and production after the 2016 bleaching event at Lizard Island, Great Barrier Reef. *Journal of Geophysical Research: Oceans*, 2019.

J. S. McNown and J. Malaika. Effects of particle shape on settling velocity at low reynolds numbers. *Eos, Transactions American Geophysical Union*, 31(1):74–82, 1950.

H. Meier, A. Höglund, K. Eilola, and E. Almroth-Rosell. Impact of accelerated future global mean sea level rise on hypoxia in the Baltic Sea. *Climate Dynamics*, 49(1-2):163–172, 2017.

L. Meire, K. Soetaert, and F. Meysman. Impact of global change on coastal oxygen dynamics and risk of hypoxia. *Biogeosciences*, 10(4):2633–2653, 2013.

L. F. Messer, M. V. Brown, M. J. Furnas, R. L. Carney, A. McKinnon, and J. R. Seymour. Diversity and activity of diazotrophs in Great Barrier Reef surface waters. *Frontiers in Microbiology*, 8:967, 2017.

K. E. Mills, A. J. Pershing, C. J. Brown, Y. Chen, F.-S. Chiang, D. S. Holland, S. Lehuta, J. A. Nye, J. C. Sun, A. C. Thomas, et al. Fisheries management in a changing climate: lessons from the 2012 ocean heat wave in the Northwest Atlantic. *Oceanography*, 26(2):191–195, 2013.

R. Mogollón and P. H. R. Calil. Counterintuitive effects of global warming-induced wind patterns on primary production in the Northern Humboldt Current System. *Global change biology*, 24(7):3187–3198, 2018.

W. Mohr, T. Großkopf, D. W. Wallace, and J. LaRoche. Methodological underestimation of oceanic nitrogen fixation rates. *PloS one*, 5(9):e12583, 2010.

M. Mongin, M. E. Baird, B. Tilbrook, R. J. Matear, A. Lenton, M. Herzfeld, K. Wild-Allen, J. Skerratt, N. Margvelashvili, B. J. Robson, et al. The exposure of the Great Barrier Reef to ocean acidification. *Nature communications*, 7:10732, 2016.

M. Mongin, M. E. Baird, A. Lenton, C. Neill, and J. Akl. Reversing ocean acidification along the Great Barrier Reef using alkalinity injection. *Environmental Research Letters*, 16(6):064068, 2021.

C. Mora, C.-L. Wei, A. Rollo, T. Amaro, A. R. Baco, D. Billett, L. Bopp, Q. Chen, M. Collier, R. Danovaro, et al. Biotic and human vulnerability to projected changes in ocean biogeochemistry over the 21st century. *PLoS Biol*, 11(10):e1001682, 2013.

A. Mora-Soto, M. Palacios, E. C. Macaya, I. Gómez, P. Huovinen, A. Pérez-Matus, M. Young, N. Golding, M. Toro, M. Yaqub, et al. A high-resolution global map of Giant kelp (*Macrocystis pyrifera*) forests and intertidal green algae (*Ulvophyceae*) with Sentinel-2 imagery. *Remote Sensing*, 12(4):694, 2020.

P. Morais, E. Dias, J. Cruz, P. Chainho, M. M. Angélico, J. L. Costa, A. B. Barbosa, and M. A. Teodósio. Allochthonous-derived organic matter subsidizes the food sources of estuarine jellyfish. *Journal of Plankton Research*, 39(6):870–877, 2017.

D. Moran, B. Robson, R. Gruber, J. Waterhouse, M. Logan, C. Petus, S. Lewis, D. Tracey, C. James, J. Mellors, U. Bove, J. Davidson, K. Glasson, S. Jaworski, C. Lefevre, A. Macadam, M. Shanahan, R. Vasile, I. Zagorskis, and J. Shellberg. Marine Monitoring Program: Annual Report for Inshore Water Quality Monitoring 2020-21. Report for the Great Barrier Reef Marine Park Authority. *Great Barrier Reef Marine Park Authority, Townsville*, 2022.

D. J. Morrisey, A. Swales, S. Dittmann, M. A. Morrison, C. E. Lovelock, and C. M. Beard. The ecology and management of temperate mangroves. *Oceanography and marine biology*, 48:43, 2010.

F. E. Moy and H. Christie. Large-scale shift from sugar kelp (*Saccharina latissima*) to ephemeral algae along the south and west coast of Norway. *Marine Biology Research*, 8(4):309–321, 2012.

B. A. Muhling, C. F. Gaitán, C. A. Stock, V. S. Saba, D. Tommasi, and K. W. Dixon. Potential salinity and temperature futures for the Chesapeake Bay using a statistical downscaling spatial disaggregation framework. *Estuaries and coasts*, 41(2):349–372, 2018.

M. R. Mulholland and P. W. Bernhardt. The effect of growth rate, phosphorus concentration, and temperature on N_2 fixation, carbon fixation, and nitrogen release in continuous cultures of *Trichodesmium* IMS101. *Limnology and Oceanography*, 50(3):839–849, 2005.

M. R. Mulholland, P. W. Bernhardt, C. A. Heil, D. A. Bronk, and J. M. O'Neil. Nitrogen fixation and release of fixed nitrogen by *Trichodesmium* spp. in the Gulf of Mexico. *Limnology and Oceanography*, 51(4):1762–1776, 2006.

A. F. Muth, M. H. Graham, C. E. Lane, and C. D. Harley. Recruitment tolerance to increased temperature present across multiple kelp clades, 2019.

T. Nakamura, K. Nadaoka, A. Watanabe, T. Yamamoto, T. Miyajima, and A. C. Blanco. Reef-scale modeling of coral calcification responses to ocean acidification and sea-level rise. *Coral Reefs*, 37(1): 37–53, 2018.

N. Nakicenovic, J. Alcamo, A. Grubler, K. Riahi, R. Roehrl, H.-H. Rogner, and N. Victor. *Special report on emissions scenarios (SRES), a special report of Working Group III of the intergovernmental panel on climate change*. Cambridge University Press Cambridge, UK, 2000.

J. Norberg. Biodiversity and ecosystem functioning: a complex adaptive systems approach. *Limnology and Oceanography*, 49(4part2):1269–1277, 2004.

W. D. Nordhaus. The economics of hurricanes in the United States. Technical report, National Bureau of Economic Research, 2006.

J. Olive, G. Ajlani, C. Astier, M. Recouvreur, and C. Vernotte. Ultrastructure and light adaptation of phycobilisome mutants of *Synechocystis* PCC 6803. *Biochimica et Biophysica Acta (BBA)-Bioenergetics*, 1319(2-3):275–282, 1997.

E. C. Oliver, J. A. Benthuysen, N. L. Bindoff, A. J. Hobday, N. J. Holbrook, C. N. Mundy, and S. E. Perkins-Kirkpatrick. The unprecedented 2015/16 Tasman Sea marine heatwave. *Nature communications*, 8(1):1–12, 2017.

R. L. Oliver. Floating and sinking in gas-vacuolate cyanobacteria1. *Journal of phycology*, 30(2):161–173, 1994.

R. L. Oliver, D. P. Hamilton, J. D. Brookes, and G. G. Ganf. Physiology, blooms and prediction of planktonic cyanobacteria. In *Ecology of cyanobacteria II*, pages 155–194. Springer, 2012.

E. Olsen, G. Fay, S. Gaichas, R. Gamble, S. Lucey, and J. S. Link. Ecosystem model skill assessment. Yes we can! *PLoS One*, 11(1):e0146467, 2016.

J. C. Orr, V. J. Fabry, O. Aumont, L. Bopp, S. C. Doney, R. A. Feely, A. Gnanadesikan, N. Gruber, A. Ishida, F. Joos, et al. Anthropogenic ocean acidification over the twenty-first century and its impact on calcifying organisms. *Nature*, 437(7059):681–686, 2005.

K. Ortega-Cisneros, L. Shannon, K. Cochrane, E. A. Fulton, and Y.-J. Shin. Evaluating the specificity of ecosystem indicators to fishing in a changing environment: A model comparison study for the southern Benguela ecosystem. *Ecological indicators*, 95:85–98, 2018.

K. Osborne, A. A. Thompson, A. J. Cheal, M. J. Emslie, K. A. Johns, M. J. Jonker, M. Logan, I. R. Miller, and H. P. Sweatman. Delayed coral recovery in a warming ocean. *Global change biology*, 23 (9):3869–3881, 2017.

M. J. Osland, N. Enwright, R. H. Day, and T. W. Doyle. Winter climate change and coastal wetland foundation species: salt marshes vs. mangrove forests in the southeastern United States. *Global change biology*, 19(5):1482–1494, 2013.

Y. Ow, C. Collier, and S. Uthicke. Responses of three tropical seagrass species to CO_2 enrichment. *Marine Biology*, 162(5):1005–1017, 2015.

R. K. Pachauri and A. Reisinger. Climate change 2007. Synthesis report. Contribution of Working Groups I, II and III to the fourth assessment report, Jul 2008.

D. Padfield, G. Yvon-Durocher, A. Buckling, S. Jennings, and G. Yvon-Durocher. Rapid evolution of metabolic traits explains thermal adaptation in phytoplankton. *Ecology Letters*, 19(2):133–142, 2016.

K. Padmakumar, B. Smitha, L. C. Thomas, C. Fanimol, G. SreeRenjima, N. Menon, and V. Sanjeevan. Blooms of *Trichodesmium erythraeum* in the South Eastern Arabian Sea during the onset of 2009 summer monsoon. *Ocean Science Journal*, 45(3):151–157, 2010.

H. W. Paerl. A comparison of cyanobacterial bloom dynamics in freshwater, estuarine and marine environments. *Phycologia*, 35(sup6):25–35, 1996.

S. L. Palacios and R. C. Zimmerman. Response of eelgrass Zostera marina to CO_2 enrichment: possible impacts of climate change and potential for remediation of coastal habitats. *Marine Ecology Progress Series*, 344:1–13, 2007.

J.-Y. Park, J.-S. Kug, J. Bader, R. Rolph, and M. Kwon. Amplified Arctic warming by phytoplankton under greenhouse warming. *Proceedings of the National Academy of Sciences*, 112(19):5921–5926, 2015.

L. Patara, M. Vichi, and S. Masina. Reprint of "Impacts of natural and anthropogenic climate variations on North Pacific plankton in an Earth System Model". *Ecological modelling*, 264:48–63, 2013.

V. J. Paul. Global warming and cyanobacterial harmful algal blooms. *Cyanobacterial harmful algal blooms: state of the science and research needs*, pages 239–257, 2008.

D. Pauly and D. Zeller. Catch reconstructions reveal that global marine fisheries catches are higher than reported and declining. *Nature communications*, 7:10244, 2016.

A. F. Pearce and M. Feng. The rise and fall of the "marine heat wave" off Western Australia during the summer of 2010/2011. *Journal of Marine Systems*, 111:139–156, 2013.

L. Peperzak. Climate change and harmful algal blooms in the North Sea. *Acta Oecologica*, 24:S139–S144, 2003.

M. Pérez and J. Romero. Photosynthetic response to light and temperature of the seagrass Cymodocea nodosa and the prediction of its seasonality. *Aquatic Botany*, 43(1):51–62, 1992.

C. T. Perry, S. G. Smithers, P. S. Kench, and B. Pears. Impacts of Cyclone Yasi on nearshore, terrigenous sediment-dominated reefs of the central Great Barrier Reef, Australia. *Geomorphology*, 222:92–105, 2014.

C. N. Pickens and M. W. Hester. Temperature tolerance of early life history stages of black mangrove *Avicennia germinans*: implications for range expansion. *Estuaries and Coasts*, 34(4):824–830, 2011.

D. Pilcher, D. Naiman, J. Cross, A. Hermann, S. Siedlecki, G. Gibson, and J. Mathis. Modeled effect of coastal biogeochemical processes, climate variability, and ocean acidification on aragonite saturation state in the Bering Sea. *Frontiers in Marine Science*, 5:508, 2018.

C. Piroddi, M. Coll, C. Liquete, D. Macias, K. Greer, J. Buszowski, J. Steenbeek, R. Danovaro, and V. Christensen. Historical changes of the Mediterranean Sea ecosystem: modelling the role and impact of primary productivity and fisheries changes over time. *Scientific reports*, 7:44491, 2017.

A. Post, Z. Dedej, R. Gottlieb, H. Li, D. Thomas, M. El-Absawi, A. El-Naggar, M. El-Gharabawi, and U. Sommer. Spatial and temporal distribution of Trichodesmium spp. in the stratified Gulf of Aqaba, Red Sea. *Marine Ecology Progress Series*, 239:241–250, 2002.

H. Putnam, A. Mayfield, T. Fan, C. Chen, and R. Gates. The physiological and molecular responses of larvae from the reef-building coral *Pocillopora damicornis* exposed to near-future increases in temperature and pCO_2. *Marine Biology*, 160(8):2157–2173, 2013.

Queensland Water Modelling Network. Critical review of climate change and water modelling in Queensland. https://science.des.qld.gov.au/__data/assets/pdf_file/0034/98863/critical-review-climate-change-water-modelling-qld.pdf, Accessed September 2020.

R Core Team. *R: A language and environment for statistical computing*. R Foundation for Statistical Computing, Vienna, Austria, 2021. URL https://www.R-project.org/.

E. Rahav and E. Bar-Zeev. Sewage outburst triggers *Trichodesmium* bloom and enhance N_2 fixation rates. *Scientific reports*, 7(1):1–8, 2017.

A. G. Ramos, A. Martel, G. A. Codd, E. Soler, J. Coca, A. Redondo, L. F. Morrison, J. S. Metcalf, A. Ojeda, S. Suárez, et al. Bloom of the marine diazotrophic cyanobacterium *Trichodesmium erythraeum* in the Northwest African Upwelling. *Marine Ecology Progress Series*, 301:303–305, 2005.

R. Reef, M. Slot, U. Motro, M. Motro, Y. Motro, M. F. Adame, M. Garcia, J. Aranda, C. E. Lovelock, and K. Winter. The effects of CO_2 and nutrient fertilisation on the growth and temperature response of the mangrove *Avicennia germinans*. *Photosynthesis research*, 129(2):159–170, 2016.

S. Reynaud, N. Leclercq, S. Romaine-Lioud, C. Ferrier-Pagés, J. Jaubert, and J.-P. Gattuso. Interacting effects of CO_2 partial pressure and temperature on photosynthesis and calcification in a scleractinian coral. *Global Change Biology*, 9(11):1660–1668, 2003.

C. Reynolds and A. Walsby. Water-blooms. *Biological reviews*, 50(4):437–481, 1975.

C. Richon, J.-C. Dutay, L. Bopp, B. L. Vu, J. C. Orr, S. Somot, and F. Dulac. Biogeochemical response of the Mediterranean Sea to the transient SRES-A2 climate change scenario. *Biogeosciences*, 16(1): 135–165, 2019.

G. Rilov, S. Fraschetti, E. Gissi, C. Pipitone, F. Badalamenti, L. Tamburello, E. Menini, P. Goriup, A. D. Mazaris, J. Garrabou, et al. A fast-moving target: achieving marine conservation goals under shifting climate and policies. *Ecological Applications*, 30(1):e02009, 2020.

B. Robson. *ereefs: Useful functions to handle eReefs and EMS model output*, 2018. URL https://ereefs.info. R package version 2.7.18.

B. Robson, J. Andrewartha, M. Baird, M. Herzfeld, E. Jones, N. Margvelashvili, M. Mongin, F. Rizwi, J. Skerratt, and K. Wild-Allen. Evaluating the eReefs Great Barrier Reef marine model against observed emergent properties. In *MODSIM2017, 22nd International Congress on Modelling and Simulation. Modelling and Simulatio n Society of Australia and New Zealand*, pages 1976–1982, 2017a.

B. J. Robson. State of the art in modelling of phosphorus in aquatic systems: review, criticisms and commentary. *Environmental Modelling & Software*, 61:339–359, 2014.

B. J. Robson, M. Baird, and K. Wild-Allen. A physiological model for the marine cyanobacteria, *Trichodesmium*. In *MODSIM2013, 20th International Congress on Modelling and Simulation. Modelling and Simulation Society of Australia and New Zealand, ISBN 978-0-9872143-3-1*, 2013.

B. J. Robson, R. E. Lester, D. S. Baldwin, N. R. Bond, R. Drouart, R. J. Rolls, D. S. Ryder, and R. M. Thompson. Modelling food-web mediated effects of hydrological variability and environmental flows. *Water Research*, 124:108–128, 2017b.

B. J. Robson, G. B. Arhonditsis, M. E. Baird, J. Brebion, K. F. Edwards, L. Geoffroy, M.-P. Hébert, V. van Dongen-Vogels, E. M. Jones, C. Kruk, et al. Towards evidence-based parameter values and priors for aquatic ecosystem modelling. *Environmental modelling & software*, 100:74–81, 2018.

B. J. Robson, J. Skerratt, M. E. Baird, C. Davies, M. Herzfeld, E. M. Jones, M. Mongin, A. J. Richardson, F. Rizwi, K. Wild-Allen, et al. Enhanced assessment of the eReefs biogeochemical model for the Great Barrier Reef using the Concept/State/Process/System model evaluation framework. *Environmental Modelling & Software*, 129:104707, 2020.

M. Rodier and R. Le Borgne. Population dynamics and environmental conditions affecting *Trichodesmium* spp.(filamentous cyanobacteria) blooms in the south–west lagoon of New Caledonia. *Journal of Experimental Marine Biology and Ecology*, 358(1):20–32, 2008.

M. Rodier and R. Le Borgne. Population and trophic dynamics of *Trichodesmium thiebautii* in the SE lagoon of New Caledonia. Comparison with *T. erythraeum* in the SW lagoon. *Marine pollution bulletin*, 61(7-12):349–359, 2010.

R. Rodolfo-Metalpa, M. O. Hoogenboom, C. Rottier, A. Ramos-Esplá, A. C. Baker, M. Fine, and C. Ferrier-Pagès. Thermally tolerant corals have limited capacity to acclimatize to future warming. *Global Change Biology*, 20(10):3036–3049, 2014.

A. J. N. Rodriguez. *Optical properties of photosynthetic pigments and abundance of the cyanobacterium Trichodesmium in the eastern Caribbean Basin*. University of Puerto Rico, Mayaguez (Puerto Rico), 1998.

R. Rodríguez-Martínez, A. Medina-Valmaseda, P. Blanchon, L. Monroy-Velázquez, A. Almazán-Becerril, B. Delgado-Pech, L. Vásquez-Yeomans, V. Francisco, and M. García-Rivas. Faunal mortality associated with massive beaching and decomposition of pelagic Sargassum. *Marine pollution bulletin*, 146: 201–205, 2019.

K. Rogers, N. Saintilan, and H. Heijnis. Mangrove encroachment of salt marsh in Western Port Bay, Victoria: the role of sedimentation, subsidence, and sea level rise. *Estuaries*, 28(4):551–559, 2005.

K. M. Romans, E. J. Carpenter, and B. Bergman. Buoyancy regulation in the colonial diazotrophic cyanobacterium *Trichodesmium tenue*: Ultrastructure and storage of carbohydrate, polyphosphate, and nitrogen 1. *Journal of Phycology*, 30(6):935–942, 1994.

G. Rousset, F. D. Boissieu, C. E. Menkes, J. Lefèvre, R. Frouin, M. Rodier, V. Ridoux, S. Laran, S. Bonnet, and C. Dupouy. Remote sensing of *Trichodesmium* spp. mats in the western tropical South Pacific. *Biogeosciences*, 15(16):5203–5219, 2018.

J. Ruiz, D. Macías, M. Losada, M. Díez-Minguito, and L. Prieto. A simple biogeochemical model for estuaries with high sediment loads: Application to the Guadalquivir River (SW Iberia). *Ecological modelling*, 265:194–206, 2013.

RWQPP. Queensland Government 2013. Reef Water Quality Protection Plan 2013. Reef Water Quality Protection Plan Secretariat, Brisbane. 2013.

V. Ryabchenko, L. Karlin, A. Isaev, R. Vankevich, T. Eremina, M. Molchanov, and O. P. Savchuk. Model estimates of the eutrophication of the Baltic Sea in the contemporary and future climate. *Oceanology*, 56(1):36–45, 2016.

S. Rysgaard, R. N. Glud, N. Risgaard-Petersen, and T. Dalsgaard. Denitrification and anammox activity in Arctic marine sediments. *Limnology and oceanography*, 49(5):1493–1502, 2004.

V. S. Saba, S. M. Griffies, W. G. Anderson, M. Winton, M. A. Alexander, T. L. Delworth, J. A. Hare, M. J. Harrison, A. Rosati, G. A. Vecchi, et al. Enhanced warming of the Northwest Atlantic Ocean under climate change. *Journal of Geophysical Research: Oceans*, 121(1):118–132, 2016.

P. Saenger. *Mangrove ecology, silviculture and conservation*. Springer Science & Business Media, 2013.

N. Saintilan, N. C. Wilson, K. Rogers, A. Rajkaran, and K. W. Krauss. Mangrove expansion and salt marsh decline at mangrove poleward limits. *Global change biology*, 20(1):147–157, 2014.

C. E. Schaum, S. Barton, E. Bestion, A. Buckling, B. Garcia-Carreras, P. Lopez, C. Lowe, S. Pawar, N. Smirnoff, M. Trimmer, et al. Adaptation of phytoplankton to a decade of experimental warming linked to increased photosynthesis. *Nature Ecology & Evolution*, 1(4):1–7, 2017.

A. Schmittner. Decline of the marine ecosystem caused by a reduction in the Atlantic overturning circulation. *Nature*, 434(7033):628–633, 2005.

A. J. Schweiger, R. W. Lindsay, S. Vavrus, and J. A. Francis. Relationships between Arctic sea ice and clouds during autumn. *Journal of Climate*, 21(18):4799–4810, 2008.

D. Scott, M. C. Simpson, and R. Sim. The vulnerability of Caribbean coastal tourism to scenarios of climate change related sea level rise. *Journal of Sustainable Tourism*, 20(6):883–898, 2012.

N. Serpetti, A. R. Baudron, M. Burrows, B. L. Payne, P. Helaouet, P. G. Fernandes, and J. Heymans. Impact of ocean warming on sustainable fisheries management informs the ecosystem approach to fisheries. *Scientific reports*, 7(1):13438, 2017.

S. Sett, L. T. Bach, K. G. Schulz, S. Koch-Klavsen, M. Lebrato, and U. Riebesell. Temperature modulates coccolithophorid sensitivity of growth, photosynthesis and calcification to increasing seawater pCO_2. *PloS one*, 9(2):e88308, 2014.

E. C. Shaw, A. J. Gabric, and G. H. McTainsh. Impacts of aeolian dust deposition on phytoplankton dynamics in Queensland coastal waters. *Marine and Freshwater Research*, 59(11):951–962, 2008.

C. Shen, J. M. Testa, M. Li, W.-J. Cai, G. G. Waldbusser, W. Ni, W. M. Kemp, J. Cornwell, B. Chen, J. Brodeur, et al. Controls on carbonate system dynamics in a coastal plain estuary: A modeling study. *Journal of Geophysical Research: Biogeosciences*, 124(1):61–78, 2019.

C. C. Shepard, C. M. Crain, and M. W. Beck. The protective role of coastal marshes: a systematic review and meta-analysis. *PloS one*, 6(11):e27374, 2011.

R. Silberstein, S. Aryal, J. Durrant, M. Pearcey, M. Braccia, S. Charles, L. Boniecka, G. Hodgson, M. Bari, N. Viney, et al. Climate change and runoff in south-western Australia. *Journal of Hydrology*, 475:441–455, 2012.

E. Simonson, A. Metaxas, and R. Scheibling. Kelp in hot water: II. Effects of warming seawater temperature on kelp quality as a food source and settlement substrate. *Marine Ecology Progress Series*, 537:105–119, 2015a.

E. Simonson, R. Scheibling, and A. Metaxas. Kelp in hot water: I. Warming seawater temperature induces weakening and loss of kelp tissue. *Marine Ecology Progress Series*, 537:89–104, 2015b.

J. Skerratt, M. Mongin, M. Baird, K. Wild-Allen, B. Robson, B. Schaffelke, C. Davies, A. Richardson, N. Margvelashvili, M. Soja-Wozniak, et al. Simulated nutrient and plankton dynamics in the Great Barrier Reef (2011–2016). *Journal of Marine Systems*, 192:51–74, 2019.

F. H. Sklar and J. A. Browder. Coastal environmental impacts brought about by alterations to freshwater flow in the Gulf of Mexico. *Environmental management*, 22(4):547–562, 1998.

D. A. Smale. Impacts of ocean warming on kelp forest ecosystems. *New Phytologist*, 225(4):1447–1454, 2020.

J. N. Smith, G. De'ath, C. Richter, A. Cornils, J. M. Hall-Spencer, and K. E. Fabricius. Ocean acidification reduces demersal zooplankton that reside in tropical coral reefs. *Nature Climate Change*, 6 (12):1124–1129, 2016.

S. C. Snedaker and R. J. Araújo. Stomatal conductance and gas exchange in four species of Caribbean mangroves exposed to ambient and increased CO_2. *Marine and Freshwater Research*, 49(4):325–327, 1998.

M. A. Snyder, L. C. Sloan, N. S. Diffenbaugh, and J. L. Bell. Future climate change and upwelling in the California Current. *Geophysical Research Letters*, 30(15):1823, 2003.

K. Soetaert, J. J. Middelburg, P. M. Herman, and K. Buis. On the coupling of benthic and pelagic biogeochemical models. *Earth-Science Reviews*, 51(1-4):173–201, 2000.

J. A. Sohm, E. A. Webb, and D. G. Capone. Emerging patterns of marine nitrogen fixation. *Nature Reviews Microbiology*, 9(7):499–508, 2011.

U. Sommer and A. Lewandowska. Climate change and the phytoplankton spring bloom: warming and overwintering zooplankton have similar effects on phytoplankton. *Global Change Biology*, 17(1): 154–162, 2011.

U. Sommer, N. Aberle, A. Engel, T. Hansen, K. Lengfellner, M. Sandow, J. Wohlers, E. Zöllner, and U. Riebesell. An indoor mesocosm system to study the effect of climate change on the late winter and spring succession of Baltic Sea phyto-and zooplankton. *Oecologia*, 150(4):655–667, 2007.

M. Stäbler, A. Kempf, S. Smout, and A. Temming. Sensitivity of multispecies maximum sustainable yields to trends in the top (marine mammals) and bottom (primary production) compartments of the southern North Sea food-web. *PloS one*, 14(1):e0210882, 2019.

P. A. Staehr and M. J. Birkeland. Temperature acclimation of growth, photosynthesis and respiration in two mesophilic phytoplankton species. *Phycologia*, 45(6):648–656, 2006.

R. S. Steneck, M. H. Graham, B. J. Bourque, D. Corbett, J. M. Erlandson, J. A. Estes, and M. J. Tegner. Kelp forest ecosystems: biodiversity, stability, resilience and future. *Environmental conservation*, pages 436–459, 2002.

A. D. Steven, M. E. Baird, R. Brinkman, N. J. Car, S. J. Cox, M. Herzfeld, J. Hodge, E. Jones, E. King, N. Margvelashvili, et al. eReefs: An operational information system for managing the Great Barrier Reef. *Journal of Operational Oceanography*, 12(sup2):S12–S28, 2019.

T. F. Stocker, D. Qin, G.-K. Plattner, M. Tignor, S. K. Allen, J. Boschung, A. Nauels, Y. Xia, V. Bex, P. M. Midgley, et al. Climate change 2013: The physical science basis. *Contribution of working group I to the fifth assessment report of the intergovernmental panel on climate change*, 1535, 2013.

D. J. Stokes, T. R. Healy, and P. J. Cooke. Expansion dynamics of monospecific, temperate mangroves and sedimentation in two embayments of a barrier-enclosed lagoon, Tauranga Harbour, New Zealand. *Journal of Coastal Research*, 26(1 (261)):113–122, 2010.

C. A. Stow, J. Jolliff, D. J. McGillicuddy Jr, S. C. Doney, J. I. Allen, M. A. Friedrichs, K. A. Rose, and P. Wallhead. Skill assessment for coupled biological/physical models of marine systems. *Journal of Marine Systems*, 76(1-2):4–15, 2009.

K. D. Strååt, C.-M. Mörth, and E. Undeman. Future export of particulate and dissolved organic carbon from land to coastal zones of the Baltic sea. *Journal of Marine Systems*, 177:8–20, 2018.

P. Straw and N. Saintilan. Loss of shorebird habitat as a result of mangrove incursion due to sea-level rise and urbanization. *Waterbirds around the world*, pages 717–720, 2006.

R. D. Stuart-Smith, C. J. Brown, D. M. Ceccarelli, and G. J. Edgar. Ecosystem restructuring along the Great Barrier Reef following mass coral bleaching. *Nature*, 560(7716):92–96, 2018.

A. Subramaniam, E. J. Carpenter, D. Karentz, and P. G. Falkowski. Bio-optical properties of the marine diazotrophic cyanobacteria *Trichodesmium* spp. I. Absorption and photosynthetic action spectra. *Limnology and Oceanography*, 44(3):608–617, 1999.

C. Sun, M. Feng, R. J. Matear, M. A. Chamberlain, P. Craig, K. R. Ridgway, and A. Schiller. Marine downscaling of a future climate scenario for Australian boundary currents. *Journal of Climate*, 25(8): 2947–2962, 2012.

P. M. Suprenand and C. H. Ainsworth. Trophodynamic effects of climate change-induced alterations to primary production along the western Antarctic Peninsula. *Marine Ecology Progress Series*, 569: 37–54, 2017.

M. Takahashi, S. Noonan, K. Fabricius, and C. Collier. The effects of long-term in situ CO_2 enrichment on tropical seagrass communities at volcanic vents. *ICES Journal of Marine Science*, 73(3):876–886, 2016.

K. Tanaka, M. W. Guidry, and N. Gruber. Ecosystem responses of the subtropical Kaneohe Bay, Hawaii, to climate change: a nitrogen cycle modeling approach. *Aquatic geochemistry*, 19(5-6): 569–590, 2013.

E. Teira, A. Fernández, X. A. Álvarez-Salgado, E. E. García-Martín, P. Serret, and C. Sobrino. Response of two marine bacterial isolates to high CO_2 concentration. *Marine Ecology Progress Series*, 453:27–36, 2012.

B. Thamdrup and S. Fleischer. Temperature dependence of oxygen respiration, nitrogen mineralization, and nitrification in Arctic sediments. *Aquatic Microbial Ecology*, 15(2):191–199, 1998.

A. Thompson, T. Schroeder, V. E. Brando, and B. Schaffelke. Coral community responses to declining water quality: Whitsunday Islands, Great Barrier Reef, Australia. *Coral Reefs*, 33(4):923–938, 2014.

H. Tian, W. Ren, J. Yang, B. Tao, W.-J. Cai, S. E. Lohrenz, C. S. Hopkinson, M. Liu, Q. Yang, C. Lu, et al. Climate extremes dominating seasonal and interannual variations in carbon export from the Mississippi River Basin. *Global Biogeochemical Cycles*, 29(9):1333–1347, 2015.

P. D. Tortell, G. R. DiTullio, D. M. Sigman, and F. M. Morel. CO_2 effects on taxonomic composition and nutrient utilization in an Equatorial Pacific phytoplankton assemblage. *Marine Ecology Progress Series*, 236:37–43, 2002.

P. D. Tortell, C. D. Payne, Y. Li, S. Trimborn, B. Rost, W. O. Smith, C. Riesselman, R. B. Dunbar, P. Sedwick, and G. R. DiTullio. CO_2 sensitivity of Southern Ocean phytoplankton. *Geophysical Research Letters*, 35(L04605), 2008.

M. Travers-Trolet, Y. Shin, and J. Field. An end-to-end coupled model ROMS-$N_2P_2Z_2D_2$-OSMOSE of the southern Benguela foodweb: parameterisation, calibration and pattern-oriented validation. *African Journal of Marine Science*, 36(1):11–29, 2014.

S. Trimborn, T. Brenneis, E. Sweet, and B. Rost. Sensitivity of Antarctic phytoplankton species to ocean acidification: Growth, carbon acquisition, and species interaction. *Limnology and Oceanography*, 58 (3):997–1007, 2013.

L. Truong, I. M. Suthers, D. O. Cruz, and J. A. Smith. Plankton supports the majority of fish biomass on temperate rocky reefs. *Marine Biology*, 164(4):73, 2017.

V. J. Tulloch, É. E. Plagányi, R. Matear, C. J. Brown, and A. J. Richardson. Ecosystem modelling to quantify the impact of historical whaling on Southern Hemisphere baleen whales. *Fish and fisheries*, 19(1):117–137, 2018.

V. J. Tulloch, É. E. Plagányi, C. Brown, A. J. Richardson, and R. Matear. Future recovery of baleen whales is imperiled by climate change. *Global change biology*, 25(4):1263–1281, 2019.

R. Turner, R. Huggins, R. Wallace, R. Smith, S. Vardy, and M. St. J. Warne. Total suspended solids, nutrient and pesticide loads (2010-2011) for rivers that discharge to the Great Barrier Reef. *Great Barrier Reef Catchment Loads Monitoring 2010-2011 Department of Science, Information Technology, Innovation and the Arts, Brisbane*, 2013.

Y. Ueno, S. Aikawa, A. Kondo, and S. Akimoto. Energy transfer in cyanobacteria and red algae: confirmation of spillover in intact megacomplexes of phycobilisome and both photosystems. *The journal of physical chemistry letters*, 7(18):3567–3571, 2016.

United Nations Educational, Scientific and Cultural Organisation. Nominations to the World Heritage List (inscribed sites). https://whc.unesco.org/en/decisions/5236, Accessed September 2020.

N. Van Oostende, R. Dussin, C. Stock, A. Barton, E. Curchitser, J. Dunne, and B. Ward. Simulating the ocean's chlorophyll dynamic range from coastal upwelling to oligotrophy. *Progress in oceanography*, 168:232–247, 2018.

M. Vancoppenolle, L. Bopp, G. Madec, J. Dunne, T. Ilyina, P. R. Halloran, and N. Steiner. Future Arctic Ocean primary productivity from CMIP5 simulations: Uncertain outcome, but consistent mechanisms. *Global Biogeochemical Cycles*, 27(3):605–619, 2013.

R. Vaquer-Sunyer and C. M. Duarte. Temperature effects on oxygen thresholds for hypoxia in marine benthic organisms. *Global Change Biology*, 17(5):1788–1797, 2011.

A. Vehmaa, A. Brutemark, and J. Engström-Öst. Maternal effects may act as an adaptation mechanism for copepods facing pH and temperature changes. *PLoS one*, 7(10):e48538, 2012.

C. Vernotte, C. Astier, and J. Olive. State 1-state 2 adaptation in the cyanobacteria *Synechocystis* PCC 6714 wild type and *Synechocystis* PCC 6803 wild type and phycocyanin-less mutant. *Photosynthesis research*, 26(3):203–212, 1990.

T. Villareal and E. Carpenter. Buoyancy regulation and the potential for vertical migration in the oceanic cyanobacterium *Trichodesmium*. *Microbial ecology*, 45(1):1–10, 2003.

S. L. Wakelin, Y. Artioli, M. Butenschön, J. I. Allen, and J. T. Holt. Modelling the combined impacts of climate change and direct anthropogenic drivers on the ecosystem of the northwest European continental shelf. *Journal of Marine Systems*, 152:51–63, 2015.

G. Walden, C. Noirot, and I. Nagelkerken. A future 1.2° C increase in ocean temperature alters the quality of mangrove habitats for marine plants and animals. *Science of the Total Environment*, 690: 596–603, 2019.

C. C. Wallace and B. R. Rosen. Diverse staghorn corals (Acropora) in high-latitude Eocene assemblages: implications for the evolution of modern diversity patterns of reef corals. *Proceedings of the Royal Society B: Biological Sciences*, 273(1589):975–982, 2006.

P. Wallhead, R. Bellerby, A. Silyakova, D. Slagstad, and A. A. Polukhin. Bottom water acidification and warming on the western Eurasian Arctic shelves: Dynamical downscaling projections. *Journal of Geophysical Research: Oceans*, 122(10):8126–8144, 2017.

A. Walsby. The properties and buoyancy-providing role of gas vacuoles in *Trichodesmium Ehrenberg*. *British Phycological Journal*, 13(2):103–116, 1978.

A. Walsby. The gas vesicles and buoyancy of *Trichodesmium*. *Marine pelagic cyanobacteria: Trichodesmium and other diazotrophs*, pages 141–161, 1992.

A. E. Walsby. The permeability of blue-green algal gas-vacuole membranes to gas. *Proceedings of the Royal Society of London. Series B. Biological Sciences*, 173(1031):235–255, 1969.

A. E. Walsby and D. P. Holland. Sinking velocities of phytoplankton measured on a stable density gradient by laser scanning. *Journal of the royal society interface*, 3(8):429–439, 2006.

K. J. Walsh, J. L. McBride, P. J. Klotzbach, S. Balachandran, S. J. Camargo, G. Holland, T. R. Knutson, J. P. Kossin, T.-c. Lee, A. Sobel, et al. Tropical cyclones and climate change. *Wiley Interdisciplinary Reviews: Climate Change*, 7(1):65–89, 2016.

D. Wang, T. C. Gouhier, B. A. Menge, and A. R. Ganguly. Intensification and spatial homogenization of coastal upwelling under climate change. *Nature*, 518(7539):390–394, 2015.

H. Wang, Q. Chen, K. Hu, and M. K. La Peyre. A modeling study of the impacts of Mississippi River diversion and sea-level rise on water quality of a deltaic estuary. *Estuaries and coasts*, 40(4): 1028–1054, 2017.

J. Wang, Z. Yu, Q. Wei, and Q. Yao. Long-term nutrient variations in the Bohai Sea over the past 40 years. *Journal of Geophysical Research: Oceans*, 124(1):703–722, 2019a.

W.-L. Wang, J. K. Moore, A. C. Martiny, and F. W. Primeau. Convergent estimates of marine nitrogen fixation. *Nature*, 566(7743):205–211, 2019b.

R. D. Ward, D. A. Friess, R. H. Day, and R. A. MacKenzie. Impacts of climate change on mangrove ecosystems: a region by region overview. *Ecosystem Health and Sustainability*, 2(4):e01211, 2016.

M. Warner, W. Fitt, and G. Schmidt. The effects of elevated temperature on the photosynthetic efficiency of zooxanthellae in hospite from four different species of reef coral: a novel approach. *Plant, Cell & Environment*, 19(3):291–299, 1996.

Y. Watanabe, A. Yamaguchi, H. Ishida, T. Harimoto, S. Suzuki, Y. Sekido, T. Ikeda, Y. Shirayama, M. Mac Takahashi, T. Ohsumi, et al. Lethality of increasing CO_2 levels on deep-sea copepods in the western North Pacific. *Journal of Oceanography*, 62(2):185–196, 2006.

R. T. Watson, D. L. Albritton, and D. J. Dokken. *Climate change 2001: synthesis report*. Cambridge University Press Cambridge, UK, 2001.

G. Wei, M. T. McCulloch, G. Mortimer, W. Deng, and L. Xie. Evidence for ocean acidification in the Great Barrier Reef of Australia. *Geochimica et Cosmochimica Acta*, 73(8):2332–2346, 2009.

T. Weisse, B. Gröschl, and V. Bergkemper. Phytoplankton response to short-term temperature and nutrient changes. *Limnologica*, 59:78–89, 2016.

T. K. Westberry and D. A. Siegel. Spatial and temporal distribution of *Trichodesmium* blooms in the world's oceans. *Global Biogeochemical Cycles*, 20(4), 2006.

A. White, D. Karl, K. Björkman, L. Beversdorf, R. Letelier, et al. Production of organic matter by *Trichodesmium* IMS101 as a function of phosphorus source. *Limnology and Oceanography*, 55(4): 1755, 2010.

A. E. White, Y. H. Spitz, and R. M. Letelier. Modeling carbohydrate ballasting by *Trichodesmium* spp. *Marine Ecology Progress Series*, 323:35–45, 2006.

C. Wilcox, G. Heathcote, J. Goldberg, R. Gunn, D. Peel, and B. D. Hardesty. Understanding the sources and effects of abandoned, lost, and discarded fishing gear on marine turtles in northern Australia. *Conservation biology*, 29(1):198–206, 2015.

B. Willis, C. Page, and E. Dinsdale. Coral disease on the Great Barrier Reef. In 'Coral Health and Disease'.(Eds E. Rosenberg and Y. Loya.) pp. 69–104, 2004.

C. J. Willmott, S. G. Ackleson, R. E. Davis, J. J. Feddema, K. M. Klink, D. R. Legates, J. O'donnell, and C. M. Rowe. Statistics for the evaluation and comparison of models. *Journal of Geophysical Research: Oceans*, 90(C5):8995–9005, 1985.

E. Wolanski and G. De'ath. Predicting the impact of present and future human land-use on the Great Barrier Reef. *Estuarine, Coastal and Shelf Science*, 64(2-3):504–508, 2005.

N. H. Wolff, P. J. Mumby, M. Devlin, and K. R. Anthony. Vulnerability of the Great Barrier Reef to climate change and local pressures. *Global change biology*, 24(5):1978–1991, 2018.

S. A. Wooldridge. Water quality and coral bleaching thresholds: Formalising the linkage for the inshore reefs of the Great Barrier Reef, Australia. *Marine pollution bulletin*, 58(5):745–751, 2009.

A. Yamamoto, A. Abe-Ouchi, and Y. Yamanaka. Long-term response of oceanic carbon uptake to global warming via physical and biological pumps. *Biogeosciences*, 15(13):4163–4180, 2018.

G. Yang and K. Gao. Physiological responses of the marine diatom *Thalassiosira pseudonana* to increased pCO_2 and seawater acidity. *Marine Environmental Research*, 79:142–151, 2012.

A. Yool, E. Popova, A. Coward, D. Bernie, and T. Anderson. Climate change and ocean acidification impacts on lower trophic levels and the export of organic carbon to the deep ocean. *Biogeosciences*, 10(9):5831–5854, 2013.

J. P. Zehr and D. G. Capone. Changing perspectives in marine nitrogen fixation. *Science*, 368(6492), 2020.

R. C. Zimmerman, D. G. Kohrs, D. L. Steller, and R. S. Alberte. Impacts of CO_2 enrichment on productivity and light requirements of eelgrass. *Plant physiology*, 115(2):599–607, 1997.